

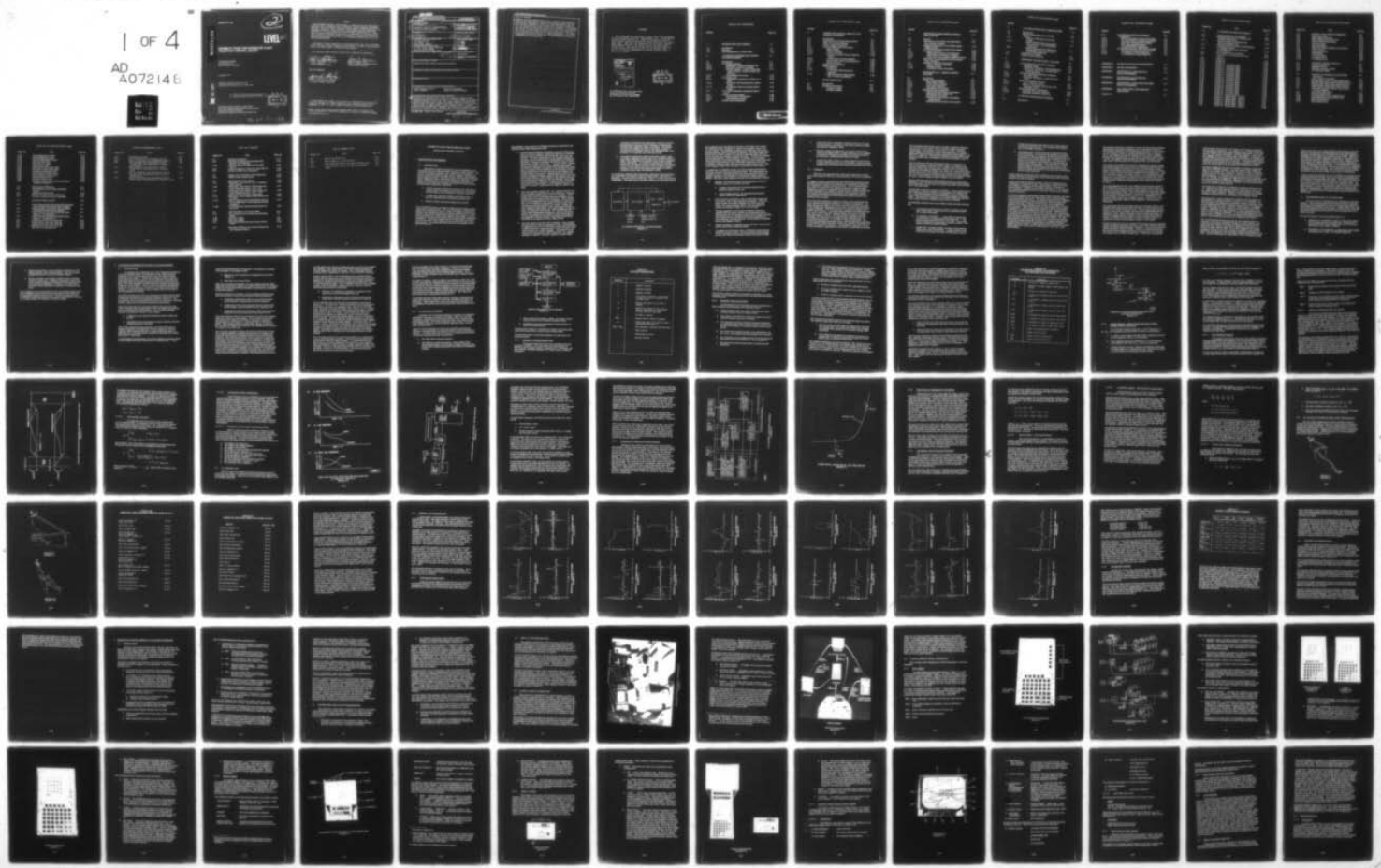
AD-A072 148 LEAR SIEGLER INC GRAND RAPIDS MICH INSTRUMENT DIV F/G 17/7  
FEASIBILITY STUDY FOR INTEGRATED FLIGHT TRAJECTORY CONTROL (AIR--ETC(U))  
JAN 77 M BIRD F33615-74-C-3083

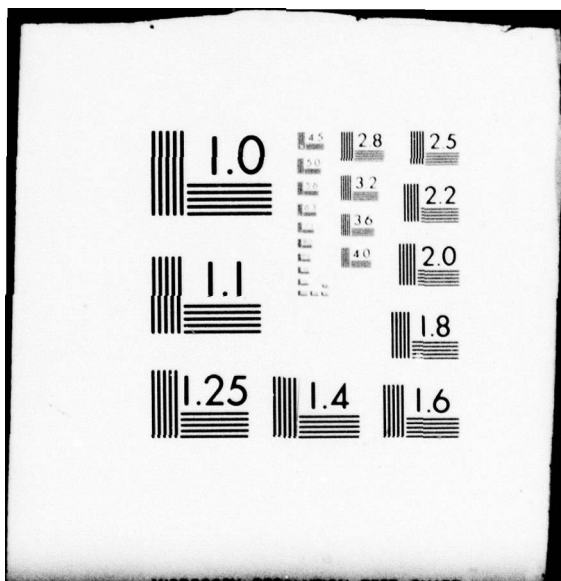
UNCLASSIFIED

AFFDL-TR-77-120

NL

1 OF 4  
AD A072148





ADA072148

AFFDL-TR-77-120

Q  
B.S.

LEVEL II

## FEASIBILITY STUDY FOR INTEGRATED FLIGHT TRAJECTORY CONTROL (AIRLIFT)

INSTRUMENT DIVISION  
LEAR SIEGLER, INC.  
GRAND RAPIDS, MICHIGAN

JANUARY 1977

TECHNICAL REPORT AFFDL-TR-77-120  
Final Report for Period June 1974 – October 1976

DDC FILE COPY

Approved for public release; distribution unlimited.



AIR FORCE FLIGHT DYNAMICS LABORATORY  
AIR FORCE WRIGHT AERONAUTICAL LABORATORIES  
AIR FORCE SYSTEMS COMMAND  
WRIGHT-PATTERSON AIR FORCE BASE, OHIO 45433

79 07 23 104

NOTICE

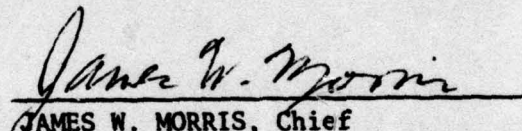
When Government drawings, specifications, or other data are used for any purpose other than in connection with a definitely related Government procurement operation, the United States Government thereby incurs no responsibility nor any obligation whatsoever; and the fact that the government may have formulated, furnished, or in any way supplied the said drawings, specifications, or other data, is not to be regarded by implication or otherwise as in any manner licensing the holder or any other person or corporation, or conveying any rights or permission to manufacture, use, or sell any patented invention that may in any way be related thereto.

This report has been reviewed by the Information Office (OI) and is releasable to the National Technical Information Service (NTIS). At NTIS, it will be available to the general public, including foreign nations.

This technical report has been reviewed and is approved for publication.

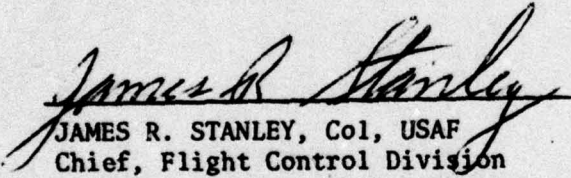


JOHN E. CHRISTENSEN, Sgt, USAF  
Project Engineer  
Control Management Group



JAMES W. MORRIS, Chief  
Control Systems Development Branch  
Flight Control Division

FOR THE COMMANDER



JAMES R. STANLEY, Col, USAF  
Chief, Flight Control Division  
AF Flight Dynamics Laboratory

"If your address has changed, if you wish to be removed from our mailing list, or if the addressee is no longer employed by your organization please notify AFFDL/FGL, W-PAFB, OH 45433 to help us maintain a current mailing list".

Copies of this report should not be returned unless return is required by security considerations, contractual obligations, or notice on a specific document.

**UNCLASSIFIED**

**SECURITY CLASSIFICATION OF THIS PAGE (When Data Entered)**

**DD FORM 1 JAN 73 1473 EDITION OF 1 NOV 68 IS OBSOLETE**

**UNCLASSIFIED**

**SECURITY CLASSIFICATION OF THIS PAGE (When Data Entered)**

**Block 20, Continued**

reference units and strapdown inertial units. Operation, with messages incoming to the cockpit via data link, was evaluated and a pilot-in-the-loop simulation was accomplished to determine an acceptable method to keep the pilot informed of command and control directives. Methods for entering this data into the guidance and control system were also analyzed. In the approach used, the cockpit consisted of CRT displays and a real-time trajectory generation routine. The data-linked information was entered directly into the central processor and acted upon by the trajectory generation. This information was then displayed to the pilot for approval/disapproval prior to being incorporated into the active flight plan. A brief discussion of follow-on recommendations is also presented.

**UNCLASSIFIED**

## FOREWORD

The investigation described in this report was performed by the Instrument Division, Lear Siegler, Inc., Grand Rapids, Michigan under Contract No. F33615-74-C-3083 for the Air Force Flight Dynamics Laboratory, Wright-Patterson Air Force Base, Ohio. The work was sponsored by the Control Systems Development Branch of the Flight Control Division under Project 2187. The report was written by Michael Bird and covers the period from June 1974 through October 1976. Mr. G. L. Fileccia (AFFDL/FG) served as technical monitor for this contract.

Accession for	
NTIS GRAAI	
DDC TAB	
Unannounced	
Justification _____	
By _____	
Distribution/	
Availability Codes	
Available/or special	
A	



RE: AFFDL-IR-77-120, Classified references, distribution unlimited-  
No change in distribution statement  
per Ms. Martha Kline, AFFDL/STINFO

## TABLE OF CONTENTS

Section		Page No.
1	INTRODUCTION AND SUMMARY	1-1
1.1	Introduction	1-1
1.2	Summary	1-5
1.3	Recommendations for Future Work	1-10
2	4-D PROFILE SYNTHESIS AND CONTROL LAW DEVELOPMENT	2-1
2.1	Introduction	2-1
2.2	4-D Profile Synthesis	2-4
2.2.1	Assignment of Missing Waypoint Data	2-5
2.2.2	Horizontal Trajectory Synthesis	2-7
2.2.3	Altitude Changes: Constant Flight Path Angle or Spiral Altitude Vertical Tra- jectories	2-11
2.2.4	Time Schedule Prediction	2-12
2.3	4-D Control Law	2-16
2.3.1	Computation of Reference Profiles Vari- ables	2-20
2.3.2	Time Error and Tracking Error Calcul- ations	2-23
2.3.3	Auto/Manual Control Command Calcul- ations	2-23
2.4	4-D Profile Synthesizer Simulation Perfor- mance	2-27
2.5	Control Law Performance	2-32
2.5.1	Final Approach Performance	2-32
2.5.2	Tracking Data Analysis	2-39
2.6	Further Recommendations	2-41

ENCLOSURE PAGE BLANK

## TABLE OF CONTENTS (cont)

Section		Page No.
<b>3</b>	<b>INTERACTIVE CONTROL-DISPLAY (C-D) CONCEPT DEFINITION</b>	<b>3-1</b>
3.1	Introduction	3-1
3.2	Information/Crew Station Requirements	3-3
3.3	Basic C-D Recommendations	3-5
3.4	Control-Display Interaction	3-5
3.5	Control-Display Detail Description	3-9
3.5.1	Status Display	3-9
3.5.2	Situation Display	3-16
3.5.3	Cursor Controller	3-19
3.5.4	Electronic Attitude Director Indicator (EADI)	3-22
3.5.5	Vertical Scale Air Data Displays	3-25
3.5.6	System Mode Control and Annunciator	3-26
3.5.7	Panel Allocation	3-26
3.6	Display System Operation	3-26
3.7	JTIDS Integration	3-27
3.7.1	Introduction	3-27
3.7.2	4-D INCADS/JTIDS Interactive Operation	3-31
3.7.3	JTIDS Information Requirements and C-D Recommendations	3-32
<b>4</b>	<b>SYSTEM SIMULATOR</b>	<b>4-1</b>
4.1	Introduction	4-1
4.2	Simulation Description	4-3
4.2.1	Transport Cockpit	4-5
4.2.2	Simulation Models	4-11

## TABLE OF CONTENTS (cont)

<b>Section</b>		<b>Page No.</b>
<b>5</b>	<b>INTEGRATED LORAN INERTIAL NAVIGATION ANALYSIS</b>	<b>5-1</b>
5.1	General	5-1
5.2	Differential Loran/Inertial and Differential Baro/Inertial Concepts	5-5
5.3	Integrated Differential Loran/Doppler Radar/AHRS Concepts	5-12
5.4	4-D INCADS Navigation System Error Model	5-15
5.5	Analytical Evaluation	5-22
5.5.1	Differential Loran/Inertial Evaluation	5-24
5.5.2	Differential Baro/Inertial Evaluation	5-31
5.5.3	Differential Loran/Doppler/AHRS Evaluation	5-36
5.6	Differential Loran/Strapdown Inertial Kalman Filter Simulation	5-41
5.7	Analysis of Data Link Parameters	5-56
5.7.1	Distance/Height of Aircraft	5-56
5.7.2	Message Content	5-57
5.7.3	Transmitter Power Calculation	5-59
<b>6</b>	<b>INTEGRATED GPS - INERTIAL SYSTEM ANALYSIS</b>	<b>6-1</b>
6.1	Introduction	6-1
6.2	Navstar GPS Description	6-2
6.2.1	Space System Segment	6-4
6.2.2	Control System Segment	6-5
6.2.3	User System Segment	6-6
6.2.4	GPS System Performance	6-6
6.3	GPS/Inertial/Baro Integration	6-10
6.3.1	GPS/Inertial/Baro System Description	6-10
6.3.2	Differential GPS Configuration	6-13
6.3.3	GPS Receiver Operation	6-15
6.3.4	GPS/Inertial/Baro System Processing Requirements	6-18
6.3.5	GPS/Inertial/Baro System Performance	6-22

**TABLE OF CONTENTS (cont)**

<b>Section</b>		<b>Page No.</b>
<b>7</b>	<b>4-D/JTIDS INTEGRATION CONSIDERATIONS</b>	<b>7-1</b>
7.1	Introduction	7-1
7.2	Mission Enhancements of 4-D/JTIDS System	7-2
7.2.1	Relevant JTIDS Data for 4-D Capability	7-2
7.2.2	Mission Enhancements of Transport Aircraft Due to 4-D/JTIDS System Capabilities	7-4
7.2.3	Mission Enhancements of Strike/Reconnaissance Type Aircraft Due to 4-D/JTIDS Capabilities.	7-7
7.3	JTIDS Relative Ranging	7-9
7.4	JTIDS Terminal Functions	7-10
<b>8</b>	<b>COMPONENT FAILURE EFFECT ANALYSIS</b>	<b>8-1</b>
8.2	Ground Equipment Reliability Prediction	8-1
8.2.1	Reliability Model	8-2
8.2.2	Reliability Calculation - Ground Equipment	8-2
8.2.3	Preliminary Operational Considerations - Ground Equipment	8-4
8.3	Airborne Equipment Reliability Prediction	8-4
8.3.1	Reliability Model	8-4
8.3.2	Reliability Calculation - Airborne Equipment	8-6
8.4	Effects of Component Failures	8-9
8.4.1	Loss of Airborne Loran	8-9
8.4.2	Effects of Component Failure for a Non-Redundant System	8-10
8.5	Recommendations for Redundancy	8-20
8.5.1	Redundant Component Approach	8-20
8.5.2	Functional Redundancy Approach	8-21
<b>9</b>	<b>4-D INCADS COMPATIBILITY STUDIES</b>	<b>9-1</b>
9.1	Introduction	9-1

## TABLE OF CONTENTS (cont)

Section		Page No.
<b>9.2</b>	<b>4-D INCADS and NAS Area Navigation Compatibility</b>	<b>9-2</b>
9.2.1	NAS Area Navigation System Description	9-2
9.2.2	Current Problems in Implementing RNAV	9-2
9.2.3	FAA RNAV Implementation Schedule	9-3
9.2.4	RNAV Navaids Requirements	9-5
9.2.5	4-D INCADS RNAV Capabilities	9-5
9.3	<b>4-D INCADS Integration With MLS and Omega</b>	<b>9-6</b>
9.3.1	Microwave Landing System Description	9-6
9.3.2	4-D INCADS and MLS Integration	9-7
9.3.3	4-D INCADS and Omega Integration	9-8
 <b>APPENDIX A</b>	<b>NAVIGATION SYSTEM MECHANIZATION</b>	<b>A-1</b>
<b>APPENDIX B</b>	<b>MATRIX DEFINITIONS</b>	<b>B-1</b>
<b>APPENDIX C</b>	<b>DIFFERENTIAL LORAN/INERTIAL ERROR EXPRESSIONS</b>	<b>C-1</b>
<b>APPENDIX D</b>	<b>DIFFERENTIAL BARO/INERTIAL ERROR EXPRESSIONS</b>	<b>D-1</b>
<b>APPENDIX E</b>	<b>DIFFERENTIAL LORAN/DOPPLER/AHRS ERROR EXPRESSIONS</b>	<b>E-1</b>
<b>APPENDIX F</b>	<b>GPS OPERATIONAL PERFORMANCE LIMITATIONS</b>	<b>F-1</b>
<b>REFERENCES</b>		<b>R-1</b>

## LIST OF ILLUSTRATIONS

Figure No.	Title	Page No.
1-1	4-D INCADS Functional Block Diagram	1-3
2-1	Profile Synthesizer Flow Diagram	2-5
2-2	Horizontal Path Between Waypoints and Defining Parameters	2-11
2-3	Velocity Profiles for Maximum and Minimum Elapsed Time	2-14
2-4	Drag and Velocity Profiles for Deceleration at Constant Throttle	2-17
2-5	4-D INCADS Control Law Functional Block Diagram	2-18
2-6	4-D Control Law Block Diagram	2-21
2-7	Cross Track, Track Angle, and Time Errors	2-22
2-8	Profile #1	2-27
2-9	Profile #2	2-28
2-10	Profile #3	2-28
2-11	Profile #1 - Automatic Mode	2-33
2-12	Profile #1 - Automatic Mode	2-33
2-13	Profile #1 - Automatic Mode	2-33
2-14	Profile #1 - Automatic Mode	2-33
2-15	Profile #1 - Automatic Mode	2-34
2-16	Profile #1 - Automatic Mode	2-34
2-17	Profile #1 - Automatic Mode	2-34
2-18	Profile #1 - Automatic Mode	2-34
2-19	Profile #2 - Automatic Mode	2-35
2-20	Profile #2 - Automatic Mode	2-35
2-21	Profile #2 - Automatic Mode	2-35
2-22	Profile #2 - Automatic Mode	2-35
2-23	Profile #2 - Automatic Mode	2-36
2-24	Profile #2 - Automatic Mode	2-36
2-25	Profile #2 - Automatic Mode	2-36
2-26	Profile #2 - Automatic Mode	2-36
2-27	Profile #1 - Manual Mode - Pilot #1	2-37
2-28	Profile #1 - Manual Mode - Pilot #1	2-37
2-29	Profile #1 - Manual Mode - Pilot #1	2-37
2-30	Profile #1 - Manual Mode - Pilot #1	2-37
2-31	Profile #2 - Manual Mode - Pilot #1	2-38
2-32	Profile #2 - Manual Mode - Pilot #1	2-38

## LIST OF ILLUSTRATIONS (cont)

Figure No.	Title	Page No.
3-1	Simulator Control-Display Configuration	3-6
3-2	System Interaction	3-8
3-3	Status Display/Keyboard	3-10
3-4	Status Display Information Flow	3-11
3-5	Present Position Information	3-13
3-6	Plan Information	3-13
3-7	Index Information	3-14
3-8	Electronic Situation Display and Controller	3-17
3-9	Cursor Control	3-19
3-10	Threat Information	3-21
3-11	EADI Display	3-23
3-12	C-D Interaction I	3-28
3-13	C-D Interaction II	3-29
3-14	C-D Interaction III	3-30
4-1	LSI Hybrid Computing Laboratory	4-2
4-2	System Configuration	4-3
4-3	Transport Cockpit	4-5
4-4	Dual Seat Transport Cockpit	4-6
4-5	A/C Simulation Model	4-12
5-1	Airborne Loran/Strapdown Inertial Navigation System	5-6
5-2	Loran-C System Principles	5-8
5-3	Representative D Value Versus Altitude Data	5-10
5-4	Airborne Differential Loran/Strapdown Inertial	5-13
5-5	TDA Secondary Phase ( $\mu$ sec) Eglin AFB Area	5-32
5-6	TDB Secondary Phase ( $\mu$ sec) Eglin AFB Area	5-33
5-7	Differential Loran/Ins Kalman Filter Simulation Block Diagram	5-46
5-8	Horizontal Flight Profile	5-47
5-9	Vertical Flight Profile	5-48
5-10	North Differential Loran Position Error	5-50
5-11	East Differential Loran Position Error	5-50
5-12	North Velocity Error	5-50
5-13	East Velocity Error	5-50

## LIST OF ILLUSTRATIONS (cont)

Figure No.	Title	Page No.
5-14	North Misalignment Angle	5-51
5-15	East Misalignment Angle	5-51
5-16	Vertical Misalignment Angle	5-51
5-17	Roll Axis Gyro Bias	5-51
5-18	Pitch Axis Gyro Bias	5-52
5-19	Aximuth Gyro Bias	5-52
5-20	Ross Axis Accelerometer Bias	5-52
5-21	Pitch Axis Accelerometer Bias	5-52
5-22	Azimuth Accelerometer Bias	5-53
5-23	North Absolute Position Error	5-53
5-24	East Absolute Position Error	5-53
5-25	Vertical Position Error	5-53
5-26	Vertical Velocity Error	5-54
5-27	Nomogram Relating Radio Horizon Distance (Height and Distance)	5-57
6-1	GPS Program Milestones	6-3
6-2	GPS/Strapdown Inertial/Baro Navigation System	6-11
6-3	Differential GPS Concept	6-13
6-4	Sequence of Operation of GPS Receiver	6-15
6-5	Process Controller/Receiver Hardware	6-17
7-1	Functional JTIDS Terminal	7-10
8-1	Ground Sensors/Data Link During IFR Approach Phase Simplified Reliability Block Diagram	8-3
8-2	Airborne System During IFR Approach Phase Simplified Reliability Block Diagram	8-5
8-3	Control/Display Simplified Reliability Block Diagram - Configuration 1	8-7
8-4	Control/Display Simplified Reliability Block Diagram - Configuration 2	8-8
8-5	Position Error and Loran Time Off	8-11
8-6	Position Error and Loran Time Off	8-12
8-7	Position Error and Loran Time Off	8-13
8-8	Position Error and Loran Time Off	8-14
8-9	Plan View of Terminal Area	8-16

## LIST OF ILLUSTRATIONS (cont)

Figure No.	Title	Page No.
A-1	Coordinate Systems	A-3
F-1	Code Tracking Loop Performance Limits	F-4
F-2	Carrier Tracking Loop Performance Limits	F-6
F-3	Code Tracking Loop Performance Limits Second Order Loop Subjected to Steps of Acceleration	F-9
F-4	Code Tracking Loop Performance Limits Third Order Loop Subjected to Steps of Jerk	F-10
F-5	Carrier Tracking Loop Performance Limits Second Order Loop Subjected to Steps of Acceleration	F-11
F-6	Carrier Tracking Loop Performance Limits Third Order Loop Subjected to Steps of Jerk	F-12

## LIST OF TABLES

Figure No.	Title	Page No.
2-I	Waypoint Parameters	2-6
2-II	Parameters Defining the Horizontal Path Between Two Waypoints	2-10
2-III	Predicted Times for Maneuvers of Flight Plan #1	2-29
2-IV	Predicted Maneuver Times for Flight Plan #2	2-30
2-V	Errors 1/2 Mile From Touchdown	2-40
3-I	Typical Voice Synthesizer Work Repertoire	3-34
3-II	JTIDS Function Requirements	3-36
5-I	Inertial System Error Source	5-23
5-II	Differential Loran/Inertial Error Equations - North Channel	5-25
5-III	Differential Loran/Inertial Performance 2nd Order Integration Filter - S/N = 0 db	5-27
5-IV	Differential Loran/Inertial Performance 2nd Order Integration Filter - S/N = +8 db	5-28
5-V	Differential Baro/Inertial Performance	5-35
5-VI	Differential Loran/Doppler/AHRS System Per- formance	5-40
5-VII	Initial Conditions and Inertial Sensors Errors for the Differential Loran/Strapdown Inertial Simulation	5-55
5-VIII	4-D INCADS Data Handling Requirements for Data Link	5-58
6-I	Characteristics of P and C/A Codes	6-5
6-II	User Equipment Set Attributes and Operating Modes	6-7
6-III	GPS User Classes	6-8
6-IV	GPS Error Budget	6-9
6-V	Integrated GPS/Inertial/Baro System Perfor- mance	6-23
8-I	Summary of Effects of Component Failures for Non-Redundant System	8-17

### LIST OF TABLES (cont)

Figure No.	Title	Page No.
B-I	Matrix $A_H$ Definition	B-4
B-II	Matrix $\Phi_H(t_{j+1}, t_j)$ Definition	B-11
F-I	Peak Transient Error for Code Tracking Loop	F-8
F-II	Peak Transient Error for Carrier Tracking Loop	F-8

## **FEASIBILITY STUDY FOR INTEGRATED FLIGHT**

### **TRAJECTORY CONTROL (AIRLIFT)**

#### **1 INTRODUCTION AND SUMMARY**

##### **1.1 INTRODUCTION**

This technical report describes the work accomplished on the Feasibility Study for Integrated Flight Trajectory Control (Airlift). The overall study program objective was to determine the feasibility of a system concept that integrates flight control, displays, and navigation into one airborne system, referred to in this report as the Four-Dimensional INtegrated Control And Display System (4-D INCADS). The objective of the system is to improve the operational performance of military aircraft operating in hostile environments with the following advanced flight management capabilities:

- a. Airborne computer synthesis of nonlinear four-dimensional profiles (three-dimensional trajectories plus a time dimension that defines a time schedule for flying the trajectory);
- b. A control law, with both automatic and manual modes, to track the synthesized four-dimensional profiles; and
- c. Mission-oriented information displays and controls.

The 4-D INCADS concept is designed to fulfill the future flight management needs of military pilots. Current developments of advanced navigation and reconnaissance sensors, multi-user digital communication systems, and expanded command and control capabilities have a direct impact on the amount of information supplied to the cockpit, and therefore necessitates an on-board system with increased flight management capabilities. Automation of flight control and information procession will allow the pilot a more significant role as system manager and decision maker. The AFFDL initiated this study to investigate the 4-D INCADS feasibility.

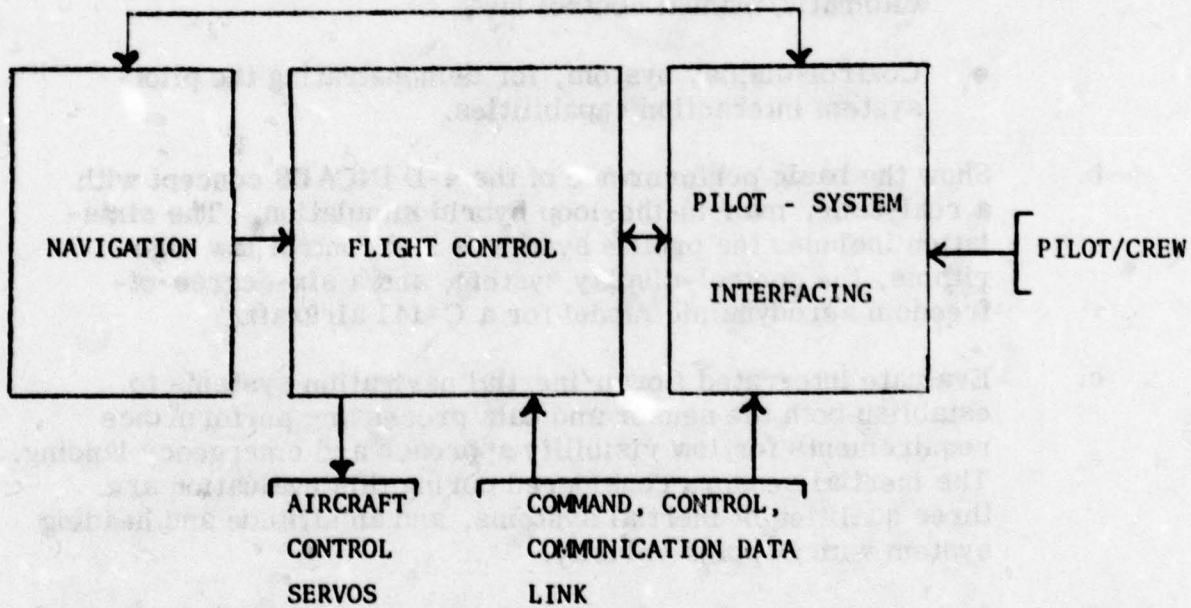
The definition of the primary 4-D INCADS functions is motivated by the following future flight management needs:

- a. A system that synthesizes and guides an aircraft along a precise 4-D profile to improve operational efficiency on missions requiring tactical assaults, tactical airlifts, and in-air rendezvous. The study concentrated on the transport approach operations where a flexible three-dimensional (3-D) trajectory capability is needed for nonlinear approaches from any direction because of flight restrictions -- such as traffic, military threats, geographic and man-made obstacles, and weather. The ability to establish the aircraft's time schedule (4th dimension) accurately allows coordination of the aircraft's activities with the operations of the other aircraft in the airspace and combat troops on the ground. Holding patterns will be minimized and a higher landing acceptance rate achieved with multi-aircraft coordination, which results in both mission time and fuel savings and increased aircraft survivability, when hostile forces are present. Both time coordination between aircraft and accurate aircraft guidance, in both position and time is required to achieve a routine and safe night/all-weather capability.
- b. FAA area navigation studies [20, 22] indicate airborne 3-D and 4-D guidance capabilities may be necessary for operation in the National Airspace System (NAS) in the 1980s. These studies were made to determine how area navigation can be implemented to increase the NAS utilization. These studies call for the implementation of 3-D navigation for enroute profile, and 4-D guidance in high density terminal areas where metering and spacing operations are needed. Besides the area navigation requirements, future operations with Microwave Landing Systems (MLS) may require guidance along nonlinear 3-D approach trajectories. The 4-D INCADS's advanced flight management capabilities, which are primarily aimed at increasing tactical military mission performance, are compatible with the potential Continental United States (CONUS) area navigation and MLS requirements.
- c. The future tasks of the pilot will be different, more complex, and more difficult than his present day tasks. Consequently, an important part of the 4-D INCADS concept is the automation of difficult and time-consuming tasks to allow the pilot to efficiently operate as a system manager. The system concept involves the following pilot relief capabilities: (1) computer synthesis of flyable 4-D profiles using all available flight

restriction information while requiring a minimum of profile specification by the pilot; and (2) reducing, by automating, the pilot effort needed for flying 4-D profiles. New generation electronic displays are part of the system concept to provide the pilot-manager relevant and meaningful data, automatically or on demand, and in the best format.

- d. Lowering the operational visual restrictions to gain a night/all-weather capability requires that the 4-D INCADS advanced flight control capability be integrated with accurate navigation sensor information. To achieve the required IFR tracking accuracies, the system concept includes navigation information from an inertial system and either Loran (a radio navigation system) or the Global Positioning System (GPS) (a satellite navigation system under development by DOD).

To provide the advanced flight management capabilities described above, the 4-D INCADS is divided into three functional areas: flight control, navigation, and pilot-system interfacing. Figure 1-1 shows this functional relationship. The flight control functional area has two interrelated parts:



4-D INCADS FUNCTIONAL BLOCK DIAGRAM  
FIGURE 1-1

path synthesis which calculates the desired 4-D profiles; and a control law which generates commands for manual and automatic aircraft trajectory control. The navigation functional area determines the current aircraft position, velocity, attitude and heading. The pilot-system interfacing area provides a medium for visually presenting system information to the pilot and manually accepting his inputs. The data link provides mission specification, traffic situation, surveillance, and reconnaissance information to the system's flight control and pilot interfacing areas. To perform these functions, the 4-D INCADS components will include an airborne computer interfaced with aircraft flight control servos, electronic displays, a data link, and radio, inertial and air data sensors.

To assess the 4-D INCADS concept, the study analyzed and simulated the basic elements of the three functional areas. The study efforts concentrated on the 4-D INCADS operation during the approach profiles of military transports with emphasis on IFR operation under hostile conditions. The major study program activities are summarized as follows:

- a. Develop, with sufficient detail for the simulation of the 4-D INCADS concept, the following elements:
  - Computer algorithms for 4-D profile synthesis and an automatic/manual control law.
  - Control-display system, for demonstrating the pilot-system interaction capabilities.
- b. Show the basic performance of the 4-D INCADS concept with a real-time, man-in-the-loop hybrid simulation. The simulation includes the profile synthesis and control law algorithms, the control-display system, and a six-degree-of-freedom aerodynamic model for a C-141 aircraft.
- c. Evaluate integrated Loran/inertial navigation systems to establish both the sensor and data processing performance requirements for low visibility approach and emergency landing. The inertial sensors considered during this evaluation are three qualities of inertial systems, and an attitude and heading system with Doppler velocity.
- d. Assess the impact of replacing Loran with GPS to form an integrated GPS/inertial navigation system.
- e. Investigate the integration of the 4-D INCADS concept with the tactical command, control, and communication data provided by the Joint Tactical Information Distribution System (JTIDS).

- f. Assess the effect of individual component failures on the system performance, and based on this failure analysis consider the system's redundancy needs.
- g. Develop a system technique that will comply with the future FAA area navigation (RNAV) requirements and will be capable of effectively utilizing the navigation information provided by the Microwave Landing System (MLS) and Omega.
- h. Develop the initial version of a system definition specification (a Type A Specification) for the 4-D INCADS, using the results obtained from the analysis and simulation tasks described above.

## 1.2 SUMMARY

While the next eight sections of this report describe the results of the study program activities, a brief summary of the work is presented here.

The digital computer algorithms that were defined and simulated during the study were developed with the objective of increasing the flight control capabilities of military aircraft systems. The 4-D profile synthesizer and 4-D control law were defined to provide an improved flight management system for transports performing low visibility airlifts into remote airfields in the presence of mobile, hostile military threats. The computer algorithms are applicable to any military air operation where the aircraft must fly to a given point (or points) and arrive at a specified time (or times).

The 4-D profile synthesizer computes a flyable, three-dimensional trajectory based on parameters defined for a sequence of waypoints. The fourth dimension is added to the profile when the synthesizer calculates a time schedule that establishes the times the trajectory passes through the given waypoints. The 3-D trajectory calculated by the profile synthesizer has two parts: a horizontal path consisting of straight lines and arcs, and a vertical path that changes altitude with either a constant flight path angle or a spiral. The time schedule synthesizer handles two cases: (1) when one or more waypoints are assigned a time-of-arrival (TOA) by the pilot, or (2) when no TOAs are specified. The 4-D profile synthesizer generates curved, three-dimensional trajectories for any feasible military approach profile and computes a realizable time schedule for flying the 3-D profile. The synthesizer algorithm will use the full aerodynamic capabilities of the aircraft in generating the profiles.

The processing requirements of the 4-D profile synthesizer algorithm can be met by current state-of-the-art airborne digital computers. Consequently, the synthesizer can be used to generate 4-D profiles while in flight. The real time creation and modification of computer-generated profiles is based on profile constraints provided either by the pilot or by a data link. This real time interaction between pilot and the system computer was demonstrated in the hybrid simulation of the 4-D INCADS.

The 4-D control law has been developed to allow a 4-D profile to be flown in an automatic mode where control signals are supplied to the aircraft's flight control servos, and in a manual mode where the pilot flies the aircraft while following flight command cues on the Electronic Attitude Director Indicator (EADI). The control law controls the aircraft attitude and throttle to null deviations from trajectory and time schedule. The control law calculates nominal attitude and throttle commands needed for turns, altitude changes and speed changes in the 4-D profile.

Section 2 describes the 4-D profile synthesis and the 4-D control law algorithms. Also discussed are three approach profiles used during the hybrid simulation, and the control law performance data collected during man-in-the-loop testing.

For the pilot's interaction with the 4-D INCADS, a control-display system featuring three electronic displays was developed for the system simulator. The basic philosophy used in developing the control-display system emphasized the pilot's role as an information manager and decision maker. The interaction capabilities are provided through the integration of the versatile electronic displays and the system's computer.

The individual elements of the control-display system and their functions are:

- a. An Electronic Attitude Director Indicator (EADI) and two air data vertical tapes, which provide the conventional situation and command information.
- b. A Cathode Ray Tube (CRT) -- whose display presentations are provided by a programmable symbol generator -- displays the horizontal portion of the 4-D profile. The orientation and scaling of the presentation are pilot selectable. This display is called the situation display.
- c. Another CRT, the status display, provides in-depth detailed alphanumeric system information. A paging concept is used to provide various types and levels of information, with the

computer automatically selecting the most relevant page for the current interaction task. The computer-selected page can be overridden by the pilot.

- d. The keyboard and a cursor controller are used by the pilot for system inputs. The pilot uses the keyboard for accuracy entry of system data, for selecting the type of information to be displayed on the status display, and for authorizing the computer to process the pilot-inserted data. The cursor controller is an alternate to the keyboard for entering data and selecting status display pages. This information is entered with the controller positioning a cross-hair symbol on the situation display, and the technique provides the pilot with a means for rapidly and effectively entering profile modifications and new threat information.

Section 3 defines and discusses the 4-D INCADS control-display system and describes how the pilots used the system during the man-in-the-loop testing on the hybrid simulator.

Section 4 describes the system simulator used for demonstrating and evaluating the 4-D INCADS concept. The simulator consists of a transport cockpit, containing the control-display system, connected to a hybrid computer. Simulated on the hybrid computer is a C-141 aircraft, the 4-D profile synthesizer and 4-D control law, and the control-display integration software.

For precise trajectory tracking the 4-D path control algorithms developed for the 4-D INCADS need to be complemented with an accurate source of aircraft position and velocity. The study has shown that four integrated Loran/inertial navigation systems provide the horizontal position and velocity accuracies 75 feet ( $1\sigma$ ) and 3 feet/sec ( $1\sigma$ ), respectively needed for low visibility guidance along curved 3-D paths down 1/2 mile from touchdown. These accuracies are achieved when the Loran system is operated in a relative (differential) navigation mode where a ground-based Loran receiver establishes the runway location. Altitude and vertical velocity accuracies of 10 feet ( $1\sigma$ ) and 2 feet/sec ( $1\sigma$ ), respectively, are attained with a barometric altimeter/inertial technique where a ground-based altimeter establishes the runway's pressure altitude. The navigation analysis also showed that the differential Loran/inertial technique provide the necessary horizontal accuracy for emergency landings, but the differential baro/inertial technique does not provide the vertical guidance accuracy needed. A radar altimeter and an independent forward-looking radar are recommended to safely perform "zero-zero" emergency landings.

The analysis covering the integration of Loran and barometric altimeter measurements with inertial navigation data is discussed in Section 5. The analysis establishes the processing requirements for Loran integration with different classes of inertial systems (20 nm/hr, 5 nm/hr, 1 nm/hr, and Doppler/Attitude and Heading Reference System (AHRS)). Kalman filter techniques will be required for integration with 20 nm/hr, 5 nm/hr, and Doppler/AHRS systems and simpler, fixed gain, second-order filters will be required for integration with 1 nm/hr systems.

This study recommends that a 20 nm/hr strapped-down inertial system be integrated with Loran to provide the 4-D INCADS navigation function. This recommendation is based on the lower cost and better maintainability of the strapped down sensors, and assumes the system computer has the memory and execution time available for the Kalman filter. However, the better quality, but higher priced, 1 nm/hr gimballed inertial systems are recommended for certain aircraft operating where Loran signals are unavailable for missions that require velocity accuracies of  $\pm 5$  feet/second. (Precision aerial delivery will require this velocity accuracy.)

The study addressed the use of the Global Positioning System (GPS) in the 4-D INCADS because the current military plans call for GPS to replace Loran as the military tactical radio navigation system when GPS becomes operational in 1984. Section 6 describes the integration of GPS into the 4-D INCADS and includes: a description of all three GPS segments (satellite, ground control, and user), the mechanization of an integrated GPS/inertial/baro navigation system, a discussion of computer processing tasks related to GPS integration, and an accuracy assessment.

The study shows that the horizontal position and velocity accuracy of an integrated GPS/inertial/baro system is equal to or better than an integrated Loran/inertial navigation system. Horizontal position accuracy relative to the runway is further improved when a differential GPS configuration is used. While reasonable vertical position information is obtained by integrating GPS, inertial, and an on-board barometric altimeter, the differential barometric altimeter technique needs to be utilized for accurate vertical guidance relative to the runway.

During the study the pilot was considered the primary source of changing mission and threat information; however, in the future another source of mission and threat information will be available - the Joint Tactical Information Distribution System (JTIDS). This is a communication system that allows several hundred participants instant access to net information anywhere in the JTIDS coverage area. JTIDS offers the potential

improvements when the data it will supply to the cockpit is integrated into the airborne equipment. The integration of the JTIDS data and the 4-D INCADS will achieve significant mission enhancement. In this integration, JTIDS will provide inputs, including waypoints, TOA's, mission changes, threats, surveillance data, and targets. In response, the 4-D INCADS will generate and guide the aircraft along 4-D profiles and display the relevant information to the pilot. A key operational improvement that will be achieved is the time/space coordination of many elements (air and ground) in the terminal area during tactical airlifts.

The study emphasized the need for automatic processing of JTIDS data with the 4-D INCADS computer. The vast amount of data JTIDS will supply to the cockpit may "overwhelm" the pilot if he has to continually monitor the data and make decisions on what data to insert into his on-board equipment. To minimize this man-machine interface problem, the 4-D INCADS will manage the JTIDS data-performing operations, such as sorting and filtering JTIDS data, displaying the relevant data needed for a pilot/manager on the electronic displays, and automatically generating new profiles for pilot approval.

The integration of JTIDS and 4-D INCADS is discussed in Sections 7 and 3.7. Section 7 discusses potential mission improvements, the use of the JTIDS relative navigation capability, and the hardware and software needed for JTIDS integration. Section 3.7 discusses the incorporation of JTIDS information into the 4-D INCADS control-display system.

During the study a failure analysis was conducted with the objective of establishing the redundant hardware needed for the 4-D INCADS. Section 8 presents this analysis and recommends standby redundancy on the ground equipment and airborne altimeter and some level of redundancy on the Loran (GPS) receiver, computer, inertial system, and display system. Redundancy for the receiver and the inertial system can be achieved either with functional redundancy, using complementary sensors, or true component redundancy. A recommended approach for the display system redundancy is to provide displays and symbol generators that are interchangeable and prioritize the displayed information.

The 4-D INCADS development and analysis work discussed above concentrated on the system capabilities needed for tactical military operations and the utilization of military navigation sensors and communication data link. However, for effective operation in the future U.S. National Airspace System (NAS), the on-board equipment for military transports will need to provide a navigation capability consistent with future FAA requirements, and utilize the navigation aids provided by the FAA. Section 9 addresses the compatibility of the 4-D INCADS concept

with the future FAA area navigation (RNAV) requirements and the integration of the Microwave Landing System (MLS) and Omega sensors. The study concludes that the 4-D INCADS has the inherent capability of navigating the FAA flight routes through and beyond 1985. Inherent in the control law and profile synthesizer capability is the ability to perform specific maneuvers required to perform offset navigation and turn radius control for conflict avoidance, and the maneuver capability to fly the SID/Enroute/STAR RNAV paths. A recommendation is made that careful consideration be given to techniques for entering FAA-designated waypoints for the RNAV profiles. The 4-D INCADS is also amenable to the integration of MLS and Omega, since both sensors provide position information and can be used in place of the Loran or GPS sensors.

A Type A system specification for the 4-D INCADS was developed as part of the study program; however, the work performed in developing this specification is not described in this report. The specification was written to conform to MIL-STD-490 and represents the initial version of a Type A specification that can be derived from a feasibility study. The specification defines the system functional requirements and the system characteristics, in terms of performance, physical structure, reliability, and maintainability. Design and construction, documentation, logistics, and quality assurance requirements are also addressed in the specification.

### 1.3 RECOMMENDATIONS FOR FUTURE WORK

The merit of the 4-D INCADS has been established in this study program. The simulations and analyses show the system's feasibility and demonstrate its applicability to tactical transport operations in terminal areas around airfields or drop zones. Another output of this study are recommendations for further analysis and simulation work that will demonstrate the operational benefits and functional capabilities of the system technique.

The major elements of the recommended program are:

- Application of 4-D INCADS to fighter aircraft mission tasks, such as weapon delivery and rendezvous. Refine the 4-D algorithms and the control-display system and demonstrate performance with a fighter simulation.
- Demonstrate, on the simulator, the operational improvements achievable with a JTIDS - 4-D INCADS integration.

- Define and implement a vertical situation presentation for the situation display in the cockpit simulator. The current study identified the need for the vertical situation display.
- Develop, simulate, and evaluate an optimal control technique for the 4-D control law. Establish if the optimal control technology provides significant tracking performance improvements over a classically designed 4-D control law and determine if an optimal control algorithm is realizable in an airborne computer.

The combination of the current study and this recommended program will firmly establish the characteristics and performance of the system and its operational benefits to the Air Force. Further development of the 4-D INCADS concept beyond these two programs would require the building of a prototype system for laboratory or airborne testing.

## **2 4-D PROFILE SYNTHESIS AND CONTROL LAW DEVELOPMENT**

### **2.1 INTRODUCTION**

To demonstrate the feasibility of the Four-Dimensional INtegrated Control And Display System (4-D INCADS) concept, digital computer algorithms for 4-D profile synthesis and control law were developed during this study program. The profile synthesis technique computes a three-dimensional (3-D) trajectory, given a sequence of waypoints and information about the desired aircraft orientation and speed at each waypoint. The fourth dimension is added when this technique calculates the trajectory's time schedule. The 4-D control law technique automatically guides the aircraft along the 3-D trajectory according to the given time schedule, or calculates guidance cues for display that allow the pilot to fly the synthesized 4-D profile.

The profile synthesis and control law techniques devised during this study program were programmed on the hybrid computer, which is part of the 4-D INCADS man-in-the-loop simulation described in Section 4. The simulator was used for demonstrating the system concept and for assessing the basic flight control performance during the study program.

This section describes the 4-D profile synthesis and control law algorithms, discusses their implementation in the 4-D INCADS system simulator, and discusses their performance. The 4-D profile synthesis technique is presented in Section 2.2 and includes:

- a. A definition of the waypoint information needed to define the profile,
- b. Descriptions of the horizontal and vertical trajectory and time schedule generation techniques.

This profile synthesis function generates a horizontal trajectory consisting of sequences of straight lines and arcs, generates a vertical trajectory whose segments may have a constant flight path angle or a spiral descent, and simultaneously combines the horizontal and vertical paths into 3-D trajectories.

In synthesizing the 4th dimension, the profile synthesizer assigns a speed to each waypoint that doesn't already have an assigned speed. Then,

using the specified speeds at the waypoints, the synthesizer calculates a time schedule for two distinct cases:

- a. When one or more waypoints are assigned time of arrivals (TOAs), or
- b. When there are no given TOAs.

When TOA information is specified, the time schedule generator determines when ground speed changes are needed to achieve the time schedule, taking into account the aircraft acceleration and deceleration constraints on each path segment.

Without a specified time schedule, the time schedule synthesizer goes into a TOA prediction mode by performing the following operations:

- a. Computing a speed profile with the current aircraft speed and the sequence of speeds given at various waypoints;
- b. Predicting the TOA at each waypoint using the speed profile and the lengths of the horizontal trajectory segments; and
- c. Computing the maximum and minimum TOA at each waypoint taking into account acceleration and deceleration limits.

This TOA prediction version of the synthesizer gives the pilot a flexible method for creating the time schedule. He can modify the predicted time schedule by changing aircraft speed, inserting or modifying a specified speed at any waypoint, or specifying TOAs at selected waypoints. When satisfied with the predicted TOA schedule or speed profile, the pilot can engage the 3-D path and TOA schedule as the reference 4-D profile for the control law.

The 4-D profile synthesis technique devised during this study is versatile; it has the capability of generating the types of 4-D profiles flown on both the NASA Terminal Configured Vehicle (TCV) and STOLAND programs. Both NASA programs [22, 23] use sequences of waypoints and a catalog of parameters defined for each waypoint to synthesize the 4-D profiles. The horizontal paths of TCV and STOLAND are similar to the horizontal trajectory generated on this study program; however, their vertical trajectory segments are limited to constant flight path angles. The TCV system uses speeds assigned at each waypoint and a planned time of arrival at one waypoint to synthesize the speed profile. The STOLAND system uses a predictive time schedule generation technique that processes specified airspeeds at waypoints, wind estimates and the current

aircraft position and velocity to predict the time of arrival at the profile's final waypoint. When the predicted TOA agrees with the required TOA, the pilot engages the profile for tracking. The 4-D INCADS synthesis technique has the capabilities of both the TCV and STOLAND techniques.

Another important part of the 4-D INCADS profile synthesis technique is the interaction between the profile synthesis function and the pilot who supplies new operational information via the control-display subsystem. The pilot can interact with the profile synthesizer and generate a new 4-D profile during the flight. The 4-D INCADS interactive control-display concept, which is discussed in detail in Section 3, gives the pilot the following profile generation capabilities:

- a. Selection of one flight plan consisting of a sequence of waypoints from a set of stored flight plans, and
- b. Generation in real time of a new 4-D profile when new waypoints and/or modified waypoint parameters are inserted,

The 4-D INCADS control law that has been developed is described in Section 2.3. The control law has been developed to allow the reference 4-D profile to be flown in an automatic mode, where the 4-D INCADS sends commands to the aircraft's flight control servos, and in a manual mode, where the pilot flies the aircraft while following flight command cues provided by the 4-D INCADS. In both modes, the control law develops error signals by comparing the current aircraft location, speed, and track to the desired location, speed, and track on the reference 4-D profile. Control surface and throttle positions are calculated by combining the path errors with the nominal attitude and speed changes needed for turns, speed and altitude changes. In the auto mode, the elevator, aileron, and throttle commands are sent to the aircraft's control servos. In the manual mode, roll command, pitch command, and throttle command are displayed on the Electronic Attitude Director Indicator (EADI). The proper anticipation is built into the nominal commands to minimize path or time tracking errors during path direction or speed changes.

The 4-D profile synthesis and control law techniques were implemented in the 4-D INCADS system simulator, where they were programmed on the simulator's IBM-370 digital computer. To demonstrate the capabilities of the 4-D profile synthesizer and control law, three flight profiles representative of different types of military approach profiles were developed. Section 2.4 describes these profiles where two profiles were developed to show the 4-D INCADS utility on operational approaches, and the third profile was used for pilot training.

The three profiles were a basic element in the piloted demonstrations of the 4-D INCADS on the system simulator. During the demonstrations, the pilots made real time modifications to the three profiles using both keyboard inputs and the situation display cursor. For a discussion of these elements of the 4-D INCADS control display system, consult Section 3.

The system simulator, which includes an aerodynamic model of a C-141 aircraft, was used for collecting data on the 4-D control law performance. Path tracking data was collected in both the automatic and manual modes to evaluate how well the control law guides an aircraft along curved 3-D trajectories while simultaneously making the aircraft fly the prescribed time schedule precisely. Manual tracking data was collected using two pilots flying the two operational approach profiles. The control law performance data is summarized in Section 2.5.

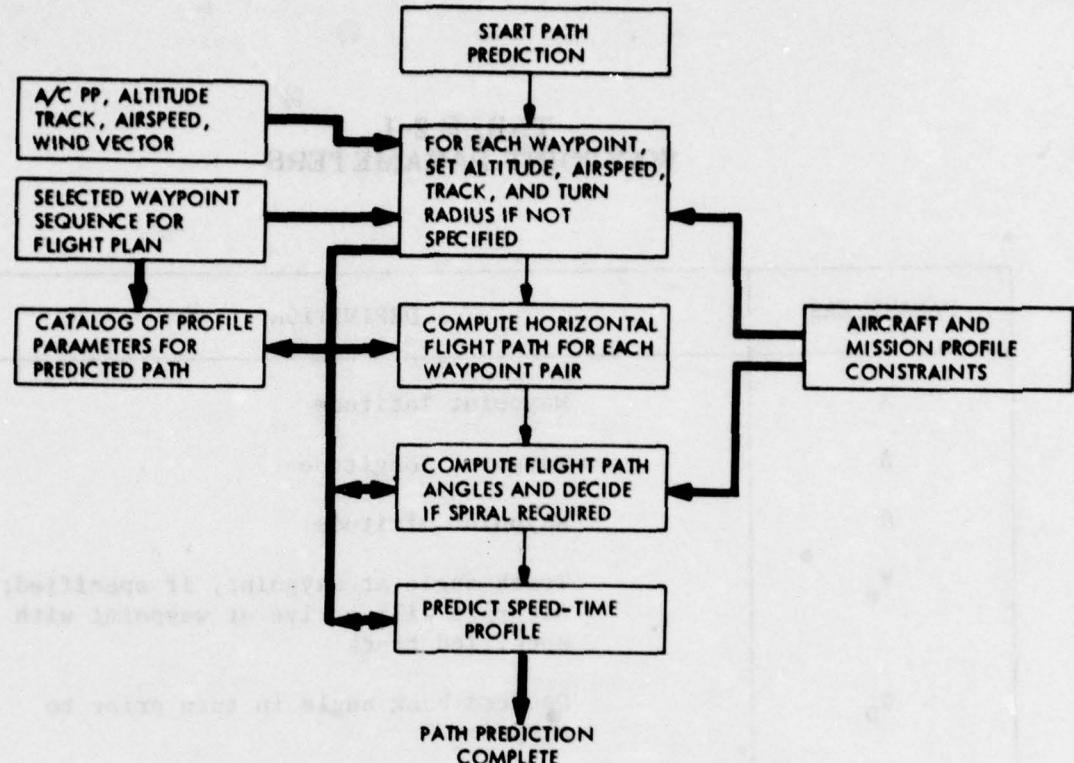
To conclude this part of the study program, Section 2.6 discusses suggested improvements in both the 4-D profile synthesis and control law techniques. These suggestions result from observing the behavior of the techniques during the concept demonstrations and performance evaluation.

## 2.2 4-D PROFILE SYNTHESIS

In general, the 4-D profile synthesizer considers the conditions specified for each pair of waypoints (in proper order) and, with this information, establishes the horizontal reference path, speed profile, and altitude profile. The profile synthesizer also accounts for aircraft flight domain limitations, such as vertical flight path angle, acceleration, and bank angle.

Figure 2-1 is flow diagram for the profile synthesizer showing the sequence of operations that are executed whenever profile syntheses is required. The figure shows that the process of synthesizing the profile involves the following four sets of parameters:

- a. The flight plan's waypoint sequence;
- b. The catalog of profile parameters, which consist of the specified parameters from the plan's waypoint sequence and all the other computed parameters that define the synthesized profile;



**PROFILE SYNTHESIZER FLOW DIAGRAM**  
**FIGURE 2-1**

- c. The current aircraft position, altitude, track angle, and airspeed provided by the 4-D INCADS navigation system
- d. Aerodynamic and mission parameters constraining the 3-D trajectory and speed profile.

The thick lines in Figure 2-1 represent the transfer of the profile parameters and waypoint data to and from the processing blocks.

The processing blocks of the profile synthesizer are described in the following sections.

#### **2.2.1 Assignment of Missing Waypoint Data**

The waypoint parameters which can be specified by the pilot are given in Table 2-I. It is not necessary that all parameters be defined for each waypoint; however, to generate the 3-D trajectory and time schedule, the profile synthesizer will assign values to undefined parameters.

**TABLE 2-I**  
**WAYPOINT PARAMETERS**

PARAMETERS	DEFINITION
$\lambda$	Waypoint latitude
$\Lambda$	Waypoint longitude
$H$	Waypoint altitude
$\psi_e$	Track angle at waypoint, if specified; Aircraft will arrive at waypoint with specified track
$\phi_d$	Desired bank angle in turn prior to waypoint
$R_d$	Desired turn radius for turn prior to waypoint (specified turn radius will override specified bank angle)
$v_A$	Airspeed at waypoint
TOA <sub>d</sub>	Desired time of arrival at waypoint
$\gamma_d$	Flight path angle to be used for achieving specified altitude, H
$ w_{Ei} , w_{Ei}$	Wind components (magnitude and direction) Flaps position Landing gear position Spoilers position

When the altitude ( $H_i$ ) of a waypoint is not specified, the altitude of the previous waypoint ( $H_{i-1}$ ) is assigned to that waypoint. When the desired airspeed ( $V_{A_i}$ ) is not specified at a waypoint, the airspeed at the previous waypoint ( $V_{A_{i-1}}$ ) is assigned to that waypoint. When the values for flaps, spoilers, or landing gear are not specified, the cleanest configuration is assigned for that waypoint. When the desired vertical flight path angle ( $\gamma_{D_i}$ ) is unspecified for a waypoint, a constant flight path angle is calculated as indicated in Section 2.2.3. When the desired bank angle ( $\phi_D$ ) is not specified for a waypoint,  $22.5^\circ$  is assigned to  $\phi_D$  for that waypoint. When the desired radius of turn ( $R_D$ ) is specified at a waypoint, this radius is used by the profile generator and  $\phi_D$  is ignored. When the desired radius of turn is not specified,  $\phi_D$  is used with the ground speed at the waypoint to produce the turn radius.

The aircraft's present location and airspeed are assigned to the initial waypoint, which by definition occurs prior to the first selected waypoint in the flight plan.

### **2.2.2 Horizontal Trajectory Synthesis**

The development of the horizontal trajectory synthesis technique considered the desirability of the following criteria:

- "Nearly optimal" path in the sense of shortest path length and hence shortest time for a given velocity.
- The number of aircraft (A/C) maneuvers required to fly the selected trajectory should be a minimum.
- The trajectories and their solutions should lend themselves to modification either under computer program control or by the pilot and resulting in a minimum amount of aircraft maneuvers.
- The trajectories should lend themselves to allowing the solution of the time schedule and altitude aspects of 4-D profile.
- The computation of any straight line and curved line distances forming the trajectory should not be unduly complicated.
- The trajectories selected should result in obvious aircraft maneuvers.

- The trajectories and quantities defining them should lend themselves to digital mechanization and computation. Quoting Ref. [8]: "The principal requirement is to construct a flyable three-dimensional trajectory that begins at the current aircraft position, heading, speed and altitude, and that terminates at a prescribed position, heading, speed, altitude and time."

There are basically three situations from which horizontal trajectory requirements may be synthesized:

- a. To fly to a waypoint and arrive with a specified bearing.
- b. To fly to a directed line in space such as a radial to a VOR or a RNAV waypoint.
- c. To fly to a waypoint with no constraint on the arrival heading.

To effect a unique solution to the horizontal synthesis problem, the criterion chosen was the minimization of the path length of the trajectory connecting the waypoints and satisfying the conditions of (a) through (c) just mentioned. A further constraint is that the bank angle be limited to some maximum value, which is equivalent to specifying that the minimum turn radius, as a function of velocity, be used for all curved portions of the trajectory. Of the three cases given, the analysis for case (a) is considerably more involved and its solution is representative of the other two. Consequently, a few general comments about cases (a) will be made at this point.

Ref. [9] derives the optimal paths for the horizontal guidance problem. The essential results may be put into two cases:

1. When the initial and final points are separated by more than four turning radii, the profiles need contain only a straight line segment with a partial turn of minimum turning radius at each end.
2. If the initial and final points are separated by less than four turning radii, the optimum profiles may contain up to three partial turns of minimum turning radius.

For reasons of geometric and control simplicity, Ref. [8] and the scheme chosen for the 4-D INCADS neglects the optimal requirements of three partial turns for the "less than four turn radii" situation and reduces this situation to a "sub-optimal" case by applying the partial turn-straight path-partial turn solution of case (a). Note that the solution is sub-optimal

only in those situations in which the waypoints in question are separated by less than four turning radii, a situation which will be true a small percentage of the time. While this simplification results in a path solution longer than optimal, the trajectory is more easily determined both mathematically and mentally, and the aircraft guidance and control requirements become less stringent.

By the last statement it is meant that because of aircraft control dynamic lags, etc., the uncertainty (or error) in performing a large number of small partial turns will be greater than those accumulated performing a fewer number of larger partial turns. Maneuver segments requiring longer relative time to perform also afford more time to apply corrective action to the flight control system for reducing guidance errors.

The switching diagrams and the equations defining these horizontal trajectories are described in Ref. [8] and were the basis of the 4-D INCADS horizontal trajectory synthesizer.

The work described in Ref. [8] is somewhat restrictive in that the radius of the initial and final turns of the trajectory are assumed to be of minimum turn radius and equal i. e., no allowance is made for velocity changes between the beginning and end of the profile which would result in the initial minimum turn radius differing from the final turn radius. Solution of the time schedule aspects of the 4-D profile synthesis problem result in velocity changes during the course of the profile and a resulting change in the final turn radius. Therefore, the following additional capabilities have been added to the work of Ref. [8]:

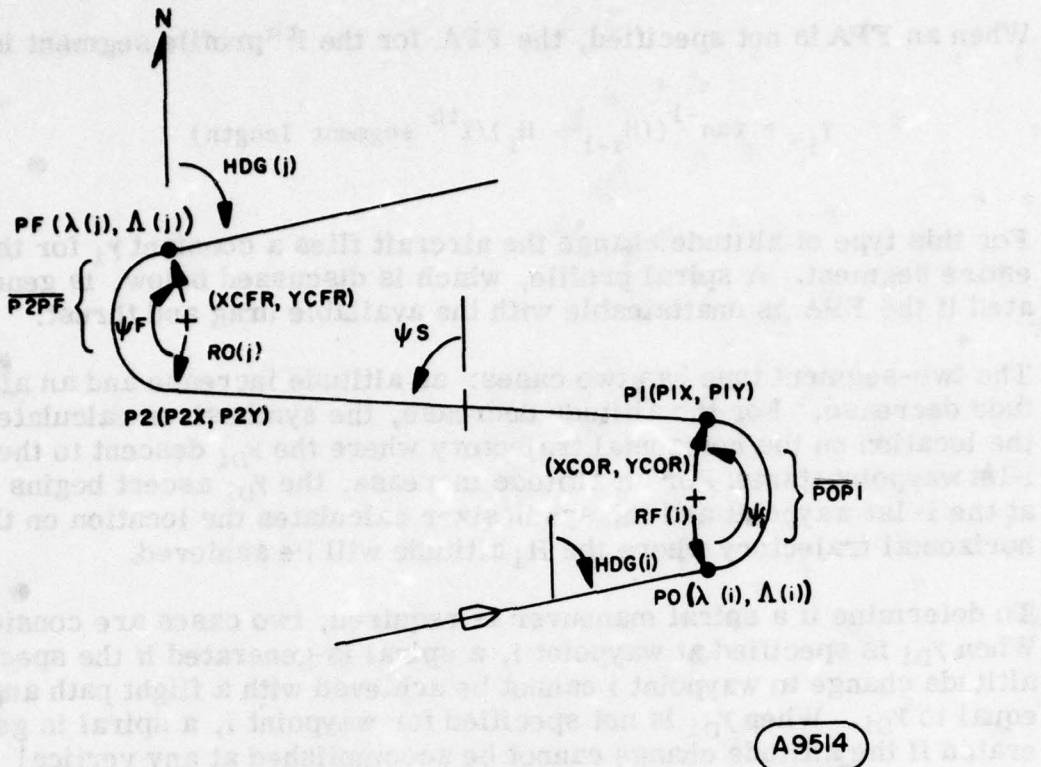
- a. Initial and final turn radii need not be equal, except when two waypoints are separated by less than 4 times the larger of the turn radii.
- b. Initial and final turn radii may be specified by the pilot as part of the parameter list in Table 2-I describing each waypoint.

The horizontal synthesizer operates on the waypoint parameters of latitude, longitude, track angle, and turn radius. The parameters that are computed to define the horizontal path between the  $i^{\text{th}}$  and  $j^{\text{th}}$  waypoints (where  $i = j-1$ ) are given in Table 2-II and shown in Figure 2-2. These parameters, which define the path from the  $j$ -1st to  $j^{\text{th}}$  waypoint, are assigned as data for the  $j^{\text{th}}$  waypoint.

Algorithms to handle all three areas (a, b, and c) of the horizontal trajectory synthesizer were developed during the program; however, only the most difficult case, case a, is mechanized in the system simulator. This requires that the pilot specify the desired aircraft track at each waypoint.

**TABLE 2-II**  
**PARAMETERS DEFINING THE HORIZONTAL**  
**PATH BETWEEN TWO WAYPOINTS**

PARAMETER	DEFINITION
$\psi_i$	Circular arc length of initial turn
$\psi_s$	Heading of straight segment length between nav points
$\psi_f$	Circular arc length of final turn
P1X	X coordinate of tangency point of initial turn circle
P1Y	Y coordinate of tangency point of initial turn circle
P2X	X coordinate of tangency point on final turn circle
P2Y	Y coordinate of tangency point on final turn circle
XCOR	X coordinate of center of initial turn circle
YCOR	Y coordinate of center of initial turn circle
XCFR	X coordinate of center of final turn circle
YCFR	Y coordinate of center of final turn circle
LS	Length of straight portion of profile
L	Length of total profile
POP1	Length of initial curved path
P2PF	Length of final curved path



A9514

### HORIZONTAL PATH BETWEEN WAYPOINTS AND DEFINING PARAMETERS

FIGURE 2-2

#### 2.2.3 Altitude Changes: Constant Flight Path Angle or Spiral Altitude Vertical Trajectories

For an altitude change between the  $i-1$  and  $i^{\text{th}}$  waypoint i.e.,  $H_i = H_{i-1}$ , the synthesizer has three different types of vertical paths:

- A constant vertical flight path angle (FPA), maintained between the two waypoints, when  $\gamma_{Di}$  is not specified.
- A two-segment trajectory consisting of a zero FPA segment and a segment with a FPA of  $\gamma_{Di}$ , when  $\gamma_{Di}$  is specified.
- A spiral descent or ascent, whenever aerodynamic constraints or a pilot-inserted  $\gamma_{Di}$  eliminates the use of the first two types of vertical paths for achieving the altitude change.

When an FPA is not specified, the FPA for the  $i^{\text{th}}$  profile segment is

$$\gamma_i = \tan^{-1}((H_{i-1} - H_i)/i^{\text{th}} \text{ segment length})$$

For this type of altitude change the aircraft flies a constant  $\gamma_i$  for the entire segment. A spiral profile, which is discussed below, is generated if the FPA is unattainable with the available drag and thrust.

The two-segment type has two cases: an altitude increase and an altitude decrease. For the altitude decrease, the synthesizer calculates the location on the horizontal trajectory where the  $\gamma_{Di}$  descent to the  $i$ -1st waypoint starts. For an altitude increase, the  $\gamma_{Di}$  ascent begins at the  $i$ -1st waypoint and the synthesizer calculates the location on the horizontal trajectory where the  $H_i$  altitude will be achieved.

To determine if a spiral maneuver is required, two cases are considered. When  $\gamma_{Di}$  is specified at waypoint  $i$ , a spiral is generated if the specified altitude change to waypoint  $i$  cannot be achieved with a flight path angle equal to  $\gamma_{Di}$ . When  $\gamma_{Di}$  is not specified for waypoint  $i$ , a spiral is generated if the altitude change cannot be accomplished at any vertical flight path angle between the maximum and minimum flight path angle constraints ( $\gamma_{Mi}, \gamma_{Ni}$ ).

The flight path angle constraints are calculated for each waypoint using the maximum available thrust ( $T_m$ ), the predicted drag ( $D_i$ ), the mass of the airplane ( $M$ ), and the acceleration due to gravity ( $g$ ).

The predicted drag ( $D_i$ ) is calculated for each waypoint based on curves fit to the C-141 aerodynamic characteristics at several airspeeds, flap settings, and altitudes. Landing gear and spoilers are modeled as equivalent flat plate drag.

#### 2.2.4 Time Schedule Prediction

The essential information used by the time schedule synthesizer is the ground speeds at each waypoint, the curved and straight trajectory segment lengths, all pilot-selected time-of-arrival (TOA<sub>d</sub>) data, and the available acceleration and deceleration values. The available acceleration and deceleration values are determined from the predicted drag ( $D_i$ ), available thrust ( $T_m$ ), and computed vertical flight path angle ( $\gamma_i$ ).

For the case when no TOAs are specified, the synthesizer computes an average speed profile based on the ground speeds at each waypoint and

turn. The synthesizer uses this speed profile to calculate the time-of-arrivals (TOAs) at each waypoint. This allows the pilot to vary his airspeed and change the predicted TOAs at any waypoint prior to engaging the synthesized profile as the active profile for the 4-D INCADS control law.

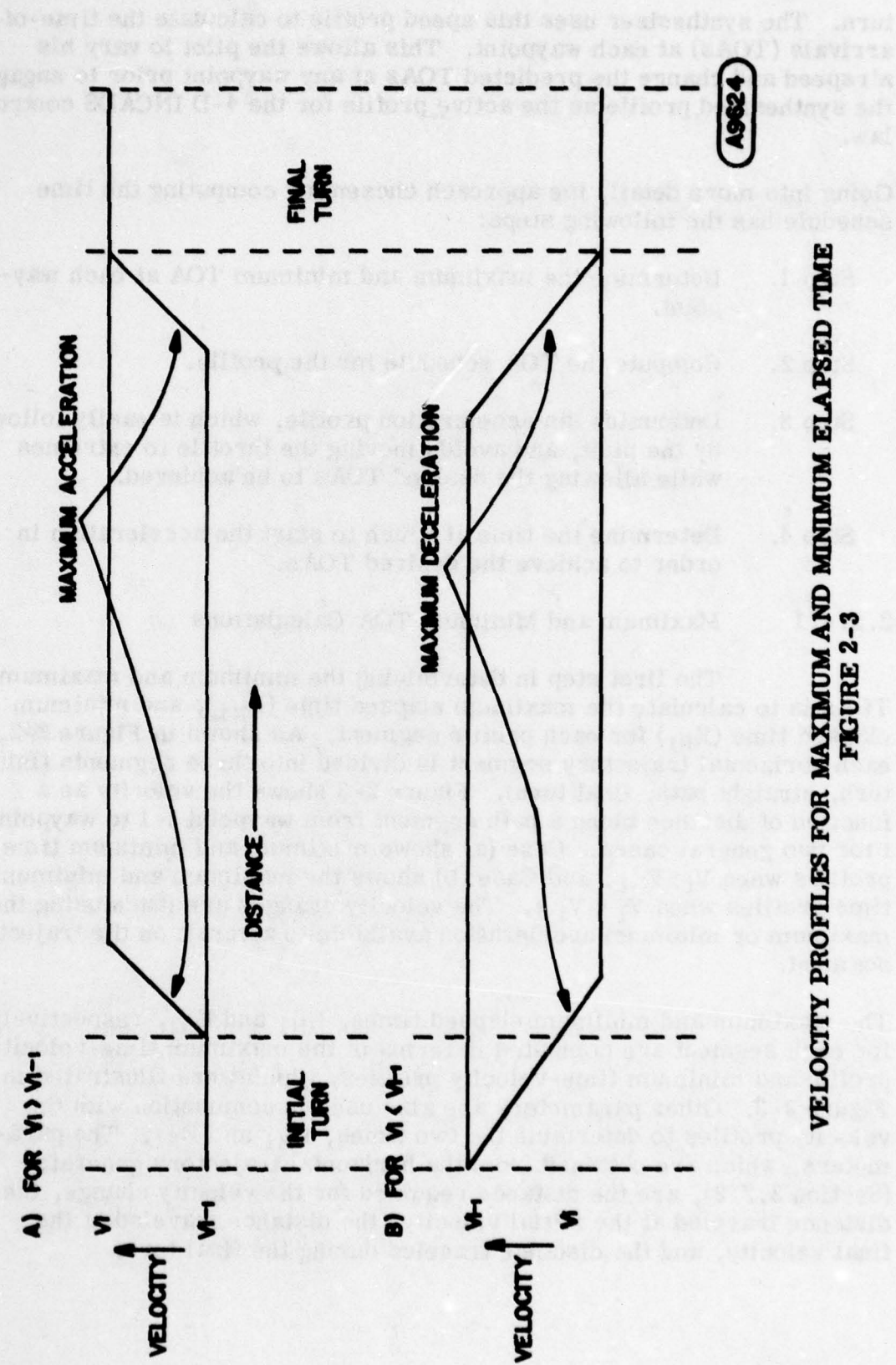
Going into more detail, the approach chosen for computing the time schedule has the following steps:

- Step 1. Determine the maximum and minimum TOA at each waypoint.
- Step 2. Compute the TOA schedule for the profile.
- Step 3. Determine an acceleration profile, which is easily followed by the pilot, and avoids moving the throttle to extremes while allowing the desired TOAs to be achieved.
- Step 4. Determine the time at which to start the acceleration in order to achieve the desired TOAs.

#### 2.2.4.1 Maximum and Minimum TOA Calculations

The first step in determining the minimum and maximum TOAs is to calculate the maximum elapsed time ( $E_{Mi}$ ), and minimum elapsed time ( $E_{Ni}$ ) for each profile segment. As shown in Figure 2-2, each horizontal trajectory segment is divided into three segments (initial turn, straight path, final turn). Figure 2-3 shows the velocity as a function of distance along a path segment from waypoint  $i-1$  to waypoint  $i$  for two general cases. Case (a) shows maximum and minimum time profiles when  $V_i > V_{i-1}$ ; and Case (b) shows the maximum and minimum time profiles when  $V_i < V_{i-1}$ . The velocity changes are made using the maximum or minimum acceleration available to aircraft on the trajectory segment.

The maximum and minimum elapsed times,  $E_{Mi}$  and  $E_{Ni}$ , respectively for each segment are computed in terms of the maximum time-velocity profile and minimum time-velocity profiles, which were illustrated in Figure 2-3. Other parameters are also used in conjunction with the velocity profiles to determine the two times,  $E_{Mi}$  and  $E_{Ni}$ . The parameters, which are obtained from the horizontal trajectory generator (Section 2.2.2), are the distance required for the velocity change, the distance traveled at the initial velocity, the distance traveled at the final velocity, and the distance traveled during the final turn.



VELOCITY PROFILES FOR MAXIMUM AND MINIMUM ELAPSED TIME  
FIGURE 2-3

To establish the maximum and minimum TOAs at each waypoint of the 4-D profile, the maximum and minimum elapsed times for the segments making up the profile are summed. To begin, the maximum and minimum TOAs for the first waypoint, which is the current aircraft location, are set to the current time. At the waypoints where a TOA is specified by the pilot, the maximum and minimum TOAs are set to the specified TOA. The maximum and minimum TOAs at the remaining waypoints are calculated sequentially as follows:

$$t_{\max,i} = t_{\max,i-1} + E_{Mi}$$

$$t_{\min,i} = t_{\min,i-1} + E_{Ni}$$

#### 2.2.4.2 Time Schedule Calculation

To compute the time of arrival for those waypoints that are not assigned TOAs, the synthesizer selects a TOA that lies between the minimum and maximum arrival times. The computation of time of arrival sequence begins at the last waypoint, denoted the  $N^{\text{th}}$  waypoint, where the time of arrival is defined as

$$t_{p,N} = \begin{cases} \text{TOA}_{dN} & \text{if } \text{TOA}_d \text{ is given} \\ \frac{1}{2} (t_{\max,N} + t_{\min,N}) & \text{if the TOA is not specified} \end{cases}$$

The remainder of the TOA sequence is calculated by iterating backwards through the waypoint sequence and calculating the TOAs with

$$t_{p,i} = \begin{cases} \text{TOA}_{di} & \text{if TOA is specified for } i^{\text{th}} \text{ waypoint} \\ t_{\min,i} + \frac{(t_{p,i+1} - t_{\min,i+1})}{(t_{\max,i+1} - t_{\min,i+1})} (t_{\max,i} - t_{\min,i}) & \text{if } i^{\text{th}} \text{ TOA is unspecified} \end{cases}$$

The  $N$  computed TOAs  $\{t_{p,1}, \dots, t_{p,N}\}$  make up the 4-D profile's time sequence.

#### **2.2.4.3 Acceleration Profile Considerations**

One of the goals of the 4-D INCADS is to fly the synthesized time schedule with a minimum increase in pilot workload. When the pilot is controlling throttles manually, minimum pilot workload means a minimum number of changes in the throttle position. The general case where both time of arrival and velocity are specified at a waypoint, and an altitude change is needed during the path segment, requires a minimum of two throttle position changes. It was assumed that extreme throttle movements were undesirable; therefore, when generating the velocity profile that corresponds to the time schedule, the 4-D INCADS synthesizer uses the maximum acceleration or deceleration only when a maximum or minimum time of arrival is required at the next waypoint. Also, the assumption was made that the velocity profile during an acceleration segment should approximate the velocity change caused by one natural movement of the throttle from one fixed position to another fixed position.

#### **2.2.4.4 Calculation of Time to Start Acceleration Profile**

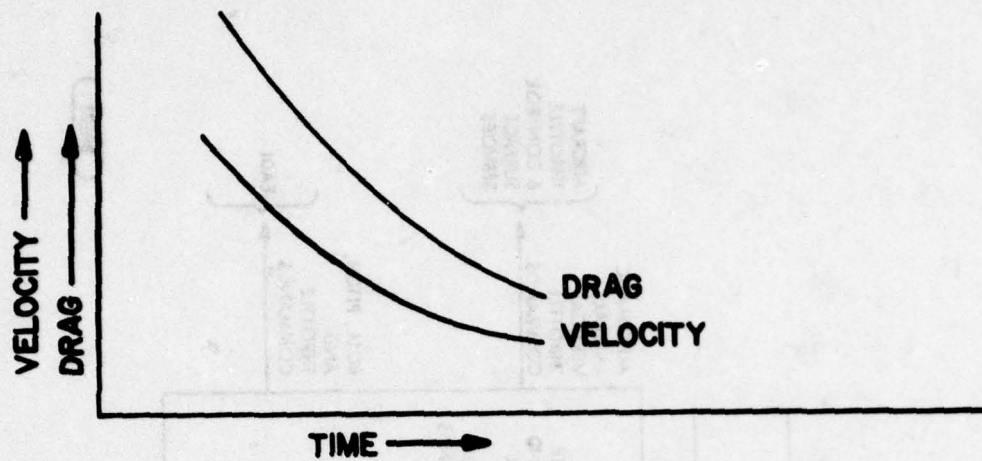
Figure 2-4 shows velocity and drag as a function of time for deceleration at constant throttle for three characteristic airspeeds. For the simulation a velocity profile similar to the curve in Figure 2-4.A was used to calculate the time required and distance covered during the acceleration segment. The time at which the acceleration must start to achieve the calculated TOA at the next waypoint is calculated from:

- a. The length of the initial turn,
- b. The length of the straight segment,
- c. The length of the final turn,
- d. The distance covered during the acceleration segment,
- e. The ground speed at waypoint  $i-1$ ,
- f. The ground speed at the end of the initial turn,
- g. The ground speed at the beginning of the final turn,
- h. The ground speed at waypoint  $i$ ,
- i. The time required for the acceleration segment,
- j. The calculated TOA at waypoint  $i-1$ , and
- k. The calculated TOA at waypoint  $i$ .

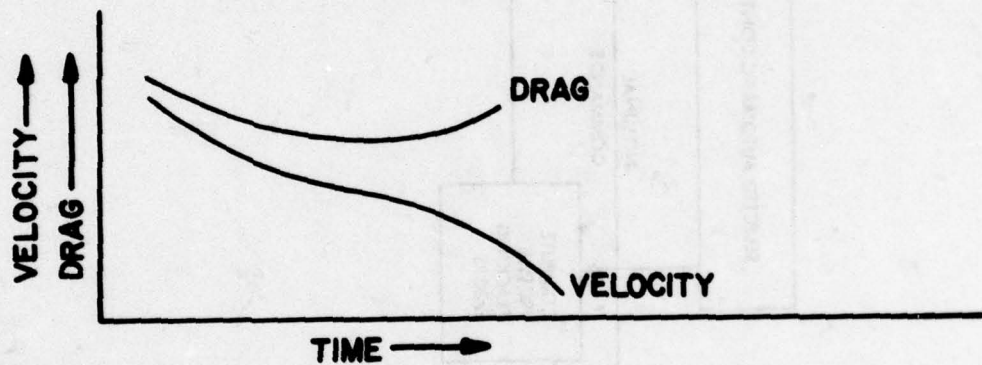
### **2.3 4-D CONTROL LAW**

The 4-D control law needed for automatic and manual control of an aircraft when flying a 4-D profile has been developed and implemented in the system simulation. Figure 2-5 is the functional block diagram of the 4-D INCADS control law.

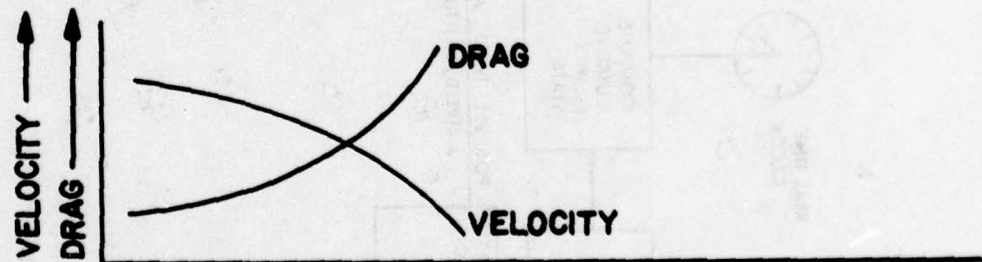
A) AT HIGH AIRSPEEDS



B) AT LOW AIRSPEEDS



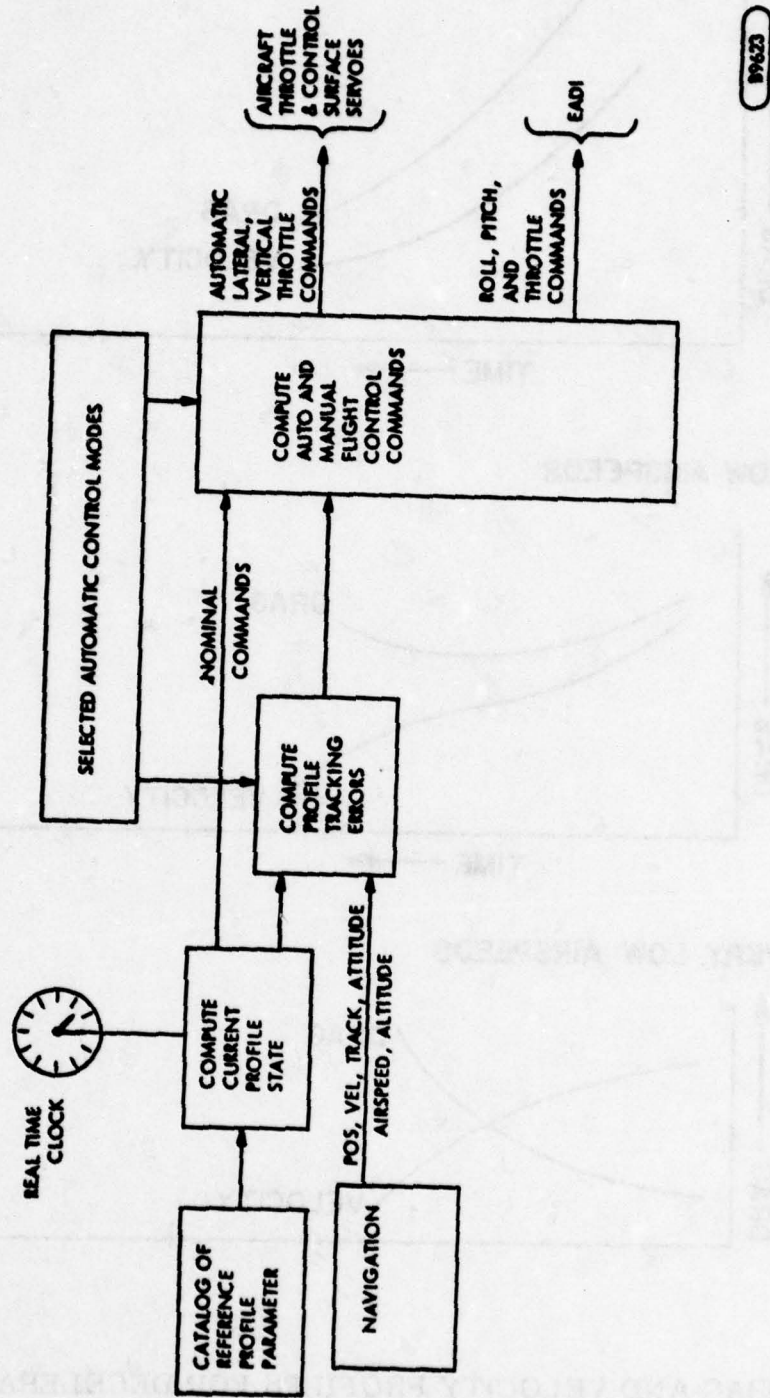
C) AT VERY LOW AIRSPEEDS



A9621

DRAG AND VELOCITY PROFILES FOR DECELERATION  
AT CONSTANT THROTTLE  
FIGURE 2-4

4-D INCADS CONTROL LAW FUNCTIONAL BLOCK DIAGRAM  
FIGURE 2-5



In general, the control law has the following parts: the 4-D INCADS navigation system provides current solutions for the aircraft state (position, velocity, track, and attitude) which are differenced with the current values of the reference profile parameters to form profile tracking errors. These error quantities are mixed with appropriate weighting factors and added to the nominal control surface and throttle commands to generate aircraft command signals. The nominal commands are needed for aircraft speed changes, altitude changes, and turns.

Depending on which control mode is selected, control commands are computed either for automatic control of the aircraft, where the commands are inputs to the aircraft's flight control servoes and to the EADI for display, or for manual control where commands are calculated for display on the EADI to allow the pilot to manually fly the aircraft along the reference profile.

For the system simulation, the following control law modes were mechanized:

- Full automatic control
- Full manual control
- Partial automatic control (manual throttle control, or manual roll and pitch control)

In full automatic mode, the control law computes pitch, roll, and throttle commands. The pitch and roll commands are input to a model of the C-141 Automatic Flight Control System and the throttle command is applied to a servo that positions the cockpit's throttle. The simulated flight control system positions the aircraft's elevator and aileron in response to the control law's pitch and roll commands. (The flight control system simulation uses a yaw damper for rudder control.)

In the fully manual mode, roll, pitch, and throttle commands are generated for presentation on the Electronic Attitude Direction Indicator (EADI) to allow the pilot to fly the 4-D profile. The automatic commands are not supplied to the aircraft in the manual mode.

In the partially automatic mode, the pilot selects the aircraft control variables that will be controlled automatically by the 4-D INCADS. By engaging only the throttle servo, the 4-D control law automatically controls the throttle while the pilot flies the roll and pitch commands on the EADI. By engaging only the automatic switch on the pilot's control stick, the 4-D control law, in conjunction with flight control model,

automatically controls the elevator and aileron displacements while the pilot moves the throttle in response to the throttle command on the EADI. For the fully automatic mode, discussed above, both the throttle servo and the automatic switch on the control stick are engaged.

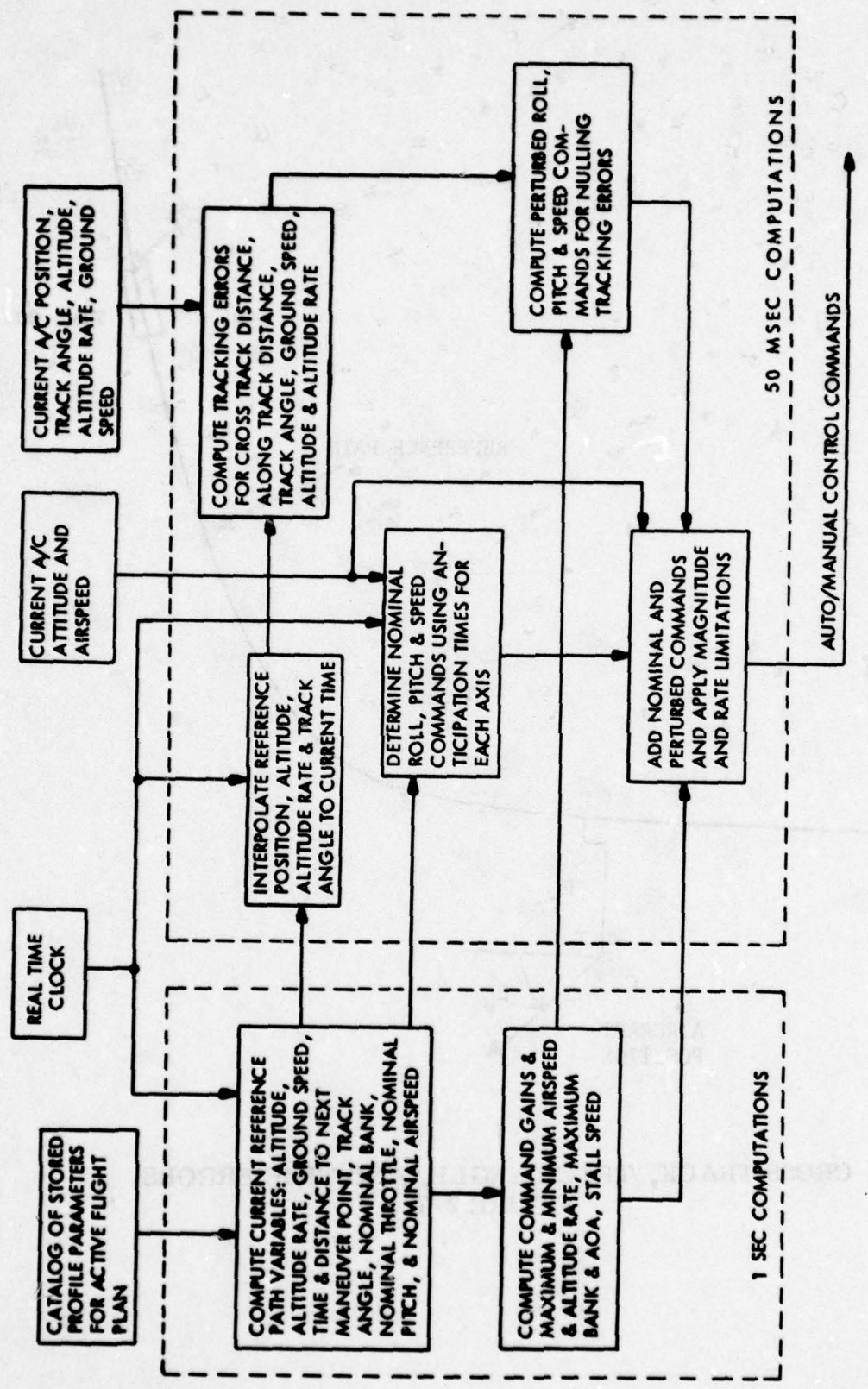
The pilot can supply manual aircraft control inputs during the full automatic control mode by means of a control wheel steering (CWS) capability where the pilot manually applies momentary corrections to the aircraft's flight path. If, during the fully automatic mode, the pilot engages CWS (by pushing a button on the control stick), the control stick displacements for the pitch and roll axes are applied as inputs to the flight control system model.

Figure 2-6 is a block diagram of the 4-D control law that has been programmed on the hybrid simulator and has been simulated using the 6-degree-of-freedom aircraft simulation, automatic Flight Control System and autothrottle models, the 4-D profile synthesizer, and pilots during man-in-the-loop operations.

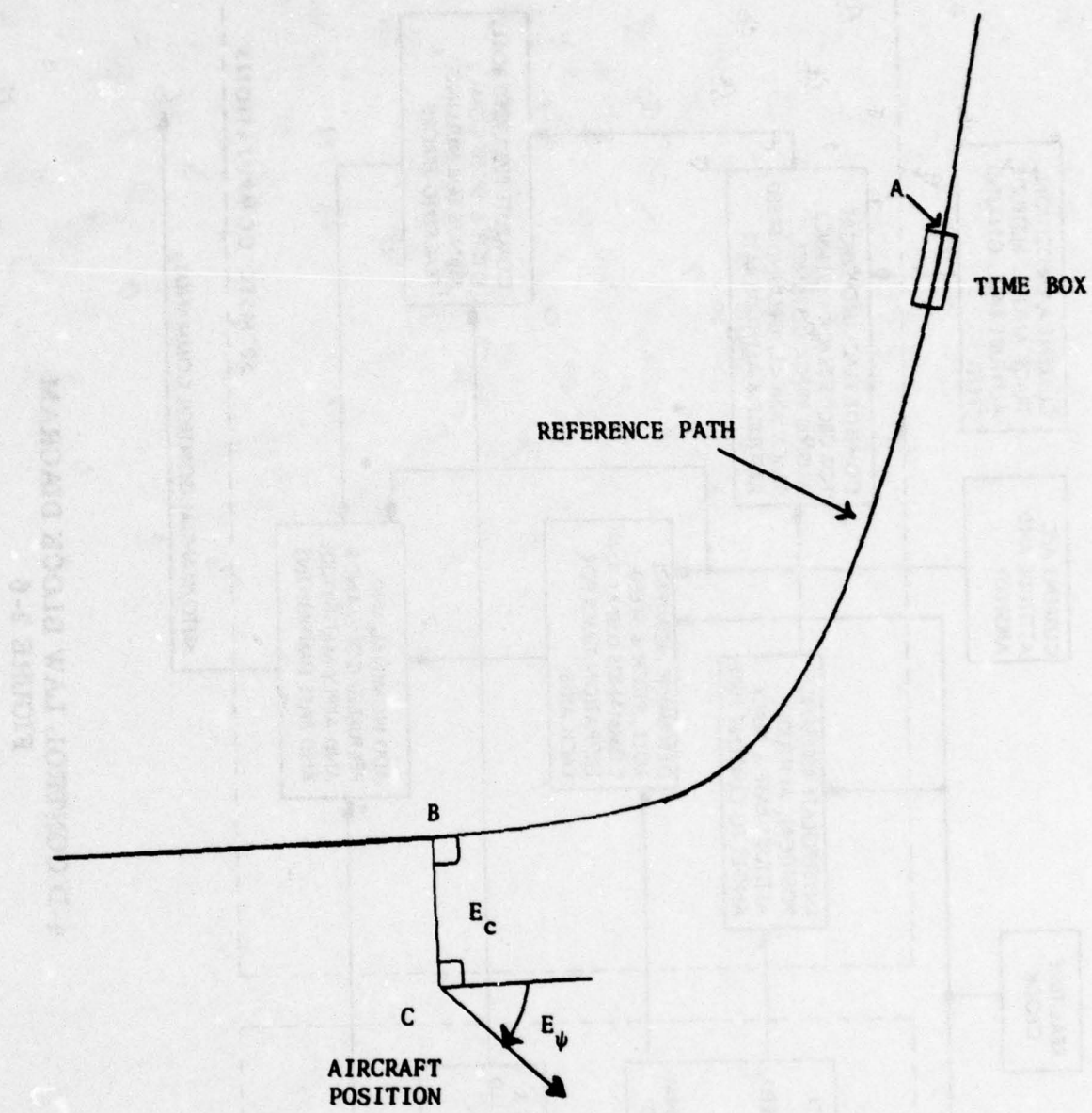
The 4-D control law, which has computations at two rates, once every second and once every 50 milliseconds, processes current aircraft position, velocity and track variables, and uses a real-time clock to determine from the set of parameters defining the 4-D reference profile the current state of the reference profile. The reference profile parameters calculated by the profile synthesizer are discussed above in Section 2.2. The following three sections describe the parts of the control law shown in Figure 2-6.

### 2.3.1 Computation of Reference Profiles Variables

This part of the control law determines the north position, east position, altitude, flight path angle, track angle, and ground speed on the reference profile for any desired time from the beginning time to the time of arrival at the last waypoint. The values of the reference profile variables are required to calculate the tracking errors and parameters for display of the profile on the situation display and status display. The situation display, Figure 3-8, requires the values of the reference profile variables for the current time, the current time plus 30 seconds, the current time plus 60 seconds, and the current time plus 90 seconds. The tracking error calculations require the values of the reference path variables for the current time and for point B of Figure 2-7. (See Section 2.3.2 for the definition of point B.) The exact values for the reference path variables are computed once each second; however, interpolation is used to determine values for these variables every 50 milliseconds.



69443



**CROSS TRACK, TRACK ANGLE, AND TIME ERRORS**  
**FIGURE 2-7**

### **2.3.2 Time Error and Tracking Error Calculations**

Cross-track error ( $E_C$ ), track-angle error ( $E_\phi$ ), and the time error ( $E_T$ ) are three error variables that define the displacement in the horizontal plane between the current aircraft position and the current reference aircraft position. Figure 2-7 defines the cross-track, track-angle, and time error variables. Point A is the reference aircraft position at the current time  $t$  (referred to as the time box), point C is the aircraft position at time  $t$ , and point B lies on the reference profile and on a line that is perpendicular to the profile and intersects the aircraft position. The time error ( $E_T$ ) equals the time it would take for the aircraft to travel from point B to the time box when flying along the path at the computed speed profile. The time error and point B location are recursively computed once each second using a predictor/corrector technique. This technique uses the speed profile to predict point B location every second and corrects this prediction with the along-track component of the aircraft to point B displacement vector.

The time error and cross track error were defined in the manner established above so that the control law is always flying the aircraft to the closest point (point B) on the profile. This technique causes the aircraft to follow the curved profile, when errors are present, preventing the control law from flying the aircraft on a direct line to the time box.

There are three other tracking error variables calculated for the control law. The altitude error ( $E_H$ ) is the reference path altitude at point B minus the aircraft altitude. The ground speed error ( $E_S$ ) is reference speed at point B minus the aircraft ground speed. The flight path angle error ( $E_Y$ ) is the reference flight path angle minus the aircraft flight path angle. These errors and the cross-track error and track-angle error are calculated every 50 milliseconds.

### **2.3.3 Auto/Manual Control Command Calculations**

The control laws transform the tracking errors and nominal commands into pitch ( $\theta_C$ ), roll ( $\phi_C$ ) and throttle ( $S_C$ ) commands. These commands are displayed on the EADI for manual mode tracking. When the full automatic mode is selected, these commands are combined in the automatic flight control system model with pitch, pitch rate, bank angle, roll rate, and dynamic pressure ( $q$ ) to drive the elevators, ailerons, and the throttle servo.

The 4-D control law looks ahead on the reference path and anticipates when an aircraft maneuver is required. Individual anticipation times for the roll, pitch, and throttle commands determine when a maneuver on

the reference path is sufficiently close to require a change in the nominal command. The throttle command has two different anticipation times for manual and automatic control modes.

The gains for the 4-D control law are calculated based on the tracking errors, the aircraft altitude, the aircraft configuration, airspeed, weight, and constraints. The roll, pitch and throttle commands are calculated as follows:

$$\phi_C = \phi_N + G_C E_C + G_\psi E_\psi$$

$$\theta_C = \theta_N + G_{\theta T} E_T + G_{\theta S} E_S + G_{\theta H} E_H + G_{\theta Y} E_Y$$

$$S_C = S_N + G_{ST} E_T + G_{SS} E_S + G_{SH} E_H + G_{SY} E_Y$$

where  $\phi_N$ ,  $\theta_N$ , and  $S_N$  are the nominal commands developed from the reference profile parameters. The above commands are modified when they exceed certain limits. These constraints are discussed below in Section 2.3.3.3. The next two subsections discuss the gains in the pitch, roll and throttle commands.

### 2.3.3.1 Lateral Channel - Roll Command Gains

The cross-track gain ( $G_C$ ) is calculated as a function of altitude, with the gain higher at lower altitudes. This gives a smoother ride and lower pilot workload at high altitudes where cross-track errors are less critical.

The track-angle error gain ( $G_\psi$ ) is computed three different ways depending on the aircraft distance from the profile, and the minimum radius of turn ( $R_M$ ) at the current aircraft ground speed. ( $R_M$  is the radius of the circular capture trajectory that corresponds to the maximum bank angle.) First, when the cross-track error ( $E_C$ ) is greater than  $2R_M$ , the gain  $G_\psi$  is set to return the aircraft back to the reference part as soon as possible. This is accomplished by calculating  $G_\psi$  to produce a zero bank command ( $\phi_C = 0$ ) when the track angle error is  $90^\circ$ . Second, when the cross-track error is between  $2R_M$  and  $0.2R_M$ ,  $G_\psi$  is calculated to produce maximum bank when maximum bank is required to prevent overshooting the desired profile. Third, if the cross-track error is less than  $0.2R_M$ ,  $G_\psi$  is a function of ground speed and is calculated in conjunction with  $G_C$  to minimize cross-track error.

### 2.3.3.2 Longitudinal Channel - Throttle/Pitch Command Gains

In determining the gains to the pitch (elevator) channel and the throttle channel several approaches were considered.

The first approach was to set  $G_{SH}$ ,  $G_{Sy}$ ,  $G_{\theta T}$ , and  $G_{\theta S}$  to zero. This approach has the advantage that altitude information is presented on the horizontal pointer of the EADI and speed information is presented on what is normally called the speed error pointer of the EADI. Pilots are already familiar with this form of presentation. It has the disadvantage that if altitude errors occur at slow air speeds, a pitch up can cause aircraft stall.

The second approach was to set  $G_{\theta H}$ ,  $G_{\theta Y}$ ,  $G_{ST}$ , and  $G_{SS}$  to zero. This approach has the advantage that it recovers quickly from any disturbance to the nominal flight conditions. The disadvantage of this approach is that the control of altitude, which is a critical parameter in the approach situation, is limited by the rate that energy can be put into or taken out of the system. Maintaining very tight control of flight path angle with this approach results in excessive throttle activity.

The previous two approaches identify the need for cross coupling between the pitch and throttle commands. For responding to altitude and FPA errors, the ideal  $G_{\theta H}$  and  $G_{\theta Y}$  gains should be based on the lift necessary to control altitude and flight path angles while  $G_{SH}$  and  $G_{Sy}$  should be determined to assure that pitch changes needed for altitude and flight path angle corrections do not disturb the ground speed of the aircraft. For speed error and time corrections, it is desirable for the calculation of  $G_{SS}$  and  $G_{ST}$  to be based on the acceleration desired to control the speed of the airplane, with the  $G_{\theta S}$  and  $G_{\theta T}$  computed to assure that the change in the dynamic pressure, caused by speed control, does not create altitude errors.

For the 4-D control law, pitch and throttle gain calculations implemented in the system simulation are an approximation to the ideal approach for correcting altitude and FPA errors, and approximately divide the control authority equally between throttle and pitch for correcting speed and time errors. To implement this approach the ratio of the pitch and throttle gains for each error variable are set equal to the ratio of the steady-state force in the X direction caused by a

change in pitch, at constant airspeed, to a force in the X direction due to a change in throttle. This gain relationship is

$$\frac{G_{\theta H}}{G_{SH}} = \frac{G_{\theta Y}}{G_{SY}} = \frac{G_{\theta T}}{G_{ST}} = \frac{G_{\theta S}}{G_{SS}} = \frac{Mg}{T_M}$$

where

M is the aircraft mass

g is the acceleration of gravity

$T_M$  is the maximum engine thrust

The altitude error to throttle command gain ( $G_{SH}$ ) is computed to put energy into the system at a rate equal to  $Mgh$  where  $h$  is the desired altitude correction rate. For large altitude errors, the altitude correction rate is limited to 10 feet per second. The FPA error to pitch command ( $G_{\theta Y}$ ) is a constant that allows stable operation without excessive throttle activity. The speed error to throttle gain ( $G_{SS}$ ) is chosen to reduce throttle activity by assuring that any energy contained in the altitude error will be used to correct the speed error. The time error to throttle command gain ( $G_{ST}$ ) is set to give the desired time error performance at the final approach waypoint. For large time errors  $G_{ST}$  is chosen to assure that the control law produces ground speeds no greater than 20% above or below the predicted ground speed.

#### 2.3.3.3 Control Law Command Constraints

Some limits are applied to the commands calculated above to make sure that large error conditions do not cause the control law to apply unsafe commands to the aircraft. The following is a list of the command limits.

- a. When the quantity  $G_{\theta S} E_S + G_{\theta T} E_T$  is greater than 0.01 radians, the pitch command is

$$\theta_C = \theta_N + G_{\theta H} E_H + G_{\theta Y} E_Y + 0.01$$

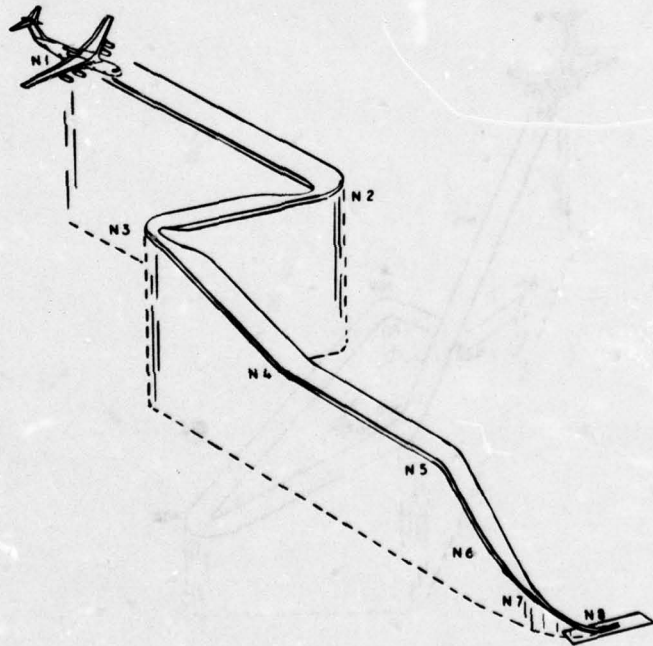
- b. When the quantity  $G_{\theta S} E_S + G_{\theta T} E_T$  is less than -0.01 radians, pitch command is

$$\theta_C = \theta_N + G_{\theta H} E_H + G_{\theta Y} E_Y - 0.01$$

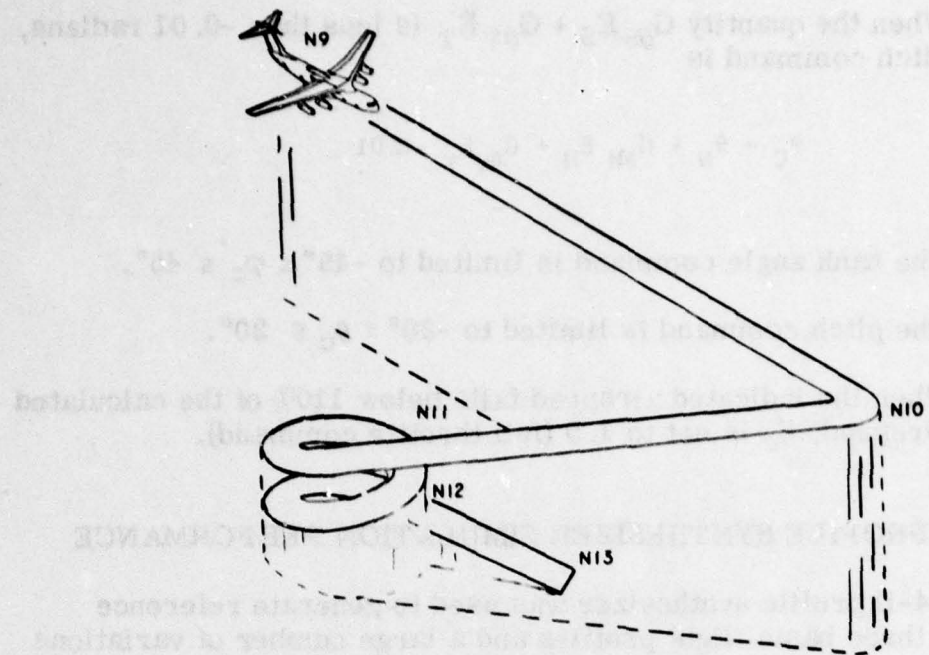
- c. The bank angle command is limited to  $-45^\circ \leq \phi_C \leq 45^\circ$ .
- d. The pitch command is limited to  $-20^\circ \leq \theta_C \leq 20^\circ$ .
- e. When the indicated airspeed falls below 110% of the calculated airspeed,  $S_C$  is set to 1.0 (full throttle command).

## 2.4 4-D PROFILE SYNTHESIZER SIMULATION PERFORMANCE

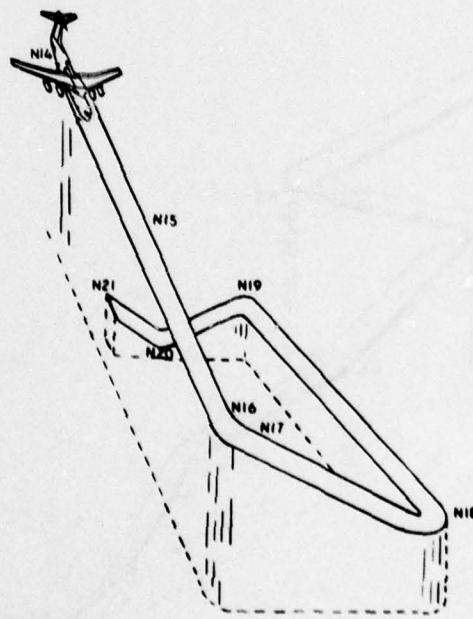
The 4-D profile synthesizer was used to generate reference profiles for three basic flight profiles and a large number of variations on these three basic flight plans. The three profiles and all the variations were synthesized in real time on the digital computer in the 4-D INCADS system simulator. Figures 2-8, 2-9 and 2-10 are illustrations of the basic flight profiles. Tables 2-III and 2-IV show the computed start and end times for profiles 1 and 2.



**PROFILE #1**  
**FIGURE 2-8**



**PROFILE #2**  
**FIGURE 2-9**



**PROFILE #3**  
**FIGURE 2-10**

**TABLE 2-III**  
**PREDICTED TIMES FOR MANEUVERS ON FLIGHT PLAN #1**

Arrive at waypoint #2	60 Sec
Start first turn	
End of first turn	110 Sec
Start of second turn	170 Sec
End of second turn	220 Sec
Arrive at waypoint #3	
Start descent to waypoint #4	
End of $1^{\circ}$ descent	355 Sec
Arrive at waypoint #4	
Start first deceleration	392 Sec
End of first deceleration segment	515 Sec
Arrive at waypoint #5	553 Sec
Start $6^{\circ}$ descent to waypoint #6	567 Sec
Change FPA to $5.3^{\circ}$	620 Sec
Arrive at waypoint #6	
Start third turn	
End of third turn	635 Sec
Start of second deceleration segment	
End of second deceleration segment	670 Sec
Arrive at waypoint #7	682 Sec
Change FPA to $\approx 3^{\circ}$	
Start third deceleration	703 Sec
End third deceleration	740 Sec
Arrive at 1/2 mile from touchdown	744 Sec
Arrive at waypoint #8	755 Sec

**TABLE 2-IV**  
**PREDICTED MANEUVER TIMES FOR FLIGHT PLAN #2**

MANEUVER	PREDICTED TIME
Arrive at waypoint #10	180 Sec
Start first turn	180 Sec
Start first deceleration	260 Sec
End of first turn	301 Sec
Start 10° penetration descent	327 Sec
End of first deceleration	392 Sec
End 10° penetration descent	432 Sec
Arrive at waypoint #11	432 Sec
Start second deceleration	444 Sec
End second deceleration	508 Sec
Start spiral	514 Sec
Start -4° spiral descent	594 Sec
Arrive at waypoint #12	932 Sec
End spiral descent	932 Sec
Start descent to touchdown ≈3.8°	932 Sec
Start third deceleration	953 Sec
End third deceleration	1020 Sec
Arrive at $\frac{1}{2}$ mile from touchdown	1024 Sec
Arrive at waypoint #13	1036 Sec

Profile 1 (Figure 2-8) is referred to as the Low Altitude Combat profile. The profile starts at 5000 feet and 232 knots indicated airspeed (250 knots true airspeed). After a short straight segment, the profile has two turns of approximately  $90^\circ$ , followed by a descent to 4000 feet with no specified flight path angle at waypoint 4. Between waypoints 4 and 5, the airplane slows from 250 knots to 170 knots to arrive at waypoint 5 at the specified arrival time. The descent to waypoint 6 is started at the position determined by the profile synthesizer for the specified flight path angle of  $-6^\circ$ . A turn of  $45^\circ$ , descent to 1000 feet, and deceleration to 148 knots are accomplished between waypoints 6 and 7. Waypoint 7 begins the final approach to waypoint 8, which is 25 feet altitude. The profile is generated with time of arrivals specified at waypoints 5 and 8.

Flight profile 2 (Figure 2-9) is referred to as the High Altitude Descent flight profile. The principal attributes of this profile are a penetration descent at a specified flight path angle of  $-10^\circ$  from 20,000 feet to 10,000 feet, and a spiral descent generated by the profile synthesizer at a specified flight angle of  $-4^\circ$  from 10,000 feet to 1000 feet.

Flight profile 3 (Figure 2-10) was synthesized primarily to acquaint pilots with the capabilities and characteristics of the 4-D INCADS. The profile has several segments which allow the pilot to exercise the control axes individually. Control activity on this profile reaches a peak when the pilot is instructed to lower the landing gear and change the flap position while in a descending, decelerating turn. It is not expected that this maneuver is representative of any practical situation. However, a pilot who can execute this maneuver smoothly should be sufficiently familiar with the 4-D control law technique to fly flight profile 1 and 2 with confidence.

Real-time modifications of the three primary profiles were routinely performed in the system simulator. Waypoints were moved to positions determined arbitrarily by the pilot while controlling the 4-D INCADS in the simulator cockpit. The new positions for these waypoints were indicated to the profile synthesizer either by the position of the cross hairs on the situation display or by latitude and longitude specified via the keyboard. The desired altitude, airspeed, track angle, flight path angle, and airplane configuration were all modified independently via keyboard inputs. The profile synthesizer successfully calculated horizontal paths for all flight profiles tested. Altitude and velocity profiles were successfully synthesized for all flight profiles when the flight path angles, velocity changes, and desired TOAs were achievable within the limits specified.

## 2.5 CONTROL LAW PERFORMANCE

A large number of simulated flights were made in manual and full automatic mode. Data taken during six of these flights is presented in this section. All flights for which data is presented were made with simulated wind shear conditions. The simulated wind had an 85 feet per second magnitude at 20,000 feet and decreased linearly to zero at sea level.

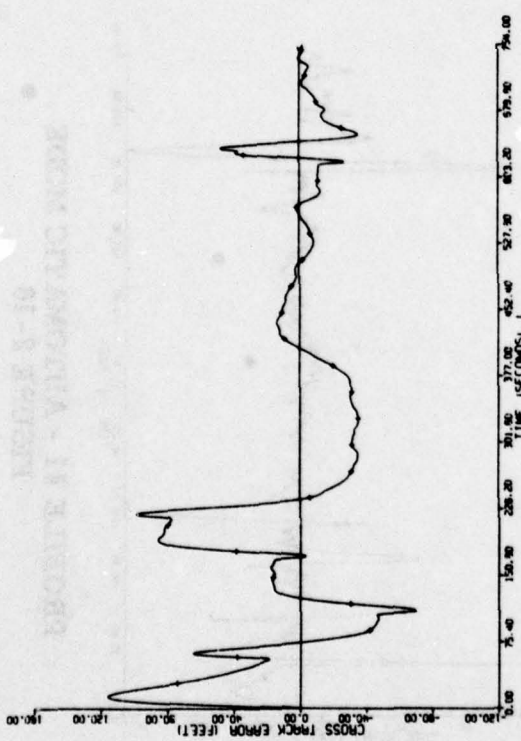
Automatic 4-D control law performance is presented in Figures 2-11 through 2-18 for flight profile #1 and Figures 2-19 through 2-26 for flight profile #2. The performance data, which shows how the 4-D control law guided the aircraft along the 3-D trajectory according to the computed time schedule, consists of cross-track error, altitude error, time error, FPA error, speed error, and track angle error. Also included are two plots showing the horizontal and vertical portions of the profile. The crosses on each plot occur every 30 seconds.

Data was collected for profiles #1 and #2 when the aircraft was under manual control. Two pilots flew both flight profiles 1 and 2. Both pilots are former Air Force pilots and each had four to six hours practice in the system simulator before the test flights were made. Pilot #1 has approximately 2,000 hours of flight time in a KC-135, 500 hours in a C-5A, 1,500 hours in a T-33, 600 hours in a T-38, 300 hours in a F-100, and 100 hours in a F-104. Pilot #2 has approximately 1,960 hours of flight time in a B-52, 120 hours in a T-37, and 120 hours in a T-33. Figures 2-27 through 2-32 show pilot #1's performance on profiles 1 and 2.

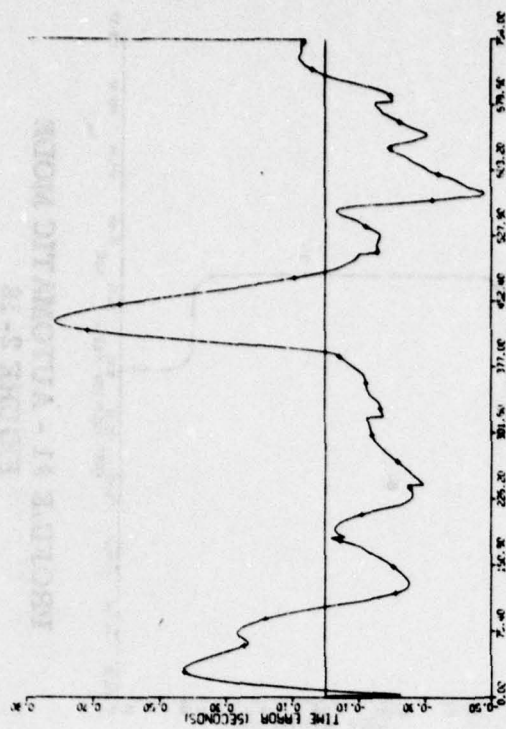
The tracking performance is analyzed in the next two sections. First, the control law accuracy in the final approach part of the profile is discussed, then an explanation is given for a few transient errors that occurred on the two profiles.

### 2.5.1 Final Approach Performance

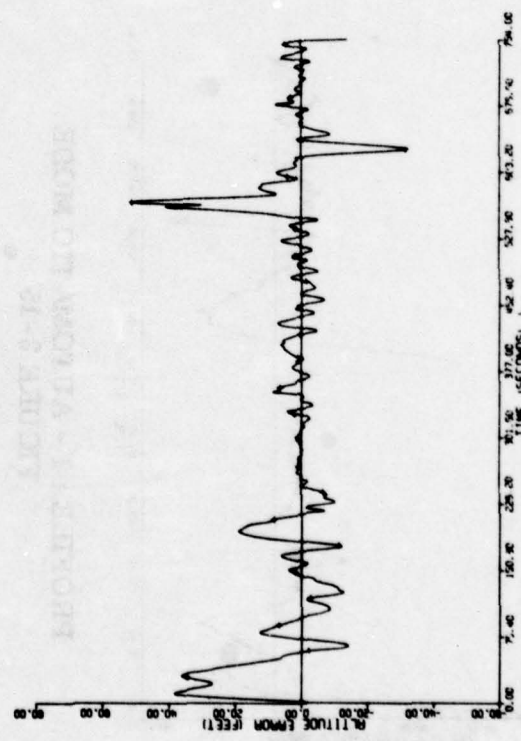
During the study emphasis was placed on the 4-D control law performance during the final approach portion of the profiles since it establishes how close in to the airfield curved 3-D trajectories with specified time schedules can be flown safely under IFR conditions.



PROFILE #1 - AUTOMATIC MODE  
FIGURE 2-11



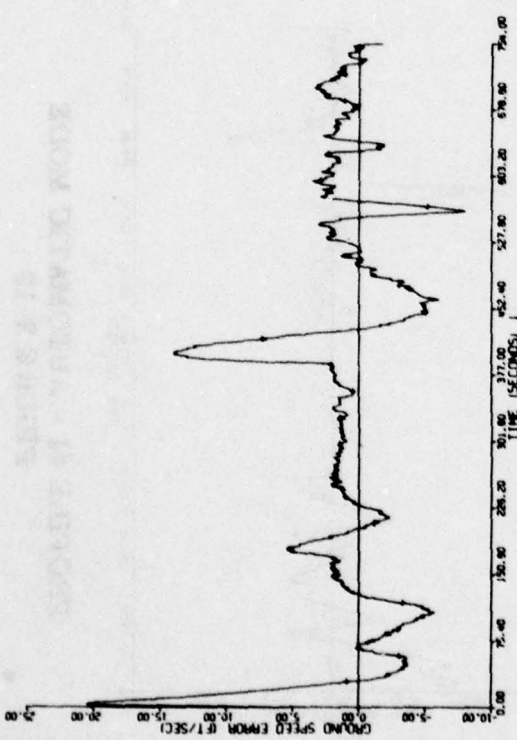
PROFILE #1 - AUTOMATIC MODE  
FIGURE 2-13



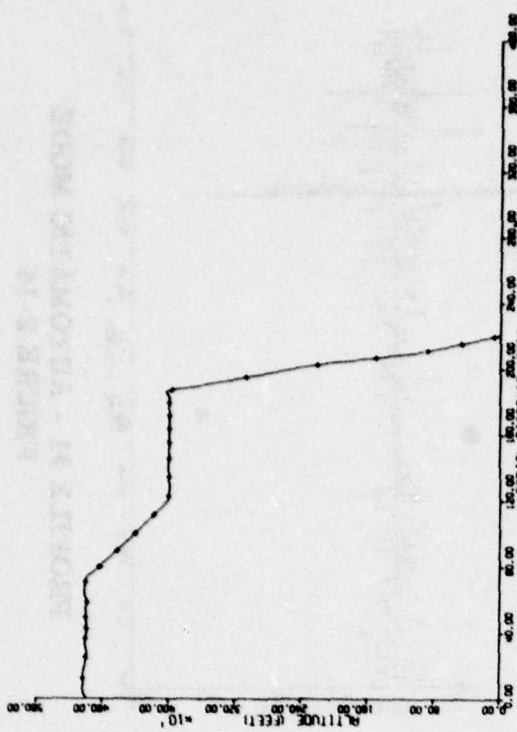
PROFILE #1 - AUTOMATIC MODE  
FIGURE 2-12



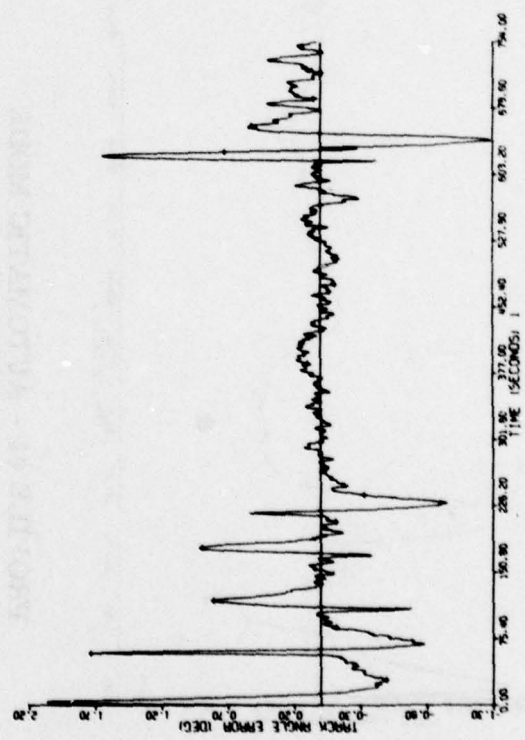
PROFILE #1 - AUTOMATIC MODE  
FIGURE 2-14



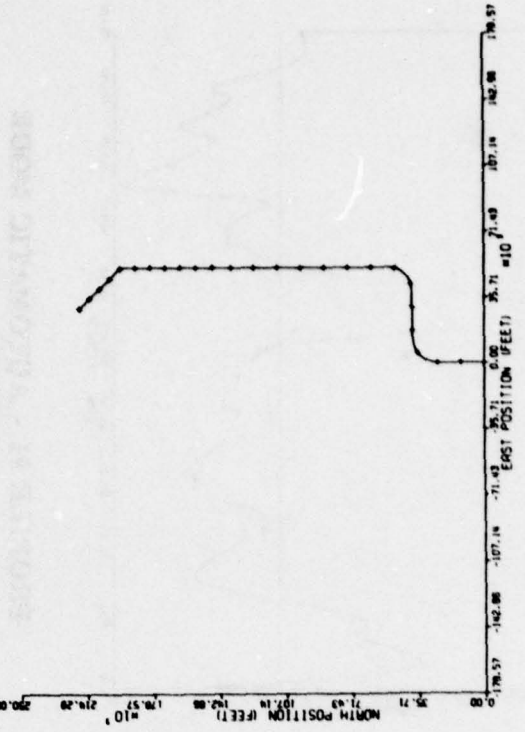
**PROFILE #1 - AUTOMATIC MODE**  
**FIGURE 2-15**



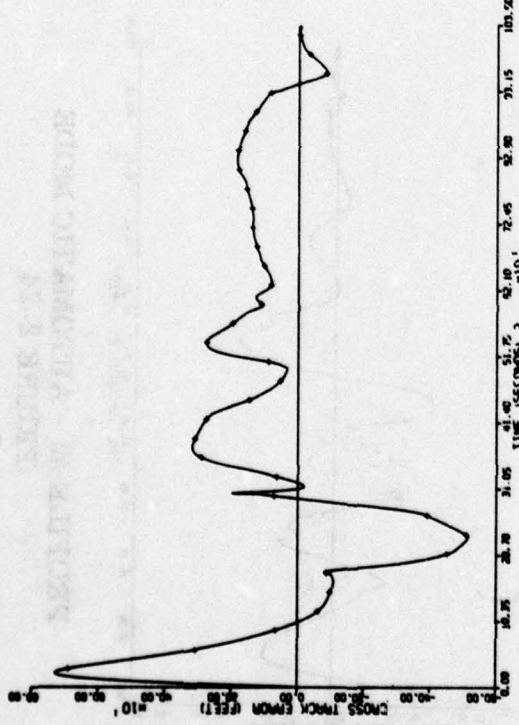
**PROFILE #1 - AUTOMATIC MODE**  
**FIGURE 2-17**



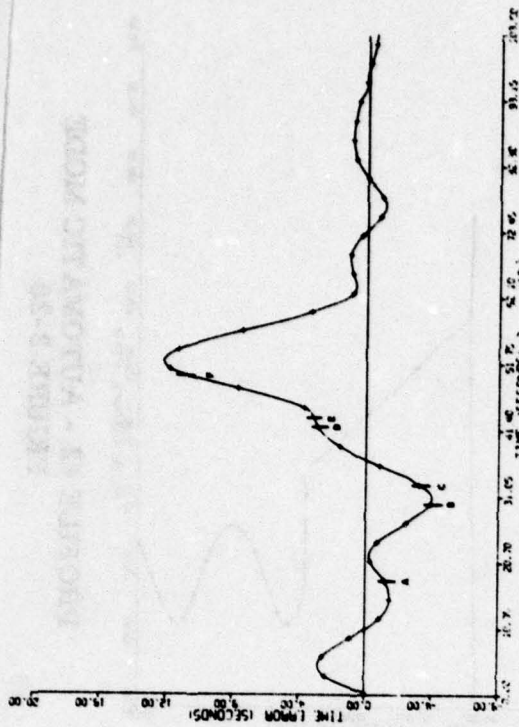
**PROFILE #1 - AUTOMATIC MODE**  
**FIGURE 2-16**



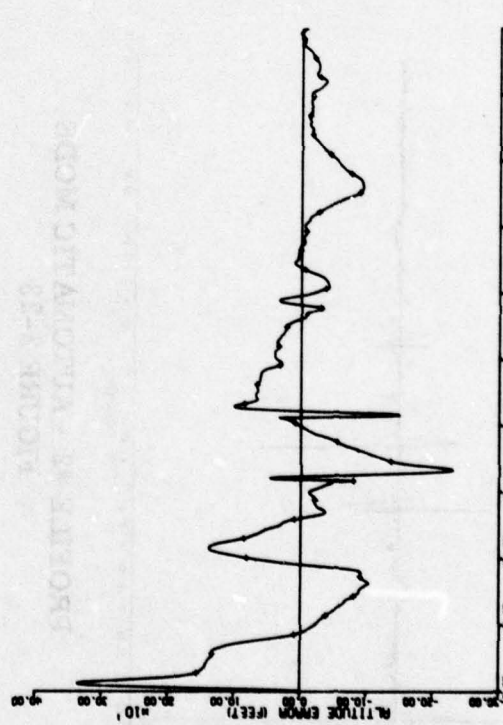
**PROFILE #1 - AUTOMATIC MODE**  
**FIGURE 2-18**



**PROFILE #2 - AUTOMATIC MODE**  
**FIGURE 2-19**

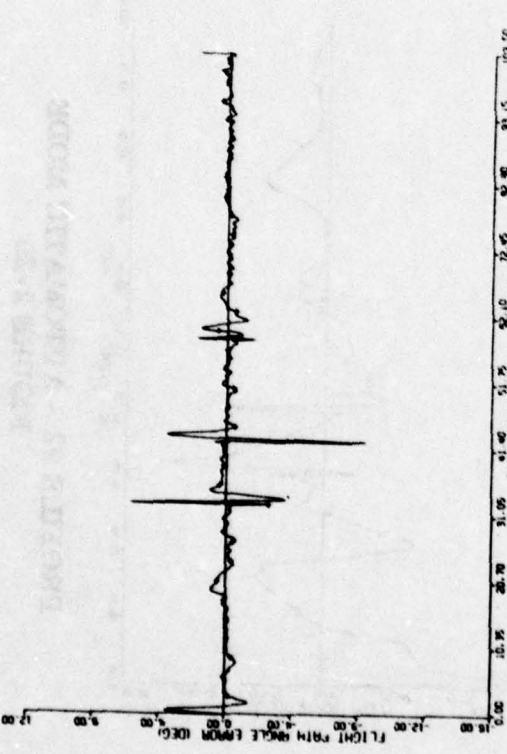


**PROFILE #2 - AUTOMATIC MODE**  
**FIGURE 2-21**

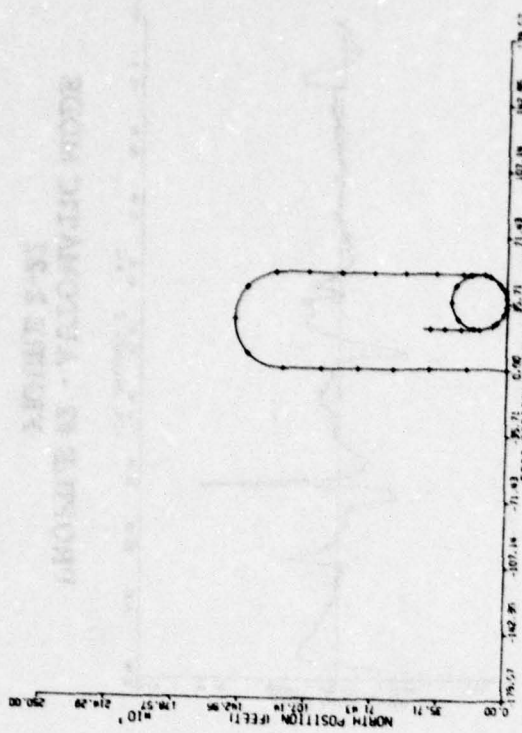


**PROFILE #2 - AUTOMATIC MODE**  
**FIGURE 2-20**

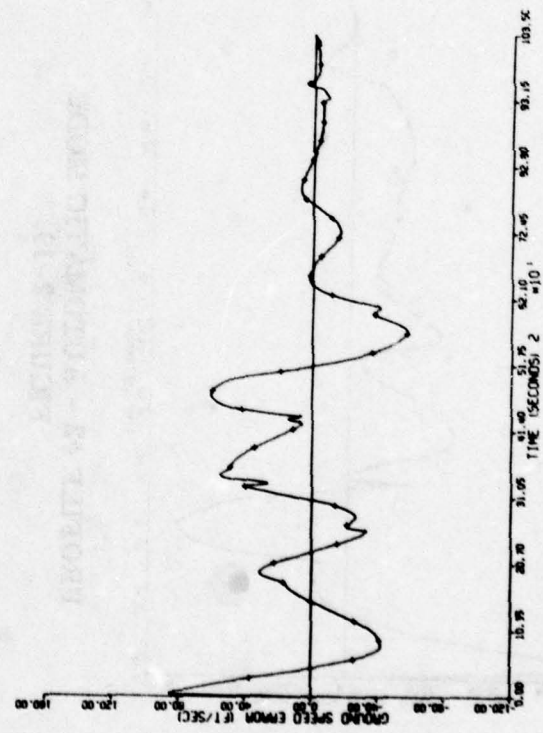
**PROFILE #2 - AUTOMATIC MODE**  
**FIGURE 2-22**



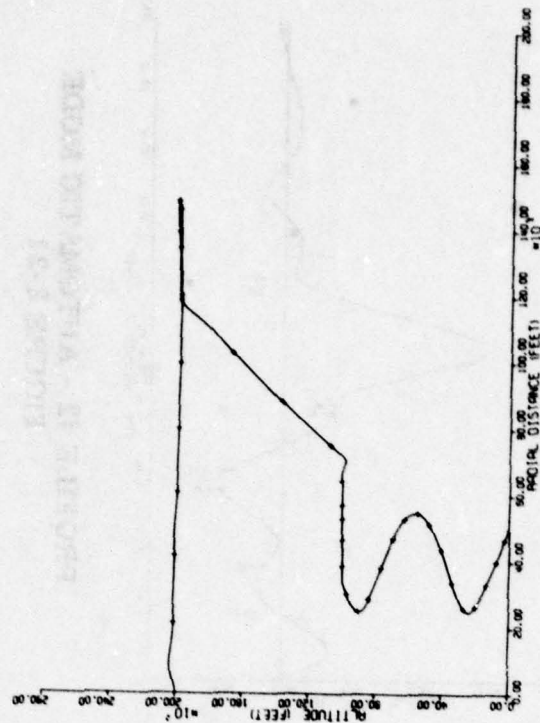
**PROFILE #2 - AUTOMATIC MODE**  
**FIGURE 2-23**



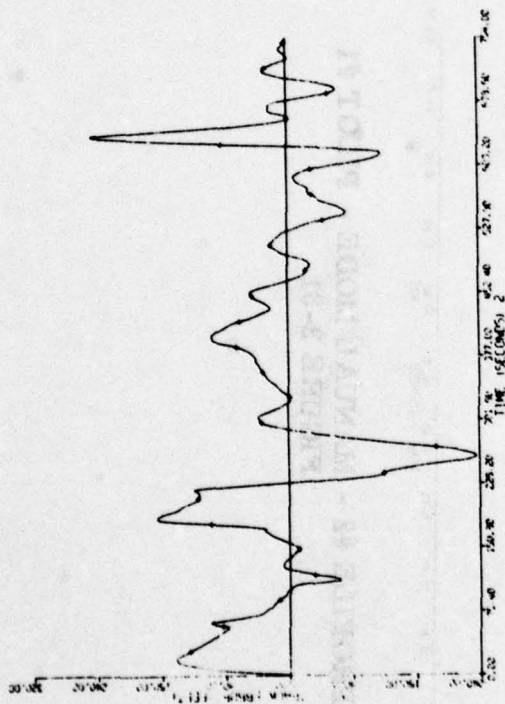
**PROFILE #2 - AUTOMATIC MODE**  
**FIGURE 2-25**



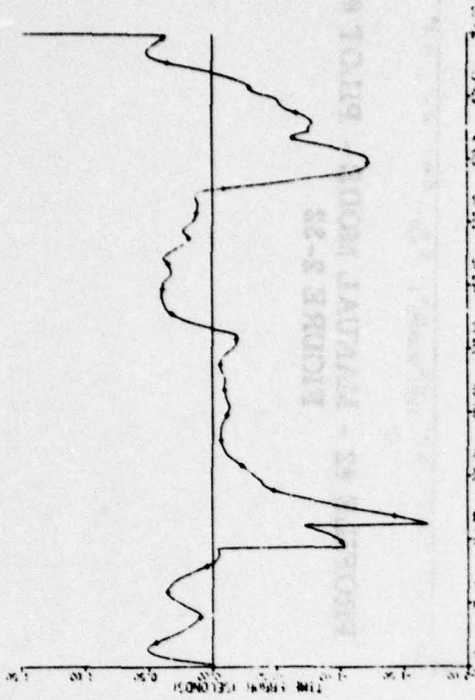
**PROFILE #2 - AUTOMATIC MODE**  
**FIGURE 2-24**



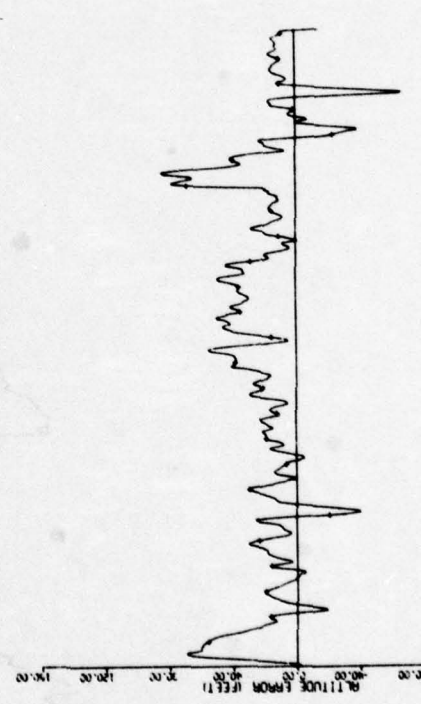
**PROFILE #2 - AUTOMATIC MODE**  
**FIGURE 2-26**



**PROFILE #1 - MANUAL MODE - PILOT #1**  
**FIGURE 2-27**



**PROFILE #1 - MANUAL MODE - PILOT #1**  
**FIGURE 2-29**

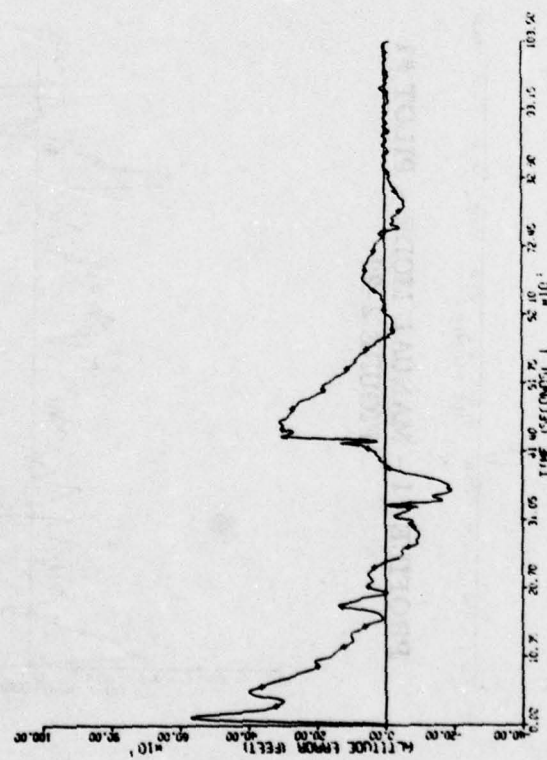


**PROFILE #1 - MANUAL MODE - PILOT #1**  
**FIGURE 2-28**



**PROFILE #2 - MANUAL MODE - PILOT #1**  
**FIGURE 2-30**

FIGURE 2-31 - ALTITUDE - PILOT MODE - PILOT #1



PROFILE #2 - MANUAL MODE - PILOT #1  
FIGURE 2-31

FIGURE 2-32 - ALTITUDE - PILOT MODE - PILOT #1



PROFILE #2 - MANUAL MODE - PILOT #1  
FIGURE 2-32

This objective was to show that the 4-D INCADS, using a radio/inertial navigation system for guidance inputs, will provide accurate aircraft control down to as close as 1/2 mile from touchdown. Sections 5 and 6 show that integrated Loran/inertial and integrated GPS/inertial navigation systems, operating in differential modes, will provide relative guidance information with the following accuracy:

Horizontal position:	75 feet ( $1\sigma$ )
Vertical position:	10 feet ( $1\sigma$ )
Horizontal velocity:	3 feet/sec ( $1\sigma$ )
Vertical velocity:	2 feet/sec ( $1\sigma$ )

The trajectory control performance also includes the effect of the 4-D control law. Table 2-V shows the control law's errors and error rates at a point 1/2 mile from touchdown for the six flights discussed above.

The data of Table 2-V shows that the control law tracking errors -- at the 1/2 mile point -- doesn't significantly increase the 4-D INCADS total profile tracking errors above the performance goals given above, with one exception. This exception has the horizontal velocity error component, the cross-track error rate, greater than the navigation system horizontal velocity goal of 3 ft/sec ( $1\sigma$ ). Because of the limited number of flights the data in Table 2-V must be treated as a preliminary assessment of the 4-D control law performance. However, by taking into consideration that an ILS beam has 230 feet width and 30 feet vertical size at 1/2 mile from the runway, the size of the navigation system plus control law errors suggests that the 4-D INCADS will reliably capture an ILS guidance beam 1/2 mile from touchdown.

### **2.5.2      Tracking Data Analysis**

The data for all test runs, both automatic and manual, exhibit similar characteristics. As the flight progresses, the average cross-track error, altitude error, and time error are reduced, and the control law response to transient disturbances becomes quicker. This is expected because the control law gains are designed to increase as the aircraft approaches touchdown.

The error plots for flight profile #2 (both automatic and manual modes), show a cross-track error bias on the order of 150 feet during the spiral descent. This bias is due to a programming error in the control law which affects the nominal bank angle during this turn. This coding error was not discovered until all test data had been collected so profile #2 data exhibited the same characteristic.

**TABLE 2-V**  
**ERRORS 1/2 MILE FROM TOUCHDOWN**

	Cross Track Error	Altitude Error	Time Error	Cross Track Rate	Altitude Rate Error	Ground Speed Error
Automatic Mode Flight Plan #1	-.3 feet	-1.2 feet	.1 sec	-.1 ft/sec	-.8 ft/sec	.69 ft/sec
Pilot #1 Manual Flight Plan #1	7.2 feet	15.2 feet	.4 sec	-1.3 ft/sec	.5 ft/sec	-2.4 ft/sec
Pilot #2 Manual Flight Plan #1	3.9 feet	6.4 feet	.6 sec	3.8 ft/sec	-1.1 ft/sec	9.7 ft/sec
Automatic Mode Flight Plan #2	-1.5 feet	-.8 feet	-.4 sec	.1 ft/sec	.8 ft/sec	-2.5 ft/sec
Pilot #1 Manual Flight Plan #2	-5.3 feet	-.2 feet	-.2 sec	-.8 ft/sec	2.2 ft/sec	-3.2 ft/sec
Pilot #2 Manual Flight Plan #2	5.7 feet	-1.5 feet	.1 sec	-5.2 ft/sec	.1 ft/sec	-13.7 ft/sec

The time error plots for flight plan #2 (both automatic and manual modes) show some significant time errors. The oscillations in the time error over the last 500 seconds of the profile are due to the fact that the profile synthesizer generates the spiral descent at nearly constant ground speed. The constant ground speed profile requires significant changes in air speed during the spiral due to the change in relative wind. This change in air speed appears as a disturbance to control law. The same effect can be seen between points A and B and between points C and D on Figure 2-21. Between points A and B the aircraft executes a 180° turn into the wind. Between points C and D the aircraft descends from 20,000 feet to 10,000 feet at a flight path angle of 10° in the presence of a significant wind sheer.

These wind effects can be reduced if the proper wind estimates are input to the profile synthesizer and to the control law. The magnitude of these errors indicate the need of further investigation in this area for accurate 4-D control.

The largest time error occurs in flight plan #2 after point E. This error results from the fact that the profile synthesizer generates the deceleration segment between points E and F based on a flaps extended aircraft configuration. The pilot, however, was instructed to extend the flaps only when the indicated airspeed dropped below 180 knots. The clean aircraft could not accomplish the deceleration without extra drag or gaining altitude. To correct this situation, the capability of the profile synthesizer can be expanded so different aircraft configurations can be assigned to different sections of each profile segment.

## 2.6 FURTHER RECOMMENDATIONS

Pilots comments indicate that the EADI commands change too rapidly during normal transitions along the flight profile. The points at which the flight plan called for a transition from level flight to a flight path angle of -6° and -10° caused particular objections. It is recommended that the normal profile be smoothed in these areas, and that rapid command transitions on the EADI be reserved for emergency situations such as collision avoidance maneuvers.

It is recommended that the profile generator not only be modified to allow configuration changes between waypoints, but also automatically compute configuration changes based on flight path angle or airspeed requirements.

The velocity profile generator at present produces velocity profiles which are consistent with the natural acceleration curve of the airplane only at airspeeds well above the airspeed for maximum lift-to-drag ratio. Throttle activity could be reduced if this algorithm were extended to include all air speeds.

The control law gains computations should be extended with particular attention being paid to the velocity and time errors and the interaction between aircraft speed and altitude.

The man-in-the-loop testing showed the desirability of displaying the reference altitude and speeds in the pilot's "T scan" (EADI, air data instruments, and situation display). The pilots were concerned when these parameters were not available when the control law was nulling out a large along-track distance error (time error). The pilots would follow

the commands (roll, pitch, and throttle) and could see on the situation display the displacement between time box and aircraft; however, they were uncomfortable because they didn't have available sufficient information (altitude and speed errors) to visualize how the control law was reducing the time error. The recommendation is to have desired speed and altitude pointers on the air data instruments which are computer driven.

### **3    INTERACTIVE CONTROL-DISPLAY (C-D) CONCEPT DEFINITION**

#### **3.1    INTRODUCTION**

The pilot is the system decision maker. He must, therefore, be given information that will enhance his decision making ability rather than burden him with endless details. The machine, in this case the 4-D INCADS, presents information which he can use in his decision process. The pilot considers the information, manipulates it as necessary to understand the impact of the decision choices available to him, and transmits his choice to the machine.

The primary emphasis of this portion of the study was focused on definition of the pilot-manager's C-D requirements. Major elements in the study were:

- To provide the basic command and control information required to fly the aircraft in the 4-D missions specified.
- To configure a C-D subsystem that would provide the basic management level information required for the pilot to make a path-changing decision. (The system's ability to generate and display information is far greater than the pilot's ability to assimilate the information so care must be exercised in selecting and formatting the information to be displayed so as to not saturate the pilot).
- To provide a rapid, efficient means by which he (the pilot) can interact with the system to:
  - a. Examine the effects of a potential path change.
  - b. Finalize a path-changing decision.
- An assessment of the compatibility of the 4-D INCADS C-D subsystem with the information requirements of the Joint Tactical Information Distribution System (JTIDS)

Constraints on the control-display definition task were that:

- The C-D configuration must utilize state-of-the-art hardware capabilities.
- Basic human factors studies were not required.

The 4-D INCADS addresses these requirements by:

- a. Configuring a C-D subsystem utilizing a combination of state-of-the-art CFE and GFE display hardware to provide the required information.
  - GFE Electronic Attitude Director Indicator - Provides pitch and roll attitude, and pitch, roll and throttle command information
  - GFE Vertical Scale Air Data Instruments - Provides altitude and air speed information
  - CFE Electronic Situation Display - Provides a graphic display of horizontal situation with respect to flight path.
  - CFE Electronic Status Display and Keyboard - Provides the means for operator interaction with the system computer.
- b. Configuring an interactive control-display operation involving multiple electronic C-D devices to provide a rapid, effective technique for inputting and reviewing path changes.
- c. Establishing the compatibility of the 4-D INCADS interactive C-D subsystem with JTIDS information and operation.
- d. Programming the 4-D INCADS C-D subsystem to demonstrate, during man-in-the-loop simulation, interactive operation for a waypoint change sequence.

Electronic CRT displays were utilized as the display media since they can be readily reprogrammed to reflect changing display requirements.

Subparagraphs of this section will explore the various elements considered in arriving at a recommended C-D configuration and will expand the reader's understanding of interactive operation by discussing a typical path change sequence.

In Section 3.2 the information requirements for a two-man flight deck complement of a tactical transport are explored with the recognition that intensive C-D integration will be required to enable the pilot and copilot to effectively complete their function as managers of a complex airborne vehicle. The need for an interactive path change concept utilizing versatile electronic displays is realized.

In Section 3.3 the conclusion is made that an EADI, an electronic situation display, a CRT status display with keyboard, and two electromechanical air data displays can provide the required flight control and navigation system information, if properly programmed.

Section 3.4 introduces the reader to the concept of the situation display and the status display working together with special controls and programming to provide management level information. This concept is labelled 'Interactive Control' since it provides the operator with a degree of system interaction and a level of information not previously attempted.

Section 3.5 contains a detailed description of each of the major C-D elements with a discussion of the information flow in the status display/keyboard. The cursor control is introduced and discussed as a central element of interactive control. The section is concluded with a discussion of the panel arrangement rationale.

Section 3.6 discusses a typical plan change interactive operation as it was demonstrated during the system simulation.

Section 3.7 discusses the effects of 4-D INCADS/JTIDS integration on the C-D subsystem. JTIDS is shown to be an automatic source of detailed tactical information replacing or supplementing the voice communication inputs assumed early in the program. JTIDS information can be integrated readily with 4-D INCADS complementing the management level information presented and reducing the operator information entry work load (since JTIDS information can enter the system automatically). An operational scenario is presented to illustrate the similarity to manual operation. It should be recognized, however, that the vast amount of data available from JTIDS can "overwhelm" any operator or display system and that, therefore, information filtering criteria and filters must be defined before an operational integration can be attempted.

### 3.2 INFORMATION/CREW STATION REQUIREMENTS

The information requirements considered were based on an analysis of the requirements of a tactical STOL transport (1) and on surveys of current 3-D and 4-D flight test programs: Terminal Configured Vehicle (TCV), STOLAND, and Speckled Trout. The analytical study included examination of:

- a. The effects of current Air Force desires to reduce crew members to a minimum by combining the navigation functions with pilot/copilot functions in transport aircraft [3].

- b. The additional information requirements imposed by 4-D guidance in a tactical environment as they apply to the 4-D terminal area vehicle control-display requirements.

The control-displays of the 4-D cockpit are configured for use in a military transport aircraft with a three-man crew -- a pilot, a copilot, and a load master. The pilot is the aircraft commander and has primary responsibility for flying the aircraft and for mission-related navigation. The copilot is the backup pilot and has primary responsibility for long term navigation and health monitoring of the various aircraft systems such as navigation, communication, etc. The load master is responsible for cargo compartment supervision and maintenance and has no flight deck responsibility. This crew complement is reflected in the current AMST requirements (Ref. [3]) and increases the pilot/copilot workload. A re-allocation of functions must be made since the crew complement maintained in Ref. [1] included a full-time navigator.

It became obvious, early in the program, that the presentation of the required variety of complex multidimensional information to the pilot-manager could be accomplished only by utilizing the versatility of electronic displays, particularly for vertical and horizontal situation information, and to present 4-D system alphanumeric status information. This conclusion was supported by reviews of the control-display configurations of the NASA Langley Terminal Configured Vehicle (TCV), NASA-Ames STOLAND, AF Speckled Trout, and AF C-141 AWLS aircraft. It was also recognized that -- as this study progressed into the simulation phase -- only electronic (CRT) displays could provide the display versatility required to illustrate the effects of potential path changes on the horizontal and vertical situation.

A further result of these program reviews was the conclusion that pilot entry via keyboard and CRT status display of the various alphanumeric data required for a path change was too slow to be practical in a high workload tactical environment. Accordingly, the study effort was directed toward:

- a. Developing a C-D concept that would fulfill the requirement for providing an effective path-change technique that could be utilized by the pilot-manager in an operation environment.
- b. Assuring the availability of versatile electronic displays for the man-in-the-loop simulation to demonstrate the path-change technique.
- c. Configuring a C-D arrangement of available electronic and electromechanical displays in the LSI fixed-base simulator that will be utilized for man-in-the-loop simulation.

### 3.3 BASIC C-D RECOMMENDATIONS

The analysis indicated that a CRT Electronic Attitude Director Indicator (EADI) and two vertical scale air data displays will satisfy the pilot's requirements for vertical and command information. A CRT situation (map) display is required to provide the horizontal situation information that will enable the pilot to understand his flight plan [5] and any accompanying threats information at a glance.

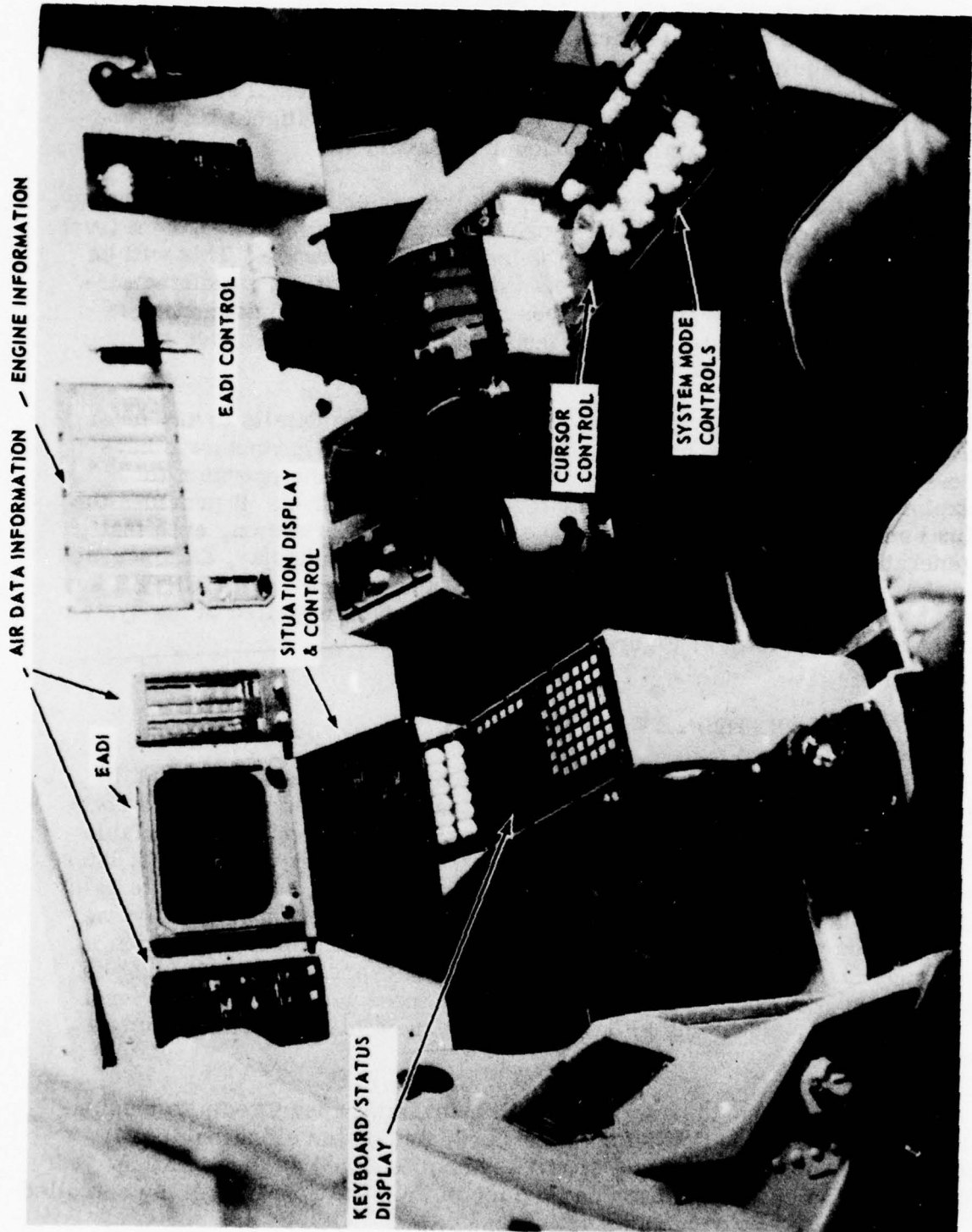
The CRT situation display, then, with the proper programming (symbology, symbol format, information), will provide the pilot with management level information about his situation in the horizontal dimension. This will be supplemented with information about the aircraft position, predicted air-position, and the desired aircraft position. This type of information is similar to that found desirable on the TCV and STOLAND studies to provide 4-D situation information.

The CRT status display provides system information details to any level selected by the operator. This display, with its full alphanumeric keyboard and with proper programming, can be used by the operator to explore system information to any level of detail desired. It provides the final communication link to the 4-D system. All information, even that generated through cursor interaction on the situation display, as discussed in the following paragraph, is entered into the system via the ENTER key as it appears on the status display. These displays installed in the system simulator are shown in Figure 3-1.

### 3.4 CONTROL-DISPLAY INTERACTION

When the pilot is considered as the system manager, he must be presented with the composite view of a situation. This composite is comprised of selected details and tentative conclusions drawn from available information. During the decision process, the manager may request information details and/or he may manipulate the available information to gain a clearer understanding of the impact of potential decisions. Ideally, he is provided with the tools to accomplish this examination/manipulation in a timely fashion and to implement his decision expeditiously. It must be so with the pilot-manager! He must be presented with management level information to assess his situation and with the tools necessary to implement a decision.

The problem of providing the pilot with management level tools to manipulate the graphic situation information presented on the situation display was addressed by providing a special symbol (cursor) on the situation display. The cursor position on the face of the situation display is controlled



SIMULATOR CONTROL-DISPLAY CONFIGURATION  
FIGURE 3-1

by a hand-operated joystick\*. The cursor shape (a large cross-hair) was chosen to provide graphic position information when referenced against scales on the situation display. Modes of cursor operation ranging from simple point interrogation to avoidance point insertion and plan changing are provided as cursor mode controls to give the pilot a wide variety of graphic interaction capability.

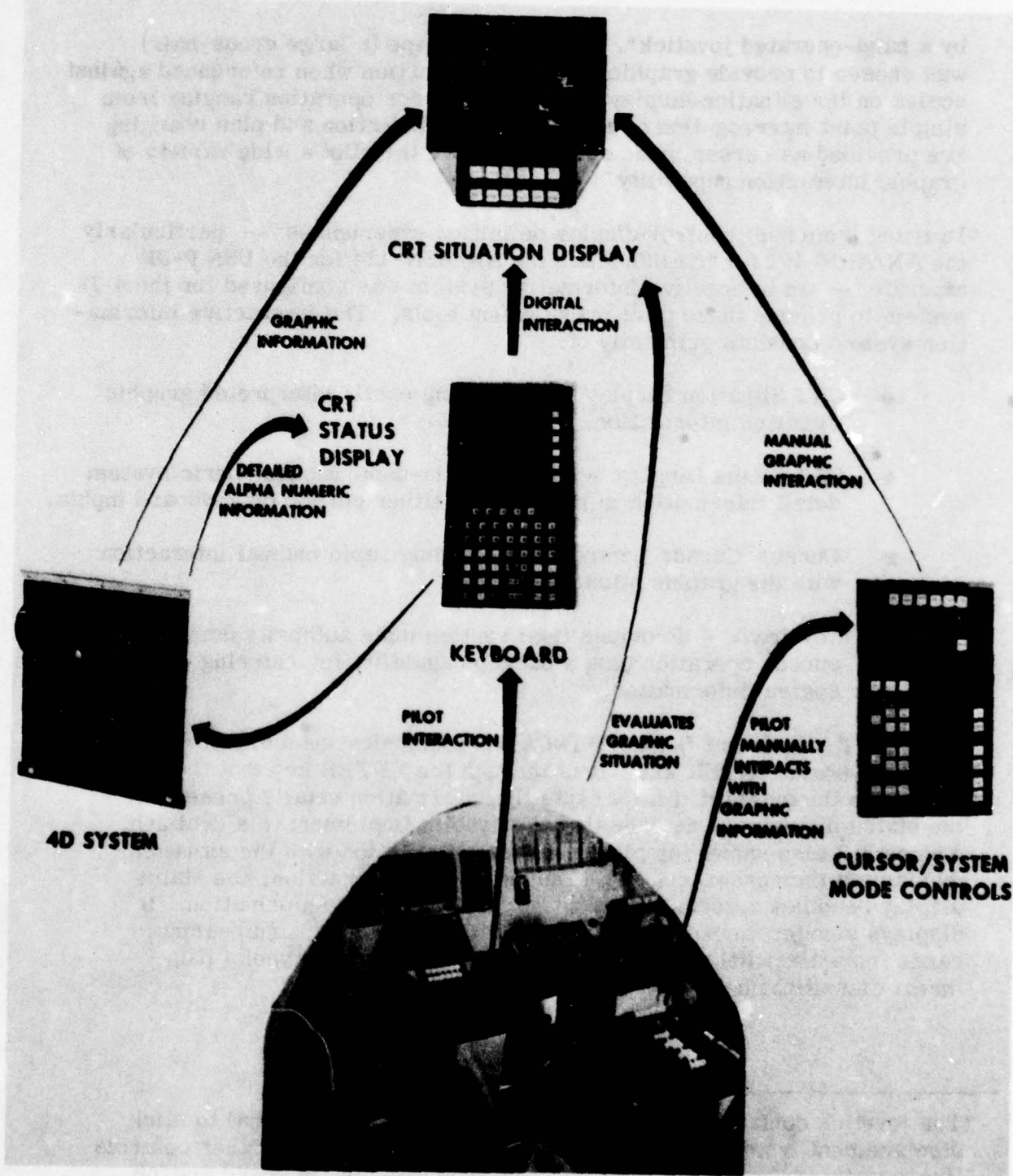
Drawing from past control-display definition experiences -- particularly the AN/ARN-101 for the USAF and the AN/ASN-124 for the USN P-3B aircraft -- an interactive information system was configured for the 4-D system to provide these pilot management tools. The interactive information system consists primarily of:

- CRT Situation Display - Providing easily interpreted graphic situation information.
- CRT Status Display - Providing in-depth alphanumeric system detail information in response to either cursor or keyboard inputs.
- Cursor/Cursor Control - Providing rapid manual interaction with the graphic situation display.
- Keyboard - Provides final system input authority during cursor operation plus a backup capability for entering detailed system information.

Figure 3-2 shows that final 4-D INCADS communication authority resides in the keyboard ENTER key. It is through the ENTER key that the pilot signals to the system that he accepts the information details presented on the status display and desires that the system implement this decision. Figure 3-2 also shows the pilot's manual interaction with the situation display via the cursor/control. During cursor interaction, the status display becomes a vernier readout of cursor position information. It displays vernier cursor position information (lat, long, and bearing, range from aircraft) plus other selected parameters (waypoint data, threat classification) based on cursor modes.

---

\*The joystick controls X, Y velocity of the cursor proportional to stick displacement from center. Studies (Ref. [7]) indicate that other controls (force sensing, trackball, etc.) may offer advantages in speed and/or accuracy - but the joystick could be obtained within the cost constraints of this program and could demonstrate the technique.



**PILOT STATION**

**SYSTEM INTERACTION  
FIGURE 3-2**

Thus, the C-D system provides a graphic display of aircraft position relative to path and threats on the situation display for rapid pilot assimilation. It provides a rapid manual interaction capability via the cursor affecting both the graphic situation display and the precise system details presented on the status display. A means (status display) is provided by which the pilot can review and accept the detailed information and signal his acceptance to the system. Finally, the interaction activity is primarily graphic with minimal use of the keyboard. The interaction of these displays, with software control, provides an advanced display system capability not found in other programs.

### **3.5 CONTROL-DISPLAY DETAIL DESCRIPTION**

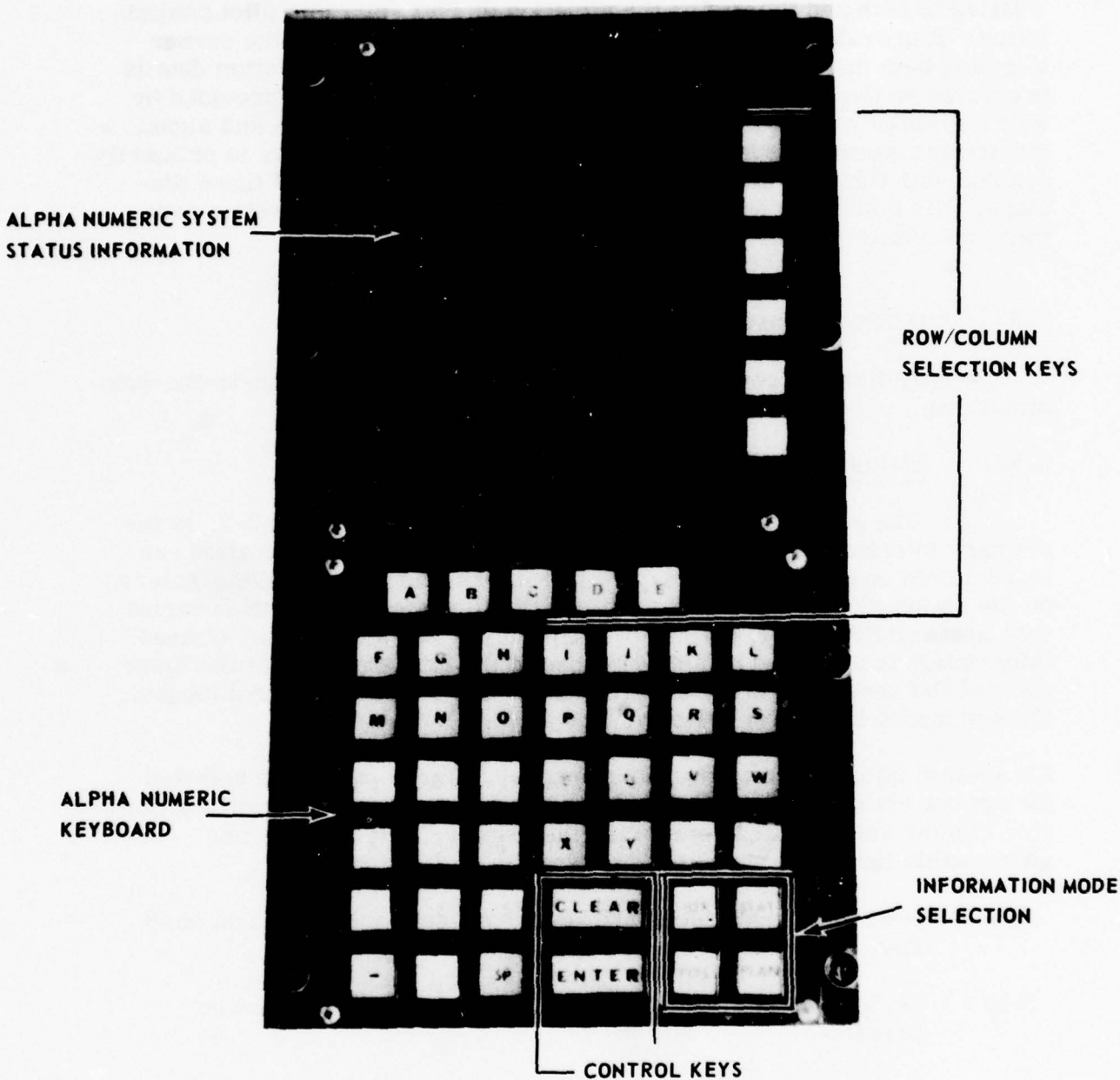
The following control-displays were utilized during man-in-the-loop simulation.

#### **3.5.1 Status Display**

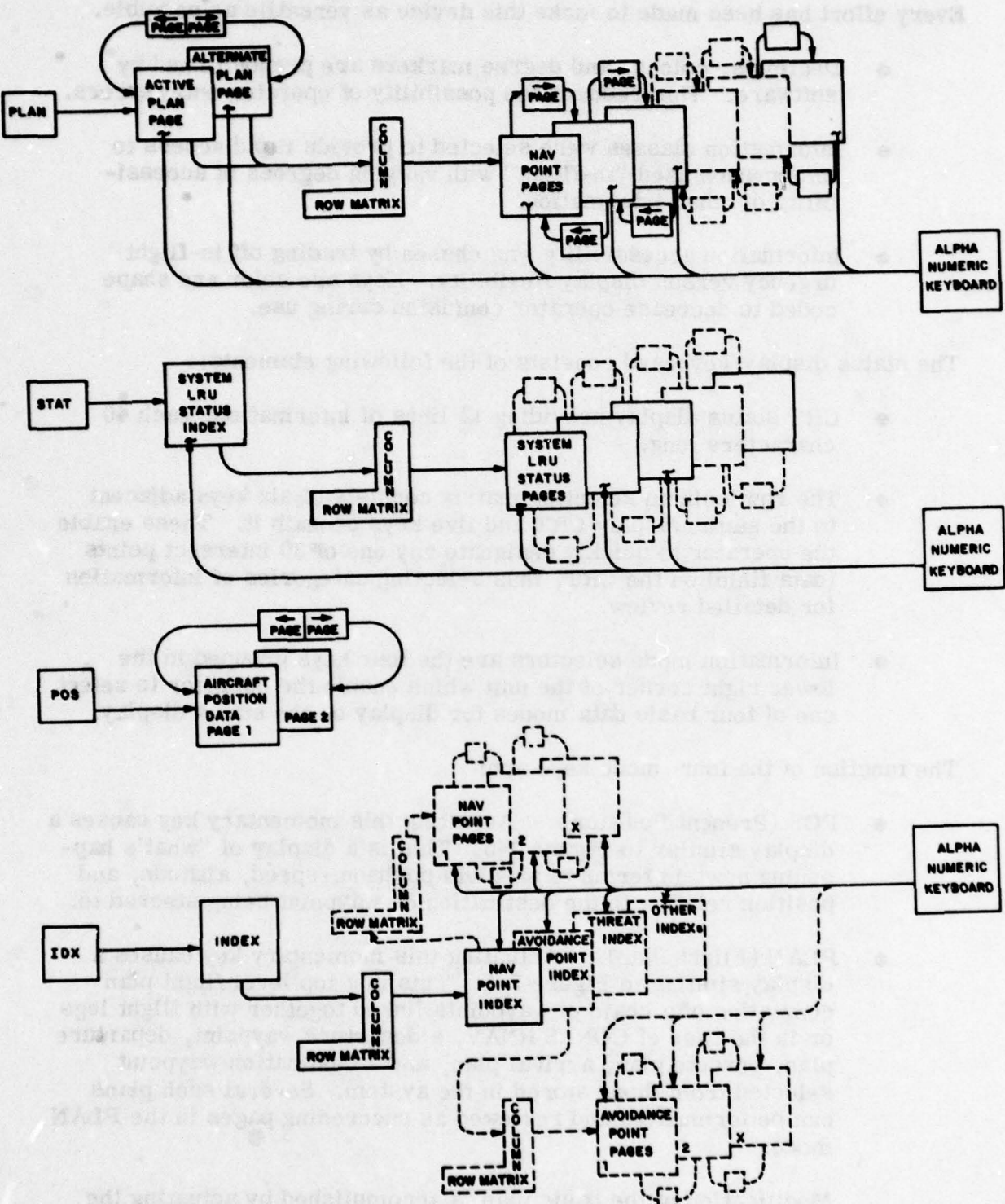
The status display and associated keyboard, Figure 3-3, is the primary interface to the navigation system. All system information can be reviewed on the status display. Most information can be edited/entered on the status display. Ease of accessibility to system information varies with accessibility levels defined by frequency of use and urgency of need. Information is accessed by actuating one of the four switches on the lower right of the keyboard, or by engaging one of the "Cursor" control modes. Cursor modes have first priority.

All system information is stored on "pages". These pages are selected for review via the four status display mode switches and the multifunction row/column select buttons bordering the display. These pages are addressable through a standard logic routine (see Figure 3-4).

- Step 1.** Select information class from one of the four lower right hand keys.
- Step 2.** Review status display for subclass or edit the information presented.
- Step 3.** Select information subclass via row/column keys.
- Step 4.** Review and edit displayed information.
- Step 5.** Insert



STATUS DISPLAY/KEYBOARD  
FIGURE 3-3



**STATUS DISPLAY INFORMATION FLOW**  
**FIGURE 3-4**

88820

**Every effort has been made to make this device as versatile as possible.**

- **Decimals, colons, and degree markers are prepositioned by software. This reduces the possibility of operator entry errors.**
- **Information classes were selected to provide rapid access to information used "in-flight" with varying degrees of accessibility of other information.**
- **Information accessibility was chosen by trading off in-flight urgency versus display flexibility. Keys are color and shape coded to decrease operator confusion during use.**

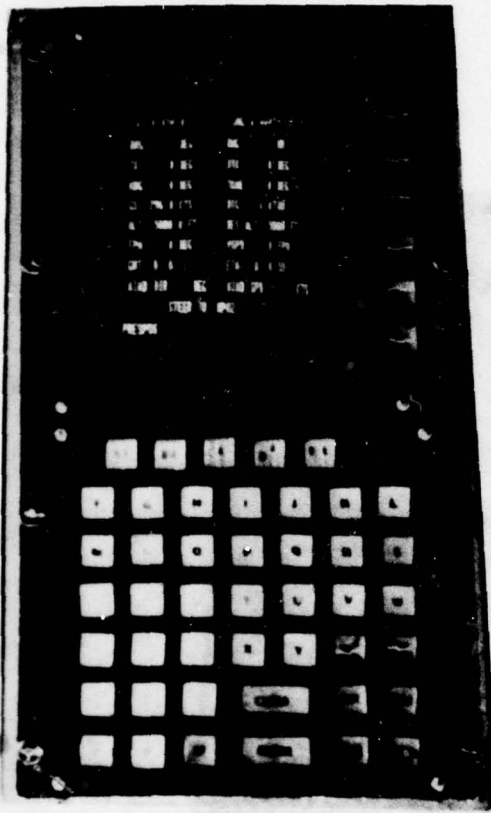
**The status display/keyboard consists of the following elements:**

- **CRT status display providing 12 lines of information, each 40 characters long.**
- **The row/column selection matrix consists of six keys adjacent to the status display CRT and five keys beneath it. These enable the operator to quickly designate any one of 30 intersect points (data field) on the CRT, thus selecting categories of information for detailed review.**
- **Information mode selectors are the four keys grouped in the lower right corner of the unit which enable the operator to select one of four basic data modes for display on the status display.**

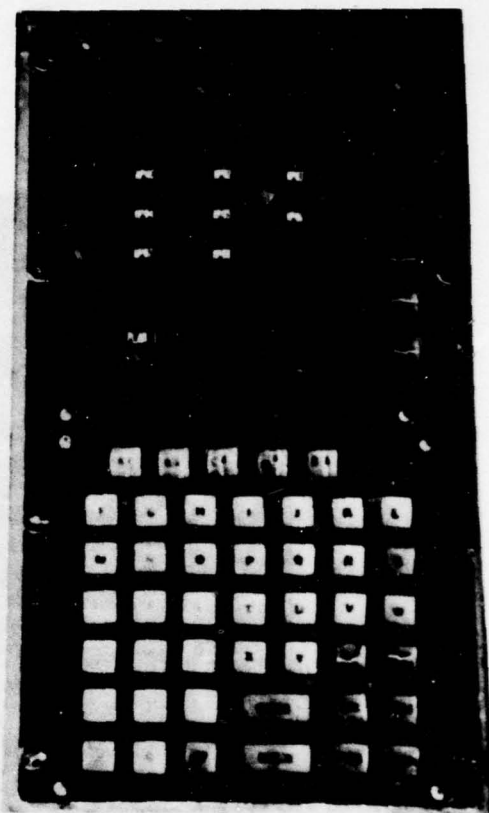
**The function of the four mode keys are:**

- **POS (Present Position) - Actuating this momentary key causes a display similar to Figure 3-5. This is a display of "what's happening now" in terms of absolute position, speed, altitude, and position relative to the destination or waypoint being steered to.**
- **PLAN (Flight Plan) - Actuating this momentary key causes a display similar to Figure 3-6. This is a top level flight plan consisting of a chain of waypoints linked together with flight legs or in the case of CONUS RNAV, a departure waypoint, departure plan, enroute plan, arrival plan, and a destination waypoint selected from those stored in the system. Several such plans can be formulated and reviewed as succeeding pages in the PLAN mode.**

**Modification of the basic plan is accomplished by actuating the line selector key to the right of the status display and selectively**



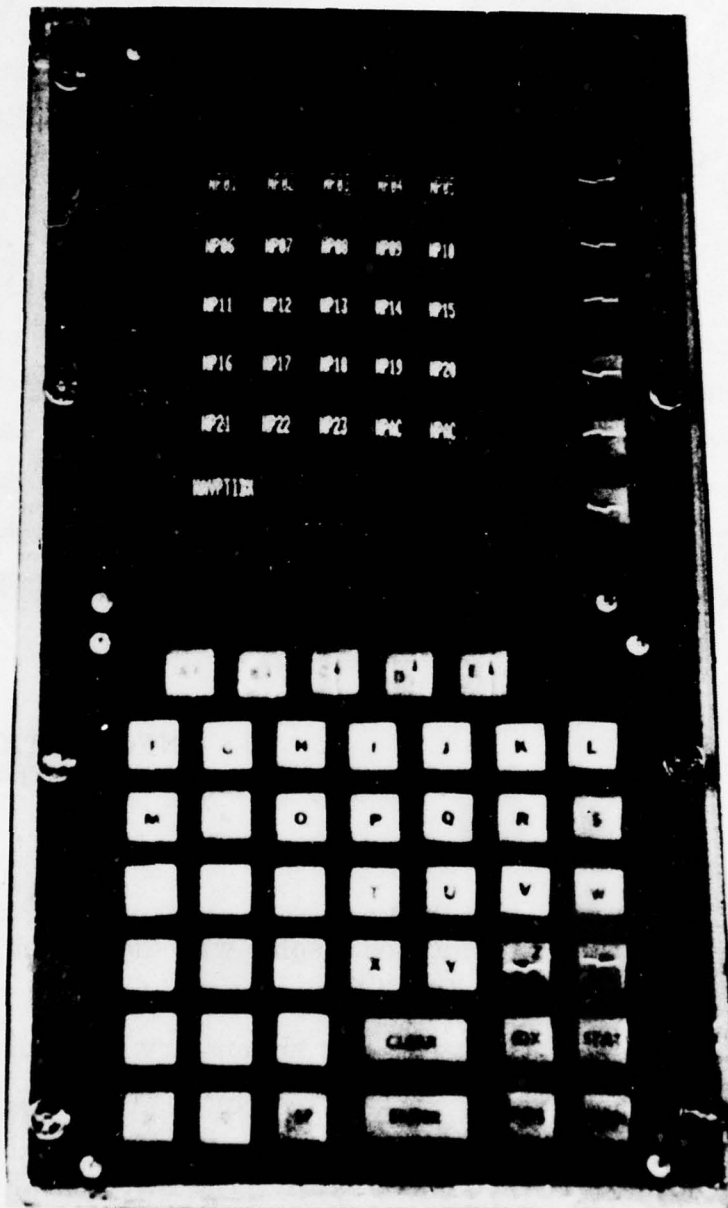
PRESENT POSITION  
INFORMATION  
FIGURE 3-5



PLAN  
INFORMATION  
FIGURE 3-6

editing the plan via the keyboard, or by chaining a sequence of waypoints on the situation display with the cursor control, and entering it via the joystick.

- **IDX (Index)** - Actuating this momentary key causes a display similar to Figure 3-7. This is a top level index of all the classes of information stored in the system. Information classes can be selected for detailed display via the associated keys in the row/column matrix. The IDX (index) capability provides for display system versatility and growth built on a logical base and utilizing established operational methods.



INDEX INFORMATION  
FIGURE 3-7

- **STAT (Status)** - Actuating this momentary switch causes system Line Replaceable Unit (LRU) status information to be displayed on the status display. Degraded mode operation trees can be generated for the 4-D INCADS depicting the mission completion capabilities remaining after failure of key system LRUs. Displays of these choices will be generated after selection of the appropriate row/column selector keys for the particular LRU.

The remaining keyboard functions are described below:

- **PAGE** - Page forward (PAGE) or page backward (PAGE) is selected by actuating these momentary keys. When either is selected, a new page is presented on the status display. The information class is the same as that previously presented via the four mode keys (POS, PLAN, STAT, or IDX) and the row/column matrix. For example, IDX mode could be selected with a subsequent row/column selection of details of NAV PT 1. The paging feature allows the operator to move within the data field one page at a time.
- **ENTER** - The ENTER key is the only way to insert displayed information from the status display into the 4-D INCADS computer. Information is inserted a page at a time after review on the status display by pressing the momentary ENTER key.
- **CLEAR** - CLEAR enables the operator to selectively erase information from the display and from the system memory. Clearing information from the system is accomplished by designating the information through the row/column matrix and pressing the CLEAR key, followed by pressing the ENTER key.
- **Space (SP)** - The cursor (underline) indicates where a character will be inserted on the status display when a key is pressed. The row/column matrix selectors have the secondary function of coarse cursor position control. That is, upon making a row/column selection, the cursor will appear beneath the left most character position in the selected data field. Pressing the SP key will move the cursor to the right one space at a time without altering the data in the field. A backspace capability is not considered necessary at this time because of the limited number of characters in any given data field and because the cursor can be returned to its left most position by making a second row/column selection.

- **Alphanumeric Keyboard** - A full alphanumeric keyboard is provided for the status display. This allows the operator to rapidly and unambiguously select from the full alphabet for RNAV, UTM\*, and threat identification. The numeric keyboard is color separated from the alpha portion. Numeric keys are arranged in a 10-key matrix similar to most hand calculators.

### 3.5.2 Situation Display

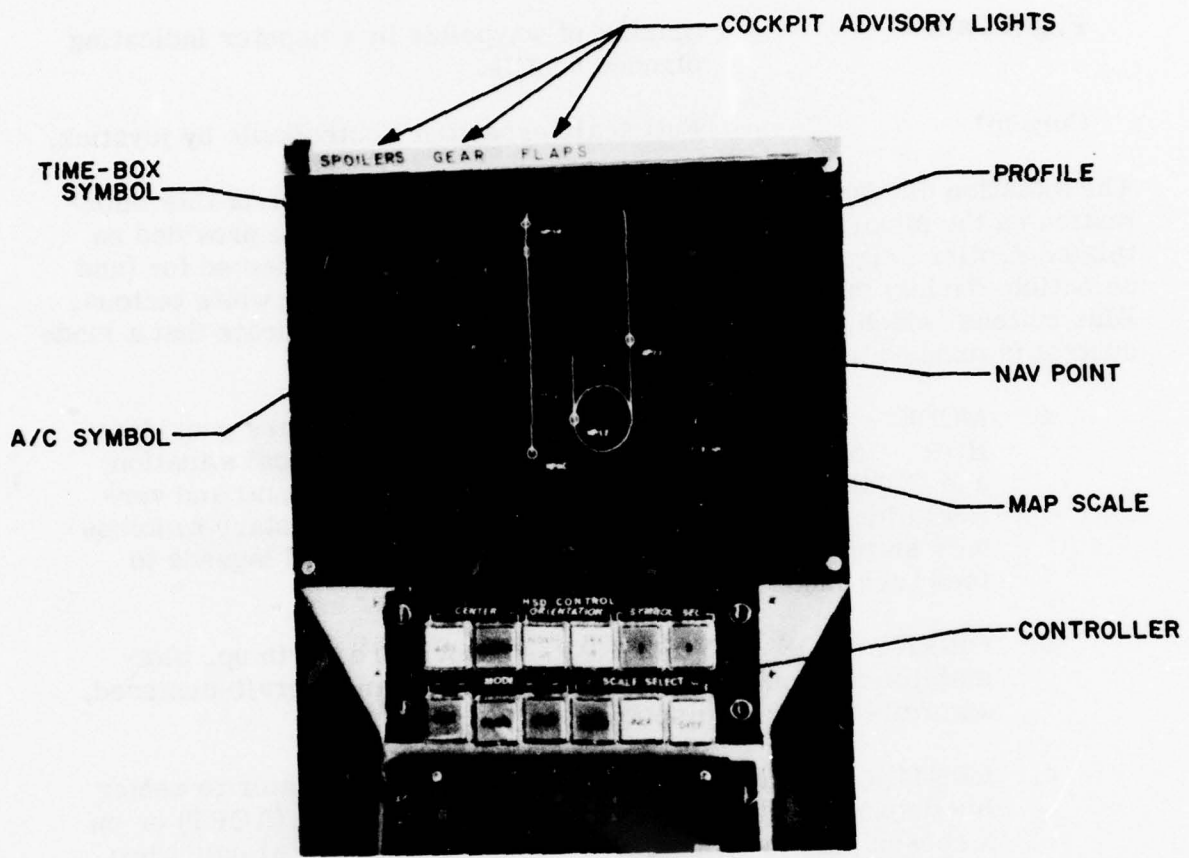
The situation display (Figure 3-8) is an electronic (CRT) display of horizontal situation relative to the flight plan. Provisions were made on the mode control for the display of vertical situation information. However, for this program only the horizontal situation was implemented. The mode control is located immediately beneath it. The aircraft position is shown relative to the planned horizontal flight path. This display allows the operator to rapidly assess the horizontal situation and make corrective inputs based on the evaluation.

The following is typical of the information presented on the situation display.

Aircraft Symbol	- Fixed at display center in "heading up" mode, moving in "north up" mode.
Alphanumerics	- Explanatory and scaling information associated with scales and parameters.
Waypoint	- Circle with alphanumeric identifiers.
Map Scale	- Scale factor explanation in nautical miles per inch.
Desired Position Window (Time Box)	- Rectangle representing desired aircraft position on the flight path at any given time.

---

\*The Universal Traverse Mercator (UTM) coordinate system is used to designate artillery coordinates and thus is a requirement for tactical navigation.



ELECTRONIC SITUATION DISPLAY AND CONTROLLER  
FIGURE 3-8

<b>Predicted Aircraft*</b>	-	Computed aircraft position in 30, 60, and 90 seconds** based on current control action.
<b>Time Box Predictor*</b>	-	Desired aircraft position on flight plan in 30, 60, and 90 seconds.
<b>Flight Path</b>	-	Linking of waypoints by computer indicating planned profile.
<b>Cursor*</b>	-	Full scale crosshair controllable by joystick.

The situation display mode control controls the presentation of this information on the situation display. Five control groupings are provided on this controller (Figure 3-8). Active control modes implemented for (and selectable during) the system simulation are denoted by the white buttons. Blue buttons (which appear as dark grey in the figures) indicate that a mode control is planned but not implemented.

- a. MODE - Three basic display operation modes are provided: HOR - horizontal situation; VERT\*\*\* - vertical situation; and COMB\*\*\* - combined (split screen) horizontal and vertical situation. These are mechanized as momentary switches with software interlocks and could utilize lighted legends to feed back mode information to the operator.
- b. ORIENTATION - NORTH UP - provides a north up, plot-stabilized display. HDG UP - provides an aircraft-centered, aircraft-stabilized display.
- c. CENTER - These two switches enable the operator to center his display, within limits, on either the aircraft (ACFT) or on a cursor position (CURSOR). These are functional only when the display is operating in a NORTH UP orientation.

---

\* Not shown in Figure 3-8.

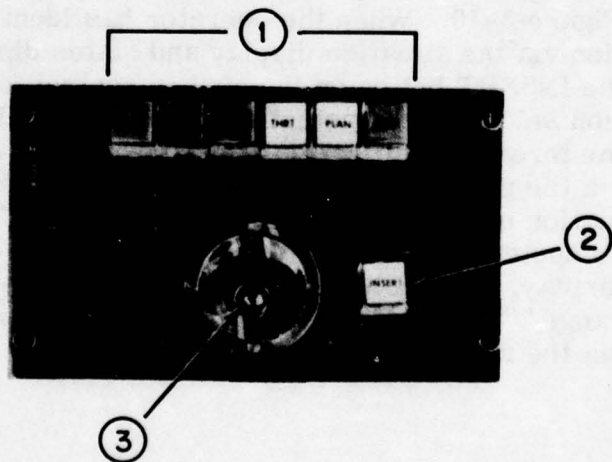
\*\* These predictors were found to be very useful during the STOLAND and TCV evaluations. The predictor spacing is a function of display scaling and aircraft velocity. Therefore, the time interval chosen for a transport will not necessarily be appropriate for a fighter. These changes are readily accommodated in the display.

\*\*\* These modes were not mechanized on this program.

- d. **SCALE SELECT** - Scaling information will be displayed as nautical miles per inch (NM/IN) on the display. If the operator wishes to change scaling he can do so by pressing INCR for increased nautical miles per inch or DECR for decreased nautical miles per inch. Each actuation will double or halve the scale factor. AUTO returns the scale factors to computer control. SCALE SELECT is functional in all modes except HSI. The plot scaling will be equal on both axes of the horizontal plane plots.
- e. **SYMBOL SELECT** - Plot symbology in all modes is under software control. These two keys enable the operator to control the amount of information on the screen at any one time. Pressing the "1" key provides more explanatory information per symbol (thus more "clutter") than does "2".

### **3.5.3 Cursor Controller**

The purpose of the cursor control (Figure 3-9) is to provide the operator with a means of rapidly and accurately entering data into the 4-D INCADS utilizing the situation display. The cursor symbol on the situation display is a large (full screen) crosshair. It appears whenever one of the cursor mode switches is engaged. While the cursor is engaged, cursor position information (lat, long,) will be displayed on the status display. Moving the joystick on the cursor control will cause a corresponding movement of the cursor symbol on the situation display and an update of cursor position information on the status display. Three control groupings, identified by number on Figure 3-9, are provided on the cursor control. Button color is used to indicate mechanization status as in Situation

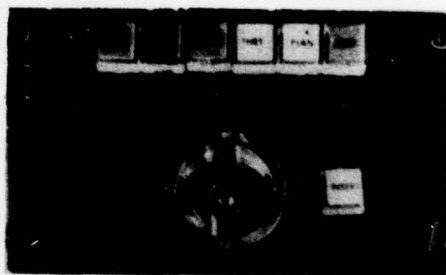
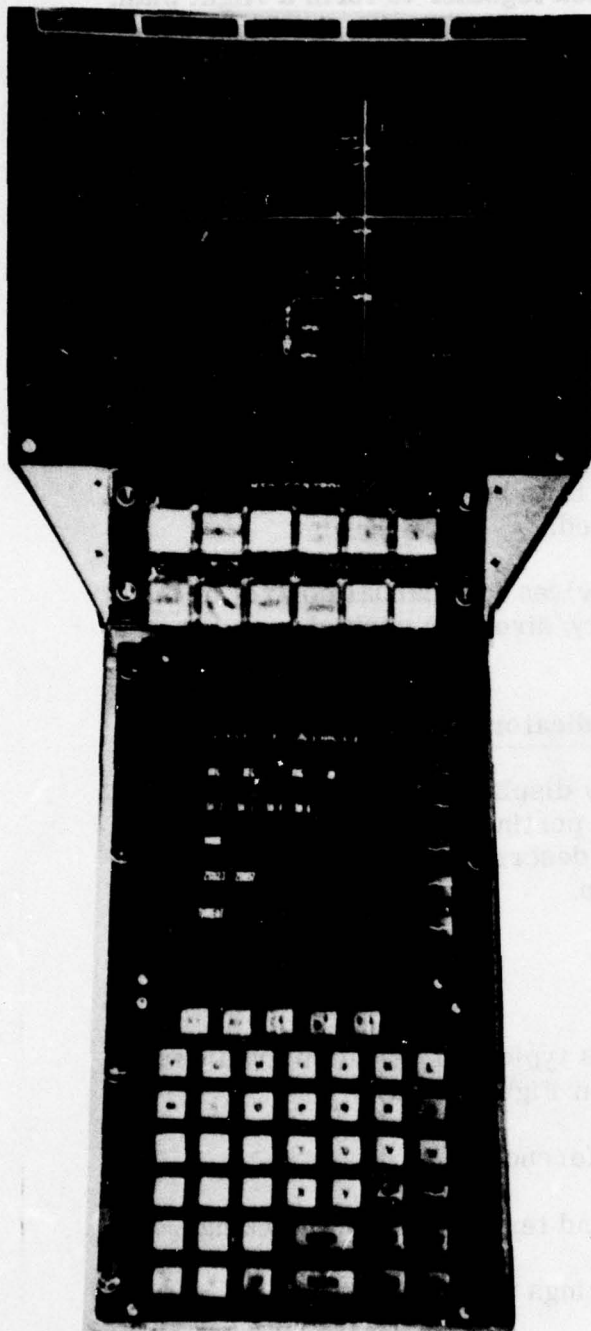


**CURSOR CONTROL**  
**FIGURE 3-9**

display mode control. White indicates a mode that is mechanized for the system simulation.

1. MODE - Provisions are made for six operational modes including OFF.

- ON - This is interrogation mode. Moving the cursor over any point on the situation display will cause the status display to present position information about that point.
- AC CURSor (Aircraft Cursor) - This is a bearing/range mode. The cursor is controlled as in the basic mode. Cursor position information including bearing range from the aircraft will be presented on the status display. When INSERT is pressed, a line is drawn from the aircraft to the cursor position.
- CURSor - This is also a bearing/range mode. It is different from the AC CURSor mode in that the line does not originate from the aircraft. The line will originate from a point designated by pressing INSERT and extend to a second point designated by pressing INSERT. Bearing and range from the first point to the second point will be displayed on the status display plus basic location information about both points.
- THRT (Threat) - This mode enables the operator to insert a threat avoidance zone via the cursor. The cursor is operated as in other modes with the status display providing position information. In THRT mode, however, the status display will also list the various threat classes as shown in Figure 3-10. When the operator has identified a threat position via the situation display and status display, he will press the INSERT button on the cursor control identifying the position selected as a potential threat area. He will then select the threat classification from those listed on the status display via the row/column matrix and enter the page of threat information using the keyboard ENTER key. This will cause the computer to position an avoidance volume on the situation display. The volume will be calculated using stored threat range/altitude parameters based on the threat situation made via the row/column matrix.



**THREAT INFORMATION**  
**FIGURE 3-10**

- PLAN - This mode enables the cursor to be used to move the waypoints that are linked together to form a flight plan. During this mode, cursor coordinates plus the flight plan page being generated/edited are displayed on the status display. The cursor is engaged via the PLAN button and moved with the joystick as before. The plan is edited by placing the cursor over the waypoint to be moved and pressing INSERT. This identifies the waypoint to be moved. Moving the cursor to the new waypoint position and pressing INSERT a second time and entering the resulting new waypoint page via the ENTER (Status Display) key causes a temporary (dashed) flight plan to be presented on the situation display. Pressing the ENTER key a second time will result in a permanent plan change.
2. INSERT - Actuation of this momentary switch designates to the system that a requested action is to be initiated about that point. No operator feedback is required.
  3. JOYSTICK - The joystick provides for manual control of the cursor position. It is a velocity/direction control.

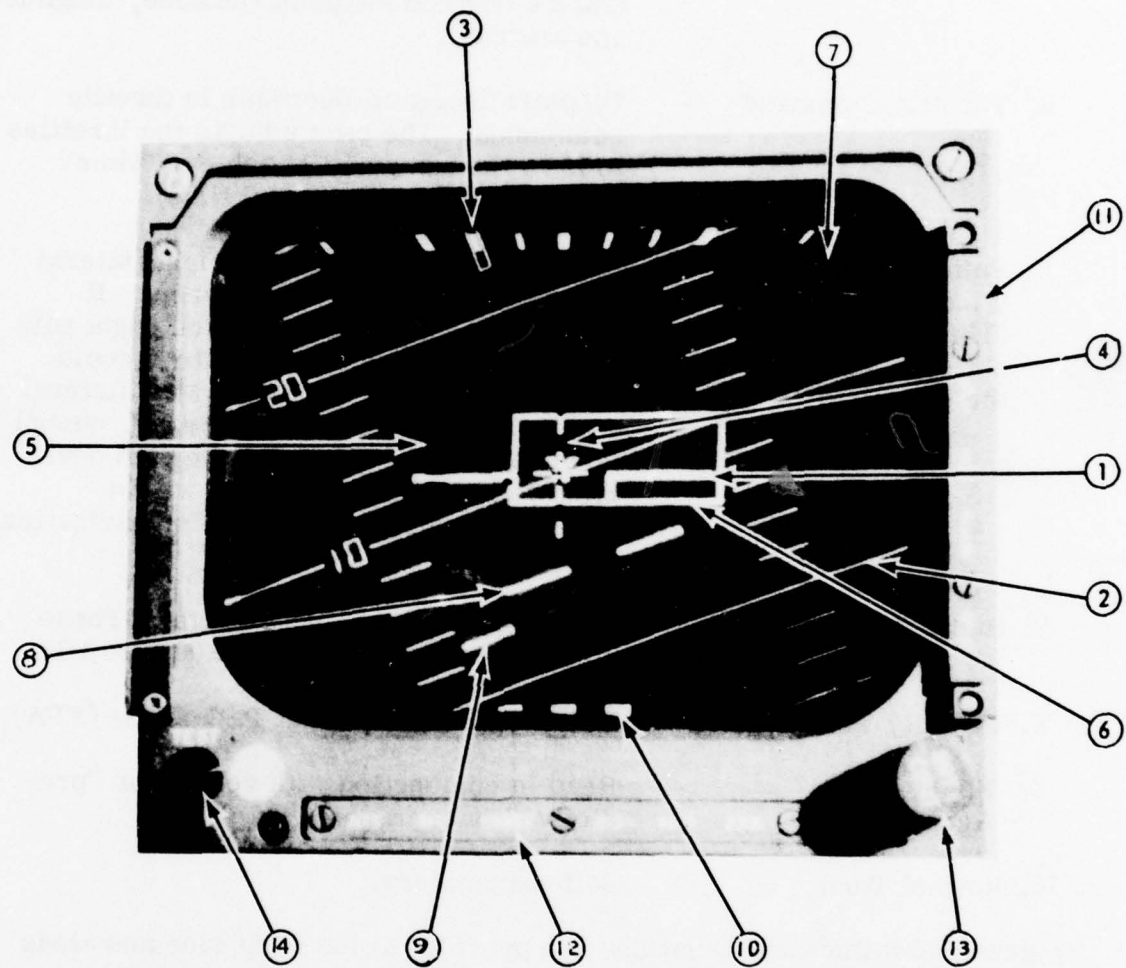
### **3.5.4      Electronic Attitude Director Indicator (EADI)**

The EADI is a GFE cathode ray display (Figure 3-11) capable of displaying a wide variety of symbology pertinent to the mode selected. The symbology shown in Figure 3-11 and described in the following paragraphs was flown in the system simulation.

#### **3.5.4.1      EADI Display**

The following information is typical of that displayed on the EADI (the numbers refer to those items on Figure 3-11).

1. Aircraft Symbol      -      Fixed reference.
2. Pitch Attitude      -      Sky-ground texture with  $2^\circ$  markings.
3. Roll Attitude      -       $10^\circ$  markings at top of display.



EADI DISPLAY  
FIGURE 3-11

- 4. Flight Director**
- Roll Command
  - Pitch Command
- Cross pointers; the pilot zeros the cross cross pointers to satisfy computed commands for the roll/pitch axis, e.g., capture and track a desired waypoint (latitude, longitude and altitude).
- 5. Throttle Command**
- Displays increase/decrease in throttle commands. The pilot adjusts the throttles to zero the command to achieve "time" constraints (speed/arrival time).
- 6. Path Deviation Window**  
**(This display was not used during the simulation)**
- Rectangular - moves left-right (lateral error); up-down (vertical error). It displays cross-track error and flight path angle error. At approach gate it could display ILS (LOC - G.S.) or MLS (lateral vertical). When the fixed aircraft symbol is within the boundaries to the path deviation window, the aircraft is within acceptable path error limits for navigation or landing.
- 7. Radar Altitude**
- Numeric display - upper right. These numerics came in view at 1200 feet AGL.
- 8. Velocity Vector**
- Defined by actual Flight Path Angle (FPA).
- 9. Flight Path Acceleration**
- Read in conjunction with vector for "predictive" information
- 10. Rate of Turn**
- Self-explanatory.

Progress and failure annunciations are provided at the right side and along the bottom of the unit. These were not used during the simulation.

- 11. Progress (typical)**
- Localizer (LOC) Armed/Engaged
  - Glide Slope (G/S) Armed/Engaged
  - Decision Height (DH)
  - Flare (FLR)
  - Go Around (G/A)

- 12. Failure (typical)**
- Attitude (roll or pitch) (ATT)
  - F/D (Flight Director)
  - ILS (LOC or G.S.)
  - SPD (Speed Errors)
  - R-Alt (Radar Altitude)
  - F.P.A. (Flight Path Angle)

Two controls on the bottom two corners of this unit are:

- 13. Brightness/Contrast** -
- 14. Test Button** - Test pattern displayed.

#### **3.5.4.2 EADI Mode Select Panel**

The EADI mode select panel (not shown) can be used to select:

##### **MODE**

**Attitude (decluttered)**

Normal - all essential symbology for particular mode  
TV - actual raster of forward scenery (runway, etc)

Pushbutton deletion of some symbols can also be selected, e.g., air speed error bug, path deviation window, flight path angle, flight director command bars.

##### **Pilot Select**

**Flight Path Angle (velocity vector)**  
**MDA (minimum decision altitude)**

#### **3.5.5 Vertical Scale Air Data Displays**

These two GFE instruments were located on either side of the EADI. They provided altitude and speed information. They are standard C-141 instruments and were totally operational during the simulation. These units are shown in Figure 3-1.

The altimeter (on the right) contains displays of barometric altitude with a manually set command altitude tab, and instantaneous vertical

velocity. Provisions are also made for local barometric pressure compensation.

The speed indicator (on the left) contains displays of indicated air speed (IAS) and Mach both with manually set command tabs.

### **3.5.6 System Mode Control and Annunciator**

Mode controls tailor the system to the aircraft and mission requirements. In this case a preliminary configuration of the mode controls has been defined for a hybrid transport simulator to demonstrate the capabilities of the 4-D INCADS. It is recognized that as the 4-D INCADS is further developed, the controls will also be reconfigured. These mode controls were not mechanized during the simulation. Switches on the throttle quadrant and control stick were used to engage auto throttle and automatic flight control.

### **3.5.7 Panel Allocation**

Instruments were arranged on the pilot's primary instrument panel to conform to the basic "T" scan pattern identified in past Air Force studies. Location of the EADI and situation display on the pilot's vertical center line with vertical scale altitude and airspeed information on the horizontal T bar to the right and left of the EADI is a proven arrangement needing no further human engineering validation. The keyboard/status display is located beneath the situation display well within the pilot's reach and vision envelope as an extension of the base of the T scan. This configuration was suggested by the TCV panel layout. Conventional shared (pilot/copilot) locations were chosen for engine information and throttle controls. The cursor control and system mode control are located in the center console aft of the throttle where they are available for shared (pilot/copilot) use. The location of the cursor control joystick was chosen to facilitate right hand use by the pilot. A side stick flight controller was installed for left hand use by the pilot. This provided a clear unobstructed view of all instruments and enabled the pilot to use his right hand to operate the keyboard, situation display, and cursor mode controls. The simulator panel allocations were made on the basis of application of proven concepts with no basic human engineering analysis in keeping with the program requirements.

## **3.6 DISPLAY SYSTEM OPERATION**

Display system interactive operation was demonstrated to each pilot who participated in the system simulation. For this demonstration the pilot was asked to fly Plan 1 and at some point in the profile to change

the latitude/longitude of a waypoint. He was instructed to use the cursor control to complete the waypoint change and given an opportunity to practice in the static mode. The pilot was asked to complete the waypoint change while flying the aircraft along the path with manual control.

A typical plan changing operational description follows: The pilot is seated in the cockpit flying Plan 1 with manual control. He has just passed through waypoint 3 and is tracking the time box in all respects. He is told that a threat has moved in near waypoint 4 and that he must move waypoint 4 east 5 miles to a new longitude of  $45^{\circ}18'$ . He presses the PLAN button on the cursor control causing the cursor to appear on the situation display and the blank waypoint page to appear on the status display (Figure 3-12). He positions the cursor on waypoint 4 using the joystick and presses INSERT. Data from the waypoint 4 page appears on the status display (Figure 3-13). He moves the cursor until he reads the latitude of  $45^{\circ}18'$  on the status display and presses the INSERT key on the cursor control. This freezes the new ( $45^{\circ}18'$ ) latitude on the waypoint 4 page and removes the cursor from view. The operator reviews data for waypoint 4 as presented on the status display. At this point he can make any additional changes necessary via the keyboard. He accepts the new waypoint 4 data into the system by pressing ENTER. This causes a temporary flight plan (dashed lines) to appear on the situation display showing the effects of moving the waypoint on the flight plan (Figure 3-14).

He presses ENTER a second time if he wants to have steering signals generated to fly the modified flight plan. This causes the dashed line flight plan on the situation display to be replaced with solid lines (Figures 3-14) indicating that commands generated are relative to the modified plan.

### 3.7 JTIDS INTEGRATION

#### 3.7.1 Introduction

A measure of the worth of a concept can be gained by examining its adaptability to new inputs. The concept of total display system interaction has been described in preceding paragraphs. It was advanced to enable the 4-D system operator to readily make changes to system information and to provide him with a rapid assessment of the effects of the new information regarding his flight plan. The information changes described were operator initiated with the thought that the basic information came to the operator through the voice radio link or sensor assessment.

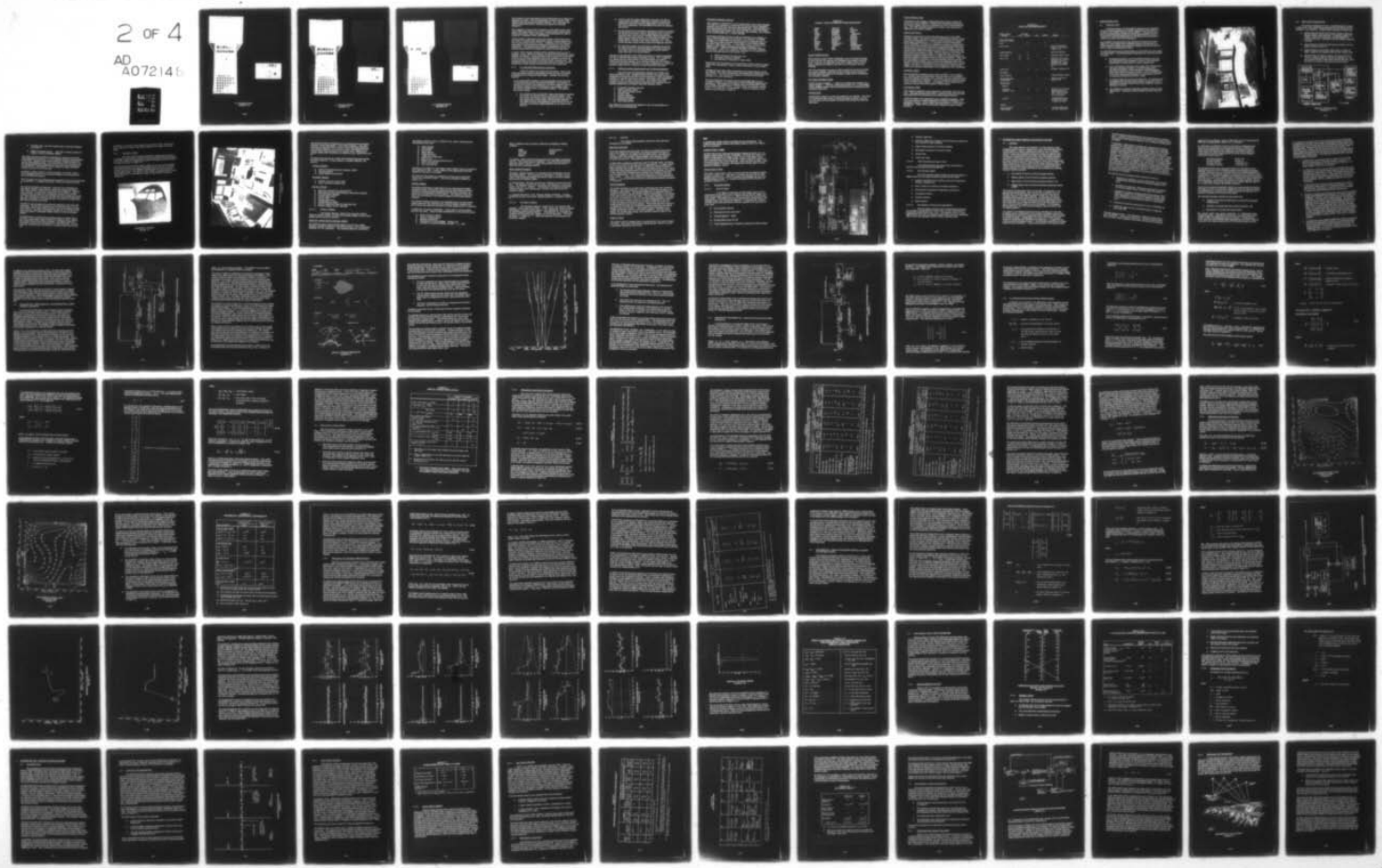
AD-A072 148 LEAR SIEGLER INC GRAND RAPIDS MICH INSTRUMENT DIV F/G 17/7  
FEASIBILITY STUDY FOR INTEGRATED FLIGHT TRAJECTORY CONTROL (AIR--ETC(U))  
JAN 77 M BIRD F33615-74-C-3083

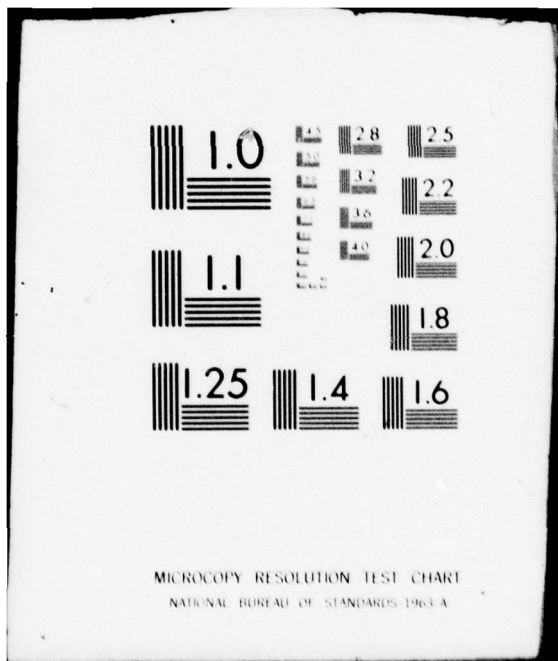
UNCLASSIFIED

AFFDL-TR-77-120

NL

2 OF 4  
AD  
A072148





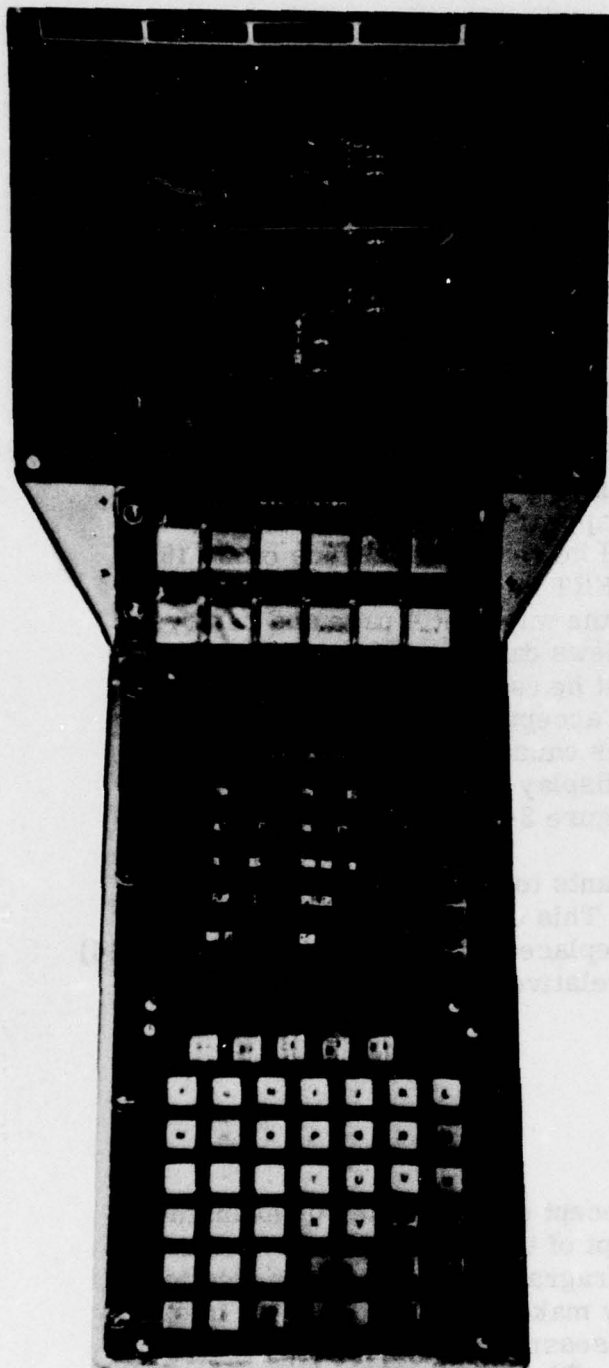
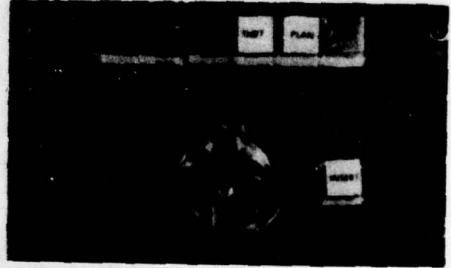
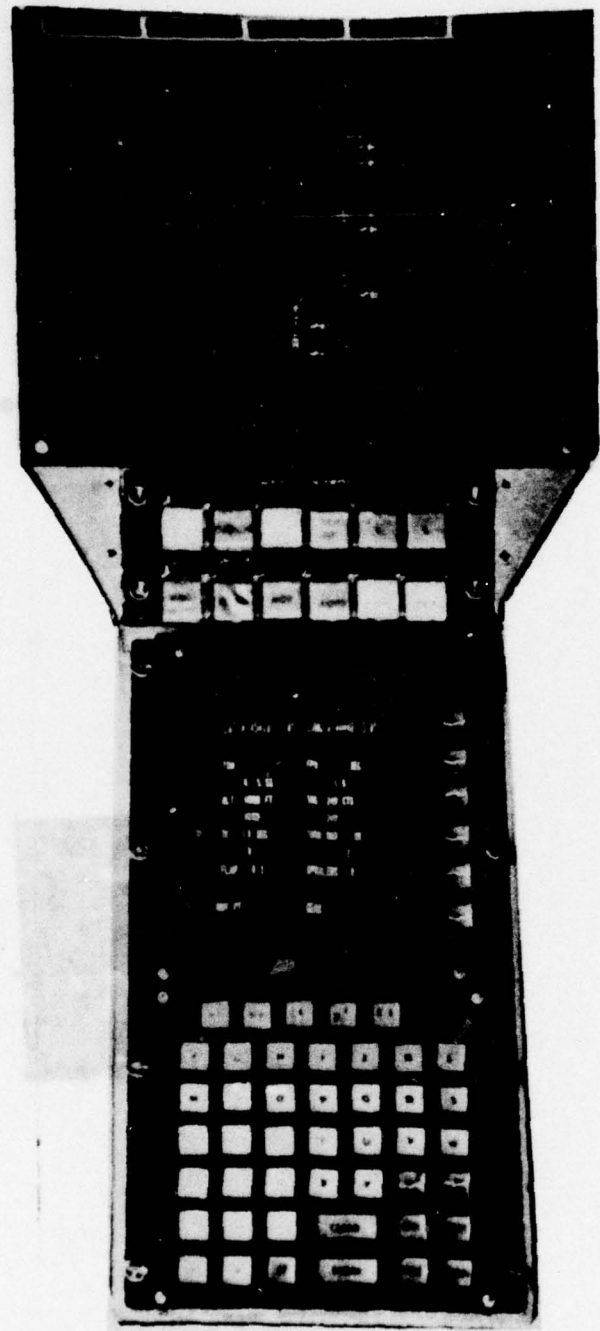
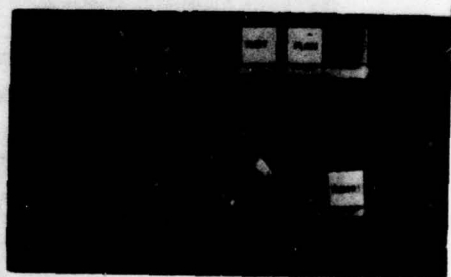
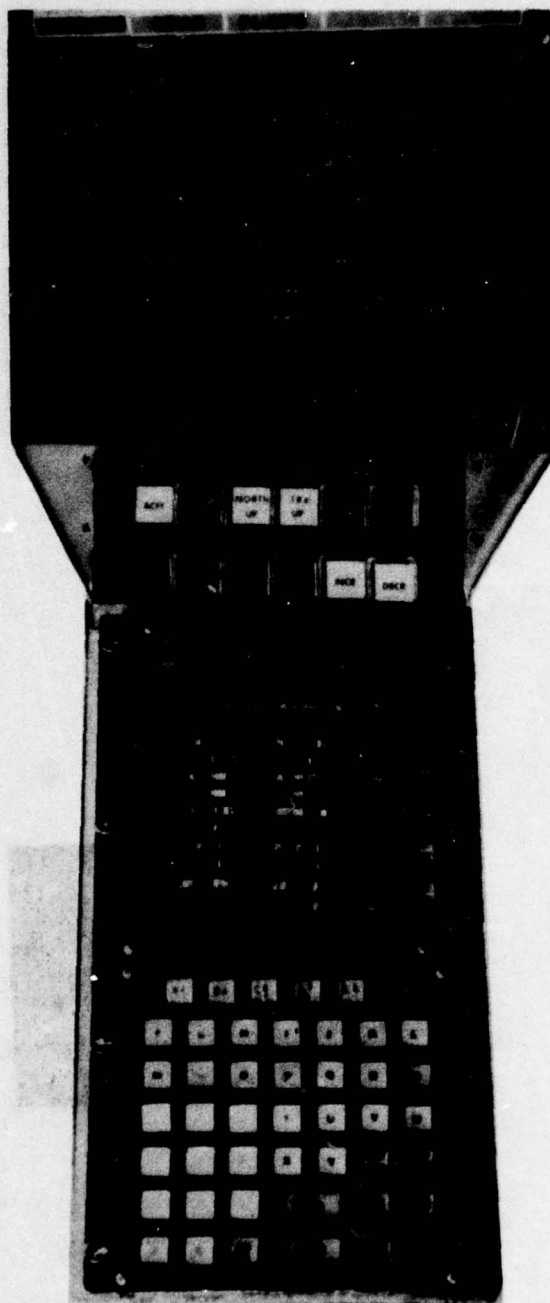


Figure 3-12 illustrates two types of C-D interaction devices. The one on the left is a large unit designed to be mounted on a wall. It features a central trackball, a 'SELECT' button, and a vertical column of small square buttons. The one on the right is a smaller, more compact unit with three buttons at the top, a trackball in the center, and a 'SELECT' button below it. Both units are designed to be used with a C-D system.

### C-D INTERACTION I FIGURE 3-12



C-D INTERACTION II  
FIGURE 3-13



C-D INTERACTION III  
FIGURE 3-14

The concept of a multi-participant tactical information net is being investigated by the USAF. This new information system is called JTIDS -- Joint Tactical Information Distribution System. Ref. [42] describes JTIDS in detail and Section 7 examines the impact of 4-D/JTIDS integration.

The remainder of this section is devoted to a description of the impact of the JTIDS information on the 4-D C-D system and its impact on the system interaction. Before proceeding, a brief discussion of JTIDS is presented to establish a basic understanding.

JTIDS embodies a data bus or party line concept in which many users time-share a common radio channel and employ a common signal structure to communicate with one another. Individual users will broadcast sequentially in synchronized pre-assigned time slots to avoid mutual interference. The equipment has integral cryptographic security and employs spread-spectrum modulation to reduce the jamming threat.

A typical JTIDS message includes various identifiers such as class of message, source, status and mission, as well as aircraft position, speed, heading, and altitude. A user can extract data from the bus on the basis of one or more of these identifiers such as for example, by sorting incoming messages on the basis of airborne threats in a given area. The information sorting criteria is an area that must be developed in further studies since manual sorting is impractical (too time-consuming).

### **3.7.2      4-D INCADS/JTIDS Interactive Operation**

JTIDS can supply vast amounts of information. Some of the JTIDS information should be assimilated directly into the 4-D INCADS and displayed as a prospective plan change. Consider the following scenario.

An incoming JTIDS message is received indicating recent detection of a mobile SAM site near the planned flight path. The operator is alerted to the threat by the appearance of a SAM avoidance volume on his situation display and by the generation of an avoidance flight plan shown as dashed lines on the situation display. The operator has several options.

- a. He can instruct the 4-D INCADS to ignore the threat by pressing the CLEAR and ENTER buttons on the status display. This will remove the temporary plan indication and revert the situation display back to the display mode previously selected. The threat will have been assigned a system ID and will be displayed on the situation display dependent on the clutter mode selected.

- b. He can accept the changed flight plan in the same way that he would accept a manually initiated plan change by pressing the ENTER key which will cause the dashed plan to become solid and, more importantly, to be accepted as the source of steering information.
- c. He can request more information regarding the threat by pressing the ON key on the cursor control, moving the cursor to the center of the threat volume on the situation display and pressing INSERT on the cursor control. A threat page will appear on the status display listing all the pertinent information about that threat such as: location, type, time of detection, etc. He can review this data as part of his accept/reject flight plan decision.
- d. He could also request more information regarding that threat by noting its ID on the situation display then using the IDX and row column matrix on the status display to get the detailed threat data page on the status display.

The point of this example is that JTIDS information is readily integratable into the 4-D INCADS with minimum procedure change. The 4-D INCADS is a system that can adapt readily to new requirements in a positive manner with minimum change. It is a system concept that will continue to provide ready operator visibility to any depth required but one which will provide a rapid overview of factors for rapid responsible decisions.

### 3.7.3 JTIDS Information Requirements and C-D Recommendations

The large amount of information available from JTIDS could easily overwhelm a user. Message sorting criteria must therefore be established and followed such that critical information is made immediately available for operator decisions or actions, while less urgent information is placed on "file" for later review/action. Accordingly, the JTIDS message catalog was examined and the messages were classified into the following categories in accordance with their message content.

- a. Emergency warning to aircrew
- b. Urgent message receipt
- c. Non-urgent message receipt
- d. Advisory data
- e. Tactical situation
- f. Steering information
- g. Emergency report
- h. Crew inserted data

The categories are explained and display for each recommendation are made in the following paragraphs.

### Emergency Warning to AircREW

This category is reserved for a very small number of incoming messages. For these it is imperative to advise the crew not only that an emergency condition exists but also what action they should take. Some examples are (a) an approaching enemy aircraft (b) a command to break off an engagement and disarm any missile which may have been launched, (c) a surface-to-air missile (SAM) site or missile warning.

Annunciating this type message is best accomplished by the addition of voice synthesis equipment to the intercom. For example, if a JTIDS message is received indicating that your aircraft is being pursued, it is not sufficient to add an airborne threat symbol to the situation display and flash a light on the EADI. A much better solution would be to synthesize a voice message indicating threat type and position, e.g., EMERGENCY - MIG 25 IN PURSUIT BEARING 180 RANGE 2 MILES, 10 O'CLOCK. With a voice synthesizer messages can be synthesized to provide immediate advice to the aircREW, e.g.,

- a. Where to look for the enemy aircraft
- b. Command to disarm a missile
- c. How and when to maneuver to evade a SAM

Synthesized voice information can be presented to both the pilot and copilot clearly and unambiguously without causing interference to their primary tasks.

Although this same data could be presented on the status display and situation display, any visual presentation would significantly increase the crew reaction time. The crew can be looking for the enemy aircraft while listening to the voice synthesizer.

The voice synthesizer is a device which accepts digital data from the navigation computer, and transcribes the data into English language aural information. The language is of adequate clarity and inflection to minimize possible misinterpretation. In other words, the computer can talk to the crew through the voice synthesizer. A typical repertoire of synthesizer words is given in Table 3-1.

**TABLE 3-I**  
**TYPICAL VOICE SYNTHESIZER WORK REPERTOIRE**

ZERO	TWELVE	AIR
ONE	HEADING	GROUND
TWO	BEARING	ANTI-
THREE	RUNWAY	AIRCRAFT
FOUR	O'CLOCK	RADAR
FIVE	ALTITUDE	DISARM
SIX	DEGREES	REFUEL
SEVEN	RANGE	RECON
EIGHT	INTERCEPT	STRIKE
NINE	THREAT	EMERGENCY
TEN	MIG	LATITUDE
ELEVEN	SAM	LONGITUDE

#### Urgent Message Receipt

Upon receipt of urgent JTIDS messages(s), the crew should be alerted in order that they can examine the message(s) and respond to the situation. However, the indication to the crew, whether visual or aural, must be significantly different than that for an emergency warning message.

The voice synthesizer will also be used to advise the aircrew of receipt of an urgent message indicating both the message type and objective. The pilot could then examine the message in detail before transmitting his compliance response.

#### Non-Urgent Message Receipt

Receipt of many messages -- which are in neither the emergency nor urgent category -- will still require alerting the crew. A non-flashing routine message display could be illuminated until the message has been reviewed by the crew.

#### Advisory Data

Labeling this category to convey its meaning is very difficult. The intent is to include that data which is important enough to present to the aircrew but which will be available to the pilot only through the status display pages.

### Tactical Situation Data

Information in this category is data which will be used to present pictorially the tactical situation. Details of the parameters presented on the situation display will also be available for review on the status display. Since MIG and SAM locations are critical, these items will be displayed on the situation display.

### Steering Information

Messages containing real-time information are a part of the JTIDS message catalog. The essence of the 4-D INCADS is its ability to generate control information for a complex trajectory defined by a series of points that are specified by z, y, z and time-of-arrival information. The 4-D INCADS C-D system is configured to respond to waypoint information and provide the pilot with top level decision-making information that he can use to accept (or reject) the changing flight plan. The command elements (flight directors) are a part of the 4-D INCADS and they would be driven directly by JTIDS inputs but doing so would relieve the pilot of his role as decision maker. It would seem that a more 4-D INCADS-compatible solution would be to utilize the JTIDS messages for end point position coordinates in lieu of steering information. This would allow the system to calculate a real-time trajectory that the pilot has the tools (situation display, etc) to review and understand rather than to blindly fly a set of command bars driven by the JTIDS steering command outputs. Therefore, a preliminary recommendation is made that the JTIDS direct-steering information not be mechanized in the 4-D INCADS.

### Emergency Report

Several emergency messages may be sent via JTIDS. Some of these, e.g., bailout, would be automatically used and thus not be contained in the control-display information list. However, the crew must have some means of signaling an emergency. This crew-initiated emergency report is the only item in this category. An emergency report switch will be located on both the pilot's and copilot's JTIDS controls.

### Crew Inserted Data

This category contains all of the quantitative information inserted by the crew. This data includes status report, request for data, and command information and will be inserted via the status display/keyboard.

JTIDS information was categorized in the preceding paragraphs. Much of the information is readily integratable in existing 4-D INCADS C-D equipment, however, certain control functions specific to JTIDS must be provided for. Table 3-II is a preliminary assignment listing of these functions.

**TABLE 3-II**  
**JTIDS FUNCTION REQUIREMENTS**

CONTROL DISPLAY FUNCTION	LOCATION		AUTO	MANUAL	REMARKS
	PILOT	COPILOT			
<b><u>SYSTEM MODE CONTROL</u></b>					
ON/OFF		X		X	
RECEIVE ONLY		X		X	15 MIN CLOCK WARM-UP REQUIRED + GMT ESTIMATE + CODE OF DAY.
TRANSMIT/RECEIVE		X			CLOCK SYNC REQUIRED.
GMT ESTIMATE	NA	NA	X		AVAILABLE FROM 4D INCADS
CODE OF DAY	NA	NA		X	INPUTS OF INITIAL FREQ, SKIP RATE, ETC., MADE ON CONNECTOR LOCATED IN EQUIPMENT BAY. LOADED BY SPECIAL MAINTENANCE MAN.
SYSTEM TEST		X	X	X	SOFTWARE & HARDWARE TEST.
<b><u>NET STATUS</u></b>					
RELAY OPERATION			X		INCOMING MESSAGE CONTROLS.
MASTER/FAC/FLIGHT LEADER/MEMBER		X		X	ASSIGNED PRIOR TO OR DURING FLIGHT
<b><u>MESSAGE DATA</u></b>					
- OUTGOING					
-EMERGENCY	X	X	X	X	MUST BE ABLE TO INDICATE EMERGENCY CONDITION & MOST INFORMATION AVAIL- ABLE IN DPU & REVIEW WILL BE NECESSARY
-ROUTINE P1 DATA		X	X	X	
- INCOMING		X			INCOMING MESSAGE MUST BE SORTED FOR URGENCY & STORED FOR REVIEW.
<b><u>TRACKER</u></b>					
SELECT TRACKING SYSTEM MANUAL		X		X	SELECTS SYSTEM TO OUT- PUT TRACK INFORMATION

## **4 SYSTEM SIMULATOR**

### **4.1 INTRODUCTION**

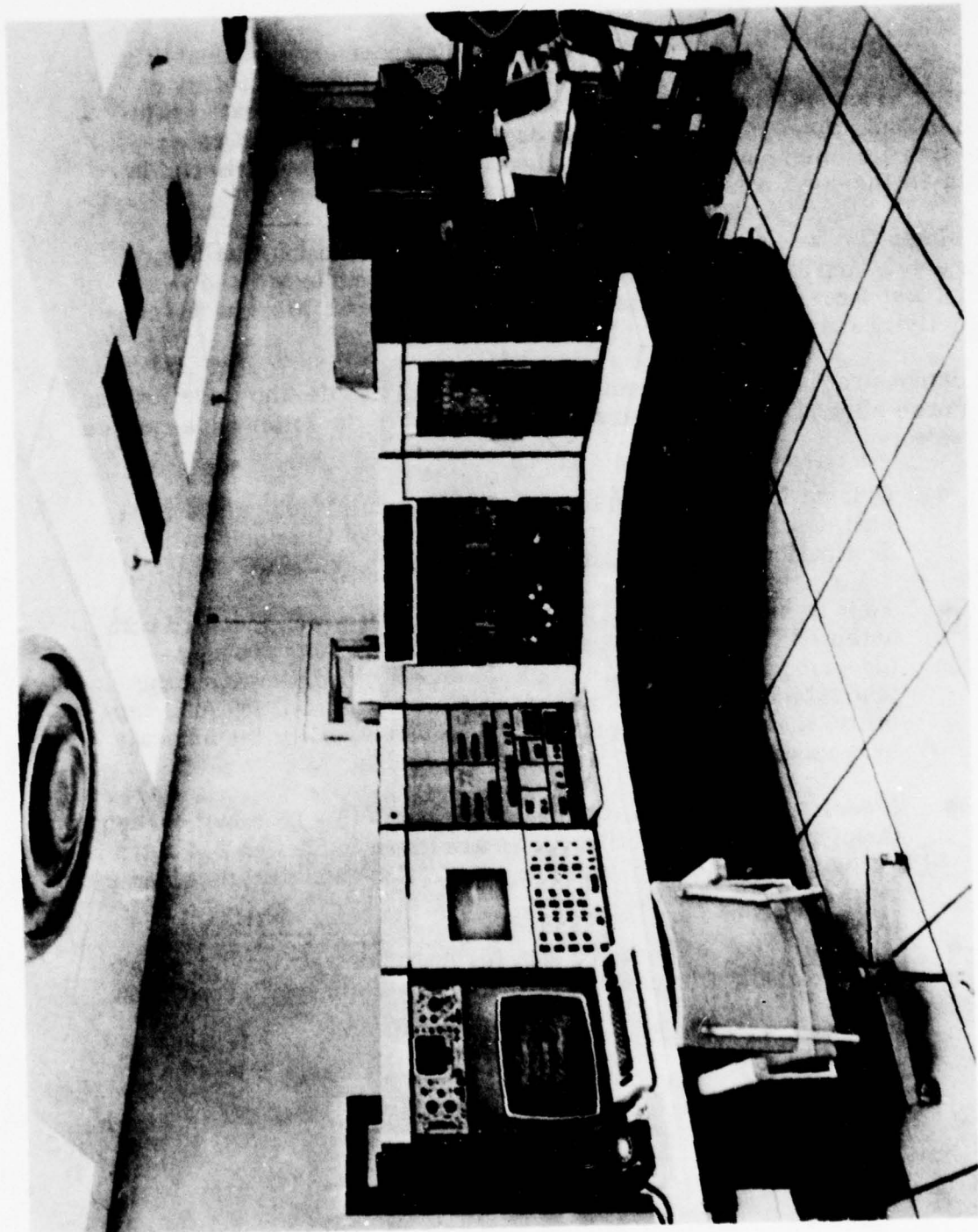
A hybrid simulator was developed to demonstrate the capability of the 4-D profile generation and control algorithms and the ability of the pilot to successfully interact with the system. The accurate evaluation of this pilot/system interaction during various phases of representative 4-D missions dictated that the simulation be accomplished in a man-in-the-loop, real-time environment.

The simulation was performed in the LSI Hybrid Computing Facility, Figure 4-1, and allowed the 4-D INCADS concept to be exercised in a typical transport cockpit environment with experienced pilots at the controls, flying four-dimensional profiles.

The demonstrations were conducted using two LSI people who were former Air Force pilots. The demonstrations consisted of the following sequence of events.

- Orientation briefing on the 4-D INCADS philosophy and a general description of the missions in terms of time criticality, destinations, and aircraft (A/C) control requirements.
- Four to six hours of training in the cockpit which involved both automatic and manual flying of a special training profile (described in Section 3.4) with the intent of familiarizing the test subject with the simulator hardware, the 4-D INCADS capability, and to give the pilot practice in controlling the aircraft in response to steering and throttle cueing.
- A series of short man-in-the-loop flights (15 - 25 minutes each). Description of the profiles flown are given in Section 2.4 and a discussion of the man-machine interaction capability is given in Sections 3.4 and 3.5.
- The collection of objective data (path tracking accuracy) on two test profiles. Discussions of the test data are given in Section 2.5.

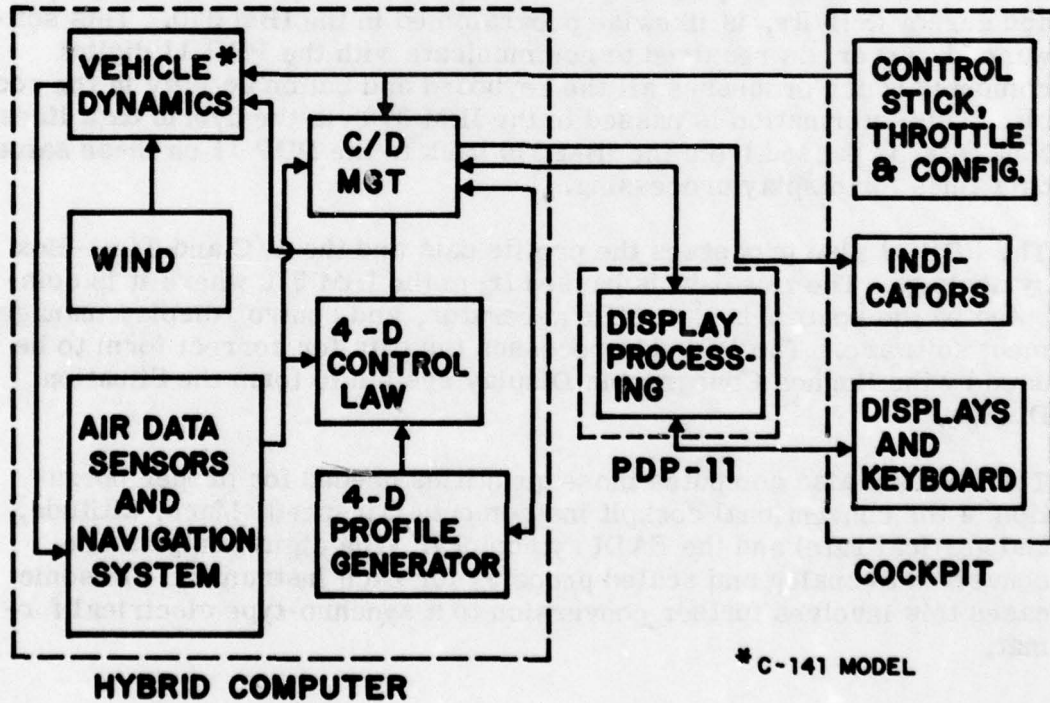
LSI HYBRID COMPUTING LABORATORY  
FIGURE 4-1



## 4.2 SIMULATION DESCRIPTION

The system configuration for the 4-D INCADS system is shown in Figure 4-2, which shows the informational flow among the various elements of the simulation. Those primary elements are listed here.

- Applied Dynamics Model AD/4 Hybrid Computer which has extensive digital logic capability, 16 analog-to-digital converters, sense and control lines, and 108 digitally set coefficient devices, in addition to the usual analog computing elements.
- Applied Dynamics Model AD/256 Analog Computer with full analog trunking to the AD/4.
- Digital Equipment Corporation (DEC) PDP 11, Model 20 digital computer with magnetic tape and disc memory units.
- IBM 370 Model 155 digital computer with associated disc memory, magnetic tape unit, printers, plotters, etc. By use of hybrid interface units (HIF & RIF) the IBM 370, AD/4 and PDP 11 are able to communicate with each other.



SYSTEM CONFIGURATION  
FIGURE 4-2

- Transport type, dual seat cockpit with its associated displays and controls.
- Hughes Conograph System - used with a cockpit-mounted TV monitor to form the situation display.

The vehicle dynamics consisted of modeling the rotational and translational equations of motion for a C-141 transport aircraft in analog fashion on the AD/4. Because of the varied operational conditions imposed by the four-dimensional profiles, it was necessary to curve-fit many of the lift and drag coefficient components and solve those curve-fits digitally on the IBM 370. The IBM 370 is used to update the digital coefficient devices on the AD/4 at a 20-Hz rate.

In addition, simple models for wind components, an air data sensor, and a navigation system were mechanized digitally and incorporated as part of the IBM 370 program.

The 4-D control law and profile generator algorithms were also programmed on the IBM 370. A complete description of these is included in Section 2.

The control and display management, which does the bookkeeping for data display changes, page requests, flight plan requests and display, and cursor activity, is likewise programmed in the IBM 370. This software, however, is required to communicate with the PDP 11 digital computer which processes all the keyboard and button activity in the cockpit. This information is passed to the IBM 370 via the hybrid data lines. New data is passed from the IBM 370 back to the PDP 11 on these same data lines for display processing.

The PDP 11 also processes the profile data and the A/C and Time-Box symbology. The raw data is passed from the IBM 370 where it is computed by the control law, profile generator, and control/display management software. The PDP 11 processes the data for correct form to be used by the Hughes Conographic Display system to form the Situation Display.

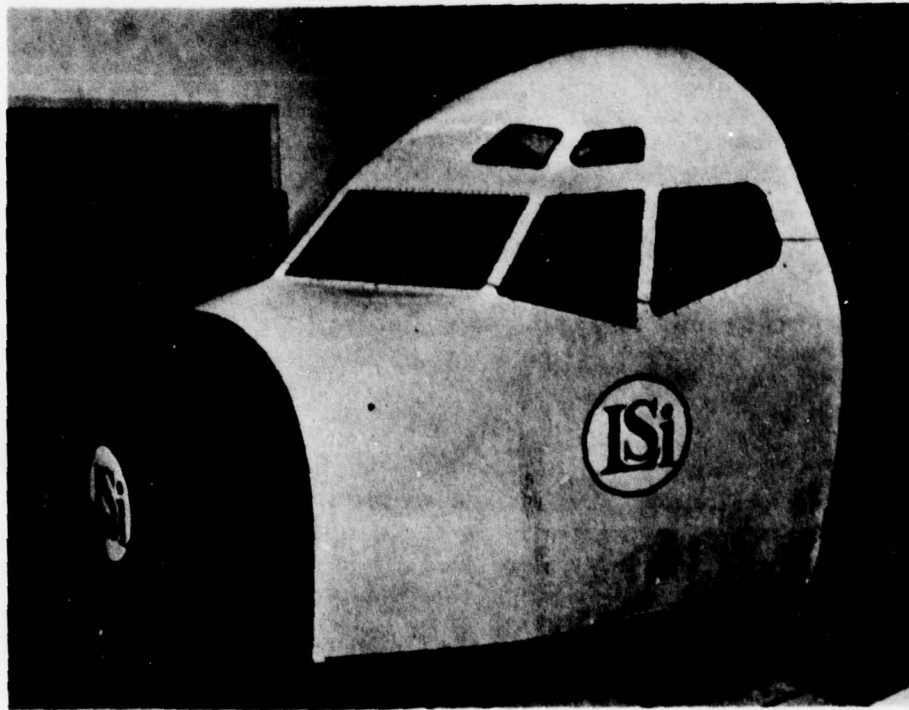
The IBM 370 also computes those quantities needed for proper operation of the conventional cockpit instruments (airspeed, Mach, altitude, and vertical rate) and the EADI symbology. The digital outputs are converted to analog and scaled properly for each instrument. In some cases this involves further conversion to a synchro-type electrical format.

In addition, the outputs of the control stick, throttle, flaps, spoiler and gear controls are routed to the hybrid computer to be used by the simulation.

#### 4.2.1 Transport Cockpit

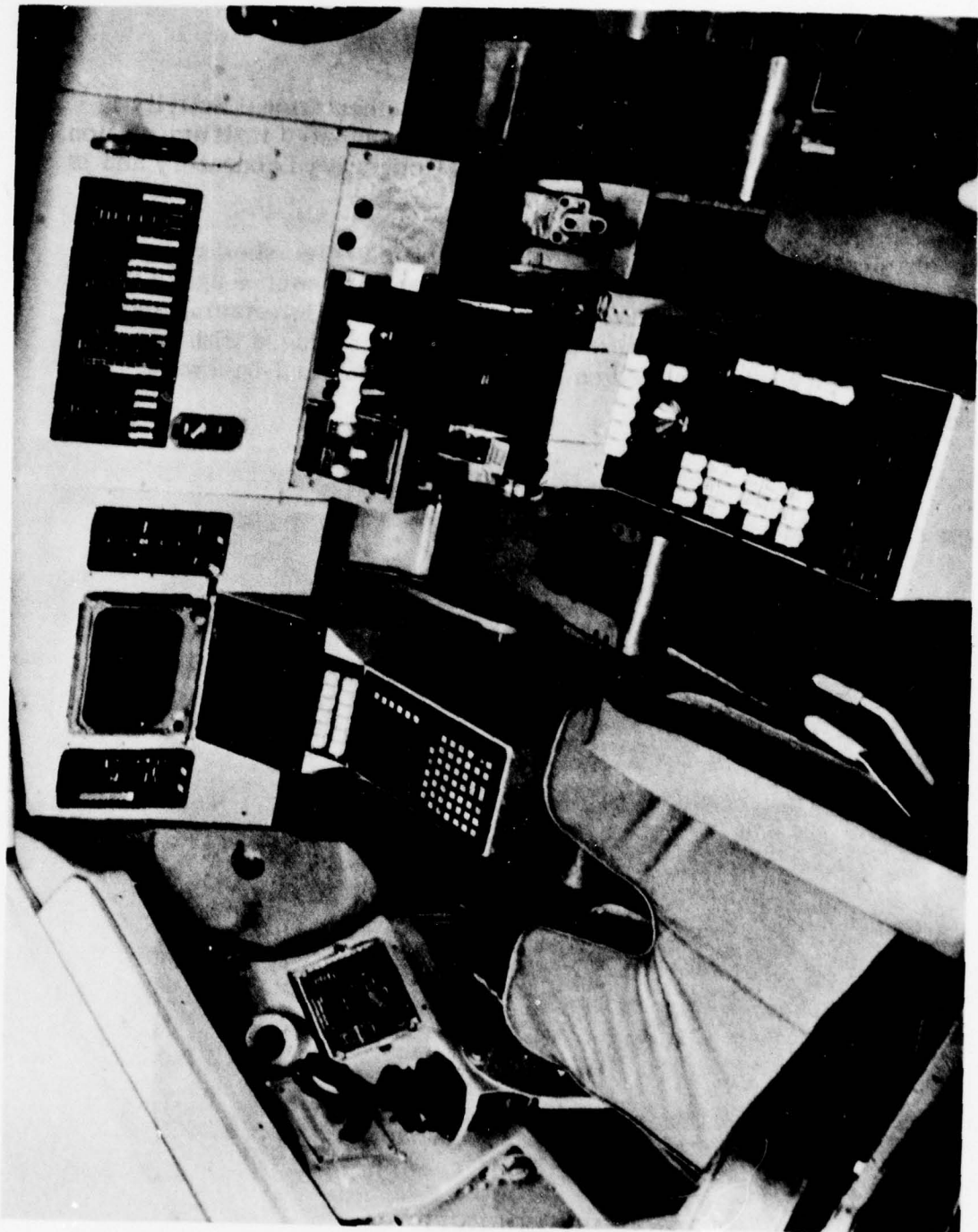
The focal point for all the simulation computational activity is a transport cockpit shown in Figure 4-3 and its associated instrumentation. A KC-135 cockpit was installed in the Hybrid Computing Laboratory and is configured as shown in Figure 4-4.

The mechanical layout of the cockpit consists of the outer shell complete with frosted windows and a blunt, fiberglass nose to conserve space but provide protection for the bulkhead-mounted electrical interfacing and power supply racks. The interior of the cockpit is equipped with two fully upholstered flight seats mounted on rails for easy forward-backward adjustment.



TRANSPORT COCKPIT  
FIGURE 4-3

DUAL SEAT TRANSPORT COCKPIT  
FIGURE 4-4



The instrument panel is augmented by an overhead panel with dummy switches, several side panels, a full throttle quadrant, a side-stick controller on the pilot's side, a center console which was enlarged to accommodate additional 4-D controllers, and a conventional KC-135 control column/wheel mounted on the copilot's side. Mechanically-coupled rudder pedal assemblies are installed in both sides of the cockpit.

For discussion purposes the cockpit instrumentation has been grouped into three categories: primary displays, secondary displays, and controls.

#### Primary Displays

- Electronic Attitude Director Indicator (EADI)
- Situation Display
- Status Display and Keyboard

#### Secondary Displays

- Altitude, Vertical Velocity Tape
- Mach, Indicated Airspeed Tape

#### Aircraft Controls

- Side-stick controller for pitch and roll
- Pitch and roll trim switch located on side-stick controller
- Servoed throttle quadrant
- Percent flaps control
- Spoiler switch
- Landing gear switch
- Cockpit advisory lights
- Control column and wheel (on right side only)
- Situation Display Cursor Controller

#### 4.2.1.1 Primary Displays

The primary displays consist of the electronic attitude director indicator (EADI), the electronic situation display, and the status display and its associated keyboard.

##### Electronic Attitude Director Indicator (EADI)

The EADI is a Sperry unit previously used on the Air Force Flight Dynamic Laboratory (AFFDL) C-141 AWLS aircraft, and is government-furnished for the simulation. The following signals are provided in

the proper electrical form as defined in the Sperry Flight Systems Specification 5512-1216:

- Pitch attitude
- Roll attitude
- Drift angle
- Radio altitude
- Flight path angle
- Flight path acceleration
- Rate of turn
- Speed error (used as throttle error)
- Pitch command bar
- Roll command bar

A backup to the EADI is a Lear Siegler Model 4058AC electro-mechanical ADI (supplied by LSI). Proper cabling and the appropriate electrical signals for this ADI are provided.

All EADI and ADI signals are updated at a 20-Hz rate to avoid CRT flicker and mechanical chatter. The EADI symbology is labeled in Figure 3-11.

#### Situation Display

The system information requirements for the government-furnished equipment (EADI, vertical tape indicators) are well defined; therefore, the effort of interfacing this equipment with the hybrid computer was required for incorporation into the system. The majority of the work was in the development of the situation display and the status display/keyboard.

The situation display presented a real challenge since a programmable symbol generator was required which would be flexible enough to present various information to the pilot in various stages of the 4-D missions.

To obtain the necessary flexibilities, a trade study of various display systems was made. These included considerations of the following items:

- Stroke written or raster
- Type of refresh memory
- Dynamic capabilities
- Flexibility for scale changing, rotation, etc.
- Potential for advanced display concepts: i.e., color

**Many companies were surveyed to determine availability of display systems:**

Adage  
Tektronix  
Ram Tek  
Hughes

Vector General  
Sanders  
Kaiser

The display system with the most potential was the Hughes Conograph System. This system has the capability of providing the situation displays described in Section 3, and of being readily reprogrammed to draw any future symbology defined.

#### Status Display/Keyboard

The status display/keyboard is a hardware item developed by LSI for the study program. The controller is interfaced to the PDP 11 computer, which transmits display formats and data to the status display and receives all keyboard inputs.

An LSI-developed CRT data terminal was modified to provide this interface. The familiar ASCII code is serially transmitted in a full duplex mode to the PDP 11 computer. The keyboard and display formats are flexible enough to allow interchange of buttons and code to meet the operator's needs.

A complete discussion of the situation display symbology, the page definitions and use of the status display/keyboard is included in Section 3.

#### **4.2.1.2 Secondary Displays**

The secondary displays consist of the two vertical tape displays, both of which were GFE. To the right of the EADI is mounted the altitude, vertical velocity display, and immediately to the left is the Mach/indicated airspeed display. Both displays are provided with properly scaled synchro-type signals for correct operation. The cockpit layout -- Figure 4-4 -- shows the placement of the primary and secondary displays.

#### **4.2.1.3      Controls**

The cockpit instrumentation controls for this real-time simulation are as follows:

##### **Side-Stick Controller**

A two-axis displacement type hand controller is provided on the pilot's side of the cockpit for the purposes of providing elevator and aileron control. In addition to providing roll and pitch control, the side-stick controller has a top-mounted, spring-loaded, four-direction switch for pitch and roll trim. Both pitch and roll trim are implemented.

A slide switch, integrally mounted as a part of the side-stick, is utilized as the on-off switch for the pitch and roll augmentation. A trigger switch, also an integral part of the side-stick, is utilized to enable the control wheel steering mode (CWS). In this mode the outputs of the control stick, rather than being coupled directly to the elevator and ailerons, are treated as rate outputs and integrated by the software to be applied to the pitch and roll augmentation. This mode allows the pilot to override any automatic modes -- which are normally providing inputs to the augmentation system -- by using the hand controller to provide perturbation commands to the system.

##### **Throttle Quadrant**

The throttle quadrant is provided with a positioning servo for automatic operation. The positioning servo is linked to the throttle through an electrically actuated clutch. The throttle position pot is attached in such a manner as to always indicate throttle position independently of the position of the servo-driven side of the clutch. The torque capability of the clutch and motor are sufficient to drive the throttle quadrant against a moderate amount of preset friction; however, the torque capability of the clutch is less than that provided by the servo motor and that which may be manually applied to the throttle handles. This allows the servo system to be manually overridden for simulated emergency situations and without damage to the servo system. The electric clutch is actuated by the master autothrottle switch on the throttle quadrant. The flap control handle, for variable flap setting, and a spoilers switch are part of the throttle quadrant console.

##### **Control Column**

The copilot's side is equipped with a conventional KC-135 control column and wheel. The column and wheel are spring-damper loaded to provide a reasonable duplication of A/C feel.

### Gear

A landing gear handle switch is provided and was operational. The position of the switch is bent to the hybrid computer where it is used in the A/C simulation.

### Cockpit Advisory Lights

Mounted between the EADI and the situation display are three red, rectangular lights labeled FLAPS, SPOILERS, and GEAR (see Figure 3-8). These are illuminated by software under control of the flight control laws to indicate that action with respect to these controls is required at some point during the current flight leg. When the action is taken, which is at the judgment of the pilot, the appropriate advisory light are extinguished by software control.

### Cursor Control Panel

The cursor control panel, which is associated with the situation display, is shown in Figure 3-9. This panel is mounted just below the throttle quadrant and is used to control the position and designate the use of the situation display cursor. A complete description of this controller is provided in Section 3.5.3.

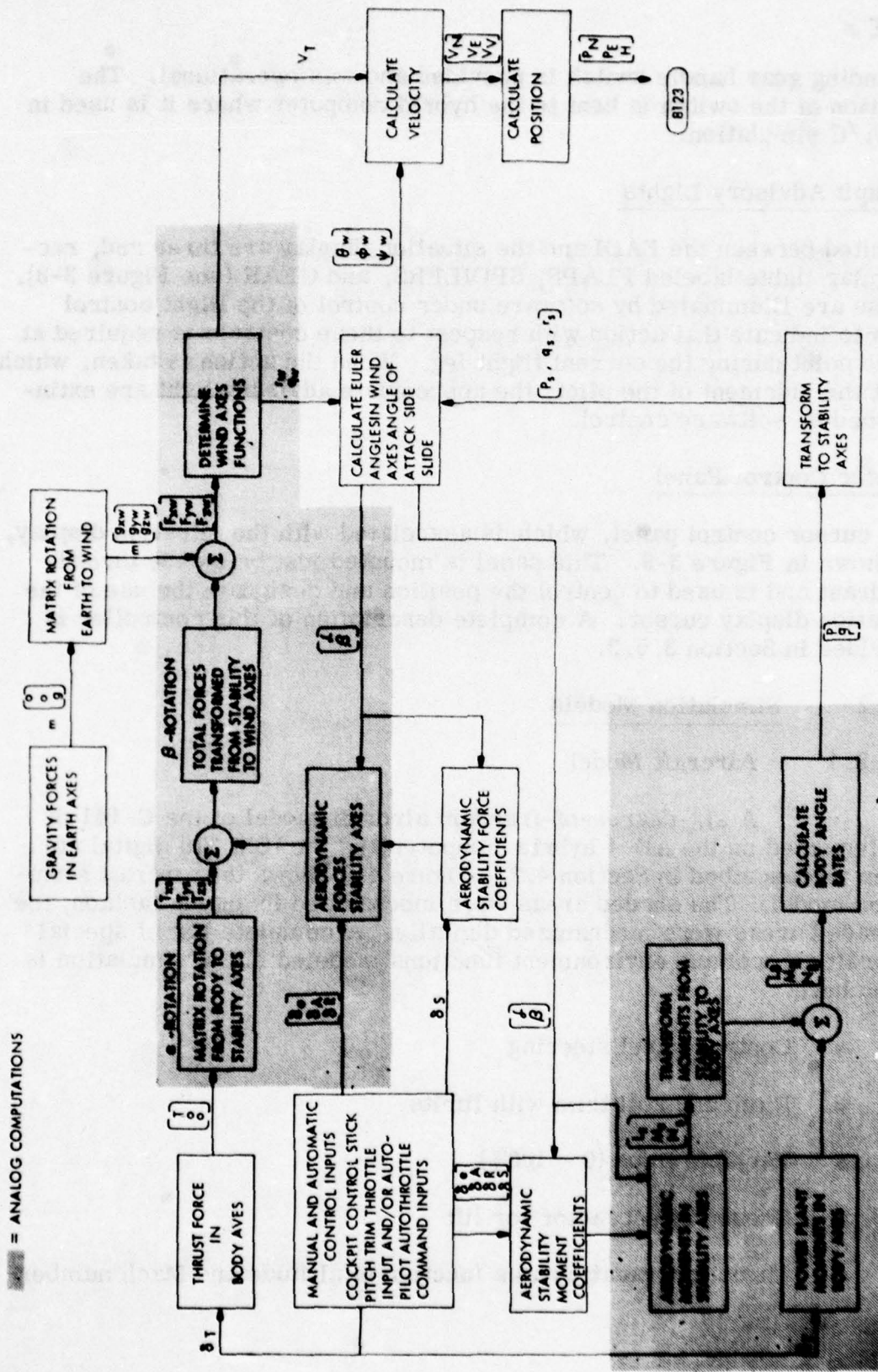
## 4.2.2      Simulation Models

### 4.2.2.1    Aircraft Model

A six-degree-of-freedom aircraft model of the C-141 is implemented on the AD/4 hybrid computer and the IBM 370 digital computer as described in Section 4.2. Figure 4-5 shows the aircraft simulation model. The shaded areas were mechanized in analog fashion; the unshaded areas were mechanized digitally. A complete list of special aircraft control and environment functions modeled in the simulation is given here.

- Control wheel steering
- Pitch and roll trim with limits
- Variable flaps (0 - 100%)
- Ground effect factor for lift
- Thrust degradation as a function of altitude and Mach number

C-141 AIRCRAFT SIMULATION FLOW CHART



A/C SIMULATION MODEL  
FIGURE 4-5

- Dynamic engine lag
- High rate digital curve fitting of A/C lift and drag coefficients as a function of flight conditions
- Engine-induced drag at low throttle settings
- Stall speed computed as a function of flaps
- Spoiler drag
- 'Gear down' drag

#### 4.2.2.2 Path Generation and Control Laws

The profile synthesis and control laws as discussed in Section 2 were programmed on the IBM 370.

#### 4.2.2.3 Environmental Model

The environmental model provided the following outputs in digital format for the cockpit indicators and the aircraft model.

- Ambient temperature as a function of sea level temperature, altitude, and lapse rate
- Sonic velocity as a function of ambient temperature
- ICAO standard atmosphere temperature and pressure
- Atmospheric density
- Pressure altitude
- Static pressure

#### 4.2.2.4 Yaw Damper and Pitch/Roll Augmentation

The yaw damper and pitch and roll augmentation functions are modeled in analog fashion on the AD-256, and are contractions of analog models described in Ref. [19]. The position servos in these augmentation units were not modeled because their rates were sufficiently high to cause only negligible effects on their respective loops.

## **5 INTEGRATED LORAN INERTIAL NAVIGATION ANALYSIS**

### **5.1 GENERAL**

This study assessed the feasibility of using different radio navigation-inertial system configurations, where each system provides aircraft position, velocity, heading and attitude to the 4-D INCADS control laws for aircraft guidance during terminal area approach and landing. Integrated navigation techniques are being considered where the system's navigational computer uses a data processing technique, referred to in this report as an integration filter, to combine the information supplied by the different navigation sensors into solutions that have more accuracy than the measurements of any sensor by itself. This study considered the Loran system and the Global Positioning System (GPS) as two possible radio navigation sensors; considered the barometric altimeter for altitude information; and considered the following classes of inertial systems:

- a. Low quality (20 nm/hr) inertial navigation systems
- b. Medium quality (5 nm/hr) inertial navigation systems
- c. High quality (1 nm/hr) inertial navigation systems, and
- d. Doppler Radar with an Attitude and Heading Reference System (AHRS)

The analysis and simulation effort of this study concentrated on the approach and landing phase, where the aircraft is guided by the 4-D INCADS down to the final approach waypoint using the radio/inertial navigation system, under IFR conditions. At this point, the system switches to the guidance signals from the airfield's landing aid instruments (ILS, MLS, or similar instruments) and uses these signals along with information from a radar altimeter and the inertial system as inputs to the path control system for aircraft landing. For emergency landing situations, the radio/inertial navigation system would be used for landing guidance.

The capture of the landing aid's beam and the switching from the radio navigation sensor measurements to the landing aid guidance signals must be repeatable and must be accomplished without significant path transients at the final waypoint. Consequently, the location of the final waypoint relative to the landing aid transmitters is significant. To maximize the use of the nonlinear approach paths -- which provide flexibility for avoiding hostile forces or obstacles -- requires minimization of the distance along

the fixed guidance beam between the final waypoint and the touchdown point. A system performance goal is to have the path tracking accuracy that allows the final approach waypoint to be as close as 1/2-mile from touchdown.

To establish a radio/inertial technique that minimizes the horizontal position error contribution to the total path tracking error, the study investigated a differential Loran configuration where the 4-D INCADS outputs accurately establish the location of the aircraft in the Loran navigation grid defined by the signals transmitted from the chain of Loran stations. To provide the location of the guidance beam, a Loran receiver on the ground establishes the location of the runway in the Loran navigation grid. To minimize the altitude error contribution to the path tracking uncertainty, this study investigated the performance of a differential baro technique, where a barometric altimeter on the ground (co-located with the ground Loran receiver) establishes the runway pressure altitude and the 4-D INCADS vertical navigation is relative to the pressure measurements, not the absolute altitude above sea level. A data link is required for transmitting the ground-measured Loran and barometric information to the airborne 4-D INCADS.

The objectives of the navigation system analysis activity are

- a. Establish the feasibility of various differential Loran/inertial configurations described above for horizontal approach guidance,
- b. Establish the feasibility a differential baro/inertial technique for vertical guidance down to the final approach waypoint,
- c. Establish the minimum decision altitude and minimum visual distance to runway for 4-D INCADS emergency landing mode where differential Loran/inertial is used for horizontal guidance and differential baro/inertial is used for vertical guidance,
- d. Establish the data link requirements for the 4-D INCADS, and
- e. Assess the impact on the 4-D INCADS system of replacing Loran with GPS.

The last analysis activity -- the integration of GPS with inertial data in the 4-D INCADS -- is discussed in Section 6. Besides Loran and GPS, there are other radio navigation sensors that can provide the navigation

inputs for the 4-D INCADS. Section 9 discusses the use of Omega and the Microwave Landing System (MLS) in the 4-D INCADS.

To determine the feasibility of each Loran/inertial configuration and baro/inertial configuration for IFR approach guidance, position and velocity performance goals were defined for the navigation system. These goals were based on well-established performance results for Loran and baro sensors integrated with one nm/hr inertial systems. These performance goals are:

Horizontal Position:	75 feet ( $1\sigma$ )
Vertical Position:	10 feet ( $1\sigma$ )
Vertical Velocity:	2 feet/sec ( $1\sigma$ )
Horizontal Velocity:	3 feet/sec ( $1\sigma$ )

The navigation performance parameters define the contribution of the navigation system to the 4-D INCADS system's path tracking uncertainty. The total uncertainty in the 4-D INCADS trajectory-following capability is a summation of the navigation system's errors and the 4-D control law path-tracking errors. Section 2 combines the navigation system's performance results with the control law tracking results to establish the total profile following performance. In assessing the trajectory-tracking capability, Section 2.5.1 establishes that the final waypoint of the nonlinear approach path can be 1/2 mile from touchdown during IFR operations.

This section's analysis establishes whether the measurements provided by the sensors in each Loran/inertial configuration have the desired accuracy, and establishes the complexity of the data processing technique that is required for integration of the sensor information.

The following navigation analysis has been performed:

- a. Analysis of the different differential Loran/inertial navigation configurations,
- b. Analysis of the differential baro/inertial technique, and
- c. Specification of the data link requirements.

The section begins with general definitions of a differential Loran strapdown inertial, a differential baro/inertial, and differential Loran/Doppler/AHRS mechanizations and then develops a comprehensive error model that includes differential equations for the errors in both the horizontal and vertical channels of the 4-D INCADS navigation system.

To evaluate the horizontal and vertical channel performance analytically, the equations of the basic error model are approximated and closed form expression derived for the sensitivities of the different differential Loran/inertial system configurations and the differential baro/inertial system to individual Loran, inertial, and barometric measurement errors. To obtain closed form expressions for the system errors it was assumed the integration filter damps out only the inertial position and velocity errors with the Loran measurements. The analytical evaluation effort resulted on the following conclusions:

- a. A differential Loran/inertial system using 1 nm/hr inertial systems does provide a horizontal position accuracy of  $\sigma^* 5$  feet ( $1\sigma$ ) and a horizontal velocity accuracy of 3 feet/sec ( $1\sigma$ ) under realistic Loran error conditions.
- b. To integrate a 1 nm/hr inertial system with differential Loran and achieve the performance goals requires a data processing technique that uses Loran to correct the position and velocity errors of the inertial system. Integration with 5 and 20 nm/hr inertial systems requires integration filters that correct the inertial position, velocity, heading and attitude errors with Loran data.
- c. A differential baro/inertial technique satisfies the vertical performance requirements for the approach phase. A pilot-inserted table of pressure vs. altitude will not be necessary to achieve the desired differential baro performance.
- d. Emergency landing using differential Loran/inertial for lateral guidance and differential baro/inertial for vertical guidance is acceptable. However, the horizontal and vertical position accuracies are not sufficient for blind landings. The decision height and runway visual range (RVR) landing parameters are dependent on the runway width and length and the type of airfield (austere, forward operating base, and main operating base). For austere airfields with short and narrow runways, 150 feet decision heights and 1/2 nm RVR's are recommended. A radar altimeter and an independent forward looking radar are recommended for use with the inertial, Loran, and barometric information to safely perform "zero-zero" emergency landings.
- e. A differential Loran/Doppler/AHRS system does not meet the horizontal velocity goal of 3 feet/sec ( $1\sigma$ ) during trajectory turns if only position and velocity damping are used in the integration filter. To meet the velocity accuracy goal, an integration filter that corrects for heading and attitude errors in the AHRS will be necessary.

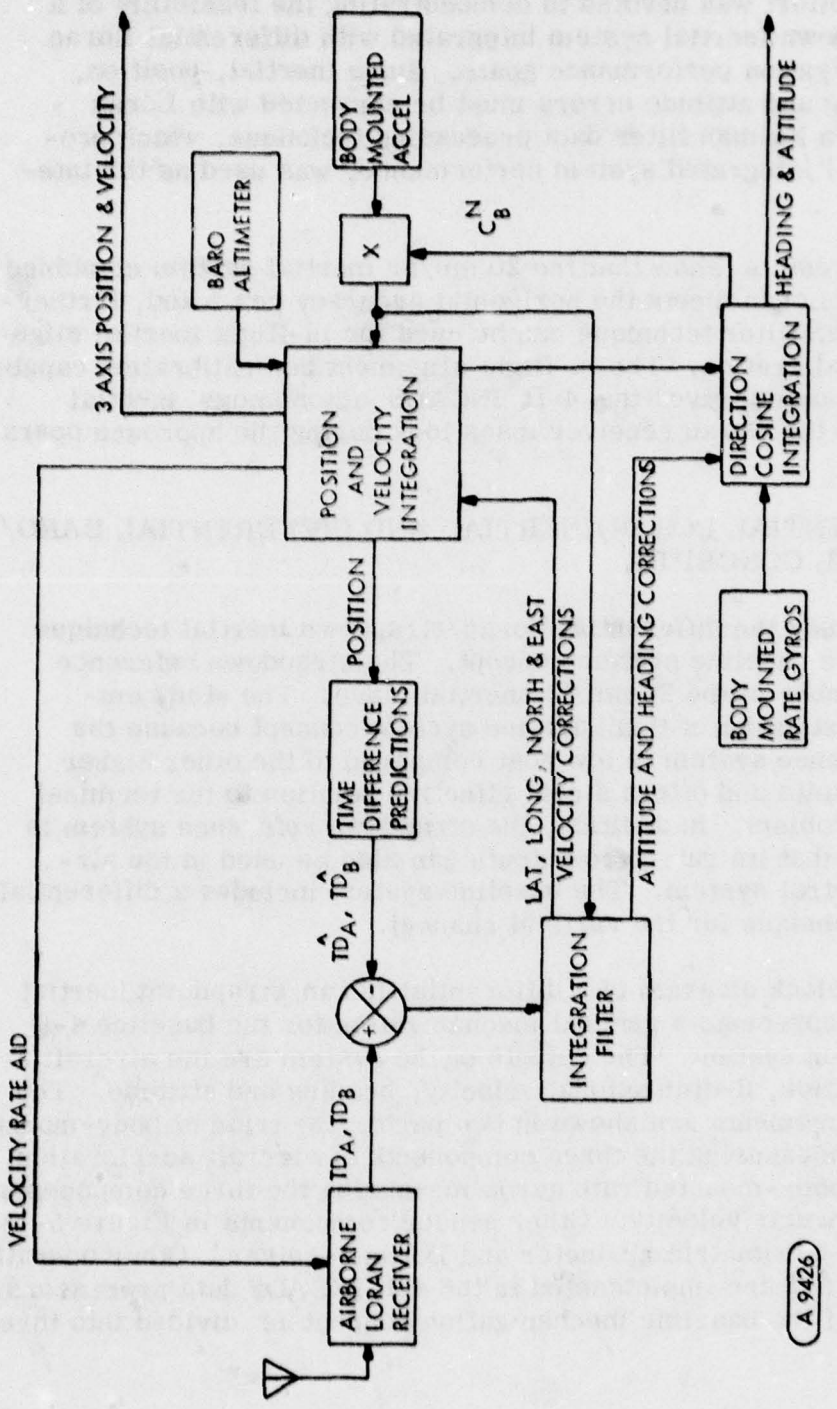
In addition to the analytical evaluation effort, the study uses a digital computer simulation to analyze the differential Loran/inertial system. The simulation effort was devoted to demonstrating the feasibility of a 20 nm/hr strapdown inertial system integrated with differential Loran to attain the navigation performance goals. Since inertial, position, velocity, heading and attitude errors must be corrected with Loran measurements, a Kalman filter data processing technique, which provides the optimal integrated system performance, was used as the integration filter.

The simulation results show that the 20 nm/hr inertial system combined with differential Loran meets the horizontal accuracy goals and, furthermore, the Kalman filter technique can be used for in-flight inertial alignment and gyro calibration. The in-flight alignment and calibration capability is important because it gives the 4-D INCADS autonomous inertial guidance in case the Loran receiver loses lock during the approach operation.

## 5.2 DIFFERENTIAL LORAN/INERTIAL AND DIFFERENTIAL BARO/INERTIAL CONCEPTS.

In this study the differential Loran/strapdown inertial technique was selected as a baseline system concept. The strapdown reference system is a member of the 20 nm/hr inertial class. The study emphasized the investigation of this baseline system concept because the strapdown reference system is low cost compared to the other higher quality inertial units and offers a cost effective solution to the terminal area guidance problem. In addition, the strapdown reference system is cost effective in that its rate gyro outputs can also be used in the aircraft's flight control system. The baseline system includes a differential baro/inertial technique for the vertical channel.

Figure 5-1 is a block diagram of a differential Loran/strapdown inertial system, which represents a general mechanization for the baseline 4-D INCADS navigation system. The outputs of the system are the aircraft 3-dimensional position, 3-dimensional velocity, heading and attitude. The strapdown measurements are shown in two parts: the triad of body-mounted accelerometers measuring the three components of aircraft acceleration, and the triad of body-mounted rate gyros measuring the three components of the aircraft angular velocity. Other sensor components in Figure 5-1 are the airborne barometric altimeter and Loran receiver. Other operations shown in Figure 5-1 are implemented in the 4-D INCADS data processors. The discussion of the baseline mechanization concept is divided into three



AIRBORNE LORAN/STRAPDOWN INERTIAL NAVIGATION SYSTEM  
FIGURE 5-1

parts: (1) Loran receiver principles, (2) strapdown inertial navigation processing and (3) integration filter processing.

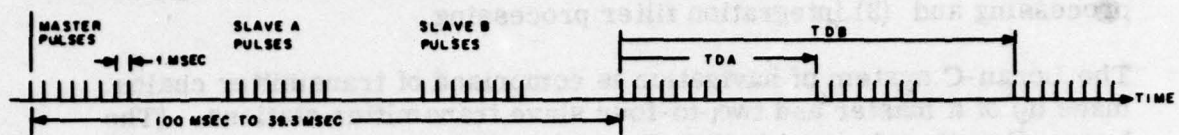
The Loran-C system of navigation is comprised of transmitter chains made up of a master and two-to-four slave transmitter stations. (The Loran-C system is used in this discussion; however, the Loran-D principles are the same--the only difference lies in the detailed signal structure.) All of these stations transmit eight pulses periodically as shown in Figure 5-2a. The spacing between pulses is 1 millisecond and the group repetition period for a given chain is fixed somewhere between 30.3 and 100 milliseconds. The Loran pulse, as shown in Figure 5-2b, has a peak at about 70 microseconds. The pulses are phase coded with 0-degree or 180-degree phasing as shown in Figure 5-2c. For identification purposes, the phase code of the master transmitter is different from that of the slave code and the master code repeats every two Loran periods as shown in Figure 5-2d. The signal transmission times for the stations of a chain are synchronized such that each slave station transmits with a predetermined emission delay after the master transmission.

The function of a Loran receiver is to receive the signals of three stations and measure precisely the difference in time of arrival between the master and each slave signal. The receiver groundwave as well as skywave signals are shown in Figure 5-2e. The skywave signals arrive later in time than the groundwave signals. For an accurate difference in signal time-of-arrival measurement, the receiver must select the highest amplitude cycle of the groundwave signal which is free of skywave contamination on all stations. Once this cycle selection has been made, measurement of its time-of-arrival via phase tracking will yield the desired time difference between the master and slave signals ( $TD_A$  for master and slave A and  $TD_B$  for master and slave B).

When a Loran receiver is located in an area where it can receive groundwave signals from the master and at least two slave stations, its position can be determined from the measured time differences. This follows from the fact that each such time difference is mapped into a constant time difference hyperbolic line of position (LOP) on the surface of the earth. The intersection of the two hyperbolae corresponding to the two measured time differences defines the present position of the receiver as shown in Figure 5-2f. Based on an earth model, the measured time differences can be converted to the latitude and longitude of the receiver.

In the differential Loran/strapdown inertial system, position is not determined directly from the time differences ( $TD_A$ ,  $TD_B$ ). Instead, the

a) Loran-C Signals

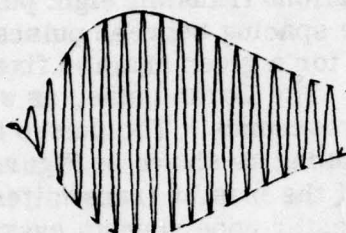


b) Loran-C Pulse

$$f(t) = \left(\frac{t}{\tau_1}\right)^2 e^{2-\frac{t}{\tau_1}} \sin \omega_0 t$$

$$\tau_1 = 70 \text{ usec}$$

$$\omega_0 = 2\pi \cdot 10^5$$



c) Phase Coding

+ or 0°



- or 180°



d) Phase Codes

0° = +

Master: + + - - + - +

Slaves: + + + + - - +

180° = -

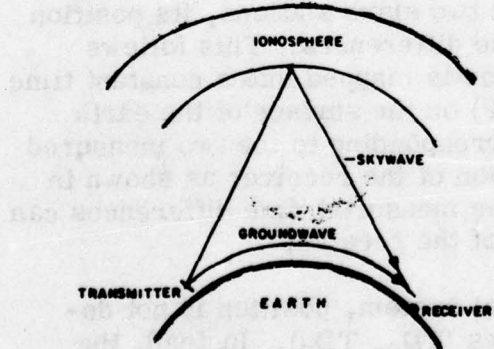
+ - - + - + -

+ + + + - - +

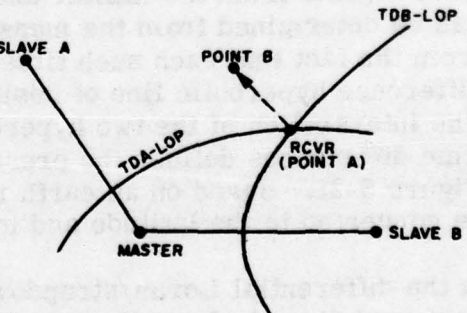
+ - - + + + +

+ - - + - + -

e) Skywaves



f) Hyperbolic Position



**LORAN-C SYSTEM PRINCIPLES  
FIGURE 5-2**

time difference information, which has good long-term tracking accuracy during non-dynamic aircraft maneuvers, is combined with the strapdown inertial system data, which provide accurate short term measurements of the aircraft state, to obtain accurate integrated navigation solutions both in the long term and the short term and during all aircraft maneuvers.

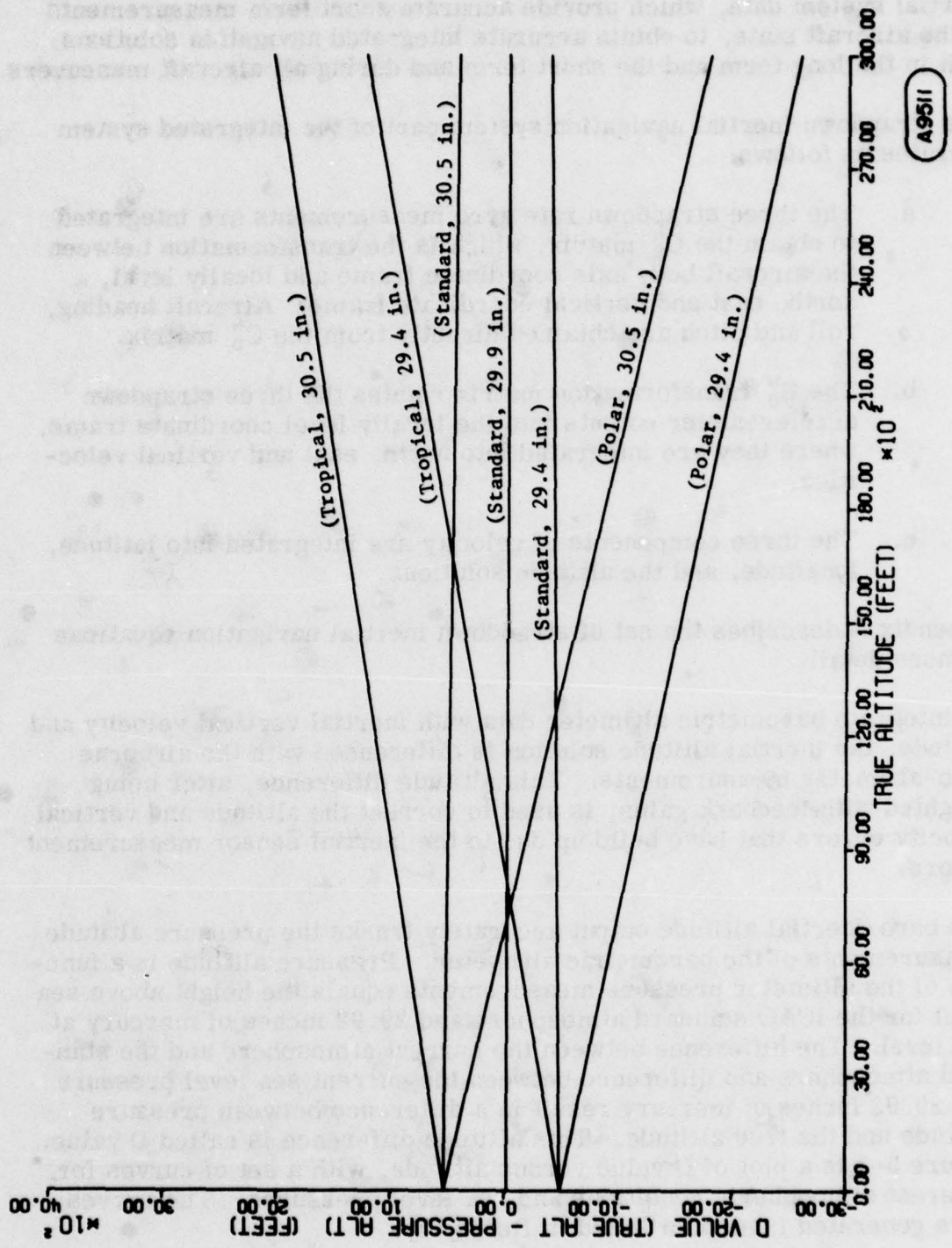
The strapdown inertial navigation system part of the integrated system operates as follows:

- a. The three strapdown rate gyro measurements are integrated to obtain the  $C_B^N$  matrix, which is the transformation between the aircraft body axis coordinate frame and locally level, north, east and vertical coordinate frame. Aircraft heading, roll and pitch are obtained directly from the  $C_B^N$  matrix.
- b. The  $C_B^N$  transformation matrix rotates the three strapdown accelerometer outputs into the locally level coordinate frame, where they are integrated into north, east and vertical velocities.
- c. The three components of velocity are integrated into latitude, longitude, and the altitude solutions.

Appendix A describes the set of strapdown inertial navigation equations in more detail.

To integrate barometric altimeter data with inertial vertical velocity and altitude, the inertial altitude solution is differenced with the airborne baro-altimeter measurements. This altitude difference, after being weighted with feedback gains, is used to correct the altitude and vertical velocity errors that have build up due to the inertial sensor measurement errors.

The baro/inertial altitude output accurately tracks the pressure altitude measurements of the barometric altimeter. Pressure altitude is a function of the altimeter pressure measurements equals the height above sea level for the ICAO standard atmosphere and 29.92 inches of mercury at sea level. The difference between the current atmosphere and the standard atmosphere and difference between the current sea level pressure and 29.92 inches of mercury result in a difference between pressure altitude and the true altitude. This altitude difference is called D value. Figure 5-3 is a plot of D value versus altitude, with a set of curves for different atmospheric conditions and sea level pressures. The curves were generated from data listed in Ref. [10].



REPRESENTATIVE D VALUE VERSUS ALTITUDE DATA  
FIGURE 5-3

With the 4-D INCADS differential baro technique, navigation is relative to pressure altitude, not true altitude. Consequently, the vertical position accuracy needed at the final approach waypoint requires that the runway pressure altitude be measured with a ground barometric altimeter and this pressure measurement used to define the altitudes of the approach path waypoints. To accurately establish the runway pressure altitude with the ground altimeter measurements, the altitude difference between the runway and the ground altimeter must also be measured. The differential baro/inertial equations are also discussed in Appendix A.

In the integration of Loran and inertial information, the following computational steps are performed:

- a. The inertial latitude and longitude solutions are transformed into predicted time differences  $\hat{TD}_A$ ,  $\hat{TD}_S$  (i.e., the two time difference LOPs that intersect at the inertial position solution are found)
- b. The receiver's measured time differences  $TD_A$ ,  $TD_S$  are differenced with the predicted time differences; and
- c. These differences, which are measurements of the errors in the inertial position solutions, are transformed by the integration filter into corrections for errors in the system's solutions for latitude, longitude, north and east velocity, heading and attitude.

These corrections are applied to the inertial position and velocity solutions and to the  $C_N^S$  direction cosine transformation. (The integration filter may also correct for gyro and accelerometer errors, but these details are not included in this mechanization discussion but are part of the error model and simulation discussions.)

The differential Loran technique was investigated in this study as a way of nulling the major contributor to the Loran position error: the uncertainty in the Loran signal propagation velocity over the non-homogeneous path between transmitter and receiver [11]. This propagation velocity uncertainty can be visualized as warpage of the constant time difference hyperbolas, shown in Figure 5-2f, since these hyperbolic LOPs are determined assuming the signals propagated over an all-seawater earth. A position fix, the estimate of the aircraft's geodetic coordinates determined from the intersection of the two hyperbolic LOPs defined by a Loran receiver's TD measurements, may be in error by as much as 2000 to 3000 feet because of the propagation velocity uncertainty.

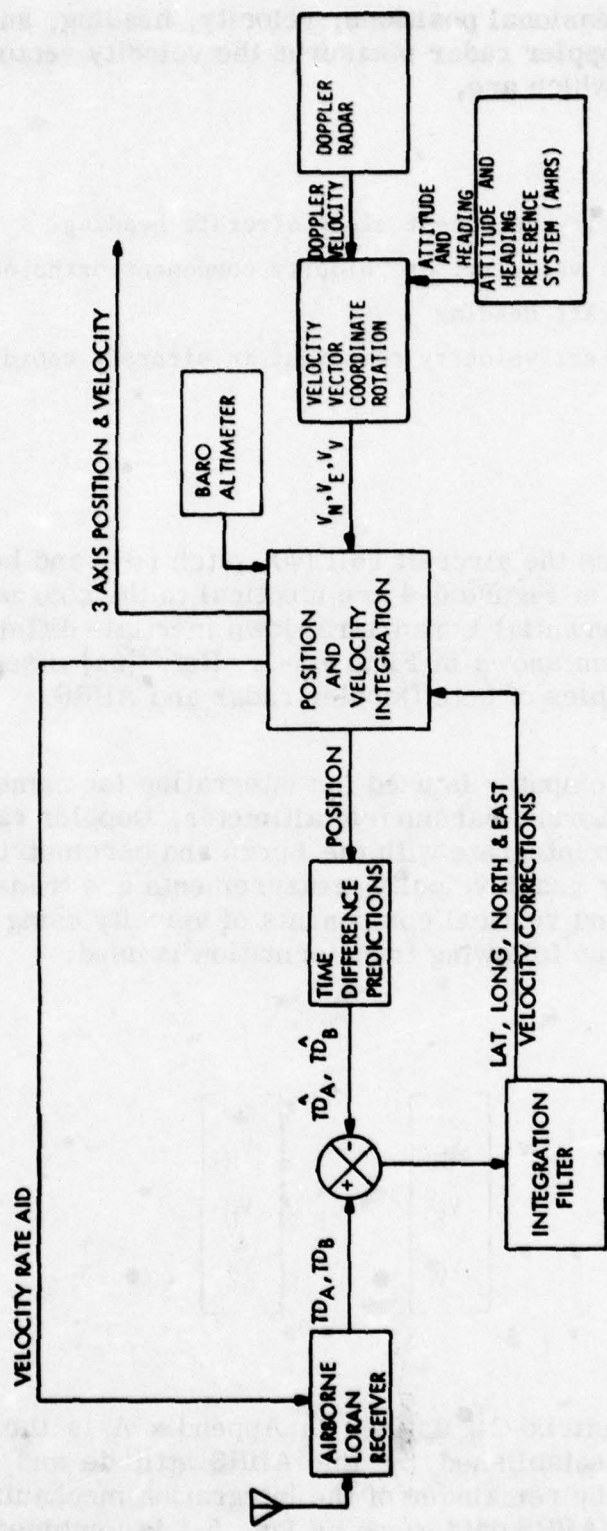
The effects of propagation velocity uncertainty are minimized with the differential Loran technique, where navigation is with respect to a Loran grid map where each geodetic point is defined by its time difference coordinates ( $TD_A$ ,  $TD_B$ ) measured by a Loran receiver. In this Loran grid system, position accuracy is determined by how accurately the navigation system measures TDs, which is significantly better (on the order of 0.05  $\mu$ sec ( $1\sigma$ ) or between 50 and 200 feet error) than the previously described position error caused by the propagation velocity uncertainty. For the 4-D INCADS to use the differential Loran technique to advantage, the runway must be located accurately within the Loran grid. This requires a ground-based Loran receiver, which is displaced a known distance from the touchdown point, to measure the Loran time differences. The need for a real-time measurement of TDs is necessary because the Loran grid is susceptible to slight shifts caused by temporal and seasonal variations in Loran signal propagation times, and slow variations in the transmitted signal waveforms.

An accurate measurement of the 3-dimensional displacement between the ground Loran receiver/baro altimeter unit and a reference point on the runway is necessary to meet the differential navigation performance requirements. This may be achieved by citing the ground unit with respect to the runway reference point, or the calibration may be performed by measuring the time differences and pressures between the two points using a 4-D INCADS-equipped aircraft.

### 5.3 INTEGRATED DIFFERENTIAL LORAN/DOPPLER RADAR/AHRS CONCEPTS

A mechanization for an integrated differential Loran/Doppler/Attitude and Heading Reference System (AHRS) is described in this section. Many parts of the differential Loran/strapdown inertial technique description provided in the previous section are applicable to the integration of Loran with Doppler and AHRS data, with the Doppler velocity and AHRS attitude and heading information combined and used in place of the inertial velocity outputs.

Figure 5-4 is a block diagram of a differential Loran/Doppler/AHRS technique and comparison with Figure 5-1 shows how the Doppler velocity and AHRS altitude and heading measurements replace the inertial accelerometers and gyro measurements. The outputs of the integrated system are



AIRBORNE DIFFERENTIAL LORAN/STRAPDOWN INERTIAL  
FIGURE 5-4

9632

the aircraft 3-dimensional positions, velocity, heading, and attitude variables. The Doppler radar measures the velocity vector's body axis components, which are,

$v_H$  = velocity component along aircraft heading

$v_D$  = drift velocity, or velocity component orthogonal to aircraft heading

$v_Z$  = vertical velocity component in aircraft coordinates

The AHRS measures the aircraft roll ( $\phi$ ), pitch ( $\theta$ ), and heading ( $\psi$ ). The other sensors in Figure 5-4 are identical to the corresponding sensors in the differential Loran/strapdown inertial - differential baro/inertial system shown in Figure 5-1. Ref. [24] discusses the fundamental principles of both Doppler radar and AHRS.

The 4-D INCADS computer is used for integrating (or combining) the information from Loran, barometric altimeter, Doppler radar, and AHRS sensors. To integrate with the Loran and barometric measurements, the Doppler radar velocity measurements are transformed into north, east, and vertical components of velocity using the AHRS measurements. The following transformation is used:

$$\begin{bmatrix} v_N \\ v_E \\ v_V \end{bmatrix} = C_B^N \begin{bmatrix} v_H \\ v_D \\ v_Z \end{bmatrix} \quad (5-1)$$

where the  $3 \times 3$  matrix  $C_B^N$  defined in Appendix A is the direction cosine transform established by the AHRS attitude and heading measurements. The remainder of the integration mechanization, where the Doppler/AHRS data given by Eqn. 5-1 is combined with Loran and

barometric measurements, is identical to the integration of inertial velocity components with Loran and baro altimeter. This mechanization technique, which uses the long term stability of the Loran and baro measurements damp out position, velocity, and altitude errors that accumulate in a Doppler/AHRS navigation system, is described in Appendix A.

The assessment of the integrated system performance is based on the error characteristics of the Doppler, AHRS, Loran and barometric altimeter sensors. The results of the performance analysis for this navigation system technique is provided in Section 5.5.3.

#### 5.4 4-D INCADS NAVIGATION SYSTEM ERROR MODEL

A dynamic error model for the differential Loran/strapdown inertial and differential baro/inertial system was developed next. (This model can be modified easily to be applicable to integrated systems using gimballed inertial units.) First, the distinction between a position error in the Loran grid and a position error in the geodetic grid were established. Consider the following variables:

$\lambda^t, \Lambda^t$  = geodetic coordinates of the aircraft

$TD_A^t, TD_B^t$  = noiseless TD measurements of aircraft receiver

$\lambda_L, \Lambda_L$  = Loran position fix defined by intersection of the  $TD_A^t$  and  $TD_B^t$  hyperlobic LOPs (this latitude and longitude defines the point in the Loran grid).

$\lambda, \Lambda$  = the 4-D INCADS navigation system measurement of aircraft position.

$R_E$  = earth's radius

The absolute north and east position errors of the 4-D INCADS are defined as

$$\begin{bmatrix} \Delta N \\ \Delta E \end{bmatrix} = \begin{bmatrix} \lambda^t - \lambda \\ \Lambda^t - \Lambda \cos\lambda \end{bmatrix} R_E \quad (5-2)$$

while the differential north and east position errors of the 4-D INCADS which determine the system position accuracy in the Loran grid are defined as

$$\begin{bmatrix} \Delta N_D \\ \Delta E_D \end{bmatrix} = \begin{bmatrix} \lambda_L - \lambda \\ \Lambda_L - \Lambda \cos\lambda \end{bmatrix} R_E \quad (5-3)$$

The difference between the absolute and differential position errors are caused by the uncertainties in the 4-D INCADS propagation time calculation, i.e., the inaccuracy in the secondary phase calculation  $T_{cs}$  in Eqn. A-4 (given in Appendix A).

The relationship between secondary phase uncertainties, absolute position errors, and differential Loran position error is

$$\begin{bmatrix} \Delta N_D \\ \Delta E_D \end{bmatrix} = \begin{bmatrix} \Delta N \\ \Delta E \end{bmatrix} - \begin{bmatrix} A & B \\ C & D \end{bmatrix} \begin{bmatrix} \Delta W_A \\ \Delta W_B \end{bmatrix} \quad (5-4)$$

where the Loran time difference warpages,  $\Delta W_A$ ,  $\Delta W_B$  represent the effects of master, Slave A and Slave B secondary phase uncertainties, and A, B, C, D account for the scale factor changes in transforming between propagation time errors, which are expressed in units of time, and position errors, which are expressed in units of distance. The geometric dilution parameters A, B, C, D are defined by the geometric

relationship between aircraft location and the three Loran stations and their equations are given in Appendix B. The variables  $\Delta W_A$  and  $\Delta W_B$  are referred to as Loran warpage.

Next, differential equations for the absolute position errors, velocity errors, heading error, and attitude errors of the differential Loran/inertial and differential baro/inertial systems are summarized. Derivations of the equations are given in Ref. [12, 13]. The heading and attitude errors of the strapdown inertial system are represented as

$$\dot{\underline{\rho}}^N = -\underline{\Omega}_{IN}^N + C_B^N \underline{\Delta W}^B - \underline{\Delta W}_{IN}^N - \hat{\underline{\rho}}^N \quad (5-5)$$

where

$$\underline{\rho}^N = [\rho_N, \rho_E, \rho_V]^T$$

$$\underline{\Delta W}^B = [G_x, G_y, G_z]^T = \text{rate gyro measurement errors}$$

$$\underline{\Delta W}_{IN}^N = [\Delta W_N, \Delta W_E, \Delta W_V]^T = \text{errors in the navigation frame's angular velocity caused by system velocity and position errors}$$

$$\underline{\xi}_N = [\xi_N, \xi_E, \xi_V]^T = \text{integration filter corrections}$$

The heading error is  $\rho_V$ , and the  $\rho_N$  and  $\rho_E$  represent the misalignments about the north and east axes, of the navigation frame "N", defined by the direction cosine matrix  $C_B^N$ , relative to the true local vertical. The matrix  $\underline{\Delta W}_{IN}^N$  is given in Appendix B.

The velocity errors in the strapdown inertial system satisfy

$$\dot{\underline{V}} = C_B^N \underline{\Delta A}^B + \lambda^N \underline{\rho}^N - \lambda_{OR}^N \underline{\Delta V}^N - \Delta \lambda_{OR}^N + \Delta g - \underline{\Delta V} \quad (5-6)$$

where

$$\underline{\Delta V}^N = [\Delta V_N, \Delta V_E, \Delta V_V]^T = \text{velocity errors}$$

$$\underline{\Delta A}^B = [\Delta A_X, \Delta A_Y, \Delta A_Z]^T = \text{accelerometer measurement errors}$$

$$\underline{\Delta g} = [g_{DN}, g_{DE}, g_{DV}] = \text{gravity deflections and gravity magnitude error}$$

$$\underline{\dot{\Delta V}} = [\dot{\Delta V}_N, \dot{\Delta V}_E, \dot{\Delta V}_V]^T = \text{integration filter velocity corrections}$$

$$\underline{\dot{A}}^N = \begin{bmatrix} 0 & -A_V & A_E \\ A_V & 0 & -A_N \\ -A_E & A_N & 0 \end{bmatrix}$$

$A_N, A_E, A_V$  = north, east and vertical accelerations

The matrix  $\hat{\underline{\Delta C}}_{OR}$  is defined in Appendix B.

The position errors satisfy

$$\dot{\underline{\Delta d}}^N = \begin{bmatrix} \dot{\Delta N} \\ \dot{\Delta E} \\ \dot{\Delta h} \end{bmatrix} = \begin{bmatrix} \Delta V_N \\ \Delta V_E \\ \Delta V_V \end{bmatrix} - \dot{\underline{d}}^N \quad (5-7)$$

where

$$\dot{\underline{d}}^N = [\dot{\Delta N}, \dot{\Delta E}, \dot{\Delta h}]^T = \text{integration filter position error estimates}$$

To incorporate the effect of the integration filter into the equations given above, the error estimates are related to the Loran errors and baro errors, using Eqns. (A-4), (A-5), (A-6), and (A-7). The difference between the receiver TD measurements and the predicted TDs, determined by the system positions ( $\lambda, \Lambda$ ), are modeled as

$$\begin{bmatrix} TD_A - \hat{TD}_A \\ TD_B - \hat{TD}_B \end{bmatrix} = \begin{bmatrix} A' & B' \\ C' & D' \end{bmatrix} \begin{bmatrix} \Delta N_B \\ \Delta E_D \end{bmatrix} + \begin{bmatrix} n_A - r_M \\ n_B - n_M \end{bmatrix} \quad (5-8)$$

where

$$\begin{bmatrix} A' & B' \\ C' & D' \end{bmatrix} = \begin{bmatrix} A & B \\ C & D \end{bmatrix}^{-1}$$

and  $n_A$ ,  $n_B$  and  $n_M$  are the receiver time of arrival errors.

In the modeling the effect of the barometric altimeter measurement, a differential baro altitude error is defined in a manner similar to the differential Loran position error. Consider the following variables:

$h^t$  = true altitude above sea level of aircraft

$\rho_s$  = true barometric pressure measure

$h_B$  = pressure altitude established by  $\rho_s$  and the standard day relationship between  $\rho_s$  and altitude

$h$  = 4-D INCADS altitude solution

$D$  = D value =  $h^t - h_B$

The absolute altitude error of 4-D INCADS is  $\Delta h = h' - h$  and the differential baro altitude error is  $\Delta h_D = h_B - h$ . The relationship between absolute and differential altitude errors is

$$\Delta h_D = -D \quad (5-9)$$

By collecting the error equations, given above, expanding the gyro measurement model to include bias, noise and maneuver dependent errors, and defining a math model for the Loran warpage errors, the following true vectors of errors can be defined for the differential Loran/strapdown inertial and differential baro/inertial system:

$$\underline{x}_H = \begin{bmatrix} \Delta N_D \\ \Delta E_D \\ \Delta V_N \\ \Delta V_E \\ \rho_N \\ \rho_E \\ \rho_V \\ G_{BX} \\ G_{BY} \\ G_{BZ} \\ \Delta A_{BX} \\ \Delta A_{BY} \\ \Delta A_{BZ} \\ \Delta W_A \\ \Delta W_B \\ G_{nx} \\ G_{ny} \\ G_{nz} \end{bmatrix} \quad = \text{differential Loran/strapdown inertial errors}$$

$$\underline{x}_V = [\Delta h_D, \Delta V_V]^T$$

where

- $\Delta A_{Bx}, \Delta A_{By}, \Delta A_{Bz}$  = accelerometer biases
- $G_{Bx}, G_{By}, G_{Bz}$  = gyro biases
- $G_{nx}, G_{ny}, G_{nz}$  = gyro noise terms, which are modeled as exponentially correlated stochastic processes

Notice that differential Loran and differential baro position errors are in the error vectors. The error vectors of the integrated system satisfy the following vector differential equation:

$$\frac{d}{dt} \begin{bmatrix} \underline{x}_H \\ \underline{d}_H \\ \underline{x}_V \\ \underline{d}_V \end{bmatrix} = \begin{bmatrix} A_H & | & A_B \\ -- & | & -- \\ A_C & | & A_V \end{bmatrix} \begin{bmatrix} \underline{x}_H \\ \underline{d}_H \\ \underline{x}_V \\ \underline{d}_V \end{bmatrix} + \begin{bmatrix} K(t)H_1 \underline{x}_H \\ K(t)H_2 \\ 0 \end{bmatrix} - \begin{bmatrix} n_A \\ n_B \\ n_M \end{bmatrix} \quad (5-10)$$

where the matrices  $A_H, A_B, A_C, A_V, H_1$  and  $H_2$  and vectors  $\underline{d}_H, \underline{d}_V$  are defined in Appendix B. In this error model the Loran warpages are modeled as exponentially correlated processes, with

$$\Delta \dot{W}_A = -\frac{|V|}{d_d} \Delta W_A + \sigma_w \sqrt{\frac{2|V|}{d_d}} U_A \quad (5-11)$$

where  $U_A$  is white noise with a unit power spectral density. This model represents the time variations of the warpage as an aircraft flies through a Loran grid with speed  $|V|$ , where the warpage spatial variation is represented with a correlation distance,  $d_d$ , and its magnitude is represented with a standard deviation  $\sigma_w$ .

The error model of Eqn. 5-10 is for an integrated system using a strap-down inertial system. It can be converted to an error model for an integrated system using a gimballed inertial system by setting  $C_B^N = I$ , where  $I$  is the  $3 \times 3$  unit matrix.

Equation 5-10 and the matrix and vector definitions of Appendix B identify the sources of navigation errors. These error sources are gyro and accelerometer meter measurements errors of the inertial system, Loran warpage and noise, D value, baro noise, and gravity deflections. Table 5-I lists the nominal gyro and accelerometer measurement uncertainties for the three classes of inertial system being considered in this study. It should be noted that the 20 nm/hr inertial system is being represented by a strapdown reference system that has a turn-on to turn-on gyro bias repeatability of 1 deg/hr. A gyro calibration on the ground before the flight or an in-flight gyro calibration is required to reduce the gyro bias uncertainty to 0.2 deg/hr, as shown in Table 5-I. This ground gyro calibration does not impose any operational limitations since it can be accomplished in the same amount of time that a normal gyro-compass heading alignment of a 1 nm/hr gimballed inertial system takes. The simulation results provided later in Section 5.6 show that a Loran/inertial Kalman filter can estimate this size of gyro bias in flight, so a ground calibration is not required for a strapdown reference system used in the 4-D INCADS.

## 5.5 ANALYTICAL EVALUATION

This section uses a simplified version of the basic error model (Eqn. 5-10) to assess the performance of differential Loran/inertial technique where the Loran is used to correct only the inertial position and velocity errors. The differential baro/inertial vertical channel performance and the differential Loran/Doppler/AHRS System are also assessed analytically in this section. This analysis effort, devoted to the second-order integration technique, was performed to

- a. Determine which of the three classes of inertial system, when integrated with Loran and baro, can meet the navigation system performance objectives given in Section 5.1.
- b. Determine those classes of inertial systems that cannot meet the performance objectives with the second-order integration technique, and establish which additional inertial errors must be corrected by a more complex integration filter.
- c. Determine which closed form analytical results can be obtained for a second-order integrated system that reasonably approximates the sensitivity of an integrated system to the major Loran, inertial, baro errors and thus provide significant performance results without a complex simulation.

**TABLE 5-I**  
**INERTIAL SYSTEM ERROR SOURCE**

	Inertial System Class		
	20 nm/hr <sup>(1)</sup>	3-5 nm/hr <sup>(2)</sup>	nm/hr <sup>(3)</sup>
x and y Gyro Bias, $\sigma_{GB}$ ( $^{\circ}/hr$ )	.2	.05	.01
z Gyro Bias, $\sigma_{GB}$ ( $^{\circ}/hr$ )	1	.1	.03
$\sigma_{GBN}$ ( $^{\circ}/hr$ )	.2	.04	.005
x,y,z Gyro Noise $\frac{\sigma}{\tau_g}$ (sec)	20	1800	3600
x,y,z Gyro Scale Factor Error, $\sigma_{GS}$ (%)	.15	.1	.05
x,y,z Gyro Mass Unbalance Drift, $\sigma_{GM}$ ( $^{\circ}/hr/G$ )	2	.2	.05
x,y,z Gyro Anisoelastic Drift, $\sigma_{GA}$ ( $^{\circ}/hr/G^2$ )	.1	.06	.06
x,y,z Accelerometer Bias, $\sigma_{AB}$ ( $\mu g$ )	1000	300	100
x,y,z Accelerometer Noise $\frac{\sigma_{An}}{\tau_A}$ ( $\mu g$ )	30	30	30
x,y,z Accelerometer Scale Factor Errors, $\sigma_{AS}$ (%)	100	100	5
	.2	.1	.05
(1) Representative of LSI Model 5152 Strapdown System with Model 1904 rate gyros.			
(2) Generic representation of the USAF Multifunction Inertial Reference Assembly (MIRA) [14]			
(3) Representative of Kearfott SKC-2300 and Litton ASN-109 Inertial Measurement Units.			

- d. Determine if Doppler Radar/AHRS -- when integrated with Loran using only position and velocity damping -- can meet the navigation system performance objectives.

### 5.5.1 Differential Loran/Inertial Evaluation

The errors for a position and velocity damped, differential Loran/inertial system are given by the vector differential equation (Eqn. 5-10) when all entries in gain matrix K set to zero, except for  $K_{11} = K_{22} = K_1$  and  $K_{31} = K_{42} = K_2$ . By neglecting the small cross coupling between the north and east channels, the error equations of Eqn. 5-10 can be divided into a set of differential equations for the north channel and a similar set of differential equations for the east channel. Since the performance of both channels are identical, except for the effects of different Loran geometric dilutions and the influence of the aircraft latitude on the east channel, only the north channel's performance is assessed.

From Eqn. 5-10, the following model for the north channel of the differential Loran/inertial system is obtained:

$$\dot{\Delta N_D} = -K_1 \Delta N_D + \Delta V_N - A[\Delta \dot{W}_A + K_1 (n_A - n_M)] - B [\Delta \dot{W}_B + K_1 (n_B - n_M)] \quad (5-12)$$

$$\dot{\Delta V_N} = -K_2 \Delta N_D - g \rho_E - A_E \rho_V + \Delta A_{BN} + g_{DN} \quad (5-13)$$

$$- K_2 [A (n_A - n_M) + B (n_B - n_M)] \quad (5-14)$$

$$\dot{\rho}_E = \Delta V_N / R_E + G B_E + G_{NE} \quad (5-14)$$

$$\dot{\rho}_V = G B_D \quad (5-15)$$

In obtaining the above equations, the gimballed inertial version of Eqn. 5-10 was used ( $C_B^N = I$ ). Also, the effects of Coriolis errors on velocity errors, the effect of heading error ( $\rho_V$ ) on the east misalignment ( $\rho_E$ ), and effects of the maneuver dependent gyro and accelerometer measurement errors were neglected in arriving at the above equations. Consequently, the analytical results obtained from this model are approximate; however, since the major error sources of the integrated system remain in the model, the results do adequately represent system performance.

Collecting Eqns. 5-12, 5-13, and 5-14 into a vector differential equation, taking Laplace transforms of all terms, and solving the equations for differential position error, velocity error, and east misalignment gives the vector equation in Table 5-II. Analytical expressions for the uncertainty in the differential position and velocity solutions caused by the Loran and inertial error sources and aircraft accelerations are derived in Appendix C using the equations of Table 5-II.

TABLE 5-II  
DIFFERENTIAL LORAN/INERTIAL ERROR EQUATIONS - NORTH CHANNEL

$$\begin{bmatrix} \Delta N_D(s) \\ \Delta V_N(s) \\ \rho_E(s) \end{bmatrix} = \frac{1}{R_E} \begin{bmatrix} s^2 + g/R_E & s & -g \\ -K_2 s & s^2 + K_1 s & -g(s+K_1) \\ -K_2/R_E & (s+K_1)/R_E & s^2 + K_1 s + K_2 \end{bmatrix} \begin{bmatrix} -A[sN_A(s) + K_1(n_B(s) - n_M(s))] - B[sN_B(s) + K_1(n_B(s) - n_M(s))] + \Delta N_D(t_0) \\ -[A_E \rho_V(s) + \Delta A_{BN}(s) + g_{DN}(s) - K_2(A(n_A(s) - n_M(s)) + B(n_B(s) - n_M(s))) + \Delta V_N(t_0)] \\ + \frac{V_E}{R_E} \rho_V(s) + \rho_E(t_0) \end{bmatrix}$$

5-25

$$D_3 = s^3 + K_1 s^2 + s(K_2 + \frac{g}{R_E}) + \frac{K_1 g}{R_E}$$

$\Delta N_D(t_0)$  = initial differential position error

$\Delta V_N(t_0)$  = initial velocity error

$\rho_E(t_0)$  = initial misalignment about east axis.

The feasibility of using a second-order integration filter with the three differential Loran/inertial configurations was judged in terms of each system's position and velocity performance in a remote airfield's terminal area after a two hour flight. Performance numbers were determined by calculating the root mean square (RMS) error contributed by the Loran and inertial error sources given in the error model of Table 5-II. This table shows that the sensitivity of the position and velocity errors to all Loran and inertial error sources, except the heading misalignment caused by z gyro bias, are not affected by aircraft accelerations. Consequently, the system performance for these error sources was characterized by steady-state position and velocity uncertainties.

The effects of heading misalignment and z gyro bias are represented by the peak values of the position and velocity errors caused by the aircraft accelerations. The largest position and velocity error transients are caused by accelerations that cause the aircraft to change its velocity vector direction within one integration filter time constant. For the analysis, a 90° turn with a 22° bank and an approach speed of 200 ft/sec was used to compute the position and velocity error peaks. The maneuver was approximated for the north channel analysis as an east velocity change of 200 ft/sec that occurred within 15 seconds. The equations of Appendix C were used to compute the errors that appear in Tables 5-III and 5-IV.

The performance of the navigation systems is dependent on the two feedback gains  $K_1$  and  $K_2$ , which were converted to their equivalent damping factor  $\zeta$  and natural frequency  $\omega_n$  in Appendix C. A unity damping factor was selected for a slightly damped system response.

The Loran signal-to-noise ratio (S/N) and the spatial variation in the Loran warpage are dominate factors in selecting the integration filter's natural frequency  $\omega_n$ . To make this selection, the combined position and velocity uncertainties caused by Loran noise and Loran warpage were constrained to 65 feet ( $1\sigma$ ) and 3.0 ft/sec ( $1\sigma$ ), respectively. The sensitivity equations of Appendix C yielded the following expressions for the combined differential position and velocity variances:

$$\sigma_{ND}^2 = (A^2+B^2)[5\omega_n^2 S_L + \sigma_w^2/\tau_w]/2\omega_n \quad (5-16)$$

$$\sigma_V^2 = (A^2+B^2)\omega_n[\omega_n^2 S_L + \sigma_w^2/\tau_w]/2 \quad (5-17)$$

**TABLE 5-III**  
**DIFFERENTIAL LORAN/INERTIAL PERFORMANCE**  
**2ND ORDER INTEGRATION FILTER - S/N = 0 DB**

$\omega_n$ = .066 rad/sec	20 nm/hr Inertial		5 nm/hr Inertial		1 nm/hr Inertial	
	Differential Position (1 $\sigma$ ) Error (feet)	Velocity Error (1 $\sigma$ ) (ft/sec)	Differential Position (1 $\sigma$ ) Error (1 $\sigma$ ) (feet)	Velocity Error (1 $\sigma$ ) (ft/sec)	Differential Position (1 $\sigma$ ) Error (1 $\sigma$ ) (feet)	Velocity Error (1 $\sigma$ ) (ft/sec)
East Gyro Bias	147.2	19.4	37.8	4.9	7.4	1.0
East Gyro Noise	3.8	.6	8.3	1.1	1.4	.2
North Accel. Bias	7.4	1.0	2.2	.3	.7	.1
North Accel. Noise	.2	.07	.2	.07	.09	.03
Loran Noise S/N = 0 db	52.1	1.5	52.1	1.5	52.1	1.5
Loran Warpage (2) $\sigma_w^2 = .256 \mu\text{sec}$ , $d_d = 12 \text{ nm}$	38.2	2.4	38.2	2.4	38.2	2.4
Gravity Deflection	.2	.06	.2	.06	.2	.06
Aircraft Maneuver (4) East velocity change of 200 ft/sec after 2 hrs. of flight	37.1	7.0	3.7	.7	1.1	.2
Root Mean Square (RMS)	165.2	20.8	75.4	5.8	65.0	3.0

(1) Differential position and absolute position errors are equal for all error sources, except Loran warpage.

(2) An approach velocity of 120 knots used for warpage calculations.

(3) Peak transient position and velocity uncertainties.

(4) The heading uncertainty is  $\sigma_{PV} = t\sigma_{GBV}$ , where  $\sigma_{GBV}$  for each inertial class defined in Table 5-1.

**TABLE 5-IV**  
**DIFFERENTIAL LORAN/INERTIAL PERFORMANCE**  
**2ND ORDER INTEGRATION FILTER - S/N = +8 DB**

$\omega_n$ = .047 rad/sec	20 nm/hr Inertial		5 nm/hr Inertial		1 nm/hr Inertial	
	Differential Position $\{\bar{P}\}$ (1 $\sigma$ ) Error (feet)	Velocity Error (1 $\sigma$ ) (ft/sec)	Differential Position $\{\bar{P}\}$ (1 $\sigma$ ) Error (feet)	Velocity Error (1 $\sigma$ ) (ft/sec)	Differential Position $\{\bar{P}\}$ (1 $\sigma$ ) Error (feet)	Velocity Error (1 $\sigma$ ) (ft/sec)
East Gyro Bias	206.9	19.4	51.7	4.9	10.3	1.0
East Gyro Noise	6.7	.7	13.6	1.3	2.3	.2
North Accel. Bias	.3	.2	.08	.06	.03	.02
North Accel. Noise	.4	.1	.4	.1	.2	.05
Loran Noise S/N = 8 db	17.4	.4	17.4	.4	17.4	.4
Loran Warpage <sup>(2)</sup>	61.8	2.8	61.8	2.8	61.8	2.8
$\sigma_w$ = .353 usec, $d_d$ = 12 nm						
Gravity Deflection	.4	.1	.4	.1	.4	.1
Aircraft Maneuver <sup>(4)</sup>						
East velocity change of 200 ft/sec after 2 hrs. of flight	52.2	7.0	5.2	.7	1.6	.2
Root Mean Square (RMS)	222.9	20.8	83.7	5.8	65.2	3.0

(1) Differential position and absolute position errors are equal for all error sources, except Loran warpage.

(2) An approach velocity of 120 knots used for warpage calculations.

(3) Peak transient position and velocity uncertainties.

(4) The heading uncertainty is  $\sigma_{PV} = \tau \sigma_{GBV}$ , where  $\sigma_{GBV}$  for each inertial class defined in Table 5-1.

where approximations were made in deriving these equations based on the size of the geometric dilution factors at Eglin AFB and the anticipated magnitudes of  $\omega_n$  and  $\tau_w$ . The variable  $S_L$  represents the Loran noise power spectral density, which is defined by S/N. Given the position and velocity accuracy constraints and a S/N, the parameters  $\omega_n$  and  $(\sigma_w^2/\tau_w)$  were determined from Eqns. 5-16 and 5-17. The warpage time constant  $\tau_w$  was set by selecting a correlation distance  $d_d$ , representative of the warpage variations in the terminal area and an aircraft speed  $|V|$ , i.e.,  $\tau_w = d_d/|V|$ . Then,  $\sigma_w$  was determined from the  $(\sigma_w^2/\tau_w)$  ratio.

To show the effect of Loran S/N ratio, two S/Ns were considered. For one case S/N = 0 db which corresponds to the Loran signal conditions at Eglin AFB, Fla. in the summer. In the winter at Eglin AFB, the Loran S/Ns are 8 db or better, so the second analysis case used S/N = 8 db. For S/N = 0 db,  $\sigma_{ND} = 65$  feet and  $\sigma_V = 3.0$  ft/sec, the solutions of Eqns. 5-16 and 5-17 are  $\omega_n = 0.066$  rad/sec and  $(\sigma_w^2/\tau_w) = (1.8 \times 10^{-4}) \mu\text{sec}^2/\text{sec}$ . For S/N = 8 db, the solutions are  $\omega_n = 0.047$  rad/sec and  $(\sigma_w^2/\tau_w) = 3.5 \times 10^{-4} \mu\text{sec}^2/\text{sec}$ .

The differential Loran/inertial system performance for the two Loran S/N cases are presented in Tables 5-III and 5-IV. These tables show the position and velocity uncertainties ( $1\sigma$ s) for the three classes of inertial error sources shown in Table 5-I. They show the Loran warpage parameters,  $\sigma_w$  and  $\tau_w$ , determined from Eqns. 5-16 and 5-17. The analysis showed that the higher the Loran S/N, the larger a variation in the Loran warpage could be allowed. Finally, the transient effects of the aircraft maneuver are shown. The peak position and velocity errors are larger for the lower quality inertial systems, because of the larger z gyro bias.

The position and velocity RMS values in Tables 5-III and 5-IV show that a second-order integration filter can adequately combine a 1 nm/hr inertial system with Loran, in a differential mode, to achieve a horizontal position accuracy of 75 feet ( $1\sigma$ ) and horizontal velocity accuracy of 3 feet/sec ( $1\sigma$ ).

The results of Tables 5-III and 5-IV indicate that higher order integration filters are required for 20 nm/hr and 5 nm/hr inertial systems. For a 5 nm/hr system, the east and north gyro biases contribute position and velocity errors that make the total system performance marginal. An integration filter that corrects the north, east, and heading misalignments, along with position and velocity errors, is required. For the 20 nm/hr inertial system, the east, north, and z gyro biases contribute position and velocity errors (both steady-state and maneuver-induced errors) that are significantly larger than the accuracy goals. An integration filter that corrects north, east, and heading misalignments, and possibly the three gyro biases, along with position and velocity errors, is required.

The differential position and velocity accuracy goals place limits on the spatial variations of the Loran warpage in the local area around the runway. These limitations are a function of Loran S/N as shown in Eqns. 5-16 and 5-17. A better understanding of the warpage variation limits is obtained by determining the warpage variation over a given distance that is equivalent to the warpage variation defined by the exponentially correlated stochastic model with parameters  $\sigma_w$  and  $d_d$ . The warpage variation significantly affects the Loran/inertial system for approximately four time constants; therefore the given distance (referred to above) corresponds to the distance the aircraft travels in four system time constants. For S/N = 0 db, the system time constant is 15.2 sec =  $1/\omega_n$ , and at a 200 ft/sec speed the aircraft flies 2.0 nm in the time interval equal to four time constants. For S/N = +8 db and  $\omega_n = 0.047$  rad/sec, this distance is 2.8 nm. The variation in Loran warpage over a distance,  $\ell$ , is

$$\begin{aligned}\sigma_{\epsilon \Delta W}^2 &= E[\Delta W(\ell) - \Delta W(0)]^2 \\ &= E\Delta W^2(\ell) + E\Delta W^2(0) - 2E[\Delta W(\ell)\Delta W(0)] \\ &= 2\sigma_w^2[1 - \text{EXP}(-\ell/d_d)]\end{aligned}$$

where E is the expected value operator. This analysis shows that the spatial variations of the Loran warpage must be bounded as follows for the Loran/inertial system, with a second-order integration filter, to meet the 75 feet ( $1\sigma$ ) position and 3 ft/sec ( $1\sigma$ ) velocity accuracies at the final approach waypoint.

S/N	Warpage Variation ( $\sigma_{\epsilon \Delta W}$ )
0 db	.15 sec over 2.0 nm
+8 db	.42 over 2.8 nm

Recent results from a Loran flight test show that the bounds given above are realistic limits for warpage variations over short distances. During this flight test (the AN/ARN-101(V) Digital Modular Avionics System flight

test), models of the Loran TD<sub>A</sub> and TD<sub>B</sub> warpages at the Eglin AFB, which are considered excessively large, were developed using measured data points [11]. Contour plots of the warpage models, which are presently being used in the ARN-101 system to compensate for Loran warpage, are given in Figures 5-5 and 5-6. These plots show the warpage changes over the 1 to 3-mile distances are significantly less than the bounds derived above.

The RMS errors presented above indicate that the differential Loran/inertial system can be used for lateral guidance during an emergency landing. However, the position RMS error of approximately 75 feet is too large for fully automated blind guidance of an aircraft to remote runways, which may be between 100 to 200 feet wide. For a safe landing, with only differential Loran/inertial guidance, the runway must be visible approximately a half mile from touchdown.

### 5.5.2 Differential Baro/Inertial Evaluation

The error equations for the differential baro/inertial vertical channel were developed in detail in Section 5.4, and are included as part of the complete set of error differential equations given in Eqn. 5-10. However, examination of Eqn. 5-10 shows that the vertical channel and the horizontal channel are loosely coupled and the performance of the vertical channel can be accurately assessed, independent of the horizontal channel.

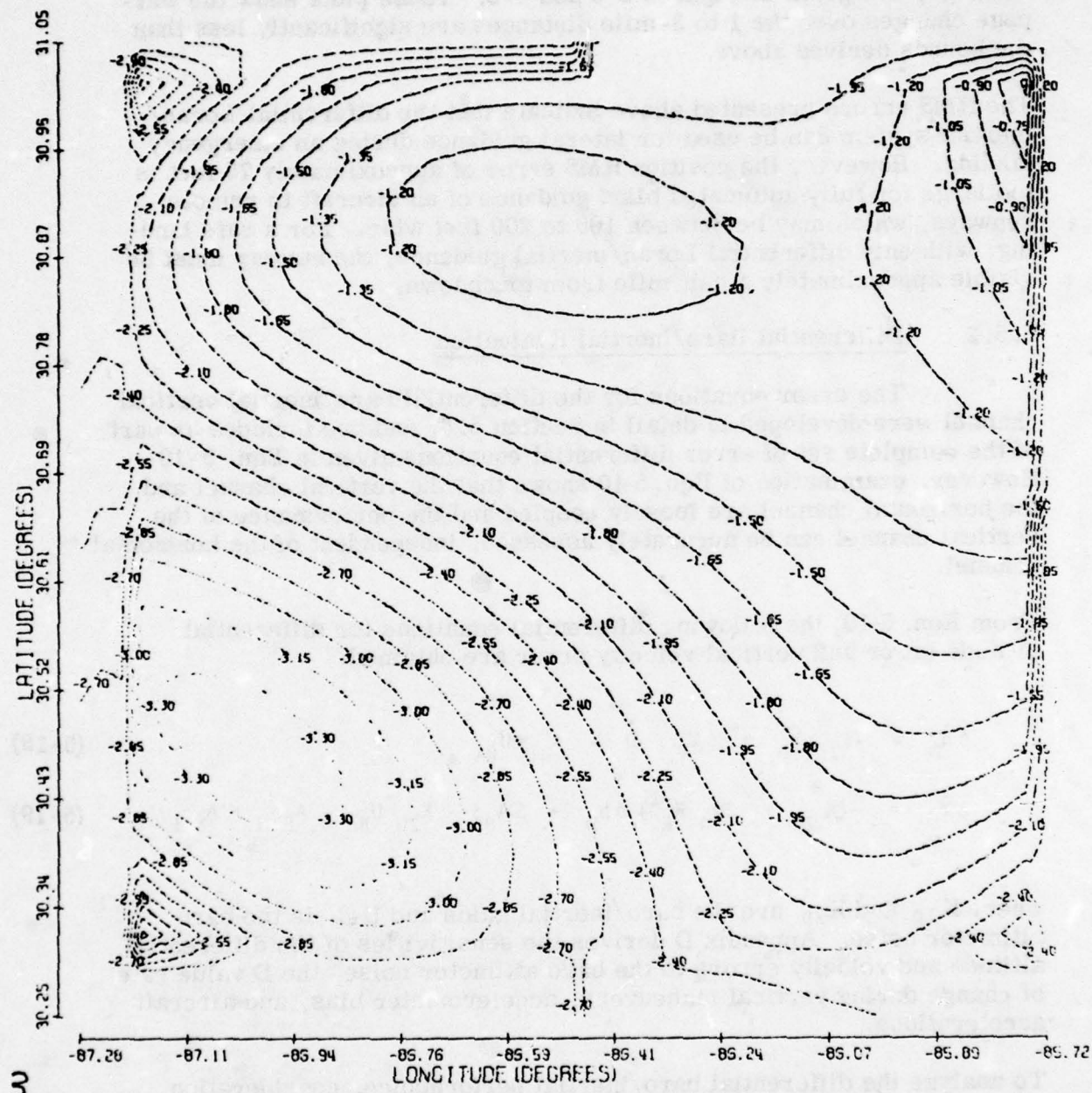
From Eqn. 5-10, the following differential equations for differential altitude error and vertical velocity error are obtained.

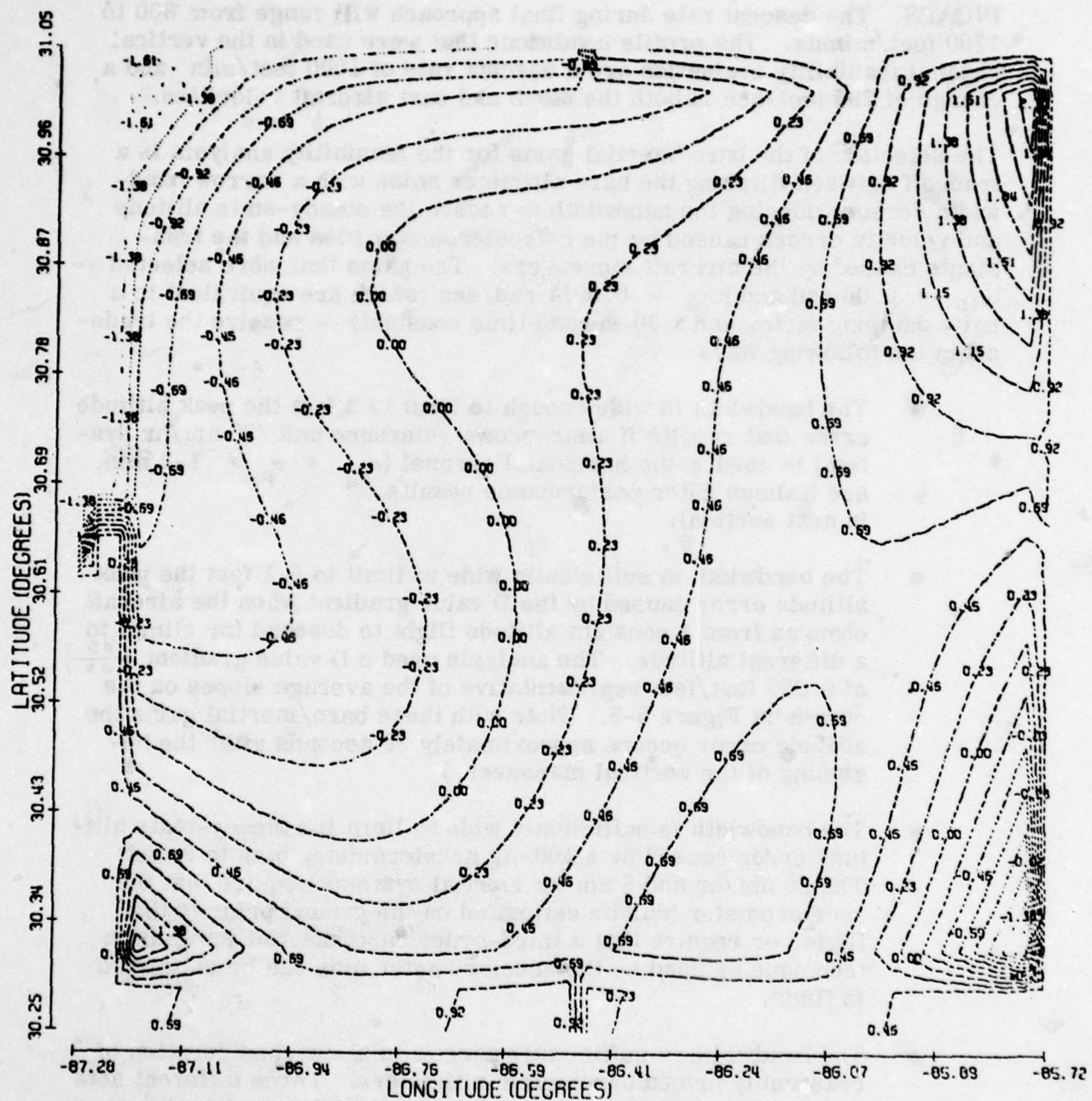
$$\Delta \dot{h}_D = -K_{1D} \Delta h_D + \Delta v_v - D - K_{1D} U_{BA} \quad (5-18)$$

$$\Delta \dot{v}_v = -(K_{2D} + 2g_0 R_E^{-1}) \Delta h_D + \Delta a_{BZ} - K_{2D} U_{BA} - a_{E^0 N} + a_{N^0 E} \quad (5-19)$$

where  $K_{1D}$  and  $K_{2D}$  are the baro/inertial gains and  $U_{BA}$  is the baro altimeter noise. Appendix D derives the sensitivities of the differential altitude and velocity errors to the baro altimeter noise, the D value rate of change during vertical maneuvers, accelerometer bias, and aircraft accelerations.

To analyze the differential baro/inertial performance, consideration must be given to the aircraft vertical profile. For the transport missions under consideration in this study, it can be expected that there





**TDB SECONDARY PHASE ( $\mu$ SEC)**  
**EGLIN AFB AREA**  
**FIGURE 5-6**

will be few changes in altitude during the enroute phase. Then, during the approach to the airfield, the aircraft can be expected to descend from as high as 20,000 feet down to the runway. Curved approach paths will be used with the 4-D path synthesis and control capability of the 4-D INCADS. The descent rate during final approach will range from 800 to 1200 feet/minute. The profile conditions that were used in the vertical channel feasibility evaluation are a descent rate of 1000 feet/min and a change of 200 feet/sec in both the north and east aircraft velocities.

The selection of the baro/inertial gains for the feasibility analysis is a tradeoff between filtering the baro altimeter noise with a narrow bandwidth versus widening the bandwidth to reduce the steady-state altitude and velocity errors caused by the z accelerometer bias and the transients caused by the aircraft maneuvers. The gains that were selected --  $K_{1D} = 0.06$  rad and  $K_{2D} = 0.0011$  rad/sec (which are equivalent to a unity damping factor and a 30-second time constant) -- resolve the trade-off in the following ways:

- The bandwidth is wide enough to limit to 2 feet the peak altitude error that results if a strapdown reference unit (20 nm/hr system) is used in the horizontal channel ( $\sigma_{\rho_N} = \sigma_{\rho_E} \approx 1-2 \text{ min}$ , see Kalman filter performance results in next section).
- The bandwidth is sufficiently wide to limit to 6.1 feet the peak altitude error caused by the D value gradient when the aircraft changes from a constant altitude flight to descend (or climb) to a different altitude. The analysis used a D value gradient ( $\frac{dD}{dh}$ ) of 0.035 feet/feet representative of the average slopes on the curves in Figure 5-3. (Note with these baro/inertial gains the altitude error occurs approximately 30 seconds after the beginning of the vertical maneuver.)
- The bandwidth is sufficiently wide to limit the steady-state altitude error caused by a 100- $\mu g$  accelerometer bias to 3 feet. The 20 nm/hr and 5 nm/hr inertial systems require that the accelerometer bias be estimated on the ground prior to the flight, or require that a third-order baro/inertial integration technique be used so the accelerometer bias can be estimated in flight.
- The bandwidth is sufficiently narrow to allow consideration of reasonably priced barometric altimeters. Three different sets of barometric measurement characterizations, which give equivalent altitude and velocity accuracies, are calculated and shown in Table 5-V.

**TABLE 5-V**  
**DIFFERENTIAL BARO/INERTIAL PERFORMANCE**

Error Source <sup>(4)</sup>	Differential <sup>(1)</sup> Altitude Error ( $1\sigma$ ) (feet)	Vertical Velocity Error ( $1\sigma$ ) (ft/sec)
<u>Baro Altimeter Noise</u>		
$\sigma_{BA} = 48.1 \text{ ft}, \tau_B = .2 \text{ sec}$	6.21 <sup>(5)</sup>	.065 <sup>(5)</sup>
$\sigma_{BA} = 21.5 \text{ ft}, \tau_B = 1 \text{ sec}$	6.21	.065
$\sigma_{BA} = 9.6 \text{ ft}, \tau_B = 5 \text{ sec}$	6.21	.065
<u>Accelerometer Bias</u>		
$\sigma_{BAZ} = 1000 \mu\text{g}$	28.9	1.93
$\sigma_{BAZ} = 300 \mu\text{g}$	8.7	.58
$\sigma_{BAZ} = 100 \mu\text{g}$	2.89 <sup>(5)</sup>	.19 <sup>(5)</sup>
<u>D Value Gradient</u>		
$\frac{dD}{dh} = .035 \text{ ft/ft}$ and $V_v = 1000 \text{ ft/min}$	6.1 <sup>(2),(5)</sup>	0.6 <sup>(5)</sup>
<u>North &amp; East Misalign<sup>(3)</sup></u>		
$\sigma_{\rho N} = \sigma_{\rho E} = 0.2 \text{ min}$	.294 <sup>(2)</sup>	.016 <sup>(2)</sup>
$\sigma_{\rho N} = \sigma_{\rho E} = 2 \text{ min}^{(5)}$	1.8 <sup>(2),(5)</sup>	.16 <sup>(2),(5)</sup>
Root Mean Square (RMS) Error	9.4	0.65

(1) Differential altitude errors and absolute altitude errors are equal for all error sources except for D value gradient.

(2) Peak transient altitude or velocity error following aircraft maneuver.

(3) Performance for an aircraft turn where both the north and east velocity values changed 200 ft/sec.

(4) Baro/inertial gains are  $K_{1D} = .066 \text{ rad}$ ,  $K_{2D} = .00111 \text{ sec}^{-1}$ .

(5) Errors included in RMS calculation.

Table 5-V summarizes the sensitivities of the differential baro/inertial errors to the major error sources discussed above. The altitude and vertical velocity RMS errors show this system technique possesses altitude accuracy of 10 feet and vertical velocity accuracy of less than 1 foot/sec ( $1\sigma$ ). The analysis showed that the vertical channel performance is attainable in the presence of a 0.035 D value gradient; consequently, the 4-D INCADS doesn't need a D value compensation technique unless the system is operated in extreme environments where larger gradients are expected. For 20 nm/hr and 5 nm/hr inertial systems, the 4-D INCADS will need to estimate the z accelerometer bias either before the flight or in flight, as part of a third-order baro/inertial mechanization.

The differential baro/inertial system can be used for vertical guidance during landing; however, the 6 feet altitude error ( $1\sigma$ ) from the air-borne baro altimeter noise is too large for safe blind landings. A 1-foot ( $1\sigma$ ) altitude error is required for a zero-zero landing, especially when landing a STOL aircraft on a short 2000-3000 foot runway where the aircraft must firmly touch down at the beginning of the runway to gain the full rollout distance. For remote landings with differential baro/inertial guidance, a 150-foot minimum decision height is recommended.

### 5.5.3 Differential Loran/Doppler/AHRS Evaluation

With the same analysis methods used for the differential Loran/inertial system described in Section 5.5.1, this section assesses the performance of the integrated differential Loran/Doppler/AHRS system. The error model for the system is established for a second-order integration technique where Loran is used to damp position and velocity errors in the integrated system. A description of the Doppler and AHRS measurement errors is given; then, using the differential Loran error sources and the flight profile described in Section 5.5.1, the system's position and velocity uncertainties are calculated.

The differential equations that describe the errors in an integrated differential Loran/Doppler/AHRS system can be divided into two sets of differential equations -- one for the north channel and one for the east channel. The performance of each channel is nearly identical so only the north channel's performance is assessed. Eqn. 5-12 describes the propagation of the north component of the differential Loran position error in terms of the Loran warpage variations  $\Delta W_A$  and  $\Delta W_B$ ; the Loran measurement noise  $n_A$ ,  $n_B$ , and  $n_M$ ; the geometric dilution factors A and B; the feedback gain  $K_1$ ; and the north velocity error  $\Delta V_N$ . Rewriting the velocity error  $\Delta V_N$  as the difference between  $V_N$ , the error in the north velocity component of Eqn. 5-1 caused by Doppler radar and

AHRS measurement errors, and the velocity damping terms,  $\Delta\hat{V}_N$ , obtained from Loran data, the differential equation for the differential Loran position error is

$$\dot{\Delta N_D} = -K_1 \Delta N_D + \epsilon V_N - A[\Delta \dot{W}_A + K_1 (n_A - n_M)] - B[\Delta \dot{W}_B + K_1 (n_B - n_M)] - \hat{\Delta V}_N \quad (5-20)$$

The north velocity error damping term is the velocity correction given by weighing the difference between the measured Loran TDs and the predicted TDs, obtained from the system position solution. This is the same type of velocity damping term obtained in the differential Loran/strapdown inertial system and shown in Eqn. A-7. The differential equation for the north velocity damping variable, expressed in terms of the north component of differential Loran position error, is

$$\dot{\Delta V_N} = K_2 \Delta N_D + K_2 [A(n_A - n_M) + B(n_N - n_M)] \quad (5-21)$$

The next step in developing the error model is to express the Doppler/AHRS north velocity error  $\epsilon V_N$  in terms of the Doppler radar and AHRS measurement errors. By using a 1st order Taylor series expansion of Eqn. 5-1, in terms of the Doppler and AHRS errors, the following relationship is established:

$$\begin{aligned} \epsilon V_N = & \cos\psi \cos\theta \delta V_H + (-\sin\psi \cos\phi + \cos\psi \sin\theta \sin\phi) \delta V_D + (\sin\psi \sin\phi \\ & + \cos\psi \sin\theta \cos\phi) \delta V_Z - V_E \delta\psi + \cos\psi V_V \delta\theta + (\sin\theta V_E + \sin\psi \cos\theta V_V) \delta\phi \end{aligned} \quad (5-22)$$

where  $\delta V_H$ ,  $\delta V_D$ , and  $\delta V_Z$  are the Doppler radar measurement errors for the body axis velocity components, and  $\delta\phi$ ,  $\delta\theta$ , and  $\delta\psi$  are the AHRS uncertainties in roll, pitch, and heading.

The Doppler radar measurement error model consists of three types of errors: bias, scale factor error, and random velocity error. Ref. [24] indicates that sea current and frequency tracker bias are sources

of Doppler velocity biases; beam direction uncertainty and over water calibration shift are scale factor error sources; and Doppler frequency fluctuation is the source of random Doppler velocity errors. The correlation time of the random error is equivalent to the frequency tracker time constant. Expressed mathematically, this error model for one component of the Doppler velocity is

$$\epsilon V_H = \epsilon V_{HB} + \epsilon SF_H V_H + n_{DH}$$

where  $\epsilon V_{HB}$  is the bias,  $\epsilon SF_H$  is the scale factor error, and  $n_{DH}$  is the random noise component.

To measure attitude and heading, an AHRS establishes a vertical reference and heading reference by using a device to sense the direction of gravity (such as a pendulum, level, or set of accelerometers), and a magnetic compass. The spin axis of two gyroscopes in the AHRS define the vertical and heading reference lines with the spin axes directions maintained over the long term with the pendulum's indication of the direction of gravity and the magnetic compass's indication of the magnetic north direction. Aircraft attitude and heading are determined by measuring the orientation of the aircraft body axes relative to the axis of the two gyroscopes by reading out the angles between the gimbals that isolate the gyros from aircraft angular motion.

The basic performance of an AHRS is described during two flight conditions: During cruise conditions the gyroscope drift errors and pendulum and compass errors contribute to attitude and heading errors that are primarily constant. During turns the pendulum and compass gives false indications of both the directions of vertical and magnetic north causing the attitude and heading errors to increase. The ability of the AHRS gyroscopes to keep its spin axes fixed relative to inertial space is used to average the false indications, thereby limiting buildup rate and magnitude of the attitude and heading errors during turns.

The performance assessment performed in this section for the integrated differential Loran/Doppler/AHRS system, which used a second-order integration filter, uses Section 5.5.1's approach to analyzing the differential Loran/inertial system. Using Eqns. 5-20 and 5-21 as the dynamic models

for the integrated system errors, Appendix E derives expressions for the position and velocity uncertainties parametrized in terms of the Doppler, AHRS and differential Loran errors. Both steady state errors during cruise and peak errors during turns are derived.

Performance numbers are determined by calculating RMS error contributed by the composite of Doppler, AHRS, and Loran errors during cruise and turn segments of the approach profile described in Section 5.5.1. The performance of the system is dependent on the two feedback gains  $K_1$  and  $K_2$ , which are expressed in terms of their equivalent damping factor  $\zeta$  and natural frequency  $\omega_n$  in Appendix E. A unity damping factor was selected for a slightly damped system response. As is the case with the differential Loran/inertial case, the spatial variation of the Loran warpage and the Loran signal to noise (S/N) are dominant factors in selecting the natural frequency  $\omega_n$ . Therefore, the gains computed in Section 5.5.1 for the two S/N ratios (S/N = 0 db and S/N = 8 db) were used in this section's analysis. It should be noted that the gains used in the system establish limits on the Loran signal strength, noise environment, and Loran warpage compensation accuracy, if the position and velocity performance objectives given in Section 5.5.1 are to be achieved.

Table 5-VI presents the differential Loran/Doppler/AHRS position and velocity uncertainties for the Doppler, AHRS and Loran error sources. Appendix E and Table 5-VI show that the steady-state position and velocity errors during cruise conditions are zero, except for effects of Doppler noise, Loran noise and Loran warpage variations. All the Doppler and AHRS error sources, except for Doppler noise, cause transient position and velocity errors during turns; however, Table 5-VI shows only the large transient errors caused by the AHRS heading error.

A number of conclusions can be drawn from the performance results shown in Table 5-VI for an integrated differential Loran/Doppler/AHRS system, using a 2nd order integration technique. First, a second order integration technique is not adequate for integrating these sensors and meeting the 75 feet ( $1\sigma$ ) position error and 3 feet/sec ( $1\sigma$ ) velocity error performance objectives. There are two error sources that limit the system performance when using a position and velocity damping integration technique: (1) the velocity error caused by Doppler noise and (2) the position and velocity error transients caused by AHRS heading error during turns. These observations lead to a second conclusion: to meet the performance objectives the

TABLE 5-VI  
DIFFERENTIAL LORAN/DOPPLER/AHRS SYSTEM PERFORMANCE

ERROR SOURCE	SNR = 0 db (1)			SNR = 8 db (1)		
	Position Error (ft)	Velocity Error (2) (ft/sec)	Position Error (ft)	Velocity Error (2) (ft/sec)	Position Error (ft)	Velocity Error (2) (ft/sec)
DOPPLER						
Bias	0.0	0.0	0.0	0.0	0.0	0.0
Scale Factor	0.0	0.0	0.0	0.0	0.0	0.0
Random $(S_d = 2.9 \text{ ft}^2/\text{sec}^2 \text{ Hz})$	3.3	1.7	3.9	1.7	3.9	1.7
AHRS						
Roll and Pitch	0.0	0.0	0.0	0.0	0.0	0.0
Heading ( $\sigma_\psi = 3 \text{ deg}$ )						
Cruise	0.0	0.0	0.0	0.0	0.0	0.0
Turn (3)	59 (4)	3.9 (4)	83. (4)	3.9 (4)	83. (4)	3.9 (4)
LORAN						
Noise	52.1	1.5	17.4	.4	1.5	.4
Warpage (5)	38.2	2.4	61.8	2.8	38.2	2.8
RSS						
Cruise	64.7	3.3	64.3	3.3	64.7	3.3
Turn	87.6	5.1	105.1	5.1	87.6	5.1

- (1) Filter bandwidth  $\omega_n = 0.066 \text{ rad/sec}$  for SNR = 0 db,  $\omega_n = 0.047 \text{ rad/sec}$  for SNR = 8 db.
- (2) Assumes frequency tracker time constant of 1 sec.
- (3) Assumed velocity change of 200 ft/sec during turn.
- (4) Peak error during turn.
- (5) Warpage  $d_d = 12 \text{ nm}$ ,  $\sigma_w = 0.256 \mu\text{sec}$  for SNR = 0 db,  $\sigma_w = 0.353 \mu\text{sec}$  for SNR = 8 db

integration technique must damp out AHRS heading errors, and the short term accuracy of the AHRS data must be used to smooth the Doppler noise in the system velocity solution. (Also AHRS roll and pitch errors will need to be damped out if the AHRS heading error is damped.)

To incorporate these additional complexities into the integrated system will probably require a Kalman filter be used for the integration technique. (A Kalman filter for integrating differential Loran with strapdown inertial is discussed in the next section.) The state vector for a Kalman filter for an integrated differential Loran/Doppler/AHRS should include the north and east position errors, three body axis velocity errors, AHRS roll, pitch and heading errors, and two Loran warpage parameters. The Kalman filter observation vector should contain the two Loran time differences and the three Doppler velocity measurements. By using a Kalman filter integration technique to smooth the Doppler noise and estimate the AHRS attitude and heading errors, the integrated system will meet the 4-D INCADS performance objectives.

## 5.6 DIFFERENTIAL LORAN/STRAPDOWN INERTIAL KALMAN FILTER SIMULATION

The analytical evaluation results of the Section 5.5.1 show that a second-order integration filter that corrects only inertial position and velocity errors is not adequate for a differential Loran/inertial system using either a 20 nm/hr or 5 nm/hr inertial system. To determine the feasibility of using these two classes of inertial systems in the 4-D INCADS, an IBM-370 simulation of the baseline differential Loran/strapdown inertial system, using a Kalman filter for the integration filter, was developed. The simulation program numerically integrates the vector differential equation (Eqn. 5-10) to simulate the errors in the differential Loran/strapdown inertial system and the differential baro/inertial system. The program uses aircraft accelerations, roll, pitch, and heading variables from a terminal area profile, representative of a military transport mission. The gain matrix, ( $K(t)$ ), in Eqn. 5-10 is computed with an 18-state Kalman filter that corrects for inertial position, velocity, attitude, and heading errors, and accelerometer and gyro biases.

The Kalman filter is an optimal data processing technique. It processes the Loran and inertial data to minimize the root mean square (RMS) of the differential Loran/strapdown inertial errors. The Kalman filter is optimum since, when compared to other data processing techniques, the filter has the smallest RMS error. In addition, as part of its processing algorithm the Kalman filter calculates the covariance matrix of the system errors. The covariance matrix is computed in one simulation run, thus eliminating the need for a Monte Carlo simulation technique for determining the error variances. (In the Monte Carlo technique, a multitude of independent simulation runs are made to accumulate enough independent samples of the system errors to accurately calculate the error variances.)

This study uses the Kalman filter error covariance matrix results to answer the following questions: (1) does a differential Loran/strapdown inertial system have the 75 foot position and 3 feet/sec velocity accuracies for the 4-D INCADS approach missions, and (2) how accurately can the strapdown inertial attitude errors, heading errors, and gyro biases be estimated with a Kalman filter? The uncertainty in the inertial attitude, heading, and gyro biases is important since they determine the autonomous inertial position and velocity performance when the Loran receiver loses lock.

For the simulation program, Eqn. 5-10 was converted to a vector difference equation that defines the trajectories of the errors at a sequence of time points,  $t_i$ . Successive time points are spaced 1 second apart; i.e.,  $\Delta t = t_{i+1} - t_i = 1$  sec. In deriving the difference equations, the rectangular integration algorithm was used to approximate each term in the vector differential equations with the exception of those terms that are functions of aircraft acceleration, attitude, or heading. These terms were expressed more accurately since they may change rapidly during the one-second integration time step. The integrals of the acceleration components and the  $C_B^N$  entries over each one-second integration step replace the  $\Delta t$  times acceleration and the  $\Delta t$  times  $C_B^N$  terms that appear in the rectangular integration algorithm. This approximation technique is discussed in more detail in Ref. [17].

The vector difference equation used in the simulation is

$$\begin{bmatrix} \underline{x}_{Hj+1} \\ \underline{x}_{vj+1} \end{bmatrix} = \begin{bmatrix} I - K_{j+1} H_1 & | & 0 \\ | & | & | \\ 1 & 0 & | \\ 0 & | & 0 & 1 \end{bmatrix} \left\{ \begin{bmatrix} \Phi_H(t_{j+1}, t_j) & | & \Delta t \Delta A_{Bj} \\ | & | & | \\ \Phi_v(t_{j+1}, t_j) & | & \Phi_v \end{bmatrix} \begin{bmatrix} \underline{x}_{Hj} \\ \underline{x}_{vj} \end{bmatrix} + \begin{bmatrix} \Delta t d_{-Hj}^* \\ \Delta t d_{-vj}^* \end{bmatrix} \right\}$$

(5-23)

$$+ \begin{bmatrix} K_{j+1} H_2 \\ | \\ | \\ | \\ 0 \end{bmatrix} \begin{bmatrix} n_{Aj+1}^* \\ n_{Bj+1}^* \\ n_{Mj+1}^* \end{bmatrix}$$

where

$K_{j+1}$  = 18 x 2 Kalman filter gain matrix defined below

$n_{Aj+1}^*, n_{Bj+1}^*, n_{Mj+1}^*$  = Loran tracking errors, which have zero means, standard deviation,  $\sigma_n$ , and correlation times  $\tau_L$

$\Phi_H(t_{j+1}, t_j)$  = 18 x 18 state transition matrix for differential Loran/strapdown Loran system (defined in Appendix B)

$\Phi_v$  = 2x2 state transition matrix for vertical channel (defined in Appendix B)

$\Phi_c(t_{j+1}, t_j)$  = 2x18 matrix which couples horizontal channel errors into the vertical channel (defined in Appendix B)

$\underline{d}_{Hj}^*, \underline{d}_{Vj}^*$  = 18x1 and 2x1 vectors of noise and dynamic measurement errors (defined in Appendix B)

The Loran noise standard deviation  $\sigma_n$  and correlation time  $t_L$  are computed from the Loran S/N. To have a Loran TOA tracking loop standard deviation,  $\sigma_n$ , in the presence of Loran-C noise, a second-order tracking loop with a 0.707 damping factor requires a time constant

$$\tau_L = \frac{3}{2} 10^{-1.1S/N} \text{GRP}/16\sigma_n^2 \omega_0^2$$

where

$$\omega_0 = 2\pi 10^5 \text{ rad/sec}$$

The set of Kalman filter matrix equations that are calculated every time instant  $t_{j+1}$ , to obtain a solution for  $K_{j+1}$ , are

$$P_{j+1}^- = \Phi(t_{j+1}, t_j) P_j^+ \Phi(t_{j+1}, t_j)^T + Q_j \quad (5-24)$$

$$K_{j+1} = P_{j+1}^- H_1^T (H_1 P_{j+1}^- H_1 + R_{j+1})^{-1} \quad (5-25)$$

$$P_{j+1}^+ = (I - K_{j+1} H_1) P_{j+1}^- (I - K_{j+1} H_1)^T + K_{j+1} R_{j+1} K_{j+1}^T \quad (5-26)$$

where

$$R_{j+1} = \begin{bmatrix} A & B \\ C & D \end{bmatrix} \begin{bmatrix} 2\sigma_n^2 & \sigma_n^2 \\ \sigma_n^2 & 2\sigma_n^2 \end{bmatrix} \begin{bmatrix} A & C \\ B & D \end{bmatrix}$$

$R_{j+1}$  = covariance matrix of Loran noise

$Q_j$  = 18x18 covariance matrix of the input vector  $\Delta t d^*_{-Hj}$

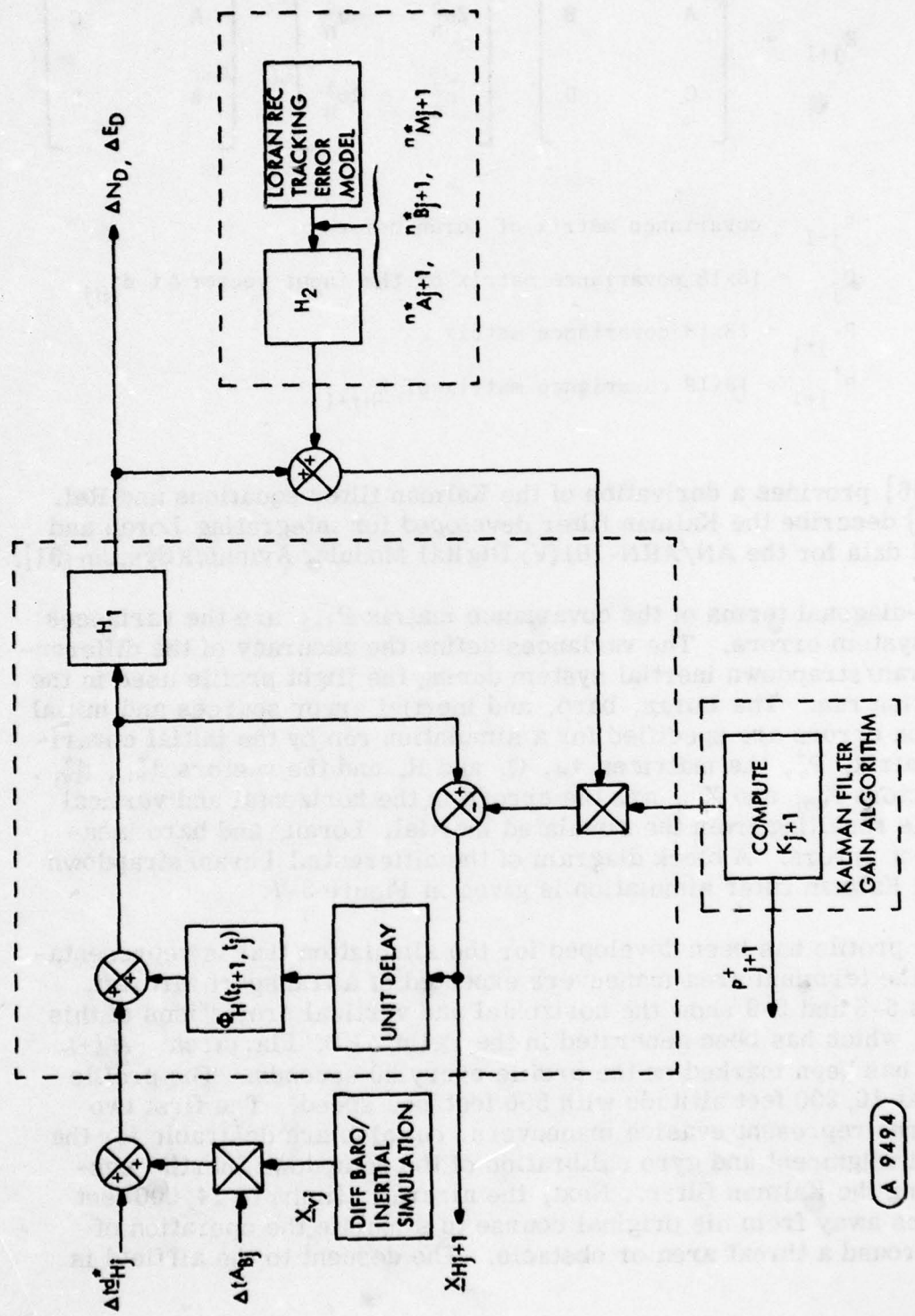
$P_{-j+1}$  = 18x18 covariance matrix

$P_{j+1}^+$  = 18x18 covariance matrix of  $X_{-Hj+1}$

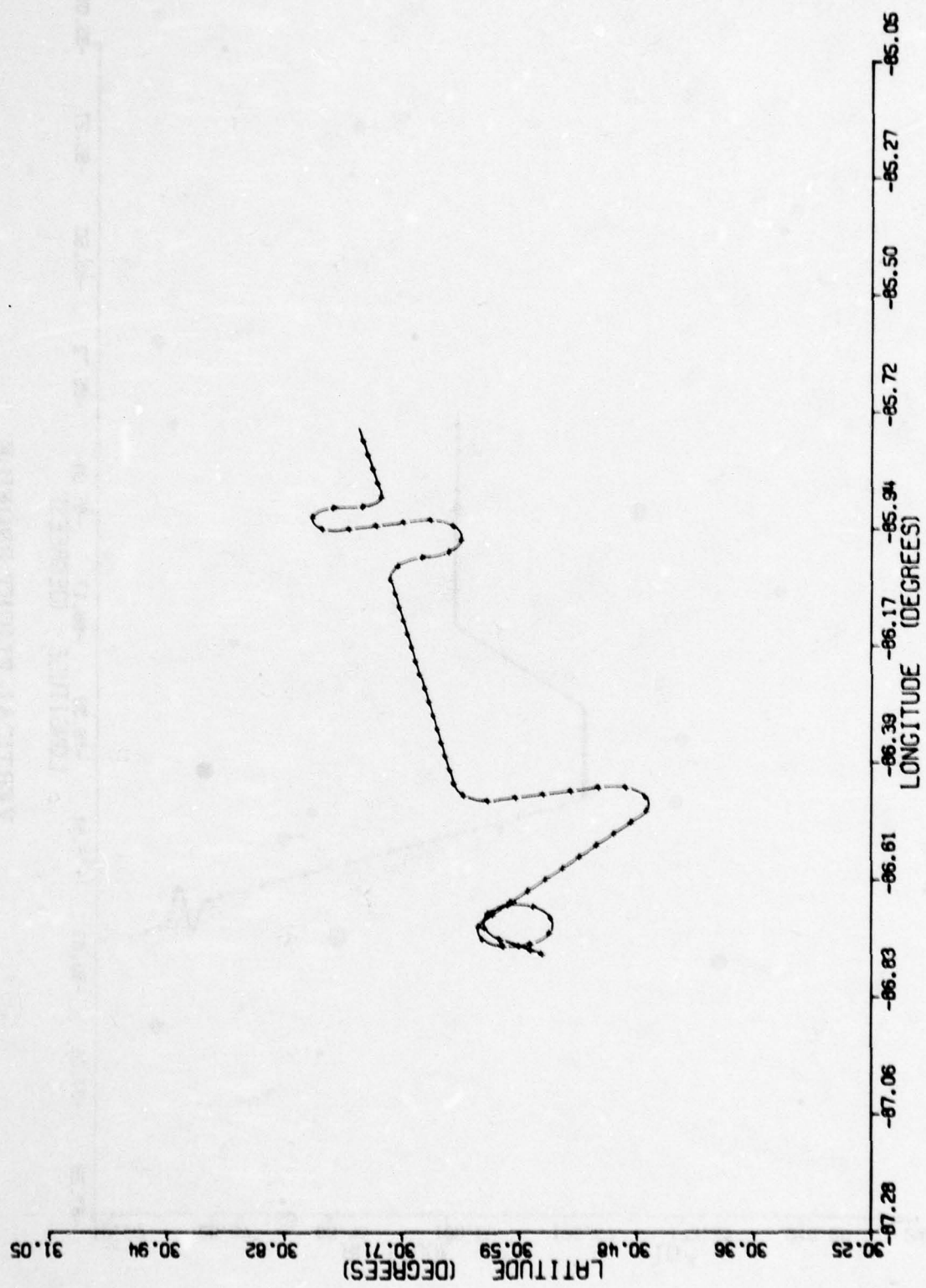
Ref. [16] provides a derivation of the Kalman filter equations and Ref. [15, 17] describe the Kalman filter developed for integrating Loran and inertial data for the AN/ARN-101(V) Digital Modular Avionics System [31].

The on-diagonal terms of the covariance matrix  $P_{j+1}^+$  are the variances of the system errors. The variances define the accuracy of the differential Loran/strapdown inertial system during the flight profile used in the simulation run. The Loran, baro, and inertial error sources and initial condition errors are specified for a simulation run by the initial covariance matrix,  $P_0^+$ , the matrices  $\Phi_H$ ,  $Q$ , and  $R$ , and the vectors  $d^*_{Hj}$ ,  $d^*_{Vj}$ . The vectors  $X_{Hj}$  and  $X_{Vj}$  are the errors in the horizontal and vertical channels resulting from the simulated inertial, Loran, and baro measurement errors. A block diagram of the differential Loran/strapdown inertial Kalman filter simulation is given in Figure 5-7.

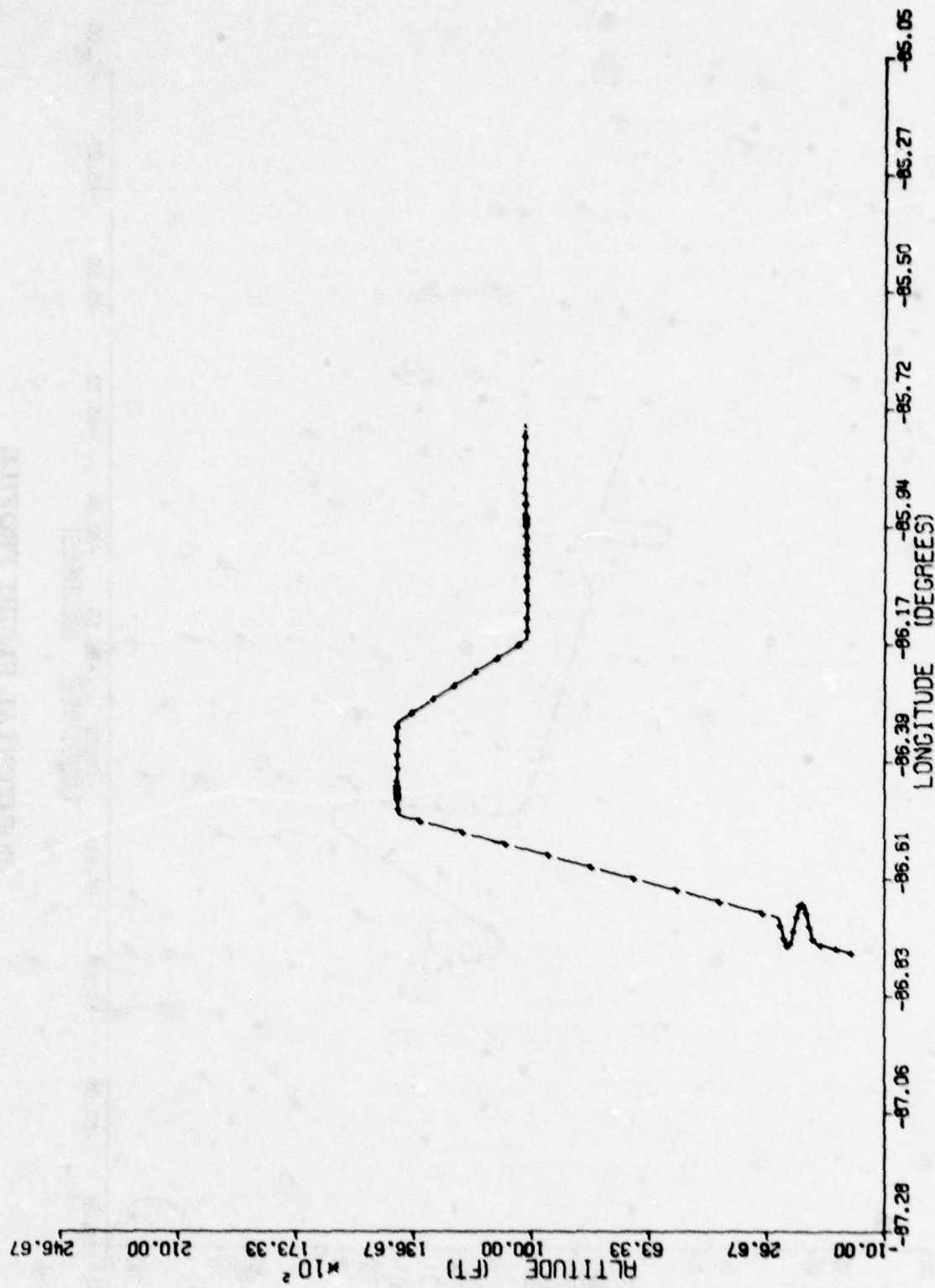
A flight profile has been developed for the simulation that is representative of the terminal area maneuvers expected of a transport aircraft. Figures 5-8 and 5-9 show the horizontal and vertical projections of this profile, which has been generated in the Eglin AFB, Fla. area. A (+) symbol has been marked on the profile every 20 seconds. The profile begins at 10,200 feet altitude with 500 feet/sec speed. The first two 180° turns represent evasive maneuvers, but also are desirable for the in-flight alignment and gyro calibration of the strapdown inertial system using the Kalman filter. Next, the aircraft climbs to 14,000 feet and turns away from his original course to simulate the operation of flying around a threat area or obstacle. The descent to the airfield is



DIFFERENTIAL LORAN/INS KALMAN FILTER SIMULATION BLOCK DIAGRAM  
FIGURE 5-7



HORIZONTAL FLIGHT PROFILE  
FIGURE 5-8



VERTICAL FLIGHT PROFILE  
FIGURE 5-9

made from 14K feet at a flight path angle of 8 degrees with a spiral, prior to final approach. The final approach velocity is 144 knots = 245 feet/sec.

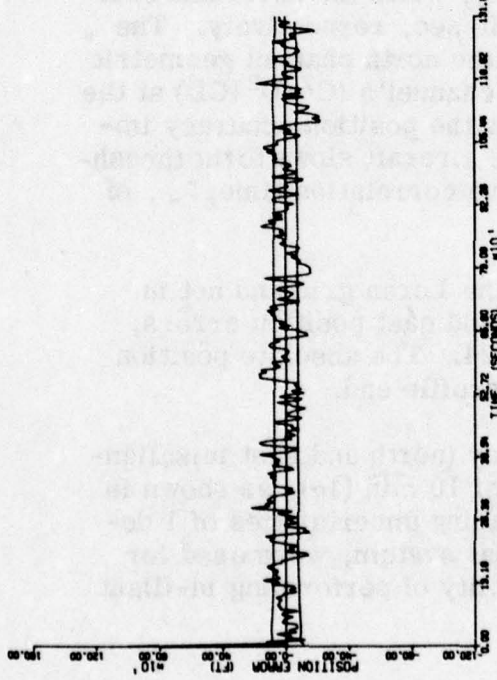
The results of a simulation run using the flight profile that shows both the in-flight alignment capability of the Kalman filter and the system position, velocity, heading, attitude, and gyro bias estimation accuracies are displayed in Figures 5-10 to 5-24. The differential baro/inertial errors for this run are given in Figures 5-25 and 5-26. On each plot the solid line defines the error that occurred during the run, and the two dashed lines define the  $1\sigma$  envelope for the error. The error standard deviations ( $\sigma$ ) were calculated by the Kalman filter (see Eqn. 5-26). On this run, the Loran conditions were an S/N = 0 db (equivalent to  $\sigma_n = 0.14 \mu\text{sec}$ , and  $r_L = 1.3 \text{ sec}$ ) and Loran warpages with  $\sigma_n = 0.2 \mu\text{sec}$  and  $d_d = 12 \text{ nm}$ . The strapdown inertial errors at the beginning of the simulation run are given in Table 5-VII.

For this simulation run, the baro altimeter noise was 12.3 feet ( $1\sigma$ ) with a correlation time,  $r_g$ , of 1 second; the D value gradient was zero.

The differential Loran/strapdown inertial position and velocity standard deviations in Figures 5-10 to 5-13 show that the 20 nm/hr inertial system combined with Loran can provide the inputs for 4-D INCADS approach guidance. The north and east position uncertainties at the final approach waypoints are 62 feet and 80 feet, respectively, while the north and east velocity standard deviations are 1.7 and 2.0 ft/sec, respectively. The north channel performance is better because the north channel geometric dilution ( $A^2 + B^2 + AB$ ) is smaller than the east channel's ( $C^2 + D^2 + CD$ ) at the Eglin AFB. Also, Figures 5-10 and 5-11 show the position accuracy improves near the end of the profile because the aircraft slows to the threshold speed of 144 knots, increasing the effective correlation time,  $r_w$ , of the Loran warpage.

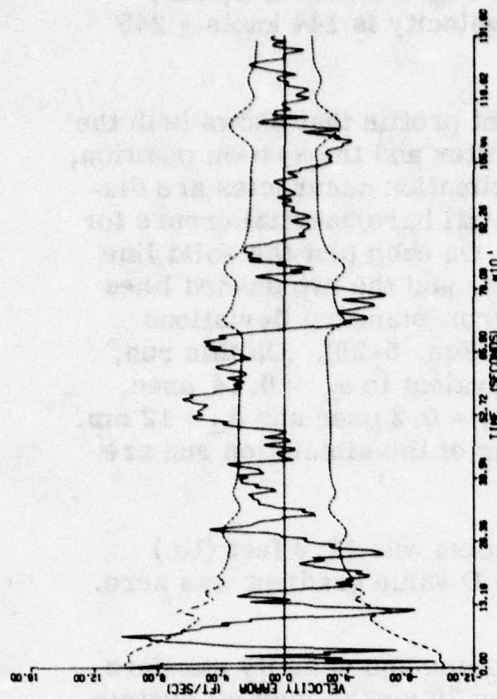
To demonstrate the reason for navigation in the Loran grid and not in the geodetic grid, plots of the absolute north and east position errors,  $\Delta N$  and  $\Delta E$ , are given in Figures 5-23 and 5-24. The absolute position errors are as large as 200 to 300 feet at the profile end.

The integrated system has an attitude accuracy (north and east misalignments) of  $1.5 \text{ min } (1\sigma)$  and heading accuracy of  $10 \text{ min } (1\sigma)$ , as shown in Figures 5-14 to 5-16. Initial attitude and heading uncertainties of 1 degree, which are typical of an unaligned inertial system, were used for this simulation run to demonstrate the feasibility of performing in-flight alignment with the Kalman filter.



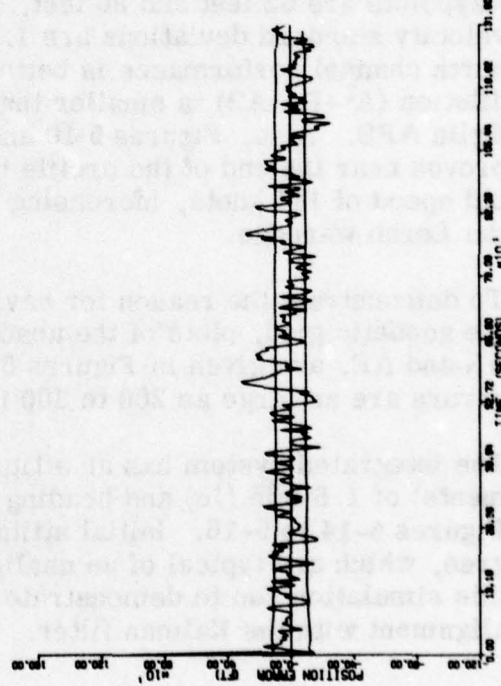
NORTH DIFFERENTIAL LORAN POSITION ERROR

FIGURE 5-10



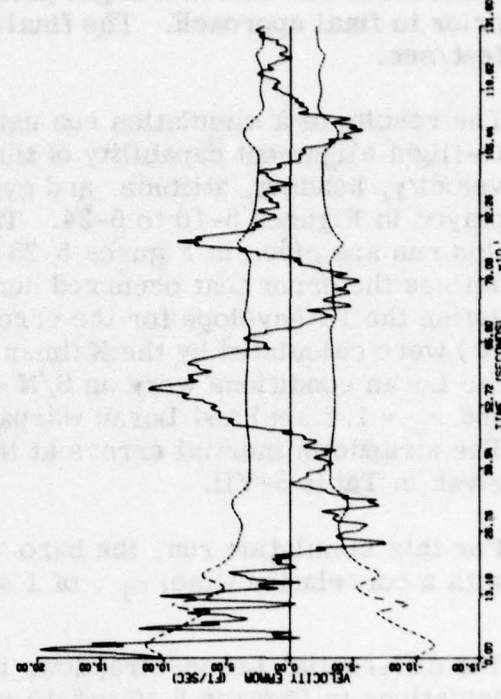
NORTH VELOCITY ERROR

FIGURE 5-12



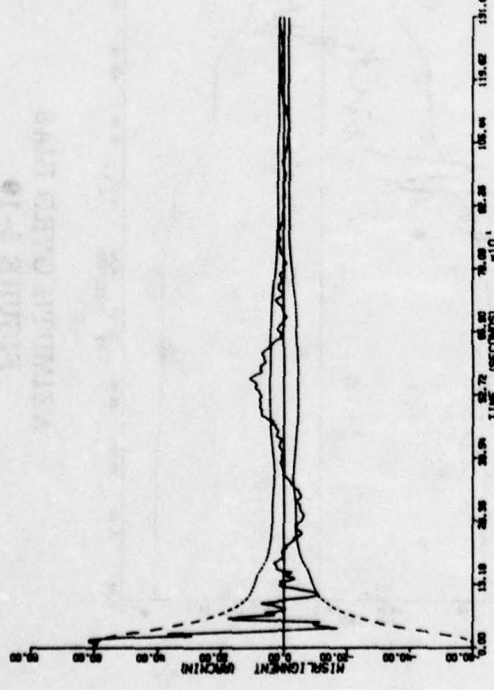
EAST DIFFERENTIAL LORAN POSITION ERROR

FIGURE 5-11

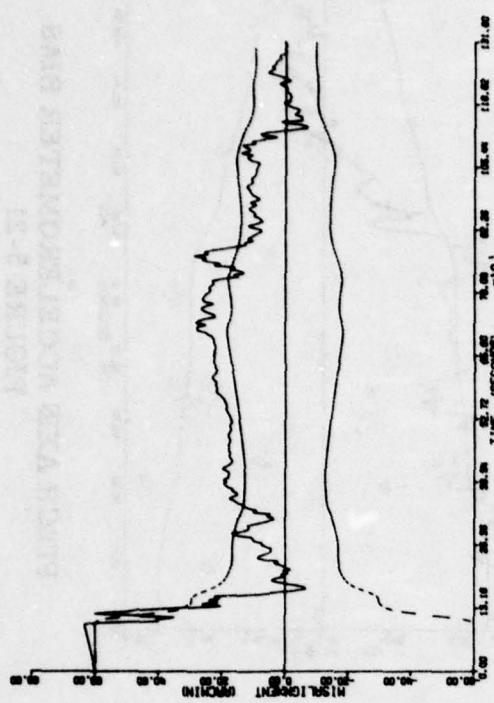


EAST VELOCITY ERROR

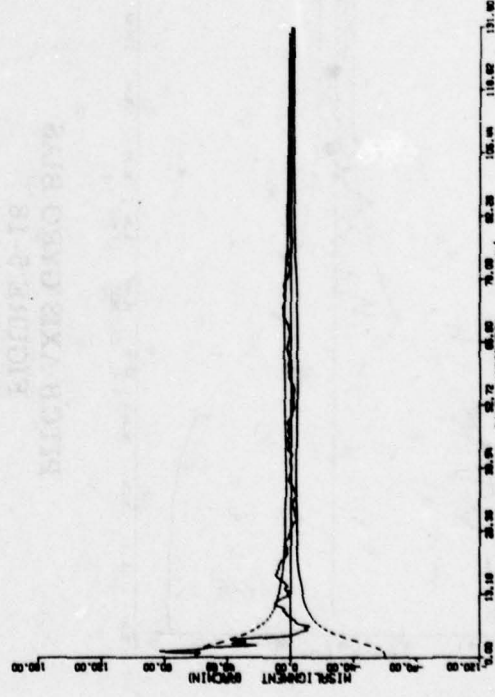
FIGURE 5-13



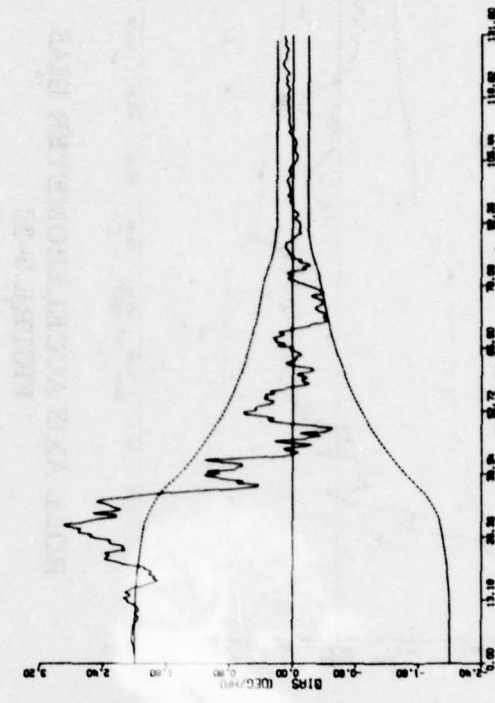
NORTH MISALIGNMENT ANGLE  
FIGURE 5-14



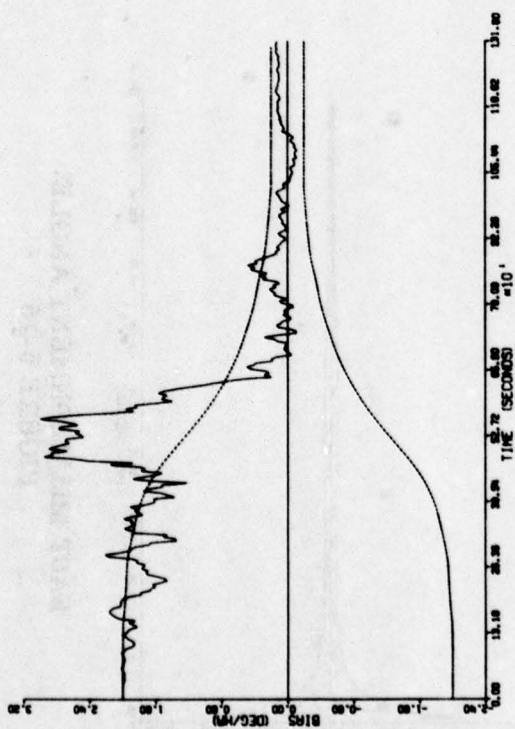
VERTICAL MISALIGNMENT ANGLE  
FIGURE 5-16



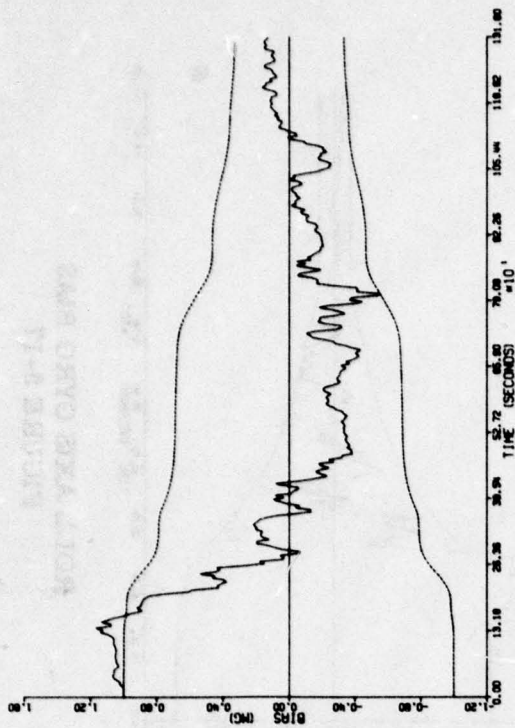
EAST MISALIGNMENT ANGLE  
FIGURE 5-15



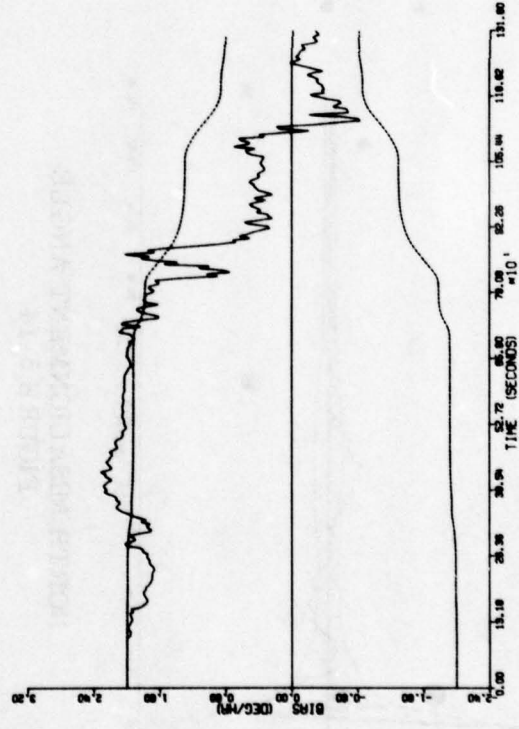
ROLL AXIS GYRO BIAS  
FIGURE 5-17



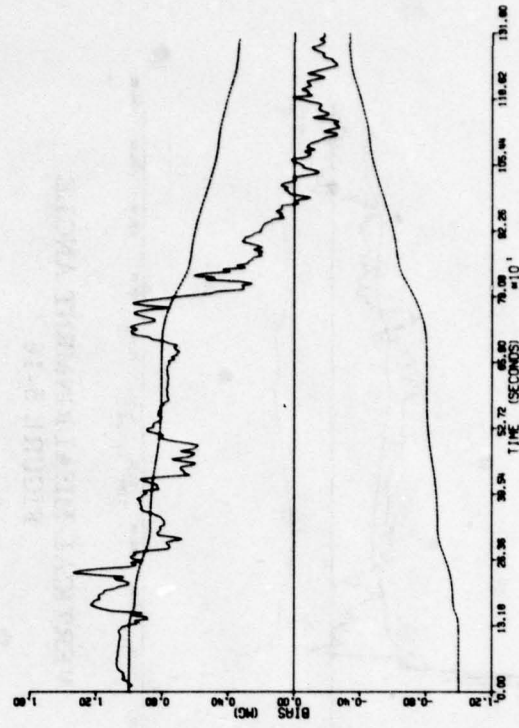
PITCH AXIS GYRO BIAS  
FIGURE 5-18



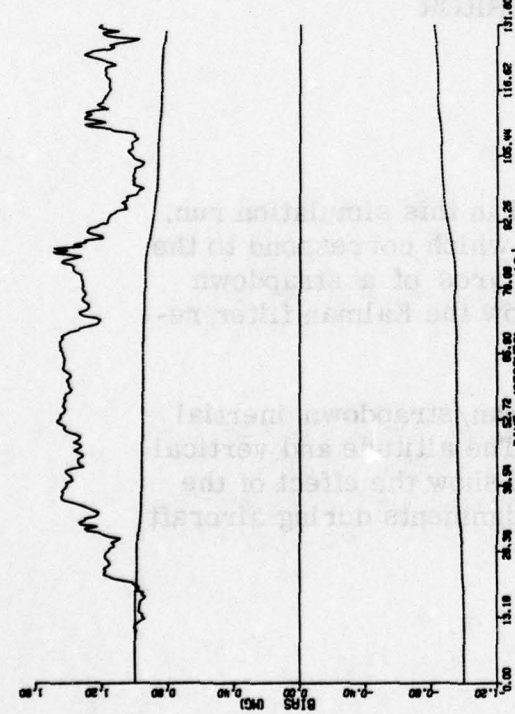
ROLL AXIS ACCELEROMETER BIAS  
FIGURE 5-20



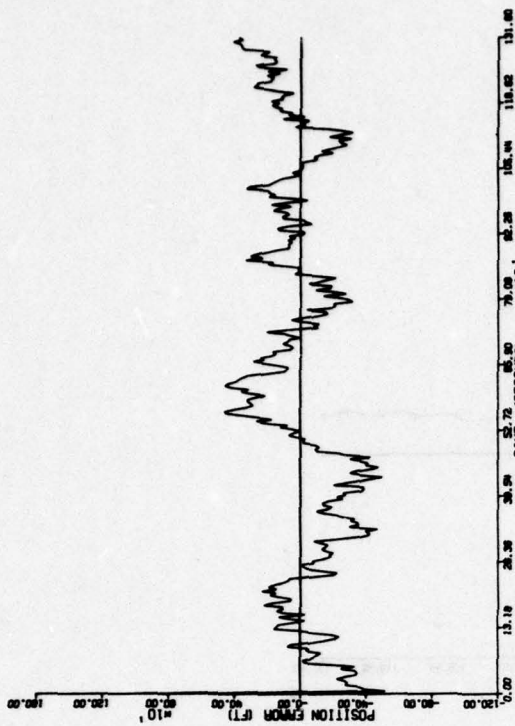
AZIMUTH GYRO BIAS  
FIGURE 5-19



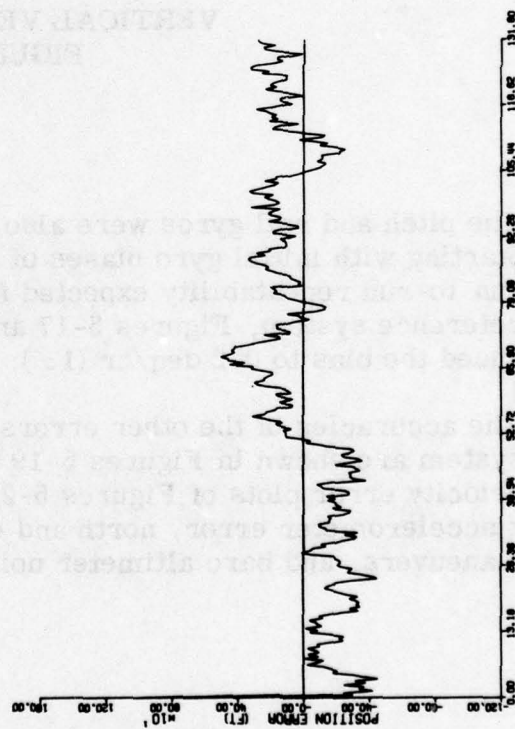
PITCH AXIS ACCELEROMETER BIAS  
FIGURE 5-21



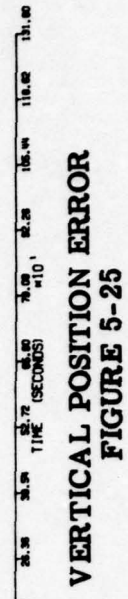
AZIMUTH ACCELEROMETER BIAS  
FIGURE 5-22



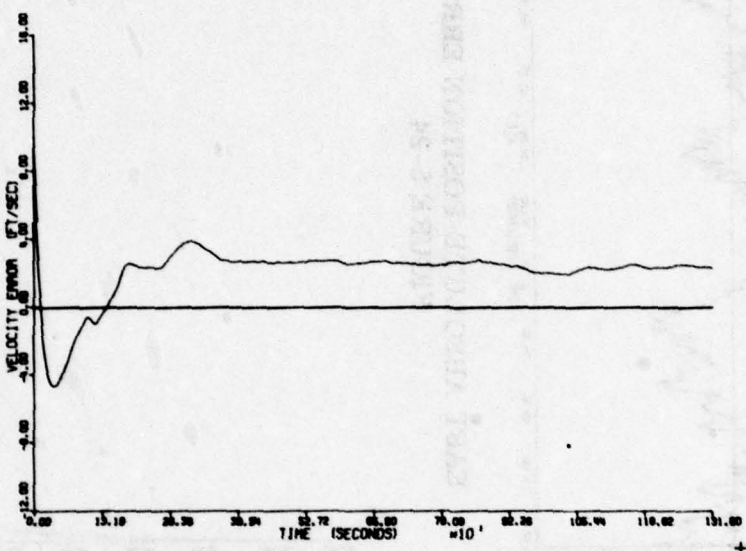
EAST ABSOLUTE POSITION ERROR  
FIGURE 5-24



NORTH ABSOLUTE POSITION ERROR  
FIGURE 5-23



VERTICAL POSITION ERROR  
FIGURE 5-25



**VERTICAL VELOCITY ERROR  
FIGURE 5-26**

The pitch and roll gyros were also calibrated in this simulation run. Starting with initial gyro biases of 2 deg/hr, which correspond to the run-to-run repeatability expected from rate gyros of a strapdown reference system, Figures 5-17 and 5-18 show the Kalman filter reduced the bias to 0.2 deg/hr ( $1\sigma$ ).

The accuracies of the other errors in the Loran/strapdown inertial system are shown in Figures 5-19 to 5-22. The altitude and vertical velocity error plots of Figures 5-25 and 5-26 show the effect of the z accelerometer error, north and east misalignments during aircraft maneuvers, and baro altimeter noise.

TABLE 5-VII  
**INITIAL CONDITIONS AND INERTIAL SENSORS ERRORS FOR  
 THE DIFFERENTIAL LORAN/STRAPDOWN  
 INERTIAL SIMULATION**

$\sigma_{ND} = \sigma_{NE} = 1000$ feet:	Initial Position Std. Dev.
$\sigma_{vN} = \sigma_{vE} = 10$ ft/sec:	Initial Velocity Std. Dev.
$\sigma_{pN} = \sigma_{pE} = 1$ deg:	Initial north and east misalignment Std. Dev.
$\sigma_{pv} = 1$ deg:	Initial heading misalignment Std. Dev.
$\sigma_{GBX} = \sigma_{GBY} = 2$ °/HR:	Initial gyro biases Std. Dev.
$\sigma_{GBZ} = 2$ °/HR:	Initial z gyro bias Std. Dev.
$\sigma_{GBNX} = \sigma_{GBNY} = \sigma_{GBNZ} = 0.2$ °/HR:	Gyro Noise Std. Dev. ( $\tau_g = 20$ sec)
$\sigma_{ABX} = \sigma_{ABY} = \sigma_{ABZ} = 1000$ $\mu g$ :	Accelerometer Bias Std. Dev.
$\Delta h_D = 1000$ feet:	Initial Altitude Error
$\Delta V_v = 10$ feet/sec:	Initial Vertical Velocity Error
GS = .15%	X, Y, Z Gyro Scale Factor Errors
GM = 2.0 °/HR/G	X, Y, Z Gyro Mass Unbalances
GA = 2.0 °/HR/G <sup>2</sup>	X, Y, Z Gyro Anisoelastic Drift
AN = 30. $\mu g$	X, Y, Z Accelerometer Noise Std. Dev.
TA = 100. sec.	X, Y, Z Accelerometer Noise Time Constants
AS = .2 %	X, Y, Z Accelerometer Scale Factor Errors

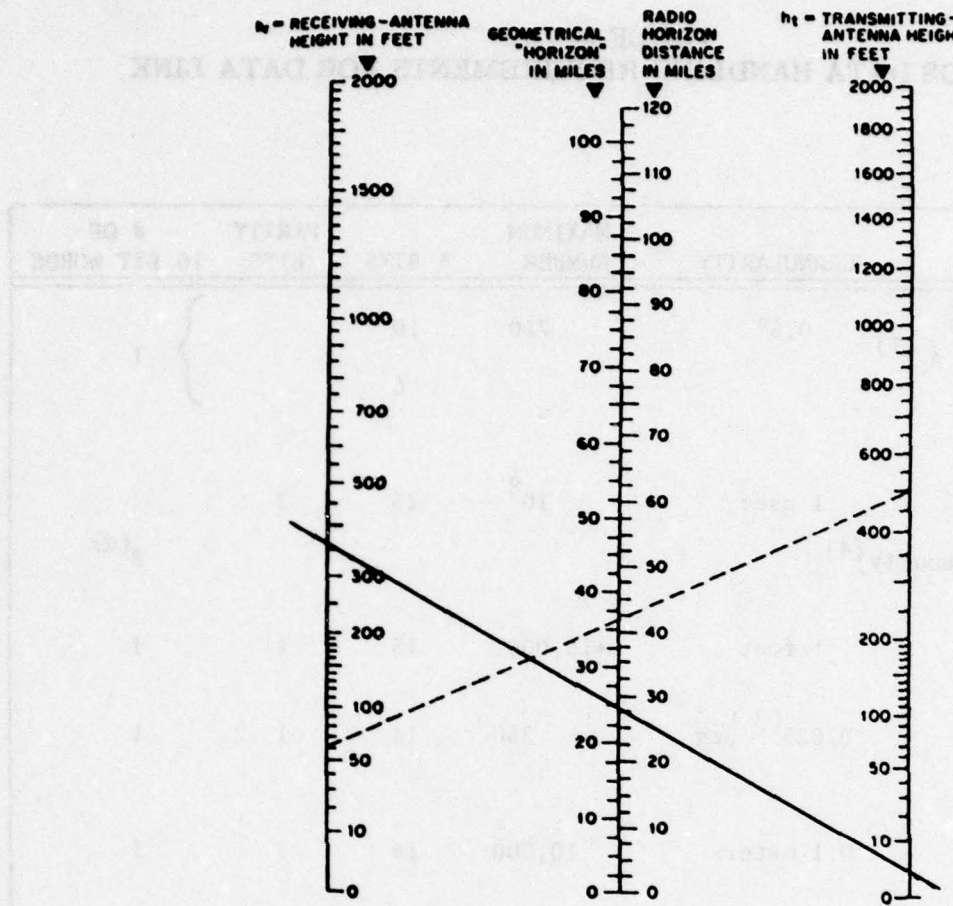
## 5.7 ANALYSIS OF DATA LINK PARAMETERS

Measurements of Loran time differences and barometric altitude from a point, whose position is accurately determined with respect to the end of the runway, are required for the differential Loran/inertial navigation mode. Another measurement that can be critical, particularly for the spiral descent maneuver to a landing strip, is the ground wind velocity and direction. If the spiral descent occurs above the airstrip there is not sufficient flight path time to determine the ground wind's magnitude and direction, and if it is a strong cross wind, foreknowledge is very important to complete the landing on the first attempt.

This section derives the "ground to air" data link parameters required to transmit ground measurements of Loran time differences, barometric altitude measurements, wind velocity, and wind direction from the airfield to the aircraft. In the following paragraphs, all of the parameters that contribute to the bandwidth and average power determination of the data link will be identified. Section 5.7.1 establishes a minimum range and altitude performance. Section 5.7.2 identifies the message content in binary word size and bandwidth required. Section 5.7.3 contains additional parameter relationships and average transmitted power calculation.

### 5.7.1 Distance/Height of Aircraft

Figure 5-27 is a nomogram of radio horizon versus transmitting and receiving height. It assumes a 4/3 earth radius which is normal for a "standard atmosphere". The solid line shows the radio horizon to be 360 feet at a range of 28 statute miles (25 nm) from a transmitted height of 2 to 4 feet. This is about the maximum practical distance that reliable communication, to an aircraft at 500 feet altitude, can be achieved. A range of 25 nm at a velocity of 360 knots provides at least 4 minutes prior to touchdown.



NOMOGRAM RELATING RADIO HORIZON DISTANCE  
(HEIGHT AND DISTANCE)  
FIGURE 5-27

#### 5.7.2 Message Content

The minimal content required from the ground station is shown on Table 5-VIII. The information includes:

- An address (that can be programmable for security reasons) and the direction of the runway.
- Four time difference measurements (maximum).
- Height of runway (above or below sea level).

**TABLE 5-VIII**  
**4-D INCADS DATA HANDLING REQUIREMENTS FOR DATA LINK**

ITEM	GRANULARITY	MAXIMUM NUMBER	# BITS	PARITY BITS	# OF 16 BIT WORDS
Airport Runway Direction From Pt A (1) Security Code or Address	0.5°	720	10	6	{ 1
Time Difference Measurements (4 Req'd simultaneously) <sup>(4)</sup>	1 nsec	$10^8$	28	2	8 <sup>(2)</sup>
Altitude of Pt A	1 foot	$\pm 15,000$	15	1	1
True Bearing from B to A	$0.025^{(3)}$ deg	360	14	1	1
Range from B to A	0.1 meters	10,000	14	1	1
Wind Velocity Ground Direction	1 Kt 2 deg	100 180	7 8	1	1
Height from B to A Test and Malfunction	1 foot	$\pm 128$	8 7	1	{ 1

(1) A is point at one end of runway  
B is location of data link

(2) Four 32 bit double precision words

(3) Requirement reduced to 0.5 degrees if data link is placed on line perpendicular to runway, through point A.

(4) Required for four slaves in a Loran transmitter chain.

- True bearing from the ground data link to the reference point on the runway.
- Range in meters from the Loran antennas to the reference point on the runway.
- Elevation difference between the barometric altimeter and the reference point on the runway.
- Wind velocity (knots) and direction (degrees).
- A digital word for fault indication.

The information requires six 16-bit single precision words and four 32-bit double precision words. The Loran stations operate at a minimum repetition rate of 10 Hz. Using a fixed sampling rate of 10 Hz for the data, the bit rate is 2240 Hz. The predetection bandwidth required by the data link receiver can be as low as 3 kHz. A bandwidth of 7 kHz used for a signal-to-noise prediction will be representative.

### 5.7.3 Transmitter Power Calculation

The equation for average transmitted power is:

$$P_T = \frac{64\pi^2 \times S/N \times R^2 \times kTB \times \overline{NF} \times L}{G_T \times G_R \times \lambda^2}$$

where

$P_T$  = average transmitted RF power in watts

S/N = signal to noise

R = range

k = Boltzmann's constant

T = Kelvin temperature

B = noise bandwidth

$\overline{NF}$  = noise figure or receiver

$G_T$  = gain of transmitter antenna

$G_R$  = gain of receiving antenna

$\lambda$  = carrier wavelength

L = RF losses due to mismatches, coupling losses, etc.

The values used in the equation are:

S/N     A value of 17.5 db will result in a bit error rate (BER) not to exceed  $10^{-4}$  [18]. Use of parity bits shown on Table 5-VIII should reduce the error further. A  $10^{-4}$  BER would result in one bit error once in every 50 complete messages.

$$R = 25 \text{ nm}$$

$$k = 1.364 \times 10^{-23} \text{ watts/degree Kelvin/Hz}$$

$$T = 300^{\circ}\text{K}$$

$$B = 7,000 \text{ Hz}$$

$$\overline{NF} = 10 \text{ db}$$

$$G_T = G_R = 4 \text{ db (vertical quarter wave dipole)}$$

$$\lambda = 0.2 \text{ meters (1500 MHz)}$$

$$L = 10 \text{ db}$$

Result:

$$P_T = 0.165 \text{ watts average of radiated power.}$$

## **6 INTEGRATED GPS - INERTIAL SYSTEM ANALYSIS**

### **6.1 INTRODUCTION**

The NAVigation Satellite Timing And Ranging Global Positioning System (NAVSTAR GPS) is currently being developed under a tri-service program [25]. NAVSTAR GPS, referred to as GPS in this report, is a radio navigation system that uses satellites as transmitters. The tri-service program's objective is to develop a high precision, global, secure radio navigation system by 1984. This study addressed the use of GPS in the 4-D INCADS since the current military plans call for GPS to replace Loran as the military tactical radio navigation system.

An integrated GPS inertial navigation system concept has been investigated for the 4-D INCADS. In this concept the 4-D INCADS computer processes real-time measurements from an on-board GPS receiver, a set of inertial sensors, and a barometric altimeter to compute a solution for aircraft position, velocity, attitude, and heading. The data processing technique -- referred to as an integration filter -- processes the sensors' measurements in a way that relies upon the long term accuracy of the GPS and barometric altimeter measurements and the short term accuracy of the inertial sensor measurements to obtain a navigation solution better than any sensor can provide by itself.

In Section 5 an integrated navigation technique using Loran as the radio navigation sensor was analyzed. The inertial navigation and barometric altimeter explanations and error models developed in that section are applicable to this section's investigation. Section 5 also analyzed a differential Loran technique for obtaining the position and velocity accuracies needed for aircraft guidance in the final approach segment. The analogous technique -- differential GPS -- is addressed here.

This section begins with a description of the three segments (space system segment, control system segment, user segment) of the GPS where the 4-D INCADS with a GPS receiver is in the user segment. Next, Section 6.3 describes the mechanization of an integrated GPS/inertial/baro navigation system for the 4-D INCADS, including the use of GPS in a differential mode. The section concludes by discussing the GPS-related processing requirements for the 4-D INCADS computer, and an assessment of the accuracy of the integrated navigation system.

In summary, the section shows that the horizontal position and velocity accuracy of an integrated GPS/inertial/baro system is equal to or better than an integrated Loran/inertial navigation system. Horizontal position accuracy relative to the runway is further improved when the differential GPS configuration is used. While reasonable vertical position information is obtained

by integrating GPS, inertial, and an on-board barometric altimeter, the differential barometric altimeter technique needs to be utilized for accurate vertical guidance relative to the runway at low altitudes.

## 6.2 NAVSTAR GPS DESCRIPTION

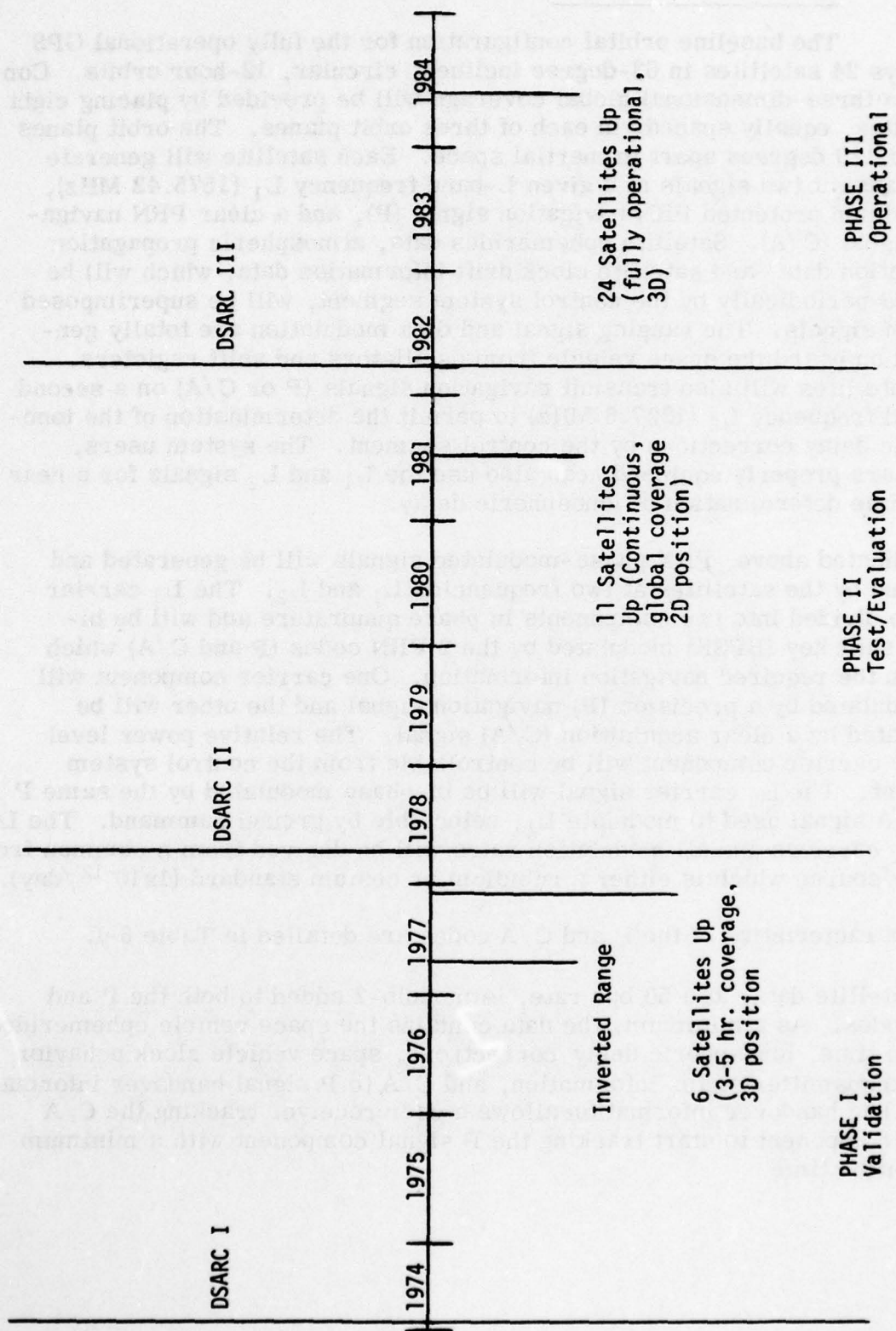
The NAVSTAR GPS is a satellite-based radio navigation system that will provide very accurate three-dimensional position fixes to properly equipped users anywhere on or near the earth, regardless of weather conditions. The system operational concept for making position fixes consists of making transit time measurements of RF signals transmitted by the GPS satellites. The RF signals are L-band signals (1 to 2 GHz) modulated with a pseudo-random noise (PRN) code. A precision timing system is used to synchronize the signal transmissions from the satellites. To avoid requiring all users to have precision clocks, enough satellites will be deployed so that all users will have available at least four satellites simultaneously from which pseudo transit time measurements can be made. Synchronized time at the user is then not required because the simultaneous reception of four satellite signals produces three independent range differences which may be used to calculate the intersection of three hyperboloids of revolution. Synchronized time can also be computed from four pseudo transit time measurements.

The objective of the tri-service GPS development program, being directed by the AF SAMSO, is to have a fully operational, 24 satellite system by 1984. The system is being developed according to the three phase schedule shown in Figure 6-1.

The GPS consists of three system segments:

- A space segment consisting of satellites in a specific orbited deployment;
- A control system segment consisting of a control center and several monitor ground stations;
- The user system segment consisting of vehicles and persons equipped with GPS receivers.

Brief descriptions of each of these segments are given in the following three subsections, followed by a subsection devoted to GPS performance.



GPS PROGRAM MILESTONES  
FIGURE 6-1

### **6.2.1      Space System Segment**

The baseline orbital configuration for the fully operational GPS employs 24 satellites in 63-degree inclined, circular, 12-hour orbits. Continuous three-dimensional global coverage will be provided by placing eight satellites, equally spaced, in each of three orbit planes. The orbit planes will be 120 degrees apart in inertial space. Each satellite will generate and transmit two signals at a given L-band frequency  $L_1$  (1575.42 MHz), a precision protected PRN navigation signal (P), and a clear PRN navigation signal (C/A). Satellite ephemerides data, atmospheric propagation correction data, and satellite clock drift information data, which will be updated periodically by the control system segment, will be superimposed on both signals. The ranging signal and data modulation are totally generated on board the space vehicle from oscillators and shift registers. The satellites will also transmit navigation signals (P or C/A) on a second L-band frequency  $L_2$  (1227.6 MHz) to permit the determination of the ionospheric delay corrections by the control segment. The system users, which are properly equipped, can also use the  $L_1$  and  $L_2$  signals for a near real-time determination of ionospheric delay.

As indicated above, PRN phase-modulated signals will be generated and radiated by the satellites at two frequencies  $L_1$  and  $L_2$ . The  $L_1$  carrier will be divided into two components in phase quadrature and will be bi-phase shift key (BPSK) modulated by the 2 PRN codes (P and C/A) which contain the required navigation information. One carrier component will be modulated by a precision (P) navigation signal and the other will be modulated by a clear acquisition (C/A) signal. The relative power level for the carrier component will be controllable from the control system segment. The  $L_2$  carrier signal will be bi-phase modulated by the same P (or C/A signal used to modulate  $L_1$ , selectable by ground command. The  $L_1$  and  $L_2$  carriers and all modulation rates will be derived from a common frequency source which is either a rubidium or cesium standard ( $1 \times 10^{-12}$ /day).

The characteristics of the P and C/A codes are detailed in Table 6-I.

The satellite data, at a 50 bps rate, is modulo-2 added to both the P and C/A codes. As a minimum, the data contains the space vehicle ephemerides, system time, ionospheric delay corrections, space vehicle clock behavior data, transmitter status information, and C/A to P signal handover information. The handover information allows a user receiver tracking the C/A signal component to start tracking the P signal component with a minimum acquisition time.

**TABLE 6-I**  
**CHARACTERISTICS OF P AND C/A CODES**

	P	C/A
Chipping Rate (Mcps)	10.23	1.023
Code Repetition Period	7 days	1 msec
Data Rate (bits/sec)	50	50
Data Frame Length*(bits)	300x; x=2,3,4,5,6	Same as P
Number of code Sequences**	37	37

\* Selectable by the control segment.

\*\* Space vehicles will generate 32; 5 others are for other transmitters.

#### 6.2.2 Control System Segment

Widely separate ground monitor stations located in Guam, Wahiawa in Hawaii, Elmendorf AFB in Alaska, and Vandenberg will track all satellites in view and accumulate ranging data received from the navigation signals. This information will be progressively processed by a data processing technique to provide a best estimate of each satellite's position, velocity, and clock drift relative to system time. This orbit determination process also derives information defining the gravitational field influencing the spacecraft motion; solar pressure parameters; the location, clock drifts and electronic delay characteristics of the ground stations; and other observable system influences. The ranging data collected from the satellites along with the information from other government installations will be used continuously to update ionospheric and tropospheric delay models. At least once per day the Master Control Station, located at Vandenberg AFB, will transmit the updated ephemeris, clock drift and propagation delay data to each satellite.

### **6.2.3      User System Segment**

There is a diverse set of potential users for GPS. These include all types of airborne vehicles (aircraft, helicopters, missiles), ships, tanks, submarines, and ground troops. All users will have a GPS receiver which tracks four satellite signals (either simultaneously or sequentially in rapid succession) and measures four independent pseudo-range measurements. The receiver also detects the data on each satellite signal and determines the satellite ephemeris, ionospheric delay, and satellite clock drift. The receiver may be designed to measure four pseudo-range rates, the rate of changes of the four pseudo ranges, by tracking the Doppler frequency of each satellite's RF signal. To obtain 3-dimensional position, time, and velocity, the receiver's measurements are processed to transform the data to the navigation coordinate frame desired by the user. Besides a receiver and digital computer, the user equipment includes an antenna and controller.

Three functional types of user equipment have been identified:

- a. A pseudo-random noise coded, four channel continuous signal receiver, designated as X model,
- b. A single channel sequential receiver, designated as Y model,
- c. A single channel, clear acquisition (C/A) signal only receiver, designated as Z model.

The attributes of each of these models is detailed more fully in Table 6-II, which was obtained from Ref. [26], the system specification for the GPS user equipment.

The three functional types of user equipment cover all user classes; however, each user class may place different environmental, size, and power requirements on the three types. Seven potential user classes (A, B, C, D, E, F, M) have been identified and are shown in Table 6-III. Referring to the aircraft horizontal position accuracy objective of 75 feet ( $1\sigma$ ), established in Section 5.1, the 4-D INCADS can be classified as a Class C user (medium accuracy, medium dynamics).

### **6.2.4      GPS System Performance**

Uncertainties in the user equipment position and velocity solutions are contributed by all three segments of the GPS. The GPS error budget is defined in terms of User Equipment Range Error (UERE), which is the error in measuring range from one satellite. This quantity is defined as user equipment measurement error, although all segments contribute errors.

**TABLE 6-II**  
**USER EQUIPMENT SET ATTRIBUTES AND OPERATING MODES<sup>(1)</sup>**

Equipment Set	Operating Frequency	Signals		Ionospheric Delay Correction Method		Auxiliary Sensor Set (2)	
		For Acquisition	For Navigation	Simultaneously Tracked Signals	L <sub>1</sub> /L <sub>2</sub> Model Using Data	Inertial Measurement Unit	Air Mass Unit
X	L <sub>1</sub> and L <sub>2</sub>	P and/or C/A	P or C/A	>4	Yes or No	Yes or No	Yes or No
Y	L <sub>1</sub> and L <sub>2</sub>	P and/or C/A	P or C/A	>1	Yes or No	Yes or No	Yes or No
Z	L <sub>1</sub> only	C/A	C/A	>1	No	Yes	No

(1) The Yes or No entries are defined as follows:

- a. For each of the operating modes, the operator shall be able to select (yes or not select) the mode.
  - b. When the operator has selected Yes for both the direct RF mode and the static model mode for ionospheric correction, the direct RF shall be the preferred mode and the system shall revert to the static model mode only when L<sub>2</sub> is unavailable.
- (2) The Yes or No entries in these columns establish if the equipment must utilize measurements provided by these additional devices.

TABLE 6-III  
GPS USER CLASSES

\*High Accuracy - better than 10 meters (32.8 feet) all axes

\*\*\*Medium Accuracy 15-150 meters (49.2 - 492 feet), accuracy will be traded within this range from costs

The components of UERE for Phase I and Phase III of the GPS Program are shown in Table 6-IV. The uncertainties in space vehicle ephemeris and group delay and part of the atmospheric uncertainty (ionospheric delay) are contributed by the space and control segments. The space vehicle group delay component accuracy is applicable two hours after the satellite has been updated by the control segment. The other error components affected by the space and control segments are applicable 24 hours after satellite update.

In Table 6-IV, the multipath, receiver noise and resolution, and part of the atmosphere components are contributed by the user segment. These components are influenced by the user's RF signal environment and receiver/navigation system mechanization.

**TABLE 6-IV  
GPS ERROR BUDGET<sup>(1)</sup>**

	<u>Phase III</u>	<u>Phase I</u>
Space Vehicle Ephemeris	5	12
Atmosphere	8 to 17 <sup>(2)</sup>	8 to 17 <sup>(2)</sup>
Space Vehicle Group Delay	3	9
Receiver Noise and Resolution	5	5
Multipath	4 to 9 <sup>(2)</sup>	4 to 9 <sup>(2)</sup>
Total R.S.S.	12 to 21	18 to 25

(1) All values are standard deviations ( $1\sigma$ ) in feet.

(2) These error quantities represent the use of different atmospheric delay correction methods and different user environment conditions.

The performance of the X, Y or Z-type receivers tracking the C code signal will be six to seven times the UERE shown in Table 6-IV.

The satellite/user geometry is a major factor in determining how the UERE will propagate into user position errors for GPS. On the average, this ratio (Geometric Dilution of Precision, or GDOP) between user position error and the total equivalent error is between two and three. Other factors influencing the user position error include simultaneous or sequential tracking of the four satellite signals, and aircraft dynamics.

Range rate will also be measured by the user equipment with a repeatability of 0.2 ft/sec ( $1\sigma$ ) for the X and Y type receivers.

### 6.3 GPS/INERTIAL/BARO INTEGRATION

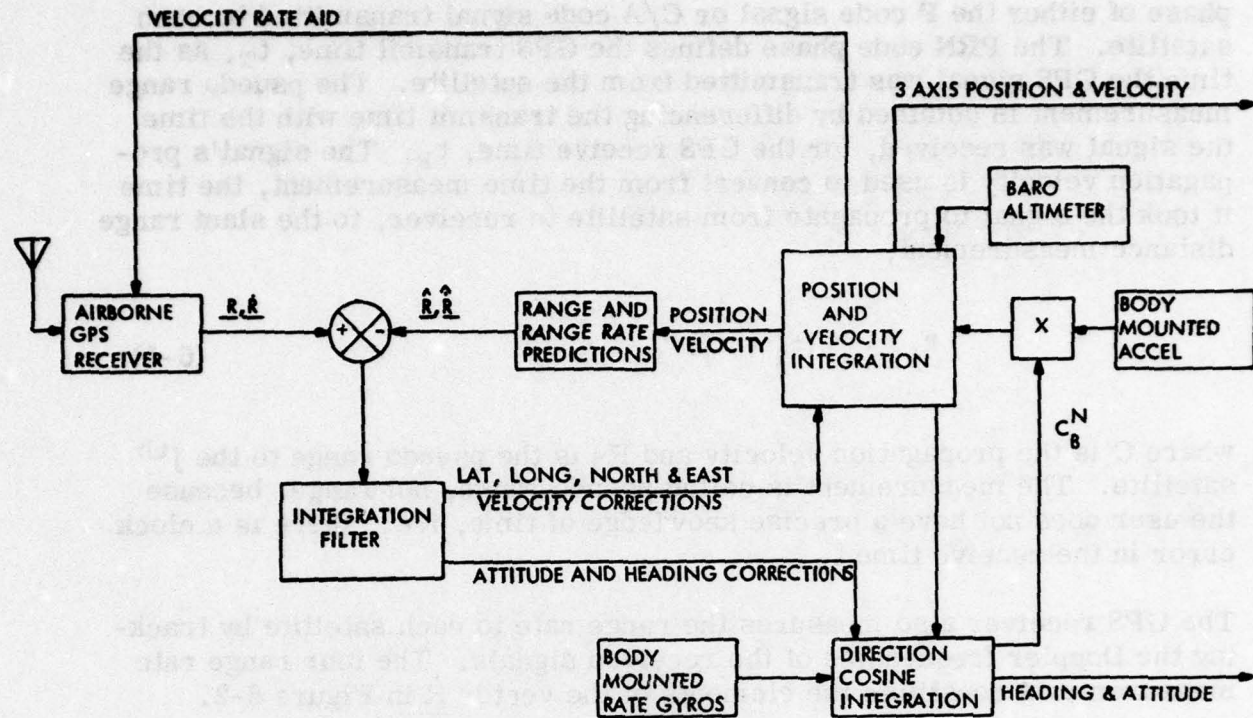
This section discusses the integration of a GPS receiver with a strapdown inertial system and a barometric altimeter. For accurate horizontal and vertical navigation relative to the airfield, the differential GPS and differential baro concepts are considered. To begin, an integrated GPS/inertial/baro system concept for the 4-D INCADS navigation system is defined. Then various parts of the integrated system are discussed. The discussions cover the following:

- a. The GPS receiver and the functions it will perform for the 4-D INCADS
- b. The digital processing tasks that need to be performed for managing the receiver, determining the GPS navigation data, and integrating GPS data with inertial and baro measurements
- c. The differential GPS configuration, and
- d. The integration filter requirements for integration of GPS with different quality inertial systems

This section concludes with a discussion of GPS/inertial/baro system accuracy.

#### 6.3.1 GPS/Inertial/Baro System Description

Figure 6-2 is a block diagram showing the functional elements of a GPS/strapdown inertial/baro navigation system. As shown, the integrated navigation system processes GPS, inertial, and baro altimeter measurements and outputs aircraft position, velocity, heading and attitude parameters to the other portions of the 4-D INCADS. Time is also an output of this system. For a discussion of the differential GPS mode consult Section 6.3.3, and



**GPS/STRAPDOWN INERTIAL/BARO NAVIGATION SYSTEM  
FIGURE 6-2**

for a discussion of the differential baro concept and its performance consult Sections 5.2 and 5.5.2, respectively.

The block diagram (Figure 6-2) of the GPS/strapdown inertial/baro system shows a functional configuration very similar to the system configuration shown in Section 5.2 where the system utilizes a Loran radio sensor in place of a GPS receiver. Instead of Loran time difference, the GPS receiver senses aircraft position information by measuring the pseudo ranges from four satellites. The four pseudo ranges, which are elements of the GPS range measurement vector  $\mathbf{R}$ , are obtained by the receiver tracking the

phase of either the P code signal or C/A code signal transmitted by each satellite. The PRN code phase defines the GPS transmit time,  $t_T$ , as the time the GPS signal was transmitted from the satellite. The pseudo range measurement is obtained by differencing the transmit time with the time the signal was received, for the GPS receive time,  $t_R$ . The signal's propagation velocity is used to convert from the time measurement, the time it took the signal to propagate from satellite to receiver, to the slant range distance measurement,

$$R_j = C(t_R - t_T) \quad (6-1)$$

where  $C$  is the propagation velocity and  $R_j$  is the pseudo range to the  $j^{\text{th}}$  satellite. The measurement is called pseudo range, not range, because the user does not have a precise knowledge of time, i.e., there is a clock error in the receive time  $t_R$ .

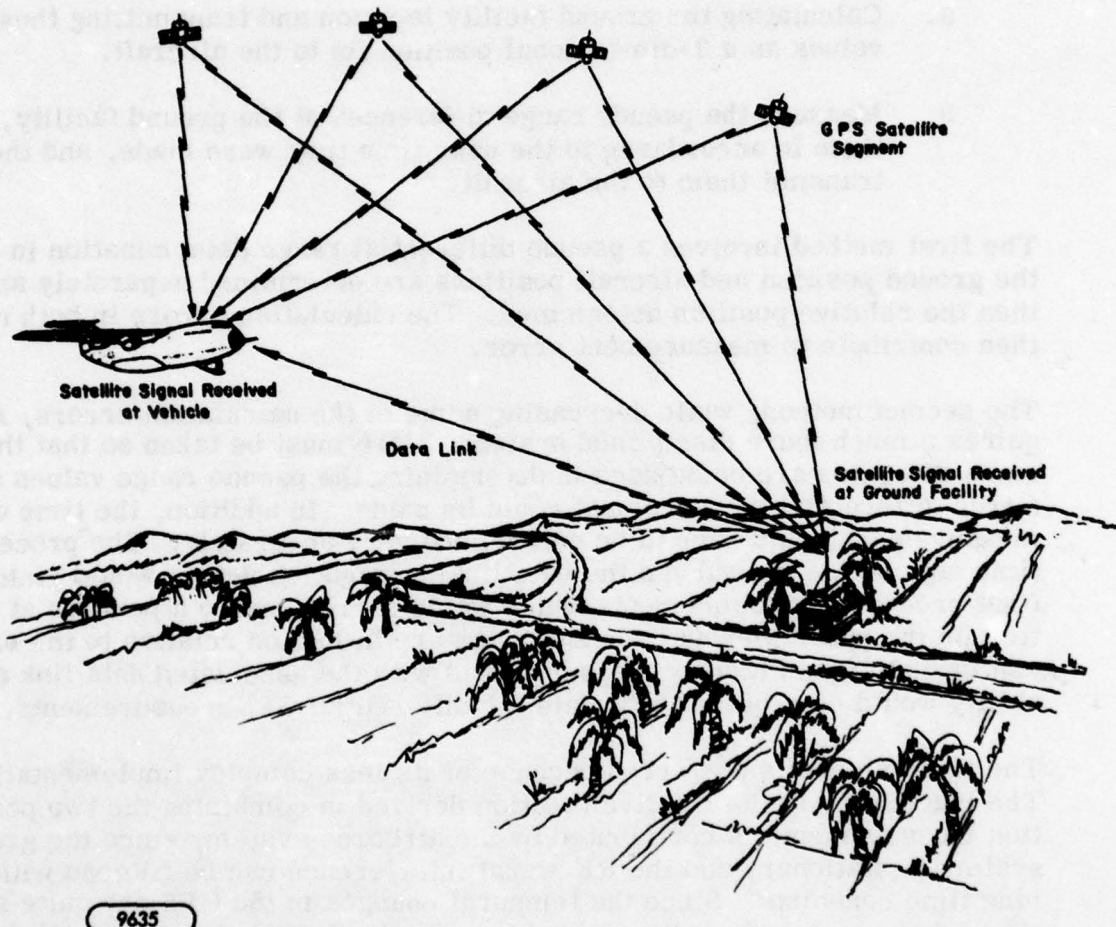
The GPS receiver also measures the range rate to each satellite by tracking the Doppler frequencies of the received signals. The four range rate measurements constitute the elements of the vector  $\dot{R}$  in Figure 6-2.

In the integrated system configuration shown in Figure 6-2, the GPS pseudo range and range rate measurements are compared with the current system predictions of the range and range rate vectors and correction signals are generated for the system position, velocity, heading, and attitude outputs. The integration filter also corrects the receiver's clock and estimates the clock drift. The GPS ranges and range rates provide measurements of altitude and vertical velocity. Consequently, the integration filter combines GPS range and range rate measurements with the barometric altimeter and inertial vertical acceleration measurements.

The system velocity solutions are used to aid the receiver's code tracking and carrier tracking loops, so that receiver operation can be accommodated over a range of aircraft dynamics and radio frequency interferences. The dynamic range and RF signal environment conditions under which the 4-D INCADS is to operate establish both steady state and transient accuracies on the velocity rate aid. Since the inertial gyro and accelerometer error sources contribute both long term and short term errors to the system velocity, the integration filter for the GPS/strapdown inertial/baro system needs to estimate inertial sensor error sources.

### **6.3.2 Differential GPS Configuration**

To decrease the errors in the relative position between the aircraft and a remote ground facility, a differential GPS configuration is considered. Figure 6-3 illustrates the general concept showing reception of the satellite-emitted navigation signals by both the airborne GPS receiver and a ground receiver at the ground facility. The data from the ground facility is transmitted to the aircraft via a data link so that a relative position can be determined. The data link requirements developed in Section 5.7 for differential Loran are applicable to this discussion along with the unique GPS considerations given below.



**DIFFERENTIAL GPS CONCEPT**  
**FIGURE 6-3**

Differential GPS minimizes many error sources that contribute to the GPS determination of the aircraft's relative position with respect to the runway. First, it alleviates the need for an accurate survey to determine the absolute runway position. This is an important consideration for tactical operations into remote, austere airfields. Second, temporal variations in the GPS signal characteristics and uncertainties in the propagation delay compensation parameters are cancelled. This significantly reduces the propagation delay correction requirements placed on the airborne system.

Two basic ways are available to accomplish the data transfer for the differential GPS configuration. They are:

- a. Calculating the ground facility location and transmitting these values as a 3-dimensional position fix to the aircraft.
- b. Measure the pseudo range differences at the ground facility, tag them in accordance to the user time they were made, and then transmit them to the aircraft.

The first method involves a pseudo differential range determination in that the ground position and aircraft positions are determined separately and then the relative position determined. The calculation errors in both units then contribute to measurement error.

The second method, while decreasing some of the calculation errors, requires a much more disciplined system. Care must be taken so that the same satellites are being used in determining the pseudo range values so a true differential measurement could be made. In addition, the time of measurement would have to be determined very accurately. The processing time lags on the ground and the data link propagation delays would yield final processed measurements which would correspond to a position at some time in the past. Because the satellites are in motion relative to the earth, continuous ground facility measurements with the associated data link availability would be required to update the differential GPS measurements.

The first method is preferred because of its less complex implementation. The inaccuracy in the relative position derived in combining the two position measurements is contributed by the airborne system, since the ground system is stationary and the RF signal interference can be filtered with long time constants. Since the temporal changes in the GPS are quite slow, only a few measured positions would be required, allowing differential GPS operation in a hostile jamming environment or at times when data link capability is not available.

AD-A072 148 LEAR SIEGLER INC GRAND RAPIDS MICH INSTRUMENT DIV F/G 17/7  
FEASIBILITY STUDY FOR INTEGRATED FLIGHT TRAJECTORY CONTROL (AIR--ETC(U))  
JAN 77 M BIRD F33615-74-C-3083

UNCLASSIFIED

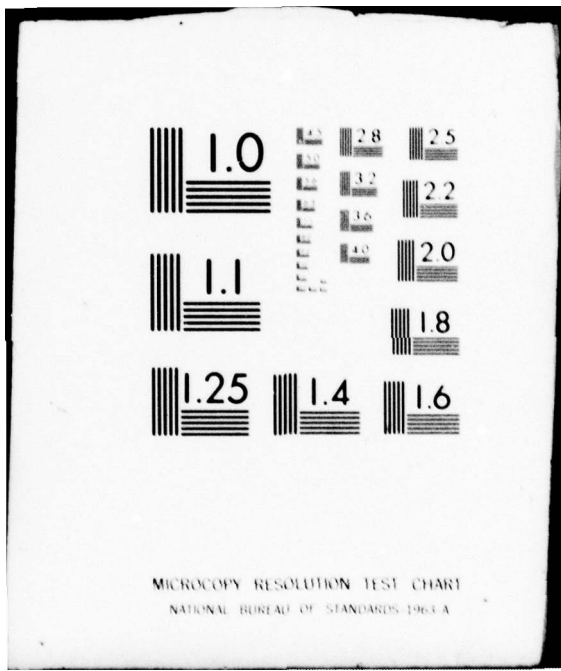
AFFDL-TR-77-120

NL

3 OF 4

AD  
A072148

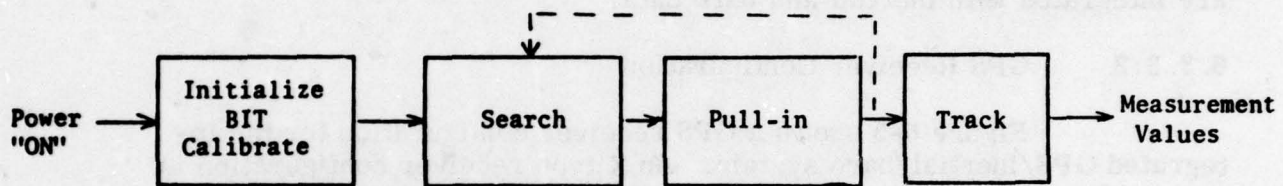




### **6.3.3 GPS Receiver Operation**

#### **6.3.3.1 Sequence of Operation of GPS Receiver**

The normal operating sequence of the GPS receiver after "turn-on" is shown in Figure 6-4.



**SEQUENCE OF OPERATION OF GPS RECEIVER**  
**FIGURE 6-4**

The first operating mode is to initialize the equipment. This includes calculating or accepting from the operator all values for beginning operation. These values include best estimates of user position, velocity, attitude, time, and their related uncertainties. Also included is determining which satellite transmitters should be selected. Before this mode is completed, the built-in-test (BIT) is exercised to verify the operation capability of all subsystems. Simulated satellite signals are presented to the receiver so that equipment measurement biases can be determined.

The Search mode is then entered. One of the selected satellites is chosen and, using the estimated values of the first mode, the search window (area of uncertainty) is determined. Depending upon the configuration of the receiver (X, Y, or Z), search to lock up the available internally generated PRN navigation signals is begun. If the signal is not found, the search window is made larger. Normal operation is to lock-on the C/A code first. This code is much easier to acquire, being at a lower chipping rate and the code sequence repeating every 1 ms. Acquisition of this code and demodulating the data allows determination of the P Code timing so very fast P code

lock-up can then occur. If direct P code acquisition is required, the time uncertainty of the user constrains the search time.

After a navigation signal has been found, the Pull-In mode is initialized. During this mode the exact code and carrier phase is determined to within the constraints of thermal noise and equipment measuring capabilities. The data is demodulated. The track mode is then initiated. This mode allows the navigation signal and carrier to be tracked dynamically so that pseudo range and range rate measurements can be made.

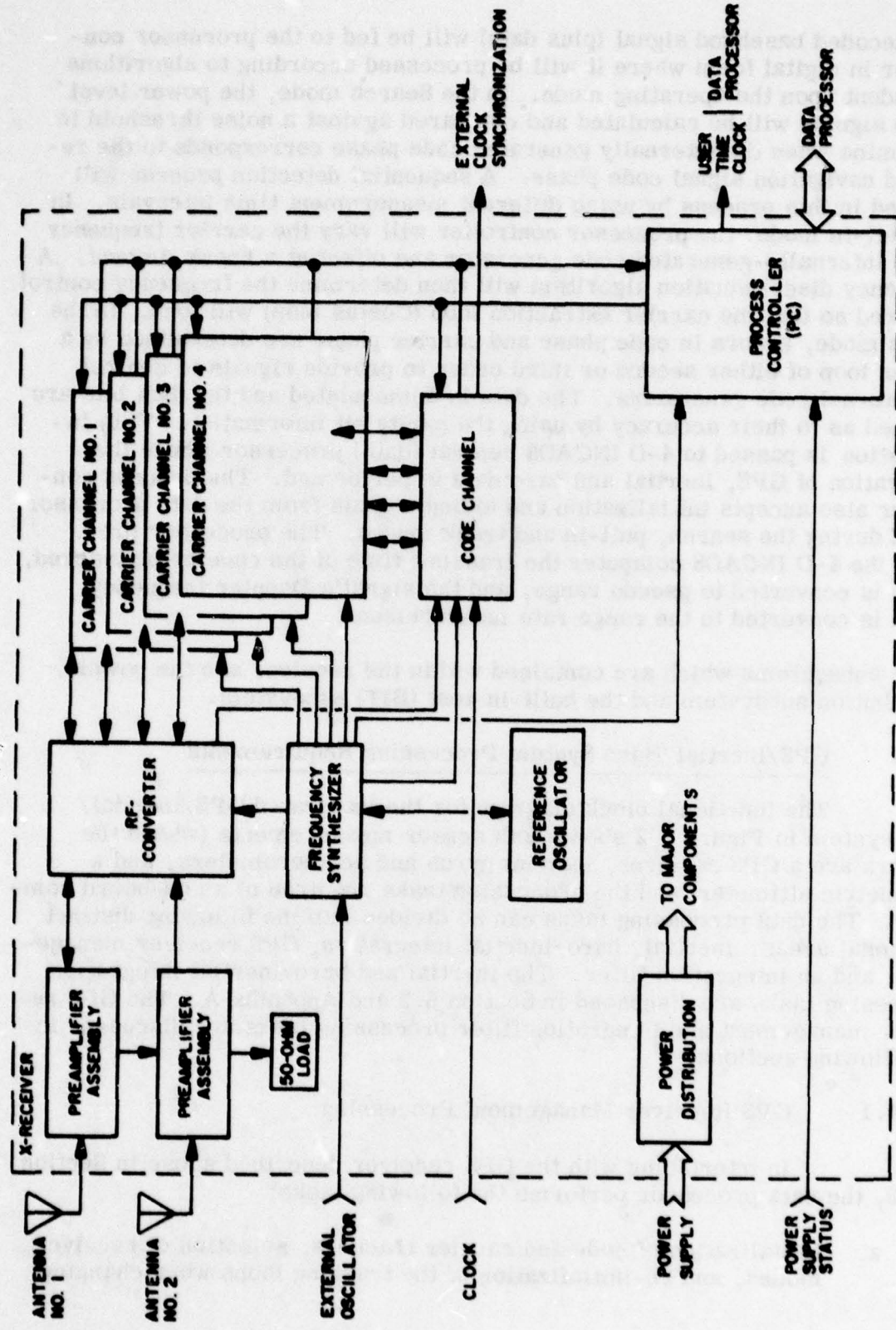
For GPS operation, four satellite signals must be searched, pulled in, and tracked. The four pseudo range and range rate measurements are supplied to the navigation portion of the integrated system, Figure 6-2, where they are integrated with inertial and baro data.

#### 6.3.3.2 GPS Receiver Configuration

Figure 6-5 shows a GPS receiver configuration for the integrated GPS/inertial/baro system. An X type receiver configuration is assumed and the receiver configuration is consistent with the AF GPS User Equipment Specification [26]. This unit receives the L-band navigation signals ( $L_1$  or  $L_2$ ) via an antenna subsystem which may consist of one, two, or even more selectable fixed pattern antennas. (The system could use steerable directional antennas to allow operation in the presence of large RF interference but those will not be considered here.) The received signal from the antennas will then be amplified in low noise amplifiers operating at RF. These amplifiers, along with the antenna gain, will determine the receiver system sensitivity. An RF converter will then convert the RF signals to a convenient Intermediate Frequency, IF, so that the code demodulation and carrier reconstruction signal processing can begin. The reference low frequencies required for the frequency conversion will be generated in a frequency synthesizer which will coherently generate these signals from either an extremely stable internal reference oscillator or from an external oscillator.

In the X type receiver, four separate carrier channel units operating in parallel will be used to track four satellite-generated navigation signals. Each of these units will include a C/A and P code generator controllable with respect to its code phase and carrier frequency from the processor controller. Each of the carrier channels will contain correlators which will be used to derive the in-phase and quadrature baseband components of the decoded navigation signal and the data information from the satellite transmitter.

A9506



PROCESS CONTROLLER/RECEIVER HARDWARE  
FIGURE 6-5

The decoded baseband signal (plus data) will be fed to the processor controller in digital form where it will be processed according to algorithms dependent upon the operating mode. In the Search mode, the power level of the signals will be calculated and compared against a noise threshold to determine when the internally generated code phase corresponds to the received navigation signal code phase. A sequential detection process will be used in this process by using different measurement time intervals. In the Pull-In mode, the processor controller will vary the carrier frequency of the internally-generated code generator and offset at a known amount. A frequency discrimination algorithm will then determine the frequency control required so that the carrier extraction loop (Costas loop) will lock. In the Track mode, errors in code phase and carrier phase are determined by a Costas loop of either second or third order to provide signals to control the internal code generators. The data is demodulated and the data bits are verified as to their accuracy by using the parity bit information. This information is passed to 4-D INCADS central (data) processor where the integration of GPS, inertial and baro data is performed. The process controller also accepts initialization and aiding signals from the data processor to aid during the search, pull-in and track modes. The processor provides the 4-D INCADS computer the transmit time of the code being tracked, which is converted to pseudo range, and the signal's Doppler frequency, which is converted to the range rate measurement.

Other subsystems which are contained within the receiver are the power distribution subsystem and the built-in-test (BIT) subsystem.

#### **6.3.4 GPS/Inertial/Baro System Processing Requirements**

The functional block diagram for the integrated GPS/inertial/ baro system in Figure 6-2 shows both sensor measurements (where the sensors are a GPS receiver, inertial gyros and accelerometers, and a barometric altimeter) and the processing tasks required of an on-board computer. The data processing tasks can be divided into the following distinct functional areas: inertial, baro/inertial integration, GPS receiver management, and an integration filter. The inertial and baro/inertial integration processing tasks are discussed in Section 5.2 and Appendix A. The GPS receiver management and integration filter processing tasks are discussed in the following sections.

##### **6.3.4.1 GPS Receiver Management Processing**

In interfacing with the GPS receiver described above in Section 6.3.3, the data processor performs the following tasks:

- a. Initialization of code and carrier trackers, selection of receiver modes, and re-initialization of the tracking loops when changing

satellites or re-acquiring satellite signals after signal loss.

- b. Establish the current position and velocity of all GPS satellites and determine the set of transmitters that will provide best position performance.
- c. Accept transmit time and Doppler frequency measurements and transmitted data from GPS receiver.
- d. Correct measurements for propagation delays, satellite clock errors, and receiver clock drift, and using the current system estimate of receive time,  $t_R$ , calculate pseudo range and range rate measurements.
- e. Compute predicted range  $\hat{R}$  and range rate  $\dot{\hat{R}}$  using the current system solution for aircraft position and velocity and the current value for satellite position and velocity.
- f. Transform the current system velocity vector solution into rate aiding signals for the receiver's code and carrier trackers. These transformations use the direction cosines which define the orientation of the vector between the aircraft and satellite. The aircraft to satellite vector is computed using the current system aircraft and satellite positions.
- g. Perform antenna switching (or antenna pointing) computations and supply the resulting antenna selection (or antenna direction cosines) to the receiver.

#### 6.3.4.2 GPS/Inertial/Baro Integration Filter

The integration filter processes the difference between the GPS receiver pseudo ranges  $\underline{R}$  and range rates  $\dot{\underline{R}}$  measurements and the current system prediction of the ranges  $\hat{R}$  and range rates  $\dot{\hat{R}}$  and, at a minimum, estimates errors in the system position, velocity, altitude, and heading variables. To update the integrated system outputs, the error estimates are added to the current system solutions.

An integration filter with the state elements (the number of state elements equals the number of errors estimated by the filter) given above will provide a system position and velocity performance equivalent to the GPS system position accuracy given in Table 6-IV and a velocity accuracy of 0.2 ft/sec ( $1\sigma$ ). However, with this minimum set of state elements, this

performance will be attainable over a limited range of interference-to-signal ratios (I/S) and aircraft maneuvers. A larger set of filter state elements are required to increase the operational performance of the system.

In examining the operational performance of radio navigation receivers, there is a tradeoff between (1) the interference-to-signal ratio threshold, below which the receiver tracking loops remain locked, and above which the tracking loop break lock; and (2) the aircraft acceleration and jerk limits, which determine the amount of maneuver the aircraft can make before the receiver will lose lock. To increase the I/S threshold, both the code tracker and carrier tracking loop bandwidths must be decreased, which reduces the allowed aircraft acceleration and jerk levels. Conversely, to handle larger aircraft dynamics, the tracking loop bandwidths must be increased, which lowers the I/S threshold.

When inertial velocities are used to rate aid the receiver code and carrier tracking loops, the aircraft maneuver limitations are relaxed for a given I/S threshold. Inertial rate aiding allows smaller receiver tracking loop bandwidths to be used during aircraft maneuvers, thereby allowing operation in the presence of more RF interference.

The errors in the inertial velocities are major factors in determining how small the receiver bandwidths can be made. Consequently, the inertial velocity errors significantly influence the I/S operating range. Appendix F discusses these operational performance limitations of a GPS receiver and the influence of the rate aiding errors on the interference-to-signal ratio threshold. Since inertial velocity errors depend on the magnitude of the error sources in the inertial accelerometer and gyros, the quality of the inertial system affects the receiver tracking performance, and consequently the integrated GPS/inertial/baro system operational performance.

In the fully integrated 4-D INCADS system, the integration filter can be designed to increase the interference-to-signal ratio operating range. This is accomplished by increasing the dimension of the filter state vector, beyond the minimum number of elements defined above. The filter will need to estimate GPS time, receiver clock drift and significant error sources in the inertial system. In addition, a Kalman filter technique will be required for the integration filter since the inertial sensor errors can be estimated only if the dynamics of the GPS and inertial measurements are part of the integration filter gain algorithm. The number of inertial error sources estimated with the Kalman filter will depend on the quality of inertial system. For a 1 nm/hr gimballed inertial system, two level accelerometer scale factor errors and three gyro drift biases can be estimated for an increase in interference-to-signal ratio operating margin. For a 20 nm/hr strapdown system,

3 accelerometer biases, 3 accelerometer scale factors, 3 gyro drift biases, and 3 gyro drift noises can be estimated. With these inertial error sources estimated, the transient inertial velocity errors during aircraft maneuvers will be reduced, allowing a smaller receiver bandwidth and larger I/S operating range. Estimation of receiver clock drift also minimizes an error source that constrains the receiver tracking loop bandwidth.

The integration of GPS with the baro/inertial system is also accomplished with the integration filter. The four GPS range measurements contain information about the aircraft altitude above sea level. The altitude output of the baro/inertial system follows the pressure altitude measurement of the barometric altimeter and differs from the true altitude above sea level by D value. (For a D value discussion see Section 5.2.) Consequently, in addition to an altitude error variable the integration filter state vector contains D value as an error source to be estimated. To compute the 4-D INCADS altitude above sea level output, the integration filter D value estimate will be added to the baro/inertial altitude output. The vertical velocity error in the baro/inertial loop is included in the integration filter state vector so that the GPS range rate information will be used to improve the system vertical velocity output.

For vertical guidance relative to the runway, the GPS altitude information will not be as accurate as the differential baro data. Consequently, when the ground baro data are available to the airborne 4-D INCADS, the system uses the baro/inertial altitude outputs for relative vertical guidance information. The vertical channel performance for this configuration is analyzed in Section 5.3.3. For this mode of operation the GPS altitude and altitude rate information is still useful since it adds functionally redundant data for the differential baro/inertial channel. The GPS measurements can be used for sensor failure detection and as backup altitude and altitude rate information in case of barometric altimeter failure.

To summarize, a Kalman filter will be used for the integration filter in the integrated GPS/inertial/baro system. For a 1 nm/hr gimballed inertial system, the Kalman filter state vector will include latitude, longitude and altitude errors, north and east velocity errors, heading and two attitude errors, GPS time error, receiver clock drift, baro/inertial altitude error (D value) and vertical velocity error, two accelerometer scale factor errors and three gyro drift biases. For a 20 nm/hr strapdown inertial system the Kalman filter will estimate all of the previous errors as well as three accelerometer biases, one more accelerometer scale factor error and three gyro drift noises. Certain inertial error elements may be dropped from the Kalman filter state vector depending on the 4-D INCADS I/S operating margin goal.

### **6.3.5 GPS/Inertial/Baro System Performance**

The GPS system error budget given in Table 6-IV has been used to assess the position and velocity performance of an integrated GPS/inertial/baro navigation system with the results given in Table 6-V. The 3-D position and 3-D velocity accuracies are dependent on the geometric relationship between the four satellites and the GPS receiver. The performance assessment optimistically assumed a GDOP of 1 for all three dimensions.

The predicted position accuracies for the integrated GPS/inertial/baro system shown in Table 6-V indicate the horizontal position accuracies are well within the 4-D INCADS horizontal position goal of 75 feet ( $1\sigma$ ) without using a differential configuration. This accuracy assumes the location of the runway is known precisely and the most accurate propagation delay compensation data is available in the system. For a differential GPS configuration these two assumptions are not necessary and Table 6-V shows that the horizontal position accuracy goal is met. Table 6-V also shows the system velocity accuracy is far better than the 3 ft/sec goal of the 4-D INCAD.

For relative vertical guidance, Table 6-V shows that the differential baro input is required to attain a performance goal of 10 feet. For this situation, the GPS measurements provide functional redundancy and a backup for the differential baro/inertial vertical channel.

**TABLE 6-V**  
**INTEGRATED GPS/INERTIAL/BARO SYSTEM PERFORMANCE\*\***

CONFIGURATIONS		AIRBORNE GPS & AIRBORNE BARO	DIFFERENTIAL GPS & AIRBORNE BARO	AIRBORNE GPS & DIFFERENTIAL BARO	DIFFERENTIAL GPS & DIFFERENTIAL BARO
Aircraft	X and Y (ft/fps)	24/.2	24/.2	24/.2	24/.2
	Z (ft/fps)	29/.2	29/.2	29/.2	29/.2
6-23	X and Y (ft/fps)	*1.2	34/.2	*1.2	34/.2
	Z (ft/fps)	*1.2	41/.2	9.4/.2	9.4/.2

6-23

\* Depends upon how accurately remote site location is known in GPS coordinates.

\*\* All numbers are  $1\sigma$  values.

## **7    4-D/JTIDS INTEGRATION CONSIDERATIONS**

### **7.1    INTRODUCTION**

The integrated 4-D INCADS concept enables time-and-space optimum aircraft flights. The potential benefits of curved trajectories, including variable velocity control, greatly enhance existing flight operations. Open questions then exist as to how the flight specifications are inserted into a 4-D INCADS implemented system and to which grids the trajectories (hence, missions) are referenced. A 4-D/JTIDS integration provides a set of answers to these questions.

The Joint Tactical Information Distribution System (JTIDS) is a digital data bus, disseminating tactical information. The data bus is a line-of-sight communication system which has extended range capability enabled by means of relaying. JTIDS is a secure system utilizing spread spectrum techniques, operating in the Tacan frequency band. Data transmissions are time-slotted (TDMA) and referenced to a master user, who can be any a priori defined user. Acquisition of the net time reference is accomplished by a passive search and track process, prior to being given the freedom to actively participate in the net. Once a user has achieved synchronization, it can begin transmitting in its assigned time slot.

The types of transmissions allowed are fixed by a message catalog, see Ref. [42]. In addition to the data bus function, JTIDS provides its users with a relative navigation capability. A user's position relative to the JTIDS grid is obtained by processing the transit times of other users' messages, and the other users' locations. Trilateration or other processing techniques, such as Kalman filtering, can be used to determine position. For a user with poor geometry relative to other users, the relative navigation accuracy can be improved by using the Round Trip Timing (RTT) message for precise slant range measurements. The relative navigation capability can be used to enhance many scenarios.

The integration features which are discussed in this section are:

- Mission enhancement of transports, and of integrated strike elements. Scenarios for each class of mission were considered utilizing the data defined in the message catalog, Ref. [42].
- Navigation grid standardization, or compatibility, using JTIDS relative navigation.
- Terminal requirements for JTIDS additions to a 4-D system.

This study also addressed the integration of JTIDS information into the 4-D INCADS control-display concept. The information is discussed in Section 3.7.

## 7.2 MISSION ENHANCEMENTS OF A 4-D/JTIDS SYSTEM

### 7.2.1 Relevant JTIDS Data for 4-D Capability

The JTIDS message catalog specifies many of the appropriate data sets (fields) which are applicable to the tactical arenas. The messages are grouped in major categories and are assigned labels. The data of particular interest to 4-D enhancements (with their labels) are the following. (Included in the list of the message groups are growth data for each group. These data suggestions are potential additions which, if included in the messages, could further enhance 4-D/JTIDS capabilities).

#### a. Waypoint (Planned Message VI-4)

1. Waypoint type: normal, rendezvous, strike initial point, and spares.
2. Latitude, longitude, altitude.
3. Time-of-arrival.
4. Flight plan sequence number.
5. Growth data: track through waypoint, desired bank or turn radius prior to waypoint, speed at waypoint, flight path - including maximum allowed - prior to or after waypoint for specified altitude change, wind at waypoint, flaps position, spoilers position, landing gear position.

#### b. Track (Air T1; Sea Surface T3; Sea Subsurface T4)

1. Friendly/non-friendly designation.
2. Latitude, longitude, altitude.
3. Heading, course, bearing.
4. Speed.
5. Track quality.
6. Growth data: avoidance radius/altitude.

- c. Status Reports (Aircraft P1; Ground Station P2; Surface Ship P3)
  - 1. System reference number.
  - 2. Status and capability.
  - 3. Latitude-longitude-altitude-speed.
  - 4. Time-position quality.
  - 5. Mission
  - 6. Growth data: rendezvous-related incremental data for entry to formation flying, or for functional coordination.
- d. Command Messages (General C1-1, A/C Control C1-11, Patr-ing C2-2, A/C Mission C2-3, ASW A/C Status C2-4, Weapon/Engagement Status C2-5, Pointer C2-11, Air Intercept Assignment M3-1)
  - 1. System reference number.
  - 2. Mission and/or mission alteration data.
  - 3. Status data.
  - 4. Growth data: expanded bridging-or-transitioning data to efficiently and smoothly move from flight segment to flight segment.
- e. Special Messages (Information 17-1, Category A, Category U, Category V, Expansion Codes 7-11, Category B, RTT Messages, Free-Text Messages)
  - 1. System reference number (when applicable).
  - 2. Source (or object) location.
  - 3. Coordination data (when applicable).
  - 4. Relative navigation data.
  - 5. Growth data: there is much that could be said, but this data will be evolved in future developments by various

operational units. Some data is suggested later in further discussions of mission enhancements due to 4-D/JTIDS system capabilities. The planned messages are a significant step in evolution of final data requirements.

#### **7.2.2 Mission Enhancements of Transport Aircraft Due to 4-D/JTIDS System Capabilities**

The function of the transport aircraft is to move personnel and/or supplies from locale to locale. Either air drop or landing may be used and the task may be accomplished in either friendly or non-friendly territory. Four transport missions are accomplished by existing fleets of C-130's, C-141's, C-5's, and the future AMST's. They are:

- a. Unit moves
- b. Logistic support
- c. Aeromedical evacuation
- d. Specialized operations support

Potential enhancements of executing these missions resulting from the addition of 4-D/JTIDS capabilities are discussed below. Each of the four missions listed above can be further divided into mission phases. They are:

- a. Preflight (including flight planning)
- b. Take-off and climb-to-altitude
- c. Enroute
- d. Cargo drop (descent for airdrop or terminal for landdrop)
- e. Egress
- f. Enroute (return-to-base)
- g. Terminal

Some enhancements in these phases are apparent.

- **Preflight Transport Mission Enhancements.**

A most important enhancement during preflight is tactical communications provided by JTIDS. Waypoints and avoidance zones can be preloaded. Planned coordination with defensive supporting elements and with

cargo-using elements can be reviewed. The 4-D INCADS situation display's presentation (described in Section 3) of the flight plan is effective in helping the operator evaluate the plan. This is particularly so in reviewing the safety aspects of the plan and the critical parameters of the plan, e.g., time/velocity tolerance at an intermediate waypoint which must be met in order to satisfy the terminal conditions at the target.

- Take-Off Mission Phase Enhancements.

Emergency data (also a feature for any mission phase) can be received from the JTIDS link which can change the flight plan, or even the major mission objective. Potentially, at least, the 4-D INCADS software could compute collision avoidance data using profile predictions based on received status (P) messages and the aircraft's profile. Relative ranging from RTT messages can monitor each aircraft's separation precisely.

- Enroute Mission Phase Enhancements.

Flight plan changes -- either new waypoints, new avoidance volumes, or even modified missions (primary or secondary) -- may be performed. The data is received from JTIDS, inserted automatically into the system, observed as a new profile (or scenario), and accepted or rejected by the pilot. A particular enroute enhancement is coordination (time and space) of in-flight refueling (an expanding requirement as seen from trans-oceanic C-5 flights). Rendezvous time, track, and turn points can be received from JTIDS and controlled by the 4-D control enhancement, thereby greatly economizing the refueling operation.

- Cargo-Drop Phase Enhancements.

Precise knowledge of relative time and an accurate execution of time-on-target, particularly for air drops, are important enhancements. Coordination is maximized with pickup units as well as with ground/air defense supporting units. Accurate relative navigation improves pop-up, drop-down performance, minimizing exposure times, and providing capabilities for improved accuracies of air drops. Secondary drop zones and their corresponding flight plans can be transmitted by means of the JTIDS net and then coordinated and flown, allowing an in-flight rescheduling. Cargo land-drop enhancement is similar to that suggested below for the terminal mission phase.

- **Egress Mission Phase Enhancements.**

Knowledge of the tactical situation enhances the egress from the drop zone. Knowledge of the tactical situation is being updated continually by the command and control centers and the results are retransmitted on the net. The crew can then use these results to program their profile.

- **Enroute (return to base, or another terminal point) Mission Phase Enhancements.**

Previously discussed enroute enhancements apply, particularly in-flight refueling.

- **Terminal Mission Phase Enhancements.**

Terminal phase enhancements are very important. The major effort of the 4-D study was directed at 4-D trajectory synthesis and control of transports in terminal phase. Both navigation accuracy and time coordination and control can be enhanced with JTIDS. Navigation accuracy from JTIDS transit times (see Refs. [43], [44], [45]) is of the same level as the differential Loran used in the analysis and simulations presented in Section 5. Ground-based JTIDS terminals located near the runway can give relative ranges (or range-differences if more terminals are used). Integration of these range measurements and on-board sensing systems can give the same capability as differential Loran or GPS.

The JTIDS navigation accuracy, broad grid-coverage, and 4-D INCADS curved-path generator give the integrated 4-D/JTIDS the capability to fly different approaches, particularly for STOL/VTOL transports. Time coordination and control can enhance the terminal mission phase. Knowledge and execution of assigned arrival time can be used to minimize holding or loitering patterns, enabling greater resource management, viz., of time-on-station, fuel management, terminal safety, etc. More accurate navigation, curved-path generation and control, and variable velocity/time specification may be used to reduce separation conditions between aircraft and increase landing rates. Automatic data insertion from the link can reduce crew work-load and expand their activity as data managers.

### **7.2.3      Mission Enhancements of Strike/Reconnaissance Type Aircraft Due to 4-D/JTIDS Capabilities**

There are many functions of strike/reconnaissance aircraft. One way to group these functions is as follows:

- a. Attack
- b. Monitor/Observe
- c. Control
- d. Assist

These categories correspond to types of missions and each mission can in turn be divided into the phases previously described for the transport aircraft. A particular characteristic of these types of missions is that they are not usually performed singly, either in type or in number of elements performing each mission type. A key, therefore, is time/position coordination and this is the unique enhancement possible with 4-D/JTIDS capabilities. Since tactical maneuvers involve elements of different squadrons and different bases, preflight, in-flight, and postflight time/position coordination is very important. An example of a tactical scenario is given below to illustrate coordination enhancements of 4-D/JTIDS capable aircraft.

A postulated attack scenario is a close air support (CAS) mission relatively close to a FEBA (forward edge of the battle air). It is assumed that there is JTIDS coverage, enemy air-air, ground-to-air defenses, and that the mission is to deliver air-to-ground ordnance (bombs, missiles) against a target. This sample tactical attack scenario (CAS) can involve strike elements (e.g., F-4), combat air patrol (CAP) elements (e.g., F-15), strike support elements (e.g., A-10 gunship), reconnaissance elements (e.g., RF-4C), forward air control (FAC) (e.g., F-4 in a limited role), search and rescue (SAR) elements, airborne tactical coordinator (e.g., AWACS), and ground-based tactical control and reporting centers. These elements require the passing around of much data. These also require time/position coordination, desirably control as well, to safely and efficiently execute their respective missions. To this end, 4-D/JTIDS capability considerably enhances their effectiveness.

The forward air controller (FAC) is an observer in the attack zone and has, depending on his capability, control of the operations in his theatre. Typically, this involves coordination of elements to perform preplanned maneuvers. The data which he would receive prior to mission execution would be his control assignment (control number, strike-force elements, communication time slots for the total control of the strike force, relevant tracks, particulars of the strike elements, strike elements on reserve in

case of contingencies, battlefield descriptions, etc.). The FAC would also probably optimize his estimate of his own time and time-rate errors with respect to net time after he arrives on station.

The combat air patrol (CAP) elements must arrive on station prior to the execution of the strike. Their role is perimeter coverage of the air space for the other strike elements. The data exchange for them is the hand-off assignment from one controller to the FAC, an extremely time-efficient input and output track-data transfer, and real-time knowledge of the position and status of the other strike elements.

A principal set of supporting elements are the ground- and air-command and reporting centers. Though it is not postulated for this sample scenario that they are the immediate control elements, it is acknowledged that they are the total battlefield commanders. They would have much more monitor capability than would the FAC and it is postulated that this is their primary role in the execution of a localized engagement. They would, however, have more capability of evaluating and changing strategies, particularly due to outside (the local battle area) influences. The dominant interface then with a localized net would be through the FAC, though they would monitor the other strike elements.

The primary active elements of the postulated CAS mission are the bomb/missile delivery systems and the air-to-ground gunnery supporting elements. It is to these elements, in particular, that the dimension of time is important. Time-on-target, and the related intermediate times at each waypoint (for coordination and prediction) are very important in performing an integrated CAS mission. The scenario of the bombing aircraft can be divided into mission phases, similar to those discussed for the transport aircraft. Flight planning, waypoint insertion, and threat presentation enhancements are analogous to those discussed before the preflight, take-off and climbout, and cruise phases. In-flight refueling would not generally be performed for CAS missions due to the proximities of the bases to the battle zones and also the desirability of minimum time (for inertial weapon delivery systems which have time-dependent errors) between system initialization and the strike. Missions of opportunity may require refueling. The principal enhancements occur, however, in the attack phase.

The attacking group, depending on the tactics planned and the resources available, would generally operate with a minimum of two aircraft and often with four or eight aircraft. A frequent scenario is to approach the target area at a low altitude, possibly performing a rendezvous at a waypoint; flying to the last waypoint prior to the target, either for system update or checkpoint, particularly if auto-steering is being used; popping up to an altitude at a course skewed to the target from which the target can

be visually acquired off to one side; rolling into and locking into the target during a dive; releasing the ordnance; and escaping however possible armed in an air-to-air defense mode. There are many variations of this scenario but it is a realistic sample. Two critical time coordinations exist for this scenario. They represent attaining flight profile time-at-position uncertainties on the order of a small number of seconds. The first critical point is the time at the top of the pop-up. At this point and following into the dive, the aircraft is particularly vulnerable to detection, tracking, and destruction by the enemy. An offensive procedure used is to lead the attacking units with strafing elements. These elements intend to keep the enemy occupied during the vulnerable portions of the attack phase. The second critical point is the time spacing between attacking units. For the case of multiple attacks on a common target, it is desirable to keep the spacing as small as possible in order to minimize exposure to the enemy air and ground defenses, but still maintain the flight safety during the many explosions occurring. Re-attacks, or re-programmed attacks, on targets of opportunities require the same planning and coordination.

Two other coordinations during the attack are important, though time uncertainties are not as restrictive. The first is the coordination between the CAS and CAP elements. Automatic status reporting by the CAS elements enables the CAP elements to know and to make judgments regarding the action which they must carry out in case of enemy sightings. Special assistance might be possible during both pre-attack and egress mission phases. The second coordination could involve all of the elements and that is to cover the detection, monitoring, and recovery of downed pilots. An integrated, efficient position/time knowledge of the downed pilot is most important as is a coordinated rescue. The cruise, let-down and land, and postflight enhancements are similar to those discussed for the transport aircraft, though more enhancement possibilities exist using JTIDS for faster attack assessments and possible follow-up efforts.

### 7.3 JTIDS RELATIVE NAVIGATION

The JTIDS relative navigation capability provides its users their positions relative to a common frame of reference. This frame of reference may only be fixed to the locations of other participants in the JTIDS net. Terminal navigation relative to ground-based JTIDS transmitters is an example of relative navigation. If the absolute positions of a few net participants are known, the entire JTIDS navigation grid can be tied to map coordinates.

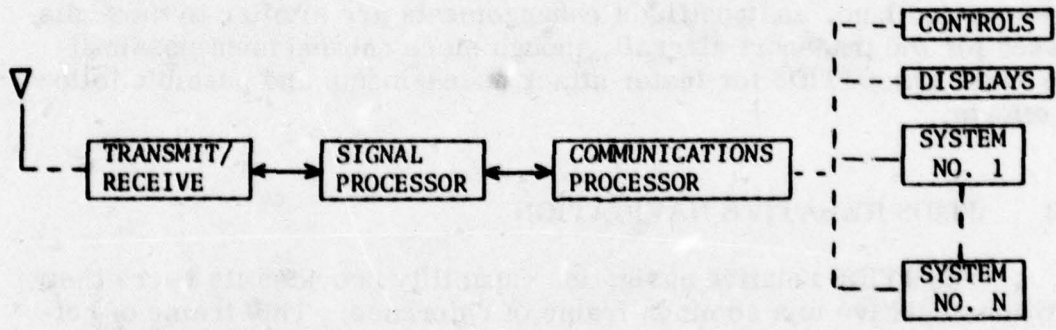
The JTIDS relative position can be used as a range gate for collision avoidance. Warning flags can be established by computing relative distances to other terminals from the position status message with respect to one's own position. Since these reports are only obtained once each 12 seconds, higher data rates can be obtained from the relative ranging of the RTT procedure.

An important capability of JTIDS' relative navigation is coordinate standardization. A range-range coordinate system can be used by different users which may have geodetic lat/long, time-difference, track/cross-track coordinate systems. A further capability is the improvement of navigation accuracy from JTIDS even of the position reference systems, such as Loran. See Ref. [47].

Loran absolute accuracy can be improved by factors of four, or more. It is not anticipated that JTIDS ranging can be used to update GPS position errors.

#### 7.4 JTIDS TERMINAL FUNCTIONS

A JTIDS terminal is a communications terminal which transmits/receives data to and from the data bus. A terminal consists of the following elements (see Figure 7-1).



FUNCTIONAL JTIDS TERMINAL  
FIGURE 7-1

The front-end of the terminal is the antenna and transmit/receive (T/R) unit, which include the encoder/decoders. The signal processor forms or detects the BIT streams during the data transmissions in each time slot. The T/R and signal processor are presently considered to be standardized hardware.

The first flexible part of the JTIDS terminal is the communications processing. It is to be noted that the communication processing may be distributed -- some going to the signal processing and some to the interconnecting systems. Essentially, communications processing contains the search/track/time-modeling algorithm, message catalog, net daily organization, error detection/correction schemes, data formatting/de-formatting, and data storage and filtering. The interconnecting elements include the controls for the terminal, displays, and using systems (No. 1-N). The using systems (not part of the terminal) may include monitor systems for fuel, stores, aircraft status and also primary mission-oriented systems such as navigation, weapon-delivery, and flight control.

The software requirements for the terminal vary considerably depending on the user capabilities and requirements. The development of JTIDS concentrated on advanced warning and control system (AWACS) and its interconnection with ground-based command and reporting centers. The development of the AWACS terminal emphasized maximum utilization of JTIDS capability employing dedicated communication processor and control-display systems. This terminal employs large bulk storage and a program to operate on all the data in the net. The terminal requirements for this type of a system are on the order of hundreds of thousands of words of a dedicated, high-speed processing system. The AWACS system, however, may not be a prime candidate for the 4-D system. The terminal requirements for a non-dedicated system are also of more interest in considering an integrated 4-D/JTIDS system. These are briefly discussed below.

The JTIDS terminal functional requirements for an integrated 4-D/JTIDS system can be considered from many potential configurations. The functional requirements themselves stand alone but feasible configurations with only slight limitations on the total JTIDS capability can be defined. The display requirements for an integrated 4-D/JTIDS system are presented in Section 3.7. The hardware requirements consist as a minimum of the front end of the terminal (antenna, T/R unit, and probably the signal processor) and a digital interface to a processing system. The communication processor function can be selectively absorbed by some other digital system, e.g., the navigation system, see Ref. [46]. The tasks which must be accomplished are:

- a. **Terminal Timing Processing:** The communication processing (CP) function must be able to passively synchronize to the net and actively participate in the net. Operating in conjunction with the signal processor, the CP function searches the net transmissions within a 12 second block of time and locks onto a set of reference transmissions. Tracking these transmissions, the terminal time uncertainty is reduced to a very small value and the results are processed in a time varying algorithm in order to model the terminal's time function. The CP function actively interrogates certain external JTIDS terminals to upgrade its time estimates. It is estimated that approximately 1% of an airborne navigation processor's time is required and about .5K of memory for the timing function.
- b. **Data Formatting/De-Formatting Function:** A very important CP function is to format or defomat the data between the net and the using systems. The net has fixed data format with a much larger bit length (in fact, the net bit length is even double the data bit length) than does the using systems. The net bit pattern is a packed data and discrete word. The formatting function is to format and preload the signal processor prior to the required time slot for transmission. The deformatting process is acceptance of data from the signal processor for each time slot (<10 ms), at least a partial defomat for some data filtering schemes, and a full defomat for data to be accepted.

A major function for receiving data from the net is data filtering. Data filtering in this context means operating on received data with respect to logical criteria and accepting or rejecting the data. Some of the parameters used for the filtering are message types (categories and subcategories), addresses, track and position locations. It is estimated that the filtering process can greatly reduce CP requirements. A further benefit, over memory storage reduction, by the filtering process enables the CP defomatting to be completed only when necessary and time-delayed over many computer cycles. This potentially saves much computer time. An estimate of computer loading is approximately 15% of cycle time and 10K of memory. It is acknowledged that these are very flexible numbers, highly dependent on the system (user) requirements.

- c. **Tactical Display Function:** A very important feature of JTIDS is real-time dissemination of tactical situation data. This data is of immense value to the crew for safety and flight

planning purposes. The addition of 4-D capability further enhances the feature because of the capability of flying curved trajectories around avoidance volumes, while maintaining flight schedules. There is a significant software function for the CP to filter (select) the important tracks for display and for profile modifications. A computer sizing estimate for radar CRT-type display and a one or two point profile avoidance warning is a 4% time estimate and a 1K memory requirement.

- d. **Man-Machine Interface Function:** The software requirements for a JTIDS C/D interface, which is discussed in more detail in Section 3.7, is for 1% computer time requirement and 5K memory requirement.
- e. **Relative Navigation Function:** The relative navigation function is part of one of the user systems, e.g., NAV, collision-avoidance, weapon-delivery, and landing system. The function utilizes the output of the CP timing function and performs its own desired task.

## **8    COMPONENT FAILURE EFFECT ANALYSIS**

### **8.1    INTRODUCTION**

The 4-D Integrated Control and Display System (4-D INCADS) provides integration of flight controls, displays, and navigation sensors to achieve three-dimensional flight control plus time schedule control. This section contains preliminary reliability calculations for a non-redundant 4-D INCADS. For this analysis, the airborne components are comprised of a Loran receiver, a system data processor, inertial measurement unit (IMU), an barometric altimeter, and an electronic control and display system. During the approach phase of a mission, a differential Loran navigation capability is achieved through the use of a ground-located Loran receiver, barometric altimeter, wind sensors, and data link.

The preliminary reliability calculations contained in Section 8.2 and 8.3 limit the mission to one-half hour before touchdown for an instrument flight with Category II visibility condition (100 feet decision height and 1200 feet runway visual range). It also assumes 100% reliability for the Loran stations and no other navigation aids airborne, or at the destination airstrip.

Section 8.4 contains an "effects of failure" of airborne and ground equipment, component-by-component, during the enroute and approach phases of a mission. Based on the "effects of failure" results for the single thread system, the redundancy needs of the 4-D INCADS are considered in Section 8.5. A conclusion is reached that to ensure mission success based solely on the 4-D INCADS components for a probability of success greater than 95 to 99%, backup redundancy should be employed on the ground equipment and airborne altimeter. Components that need some level of redundancy to improve reliability are the Loran receiver, data processor, and inertial system. This redundancy can be achieved either with functional redundancy (Ref. [29]) where complementary sensors both provide the critical information, or with true component redundancy, where two or more identical components measure the same critical parameters. Quantitative estimates for the amount of redundancy require more extensive component definition and analysis of voting techniques and switching criteria.

### **8.2    GROUND EQUIPMENT RELIABILITY PREDICTION**

The preliminary reliability estimate for the ground equipment during an IFR approach is based on the simplified reliability block diagram (Figure 8-1). The single mission duration for the ground equipment could be as short as one-half hour predicated on a single aircraft arrival. More realistically, it would be as long as eight hours to accommodate a more complex schedule of many transport arrivals and departures.

### **8.2.1 Reliability Model**

Figure 8-1 shows the simplified reliability block diagram of the ground sensor and data link equipments. The Loran receiver/computer measures time differences on the ground. Ground wind velocity, direction, and atmospheric pressure are also measured. These signals are converted to a binary form, multiplexed, and then used to modulate an RF data link transmitter feeding an omnidirectional antenna.

The failure rates for the Loran equipment are derived from test data for the AN/ARN-101 Digital Modular Avionics System. The Loran antennae and preamp are shown in parallel. The failure rate for the power amplifier assumes a solid-state amplifier capable of delivering RF power of up to 5 watts average. If higher RF power levels are required due to intentional or untoward EMI, a traveling wave tube or cavity amplifier may be required with an attendant increase in failure rate.

The power generator has not been defined. It could take the form of a battery or, depending on final power requirements and mission duration, perhaps a gasoline engine-generator combination. The power generator for either class of device requires routine maintenance at frequent intervals. A standby power generator unit, or extended fuel reserves, may be required to achieve adequate reliability. A failure rate of 1000 per  $10^6$  hours will be used in this model with the caution that the generic origin of the device is not yet identified. For reference, a budgetary estimate of generated power to operate the ground equipment as postulated is:

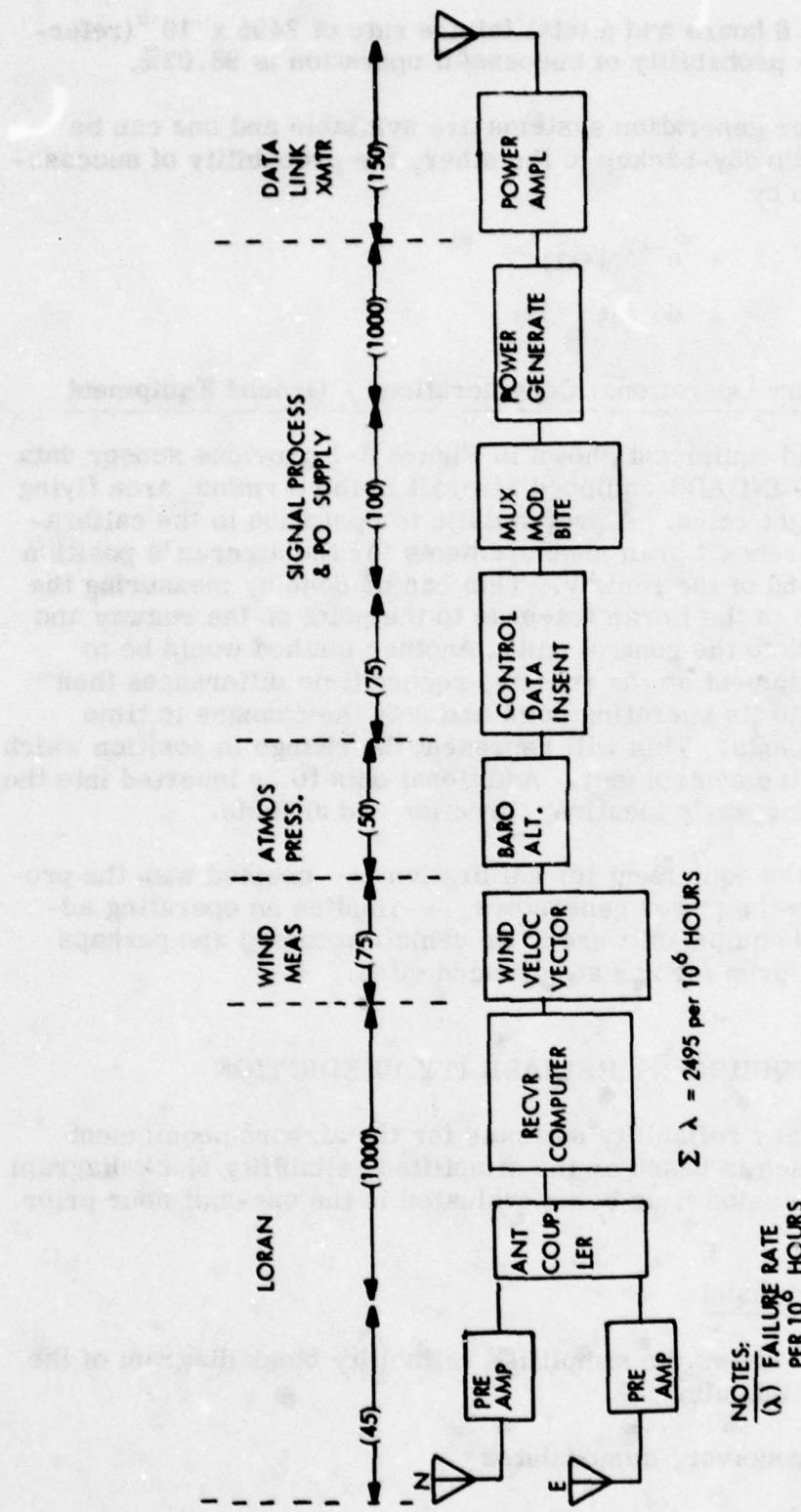
Loran Receiver/Computer	150 watts
BITE/MUX/MOD	50 watts
RF Power Amp (5 watts output)	40 watts
A/D or Encoder	10 watts
Power Regulator	75 watts

### **8.2.2 Reliability Calculation - Ground Equipment**

The reliability of the single thread ground equipment (reference Figure 8-1), where reliability is the probability of successful operation [30], is given by

$$R = e^{-\lambda T}$$

where R is the probability of successful operation,  $\lambda$  is the number of failures per operating hour, and T is the specified operating time. For



GROUND SENSORS/DATA LINK DURING IFR APPROACH PHASE  
 SIMPLIFIED RELIABILITY BLOCK DIAGRAM  
 FIGURE 8-1

an operating time of 8 hours and a total failure rate of  $2495 \times 10^{-6}$  (reference Figure 8-1) the probability of successful operation is 98.02%.

If two complete power generation systems are available and one can be considered to be a standby-backup to the other, the probability of successful operation is given by

$$\begin{aligned} R &= e^{-\lambda T} (1 + \lambda T) \\ &= 99.98\% \end{aligned}$$

### **8.2.3 Preliminary Operational Considerations - Ground Equipment**

The ground equipment shown in Figure 8-1 provides sensor data for use aboard a 4-D INCADS-equipped aircraft in the terminal area flying under instrument flight rules. A prerequisite to operation is the calibration of the time difference Loran measurements for the aircraft's position with respect to the end of the runway. This can be done by measuring the bearing and range from the Loran antennae to the point on the runway and inserting the values into the control unit. Another method would be to place the ground equipment on the runway, record time differences then move the equipment to its operating point and note the changes in time difference measurements. This will represent the change in position which can be inserted into the control unit. Additional data to be inserted into the control unit are the runway's location, direction and altitude.

The ability to move the equipment for calibration -- coupled with the probable need to service the power generators -- implies an operating advantage if the ground equipment were to be vehicle mounted and perhaps capable of parachute drop for use at advanced sites.

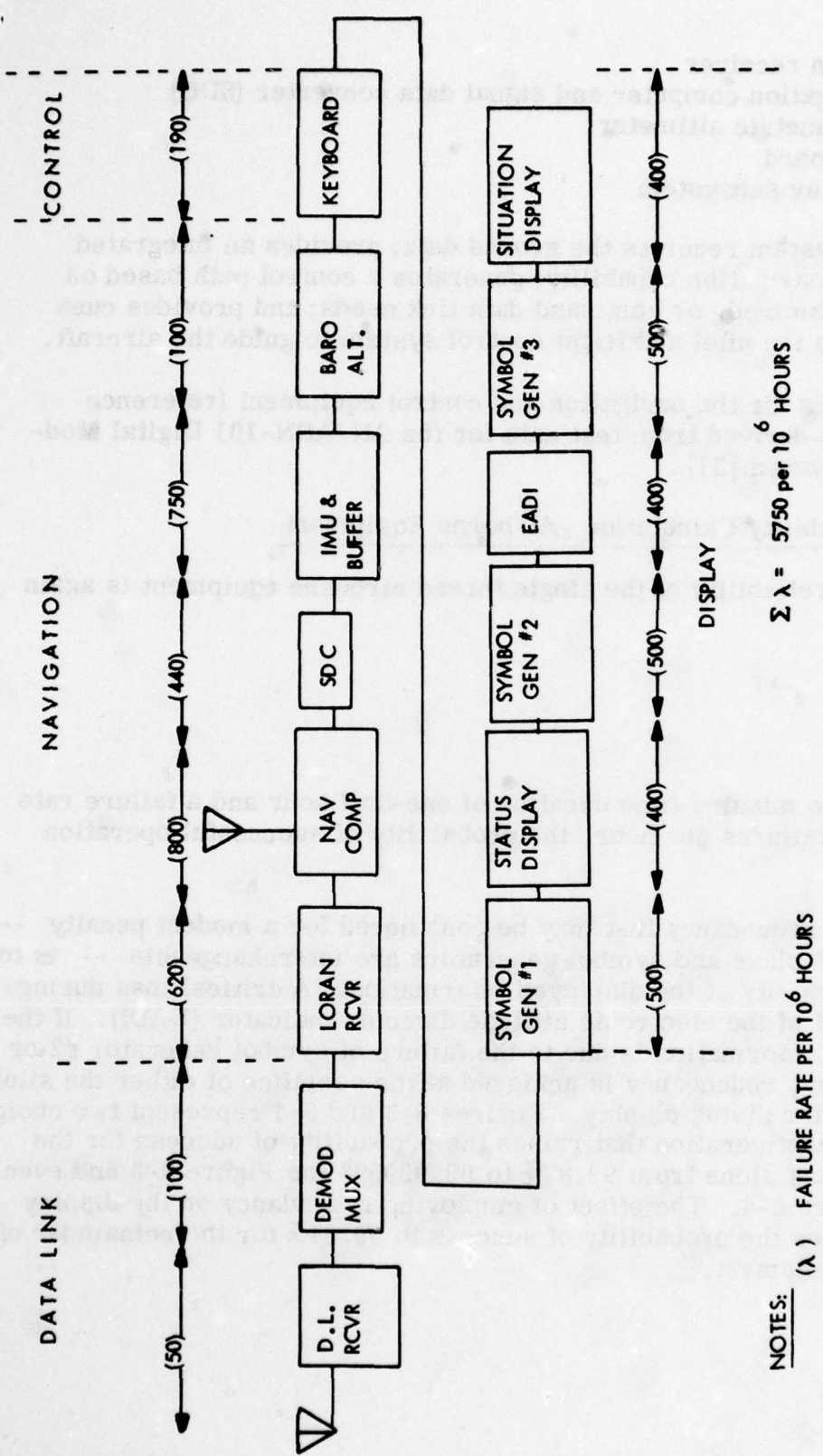
## **8.3 AIRBORNE EQUIPMENT RELIABILITY PREDICTION**

The preliminary reliability estimate for the airborne equipment during an IFR approach is based on the simplified reliability block diagram (Figure 8-2). The mission time being evaluated is the one-half hour prior to touchdown.

### **8.3.1 Reliability Model**

Figure 8-2 shows the simplified reliability block diagram of the airborne equipments including:

- a. Data line receiver, demodulator



AIRBORNE SYSTEM DURING IFR APPROACH PHASE  
SIMPLIFIED RELIABILITY BLOCK DIAGRAM  
FIGURE 8-2

- b. Loran receiver
- c. Navigation computer and signal data converter (SDC)
- d. Barometric altimeter
- e. Keyboard
- f. Display subsystem

The airborne system receives the ground data; provides an integrated Loran/inertial navigation capability; generates a control path based on pilot, preprogrammed, or command data link needs; and provides cues or commands to the pilot and flight control system to guide the aircraft.

The failure rates for the navigation and control equipment (reference Figure 8-2) are derived from test data for the AN/ARN-101 Digital Modular Avionics System[31].

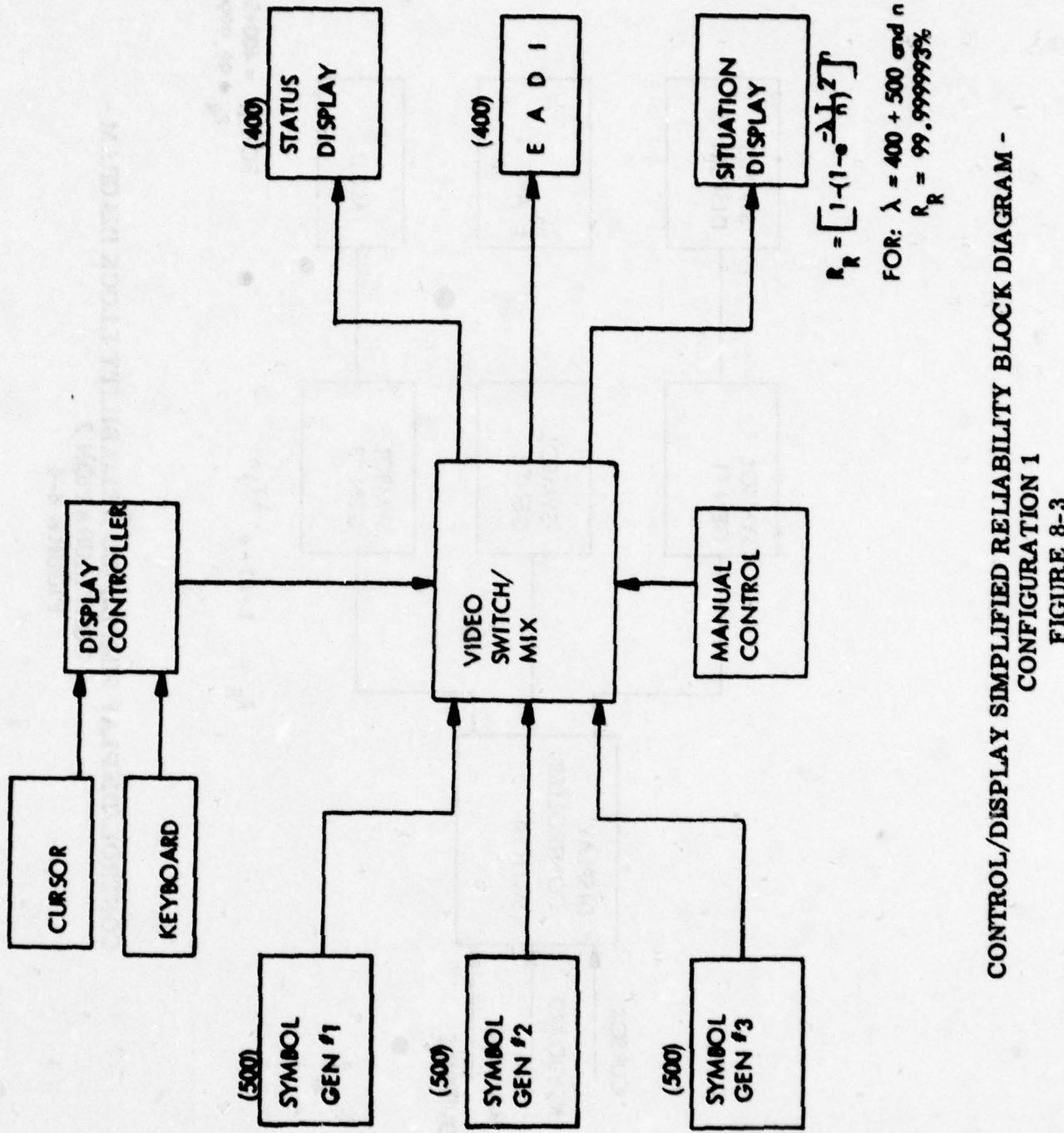
#### **8.3.2 Reliability Calculation -Airborne Equipment**

The reliability of the single thread airborne equipment is again given by

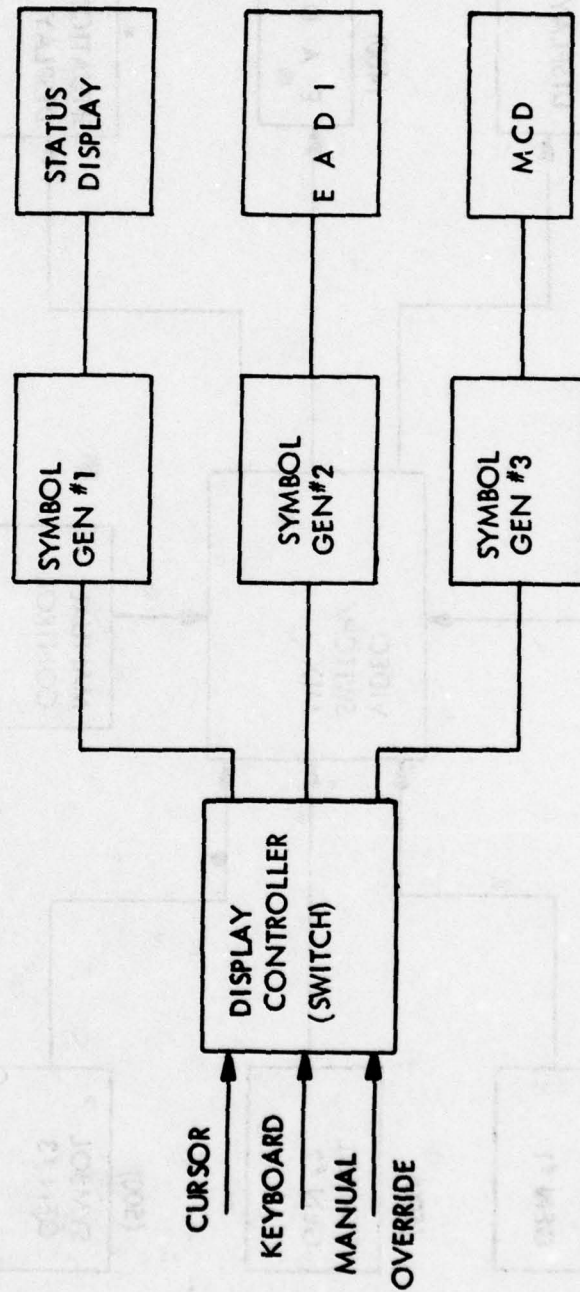
$$R = e^{-\lambda T}$$

For an approach mission time duration of one-half hour and a failure rate of  $5750 \times 10^{-6}$  failures per hour, the probability of successful operation is 99.71%.

An approach to redundancy that may be considered for a modest penalty -- providing the displays and symbol generators are interchangeable -- is to establish the priority of the displayed information. A critical loss during approach is that of the electronic attitude director indicator (EADI). If the failure of EADI information is due to the failure of symbol generator #2 or the EADI display, redundancy is achieved at the sacrifice of either the situation display or the status display. Figures 8-3 and 8-4 represent two choices of redundancy configuration that raises the probability of success for the display equipment alone from 99.87% to 99.999993 for Figure 8-3 and even better for Figure 8-4. The effect of employing redundancy on the display subsystem raises the probability of success to 99.84% for the remainder of the airborne equipment.



CONTROLLERS  
CONFIGURATION 2  
BLOCK DIAGRAM



$$R_R = 1 - (1 - e^{-\lambda T})^n$$

$$\text{FOR: } \lambda = 400+500 \text{ and } n=3 \\ R_R = 99.99999999999999\%$$

CONTROL/DISPLAY SIMPLIFIED RELIABILITY BLOCK DIAGRAM -  
CONFIGURATION 2  
FIGURE 8-4

## 8.4 EFFECTS OF COMPONENT FAILURES

Some failures for a single thread system, such as navigation computer failures, result in the total denial of a Loran or inertial navigation capability. For other failures, such as the Loran receiver or inertial measurement unit, a degraded navigation capability exists by using the alternate sensor. The effects of component failures are addressed in the following paragraphs.

### 8.4.1 Loss of Airborne Loran

The navigation system operating in the differential Loran/inertial mode provides position accuracies, relative to the Loran grid in Loran time differences, better than 75 feet rms. Gradual degradation of position versus time loss of airborne Loran measurements must include the following error sources.

- a. Gyro bias error
- b. Platform vertical alignment
- c. Lateral velocity
- d. Loran warpage

where the initial conditions are established by the differential Loran/inertial performance. The position error from the time of loss of airborne Loran measurements if given by:

$$\sigma_e(t) = \left[ \sigma_{\Delta N(0)}^2 + R^2 \left( t - \frac{1}{\omega_s} \times \sin \omega_s t \right)^2 \sigma_{GB(0)}^2 + R^2 (1 - \cos \omega_s t)^2 \sigma_p(0)^2 + \frac{1}{\omega_s^2} \times \sin^2 \omega_s t \times \sigma_{\Delta V(0)}^2 + 2(A^2 + B^2) \sigma_w^2 (1 - e^{-t/\tau_w}) \right]^{\frac{1}{2}} \quad (8-1)$$

where

$\sigma_e(t)$  Position error (rms) versus loran time off

$\sigma_{\Delta N(0)}$  Initial differential loran/inertial position error (rms)

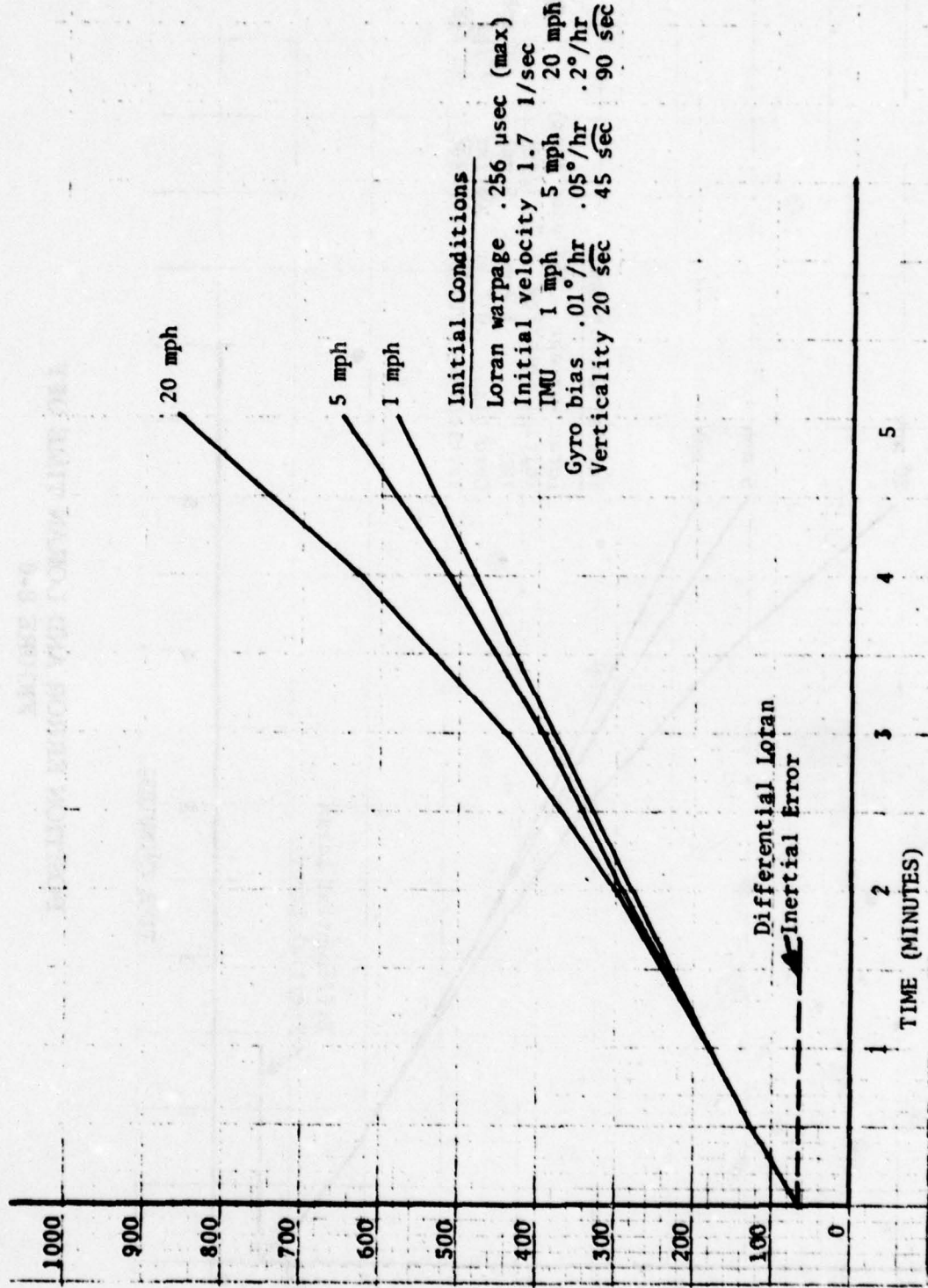
$R^2$	Earth's radius
$\omega_s$	Schuler angular rate = $g^2/R^2$
$t$	Time
$\sigma_{GB(o)}$	Initial gyro bias error (rms)
$\sigma_p(o)$	Initial vertical uncertainty (rms)
$\sigma_{\Delta V(o)}$	Initial velocity error (rms)
A, B	Loran warpage factors, feet per $\mu$ sec of time difference
$\sigma_w$	Loran warpage error (rms)
$\tau_w$	Loran warpage time constant
g	Gravity

Equation 8-1 was evaluated for three classes of inertial platform (1, 5, and 20 nmi per hour), and warpage factors, errors and time constants derived from the AN/ARN-101 flight test program at Eglin AFB. The results are plotted in Figures 8-5 to 8-8.

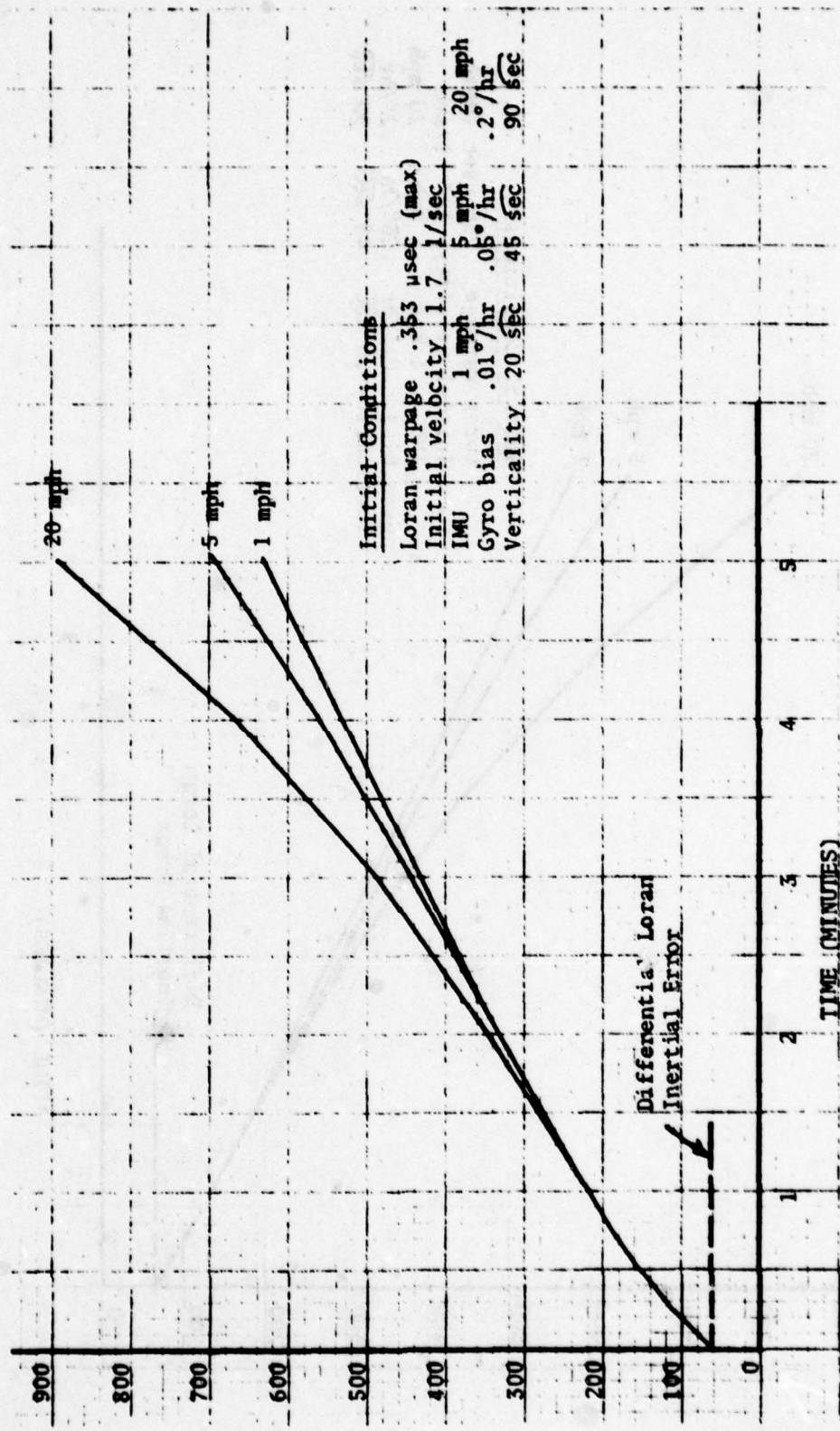
Examination of the contributing sources of error shows that during the first 1-1/2 minutes the error sources are from the Loran warpage and the initial velocity terms. Further (reference Figures 8-5 to 8-8) the total position error becomes 100 feet rms within the first 1/4 minute for all three classes of inertial platforms. The conclusion is that if the airborne Loran signal is lost in the differential Loran/inertial mode during approach, and if ILS or MLS is not available, the lateral position error growth will prevent completion of the landing if the time from touchdown exceeds 1/4 minute, independent of INS class.

#### 8.4.2 Effects of Component Failure for a Non-Redundant System

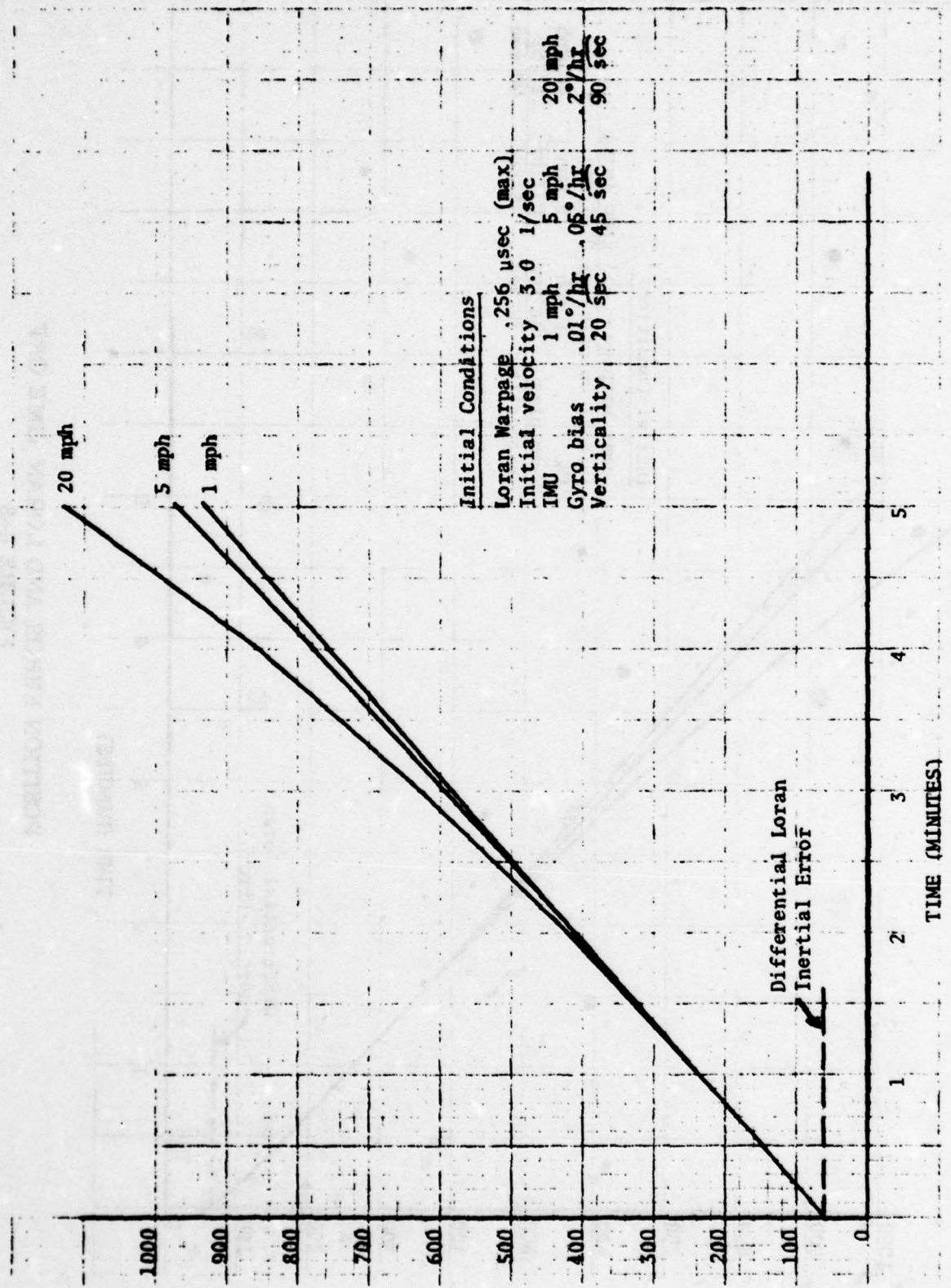
This section identifies the effect of individual component failures in terms of what action should follow the failure. Two actions are considered, either proceeding with the mission or aborting the mission.



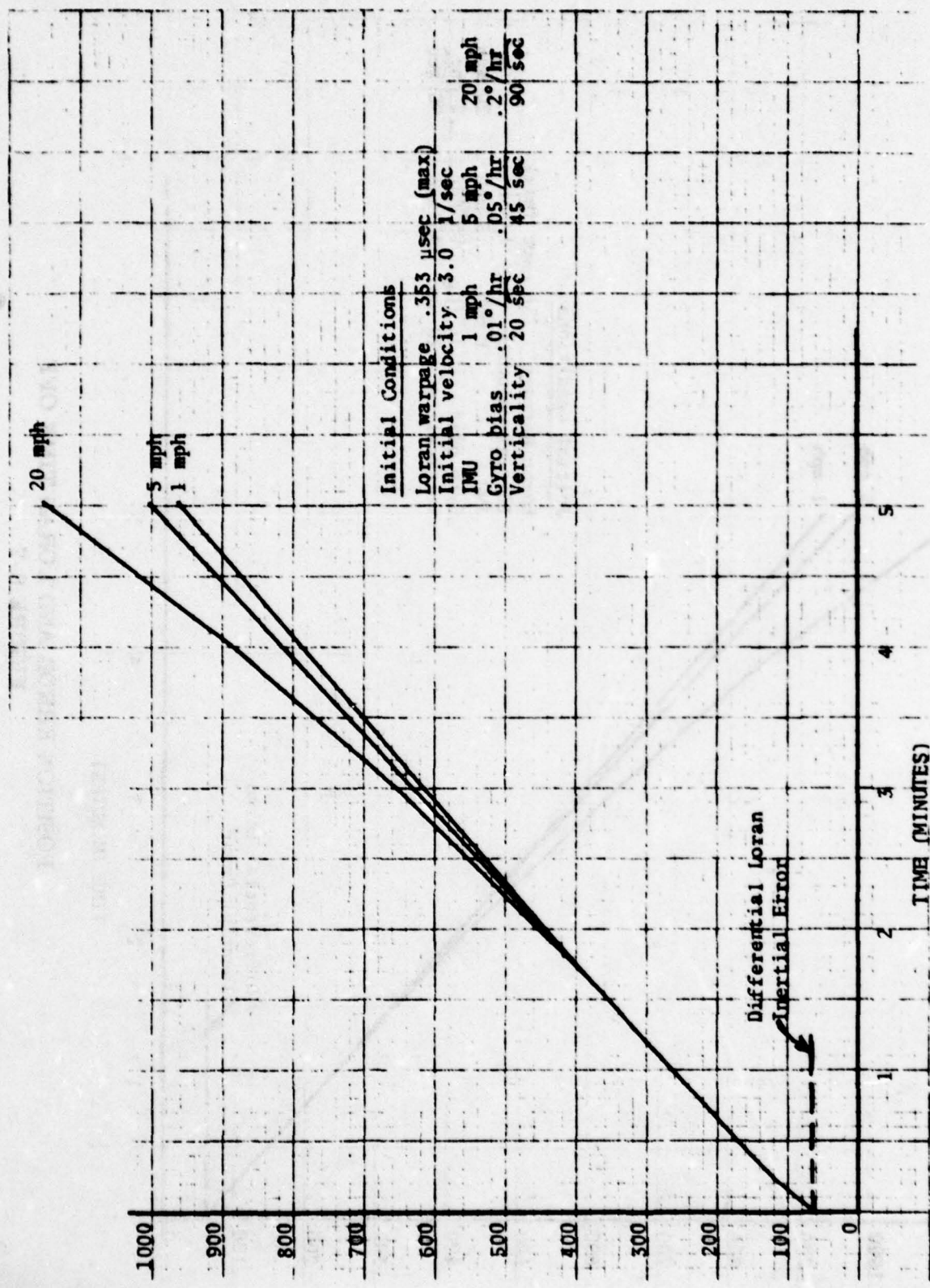
POSITION ERROR AND LORAN TIME OFF  
FIGURE 8-5



POSITION ERROR AND LORAN TIME OFF  
FIGURE 8-6



POSITION ERROR AND LORAN TIME OFF  
FIGURE 8-7



POSITION ERROR AND LORAN TIME OFF  
FIGURE 8-8

#### **8.4.2.1 Underlying Assumptions**

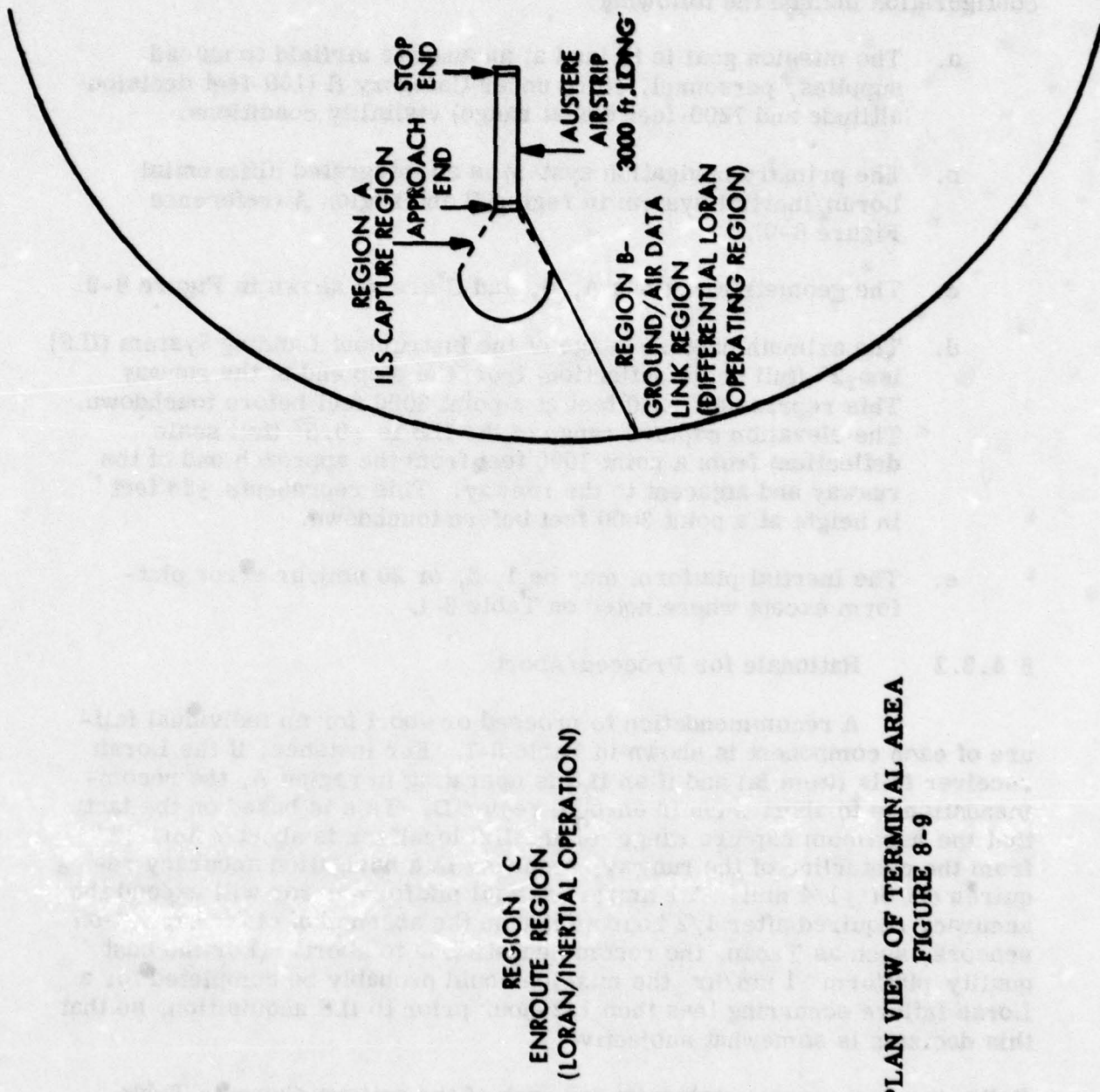
**Assumptions made about the approach profile and system configuration include the following:**

- a. The mission goal is to land at an austere airfield to unload supplies, personnel, etc., under Category II (100-feet decision altitude and 1200-feet visual range) visibility conditions.
- b. The primary navigation system is an integrated differential Loran/inertial system in region B and region A (reference Figure 8-9).
- c. The geometric regions A, B, and C are as shown in Figure 8-9.
- d. The azimuth capture range of the Instrument Landing System (ILS) is  $\pm 2^\circ$  (full scale deflection) from the stop end of the runway. This represents  $\pm 210$  feet at a point 3000 feet before touchdown. The elevation capture range of the ILS is  $\pm 0.5^\circ$  (full scale deflection) from a point 1000 feet from the approach end of the runway and adjacent to the runway. This represents  $\pm 38$  feet in height at a point 3000 feet before touchdown.
- e. The inertial platform may be 1, 5, or 20 nmi/hr error platform except where noted on Table 8-1.

#### **8.4.2.2 Rationale for Proceed/Abort**

A recommendation to proceed or abort for an individual failure of each component is shown in Table 8-1. For instance, if the Loran receiver fails (item 1a) and if an ILS is operating in region A, the recommendation is to abort when in enroute region D. This is based on the fact that the maximum capture range for the ILS localizer is about 7 nm,  $\pm 2^\circ$  from the centerline of the runway, resulting in a navigation accuracy requirement of  $\pm 1/4$  nmi. A 1 nm/hr inertial platform error will exceed the accuracy required after 1/2 hour so that in the absence of other navigation sensors, such as Tacan, the recommendation is to abort. (For the best quality platform 1 nm/hr the mission could probably be completed for a Loran failure occurring less than 1/2-hour prior to ILS acquisition, so that this decision is somewhat subjective.)

Following is a concise statement for each of the actions shown in Table 8-1.



PLAN VIEW OF TERMINAL AREA  
FIGURE 8-9

**TABLE 8-1**  
**SUMMARY OF EFFECTS OF COMPONENT FAILURES FOR NON-REDUNDANT SYSTEM**

		REGION C PRIOR TO DIFF LORAN		REGION B DIFF LORAN BUT PRIOR TO ILS		REGION A ILS DIFF LORAN	
		1	2	1	2	1	2
I.	AIRBORNE EQUIPMENT						
a)	Loran	Abort	Abort	Proceed *	Abort	Proceed	Proceed **
b)	Nav Comp SDC	Abort	Abort	Abort	Abort	Proceed	Abort
c)	IMU	Proceed	Proceed	Proceed	Proceed	Proceed	Proceed
d)	Baro Altimeter	Abort	Abort	Abort	Abort	Proceed	Abort
e)	Control/Display	Abort	Abort	Abort	Abort	Proceed	Abort
II.	GROUND EQUIPMENT						
a)	Loran	Proceed	Abort	Proceed	Abort	Proceed	Proceed **
b)	Baro Altimeter	Abort	Abort	Abort	Abort	Proceed	Abort
c)	Wind Sensors	-----	-----	Proceed for straight in approach or during periods of light winds -----	-----	-----	-----
d)	MUX/MOD/XMTR	Abort	Abort	Abort	Abort	Proceed	Abort
e)	Power Gen.	Abort	Abort	Abort	Abort	Proceed	Abort

NOTE: Mission is to land at austere airfield during Cat. II visibility conditions: (1) with ILS;  
(2) without ILS.

\* Change to abort if IMU is 5 nmi or 20 nmi/hr quality.

\*\* Change to abort if more than  $\frac{1}{2}$  mile from touchdown.

<u>Failed Item</u>	<u>Region</u>	<u>ILS</u>	<u>Decs'n</u>	<u>Reason</u>
		<u>1</u>	<u>2</u>	
Ia (Loran)	C	X	Abort	IMU accuracy inadequate to acquire ILS localizer signal (refer to text for exception).
	C	X	Abort	IMU accuracy inadequate for approach guidance.
	B	X	Proceed	Accuracy of 1 nmi/hr IMU is adequate to acquire ILS beam.
			(Abort)	(Accuracy of 5 or 20 nmi/hr IMU probably not adequate to acquire ILS beam.)
	B	X	Abort	IMU accuracy inadequate for final approach guidance.
	A	X	Proceed	ILS guided approach.
	A	X	Proceed	Change to abort if more than $\frac{1}{2}$ nmi from touchdown due to growth of error.
Ib (Nav Comp, SDC)	C	X	Abort	No onboard navigation computation capability.
		X	Abort	No onboard navigation computation capability.
	B	X	Abort	No onboard navigation computation capability.
		X	Abort	No onboard navigation computation capability.
	A	X	Proceed	ILS guided approach.
		X	Abort	No onboard navigation computation capability.
Ic (Inertial Measurement Unit)	C	X	Proceed	Loran only accuracy adequate to acquire ILS localizer signal.
		X	Proceed	Loran only accuracy adequate for approach guidance.
	B	X	Proceed	Differential Loran accuracy adequate to acquire ILS localizer signal.
		X	Proceed	Differential Loran accuracy adequate for approach guidance.
	A	X	Proceed	ILS guided approach.
		X	Proceed	Differential Loran adequate for approach guidance.

<u>Failed Item</u>	<u>Region</u>	<u>ILS</u>	<u>Decs'n</u>	<u>Reason</u>
		<u>1</u> <u>2</u>		
Ia (Baro Altitude)	C	X	Abort	Loss of altimeter precludes IFR approach.
		X	Abort	Same as above.
		B	X	Abort
		X	Abort	Same as above.
		A	X	Proceed
		X	Abort	ILS guided approach.
				Loss of altimeter precludes IFR approach.
	D	X	Abort	No navigation guidance information.
		X	Abort	Same as above.
		B	X	Abort
		X	Abort	Same as above.
		A	X	Proceed
Ie (Control/Display)	C	X	Abort	ILS guided approach.
		X	Abort	No navigation guidance information.
		B	X	Abort
		X	Abort	Same as above.
		A	X	Proceed
	D	X	Abort	ILS approach unimpaired.
		X	Abort	No navigation guidance information.
		B	X	Proceed
		X	Abort	Loss of differential Loran precludes IFR approach.
		A	X	Proceed
IIa (Ground Loran)	C	X	Proceed	ILS approach unimpaired.
		X	Abort	Loss of differential Loran precludes IFR approach.
		B	X	Proceed
		X	Abort	Loss of differential Loran precludes IFR approach.
		A	X	Proceed
	D	X	Proceed	ILS approach unimpaired.
		X	Proceed	Change to abort if more than $\frac{1}{2}$ nmi from touchdown due to growth of error.
		B	X	Proceed
		X	Proceed	ILS approach unimpaired.
		A	X	Proceed
IIb (Ground Baro Altimeter)	C	X	Abort	Loss of differential altitude precludes IFR approach.
		X	Abort	Same as above.
		B	X	Abort
		X	Abort	Same as above.
		A	X	Proceed
	D	X	Abort	ILS approach unimpaired.
		X	Abort	Loss of differential altitude precludes IFR approach.
		B	X	Proceed
		X	Abort	Lack of cross wind data will restrict approach profile.
		A	X	Proceed
IIc (Ground Wind Sensors)	C	X	Proceed	Same as above.
		X	Proceed	Same as above.
		B	X	Proceed
		X	Proceed	Same as above.
		A	X	Proceed
	D	X	Proceed	Same as above.
		X	Proceed	Same as above.
		B	X	Proceed
		X	Proceed	Same as above.
		A	X	Proceed

<u>Failed Item</u>	<u>Region</u>	<u>ILS</u>	<u>Desc'n</u>	<u>Reason</u>
		<u>1</u>	<u>2</u>	
IId and IIe (Ground MUX/ MOD/SMTR and Power Gen.)	C	X	Abort	Loss of differential altitude precludes IFR approach.
			X Abort	Same as above.
	B	X	Abort	Same as above.
			X Abort	Same as above.
A	X		Proceed	ILS approach unimpaired.
			X Abort	Loss of differential altitude precludes IFR approach.

## 8.5 RECOMMENDATIONS FOR REDUNDANCY

Reliability has been quantified and tabularized based on a single thread system in Sections 8.2.2 and 8.3.2 for the approach phase of the mission. Redundancy required to accomplish a "must be performed" transport mission can be based on one of two approaches. One is to recommend redundant components based on the system configuration shown in Section 8.2.3 and the other is to employ other navigation aids, or systems, that are normally available on military transports and have proven capability.

### 8.5.1 Redundant Component Approach

In order to improve the probability of achieving the intended transport mission this section delineates the components that provide a standby redundancy capability. Standby redundancy implies that when a unit fails one can turn on an identical unit to replace the failed element. The extra components to be added should consist of:

- a. Loran receiver
- b. Navigation computer and interface equipment
- c. Inertial measurement unit (The backup platform could be a lower accuracy system.)
- d. Barometric altimeter

- e. Ground equipment complete with data link, Loran receiver power generator, barometric altimeter, etc.

NOTE: Based on the ability to prioritize the displays and symbol generator, it should not be necessary to add display equipment. The assumption of standby redundancy for the ground equipment (item e) is valid if an operator is in attendance to switch from one system to the other.

As a backup unit for the barometric altimeter (item d), a radar altimeter of the type that has no minimum blind range (FW-CW), and sufficient accuracy to assist in an emergency landing conditions, is recommended.

Standby redundancy components for the Loran receiver, navigation computer and inertial measurement unit require additional switching and monitoring circuits to perform "redundancy management" in order to improve reliability since these components cannot be replaced, simply, by an operator. Improvement in reliability for these components will require a more detailed study that identifies the equipment components and software in order to permit an evaluation of reliability.

#### **8.5.2 Functional Redundancy Approach**

A method of achieving redundancy through the use of alternate equipment can be achieved by use of Tacan and a radar altimeter. This presupposes that a portable or easily transportable Tacan station can be placed near the destination airfield. An advantage to this approach is the recognition that aircraft Tacan equipment is an existing component on the aircraft, and by selecting a suitable approach profile, it can be used to acquire the ILS localizer beam.

A further consideration of an independent system would be the use of a high resolution, short range, forward looking radar capable of mapping the runway, and which, in conjunction with a radar altimeter, could provide an emergency landing capability. The Hughes bistatic thinned array radar (BISTAR) would be a possible candidate for evaluation.

## **9    4-D INCADS COMPATIBILITY STUDIES**

### **9.1    INTRODUCTION**

Air traffic control, under the Federal Aviation Administration (FAA), is undergoing large scale changes in the methods of monitoring and controlling aircraft position during the enroute phase, for approach control, and guidance and designation of flight paths. The major growth items with respect to the aircraft equipage are area navigation (RNAV), Microwave Landing System (MLS), Omega, and Discrete Address Beacon System (DABS). For effective operation of the U.S. National Airspace System (NAS) in the future an advanced navigation, control and display system technique for military transports will need either to utilize the FAA systems or to provide the capability required by the FAA systems. This section discusses the compatibility of the 4-D INCADS technique with RNAV, MLS and Omega.

Section 9.2 is concerned with RNAV compatibility for continental United States (CONUS), specifically for military jet aircraft Standard Instrument Departure (SID), enroute above 18,000 feet, and a Standard Terminal Arrival Route (STAR). The need for inserting the waypoints that define the desired profile into the 4-D INCADS, in a timely and error free manner, is discussed.

The integration of MLS and Omega into the 4-D INCADS is discussed in Section 9.3. Both systems provide aircraft position information. Omega provides 2-dimensional position for enroute and terminal guidance, with a differential Omega configuration providing more accurate terminal guidance information. MLS provides 3-dimensional position information for terminal and landing guidance. With the 4-D INCADS technique, Omega and MLS provide the same information as GPS or Loran with the only significant difference between the sensors, from a system performance point of view, lying in their error characteristics. Omega is not as accurate as either GPS or Loran, even in the differential Omega mode, but if the Omega (differential Omega) navigation accuracy is acceptable -- which it will be for enroute (terminal area) guidance in the NAS -- Omega can replace GPS or Loran in the 4-D INCADS. MLS provides the spherical coordinates of the aircraft over an airfield's terminal airspace defined by a +60° azimuth scan, a 0.5 to 20° vertical scan, and a 20 nm range [32]. Consequently, with a 4-D INCADS, GPS, Loran or Omega will be necessary for enroute guidance up to the MLS coverage area, where the system will switch to MLS for guidance relative to the runway. Differential GPS, differential Loran and differential baro will not be required for relative navigation; however, GPS or Loran provide functional redundancy for the MLS information.

This study did not address the integration of the air traffic control (ATC) data that may be provided by DABS into the 4-D INCADS. The DABS is being developed to provide a surveillance and data link communication capability for an automated ATC [33]. The DABS data link communication capability will be used as part of an automated ground-based collision avoidance system called Intermittent Positive Control (IPC) [34]. The IPC data received in the cockpit consists of proximity warnings and collision avoidance commands which are to be displayed on an IPC display being specified as part of the IPC program [34]. As presently configured, the IPC data is derived on the ground and the only potential for integration of DABS with 4-D INCADS is in the display of IPC warning and command data. More integration will be possible in the future, if the ground-to-air and air-to-ground data carrying capability of DABS is exploited.

## 9.2 4-D INCADS AND NAS AREA NAVIGATION COMPATIBILITY

### 9.2.1 NAS Area Navigation System Description

The RNAV capability for the U.S. NAS [35] requires a system which calculates a control path (RNAV route) between a series of designated waypoint pairs whose position is referenced to VORTAC stations. Since the control path is offset from the VORTAC station, the system must be able to compare measurements of actual position with the designated RNAV route, and provide the guidance commands required to fly the designated path. The expected benefits of an RNAV system are to:

- a. Relieve congestion at VORTAC terminals caused by aircraft flying on VOR radial path.
- b. Provide a method of flying "offset" from the RNAV route as required to relieve congestion without increasing pilot workload or requiring radar vectoring by air traffic control.
- c. Permit automatic flight control for the approach phase, thereby reducing the aircrew workload. (Automatic flight control during the approach phase implies that a 3-D RNAV capability, including vertical flight control, should be the minimum capability.)

### 9.2.2 Current Problems in Implementing RNAV

The success of the RNAV concept depends to a large extent on the degree of automation available both to the Air Traffic Controller and to the air crew. At present, the FAA prefers that an RNAV route

be "ground filed" (Ref. [36]) because air filing places an additional burden upon the air traffic control system. Computerized evaluation of RNAV route congestion is being improved and will probably be adequate by 1982.

Changes of waypoints during the approach phase could require insertion of latitude and longitude (14 digits) for each waypoint, and the approach path may require from 6 to 10 waypoints for an IFR approach. The ability of the air crew to insert the data without error in a limited time is tenuous. It is mandatory that the waypoints be stored in system computer memory, or readily insertable from cards or magnetic cassettes.

The problems being encountered in implementing RNAV (Ref. [37]) may be summarized as follows:

- a. Many requests for RNAV routes lack optimum planning for continuity between enroute and the terminal environments.
- b. Inability of the ground facility to handle impromptu route requests.
- c. Difficulty in changing instructions in the airborne RNAV equipment.
- d. Ground radar video clutter precluded depicting RNAV routes on the controller's display.
- e. Too many waypoints in the terminal area.
- f. Current methods of charting and route definition constrain optimum route design and complicate navigation.
- g. Methods of updating the airborne data file, in some systems, are complicated and costly.

#### **9.2.3 FAA RNAV Implementation Schedule**

A fundamental on-going task for the FAA RNAV implementation is waypoint location, designation, and route definition. When possible, a waypoint will be located at a point where the aircraft, flying at 18,000 feet and above, will be in the good signal region of a VORTAC station. The waypoint will be identified with a pronounceable 5 alpha

name, the VORTAC station, and the latitude and longitude of the waypoint to an accuracy of 0.1 min. For example:

SHAWN

16.3 DEN

219/42

N 039° 25.8' W 105° 27.5'

The pronounceable alpha 5 name is unique for each point, is helpful in aural exchanges between the pilot and the air traffic controller, and is a useful identifier for accessing a computer memory.

The specific criteria for designating the location points for standard instrument departure (SID), enroute and general terminal area, and standard terminal arrival route is too lengthy for this report, but is explained in depth in Ref. [38]. The number of points typically needed for takeoff, based on the standard terminal area waypoint designator, is typically 2 or 3. Enroute transition would require from 3 to 12 depending on the flight path. The number of points for an RNAV arrival is expected to be between 4 and 6. Thus a typical flight might be performed with a total of 9 to 21 prestored waypoints with a possibility, due to weather changes and impromptu destination changes, of perhaps doubling those numbers.

The RNAV implementation schedule given in the early documents (Ref. [37], [38], [39]) have indicated that RNAV along predetermined, charted routes above 18,000 feet would be a required capability in 1977, and that VOR radial routes would be deleted at that time. Further, in 1982 the use of predetermined (charted) routes would be dropped and flight plans would be submitted based on preplanned direct routes.

A subsequent publication of the National Aviation System plan for fiscal year 1976-1985 states that a comprehensive cost/benefit analysis to determine user and ATC system payoffs is a prerequisite to implementation of the RNAV task force plan. It also reveals, contrary to the earlier documents (Ref. [37], [38], [39]), the following:

- a. Existence of jet VOR routes through 1985.

- b. Designation of jet RNAV routes through 1985 (which implies deletion of the preplanned RNAV routes).
- c. Decreased emphasis on current STAR/SID procedures during the period 1976-1985.

FAA requirements for a 4-D RNAV capability at busy terminals have been discussed in the references. However, all of the references indicate that any decision has been deferred in time to permit an assessment of the need for a 4-D navigation capability.

#### **9.2.4 RNAV Navaids Requirements**

The VORTAC-referenced RNAV implementation does not preclude the use of any other navigation systems -- such as Omega, GPS, inertial-VORTAC, and Loran-inertial -- that can navigate with the required accuracies. However, use of navaids other than VORTAC does not preclude the need for storing or accessing the RNAV waypoint information, since the waypoints define the RNAV enroute path, and RNAV points for the SID and STAR. VORTAC is going to be retained indefinitely as a ground-referenced navaid, and it will be upgraded in terms of achievable accuracy to reduce the aircraft position error.

#### **9.2.5 4-D INCADS RNAV Capabilities**

A military aircraft with a 4-D INCADS has the inherent capability of navigating the FAA flight routes through and beyond 1985. Inherent in the control law and path generation capability is the ability to perform the specific maneuvers required to perform offset navigation and turn radius control for conflict avoidance, and the maneuver capability to fly the SID/enroute/STAR RNAV paths.

A problem that needs addressing is the insertion of the FAA-designated waypoints for the:

Departure Path  
Enroute Path  
Arrival Path

Conceivably, all the points could be inserted via keyboard before takeoff and with an uneventful takeoff, the enroute waypoints, 200 nm apart, could be inserted manually. At arrival time there will be a 90 nm diameter circle with 4 quadrants of 6 to 10 waypoint sets per quadrant. If wind changes, storm activity or changes in destination occur, the pilot may be required to insert latitude and longitude to 0.1 min for 10 points, error free, in a relatively short time.

A method of automatically loading the system computer or having the computer rapidly accessing the RNAV waypoints should be investigated for the 4-D INCADS. Having the waypoints available to the computer will improve the accuracy and reduce response time of waypoint insertion. Current methods include bulk storage of all waypoints (for SID, enroute and STAR) for the United States, magnetic tape cartridges for sections of the United States, or card data entry for a limited number of points.

### 9.3 4-D INCADS INTEGRATION WITH MLS AND OMEGA

#### 9.3.1 Microwave Landing System Description

The Microwave Landing System (MLS) is under development by the FAA as a replacement for the UHF/VHF Instrument Landing System (ILS). The MLS will have the following features [40]:

- a. Accurate guidance signals that will be relatively insensitive to weather, terrain, airport structures, and other aircraft. MLS will provide an improved all-weather approach and landing operation.
- b. It will cover a large volume of airspace to permit a broad choice of approach paths. Flexible flight paths will be an aid to noise abatement and increased airport capacity.
- c. Accurate guidance signals that will provide the capability for simultaneous operations on closely spaced parallel runways.
- d. The system will satisfy the complete range of civil, military and general aviation requirements on fully compatible bases.

The FAA conducted a competitive MLS development program from 1973-1975 and selected the Time Reference Scanning Beam (TRSB) technique. This MLS technique has been submitted to the International Civil Aviation Organization (ICAO) for consideration as an international MLS standard [41].

The TRSB is an air-derived data system with ground stations generating coded signals that enable an airborne receiver/processor unit to derive precisely the aircraft's azimuth angle, elevation angle, and range. The TRSB signal format includes a ground-to-air data link which provides runway identification and condition, MLS operational status, and weather information. The TRSB has a time-multiplexed signal format and, in each assigned time slot, a narrow fan beam is rapidly scanned "to" and

"from" (back and forth for azimuth and down and up for elevation) at a precise rate over the coverage area to measure angle. The key feature of TRSB is that angular position is determined by measuring the time interval between the arrival times of the "to" and "from" scans. In one complete 15--millisecond TRSB time frame, azimuth, elevation, flare, back azimuth and 360° azimuth scanning beams and the auxiliary data are transmitted. Aircraft range is measured with Distance Measuring Equipment (DME), which is an asynchronous and independent part of the MLS. The DME uses separate frequencies and is not time-multiplexed. For a more detailed description of the TRSB MLS technique, see Ref. [32] and [41].

### 9.3.2 4-D INCADS and MLS Integration

To implement all the MLS features listed in the previous section, an on-board system will need more than a receiver/processor unit for measuring the aircraft's spherical coordinates. The on-board system needs the capability for generating flexible, nonlinear flight paths to utilize the large airspace volume covered by MLS and it will need a control law for flying curved paths accurately under IFR conditions. These are the same capabilities the 4-D profile synthesizer and control law algorithms are providing for the 4-D INCADS. Consequently, the ability to use the full potential of MLS is inherent in the 4-D INCADS, where MLS is treated as a 3-D position sensor for navigation relative to the runway. Since the MLS is being designed to handle both civil and military applications, the same system hardware can be used for receiving the military and civil MLS signals.

To integrate the MLS position data into the 4-D INCADS navigation system, the 3-dimensional position data, after the appropriate transform, can replace the 3-D position information provided by GPS.

In the 4-D INCADS, the inertial system is the source of velocity information; however, the integration of MLS and inertial measurements will provide a number of benefits. First, the inertial velocities will provide smooth position and velocity solutions between the discrete-time MLS measurements. Second, the inertial velocities can be used to rate aid the MLS receiver, and the short term accuracy of the inertial data will allow the MLS receiver to average the raw MLS data longer, thereby reducing the in-beam multipath errors. Also, the inertial position and velocity data will allow the thresholds for the time gates that reject out-of-beam multipath to be lowered. This increases the effectiveness of the time gating technique resulting in a more accurate MLS position input to the integrated MLS/inertial navigation system in the 4-D INCADS.

### **9.3.3    4-D INCADS and Omega Integration**

Omega is a very low frequency (VLF) navigation system operating in the internationally allocated frequency band of 10 to 14 kHz. Global coverage, with continuous 24-hour operation, is obtained with eight transmitting stations. Omega has an accuracy of approximately one to two miles, which is achieved through the use of predicted sky-wave correction tables. Although these accuracies are acceptable for operations over the sea, they are not adequate for the future IFR navigation needs in the CONUS, where the projected lane widths for enroute flights are  $\pm$  2.5 nm, and  $\pm$  1.5 nm. for terminal operations.

One method under consideration for using Omega to meet these navigation aid requirements is differential Omega [48]. With this method, ground monitor stations would receive the Omega signals and calculate differential corrections from one or more ground monitors would be incorporated into a digital message and data linked to the aircraft. In the on-board equipment the corrections would be applied to the outputs of the Omega receiver. Differential Omega is based on the experimentally verified phenomenon that VLF propagation phase variations are highly correlated within reasonable large area. The differential accuracies are highly dependent upon the monitor-to-aircraft distance. For a monitor-to-aircraft distance of 50 nm, the differential accuracy is 0.2 nm ( $1\sigma$ ) and a differential accuracy of 0.4 nm ( $1\sigma$ ) is attainable for a monitor-to-aircraft distance of 200 nm [48]. Based on a 200 nm radius coverage area, 50 monitor stations will be required to cover the CONUS with a 0.4 nm ( $1\sigma$ ) accuracy.

Since differential Omega provides a 2-dimensional aircraft position measurement, it can be incorporated into the 4-D INCADS in the same way that Loran position information is processed. Differential Omega will establish the aircraft in the radio navigation grid established by the Omega ground monitor stations, the barometric altimeter will provide altitude information, and the on-board inertial system will provide velocity information. In terms of hardware requirements, an airborne Omega receiver for the primary phase measurements, and a data link terminal for receiving the differential corrections are required.

The performance goals of the differential Omega configuration of the 4-D INCADS will not be as ambitious as the differential Loran/inertial system goals of Section 5. Consequently, all three qualities of inertial navigation systems (20 nm/hr, 5 nm/hr, and 1 nm/hr) and the Doppler radar/AHRS system can be integrated with the Omega data. Furthermore, second order integration techniques, where the differential Omega data is used for position and velocity damping of the inertial errors, can be used for Omega-inertial integration.

APPENDIX A  
NAVIGATION SYSTEM MECHANIZATION

Information systems are called to a mission will be derived from selected information which contains information on flight navigation, health and safety of the crew, and applications which may be required to assist the pilot in his choice and to control the attitude, motion and position of the aircraft.

APPENDIX A

**NAVIGATION SYSTEM MECHANIZATION**

## APPENDIX A. NAVIGATION SYSTEM MECHANIZATION

The purpose of this appendix is to define an integrated differential Loran/strapdown inertial navigation technique and a differential barometric altitude/inertial system technique. A general set of equations are defined for these mechanizations. Derivation of the equations defined below are available in references [12,15].

### A.1 COORDINATE FRAME DEFINITIONS

Two coordinate systems are used. These are the body coordinates and the navigation coordinates as shown in Figure A-1. The body axes are an orthogonal set of axes attached to the aircraft with:  $X_B$  along the longitudinal reference axis and positive forward;  $Y_B$  perpendicular to the  $X_B$ - $Z_B$  plane and positive to the right; and  $Z_B$  perpendicular to  $X_B$  in the plane of symmetry of the aircraft and positive down. The navigation coordinates are an orthogonal set centered at the strapdown sensor package with the  $X_N$  axis aligned north-south, positive north; the  $Y_N$  axis aligned east-west, positive east; and the  $Z_N$  axis aligned along the local vertical, defined by local  $g$ , with positive down.

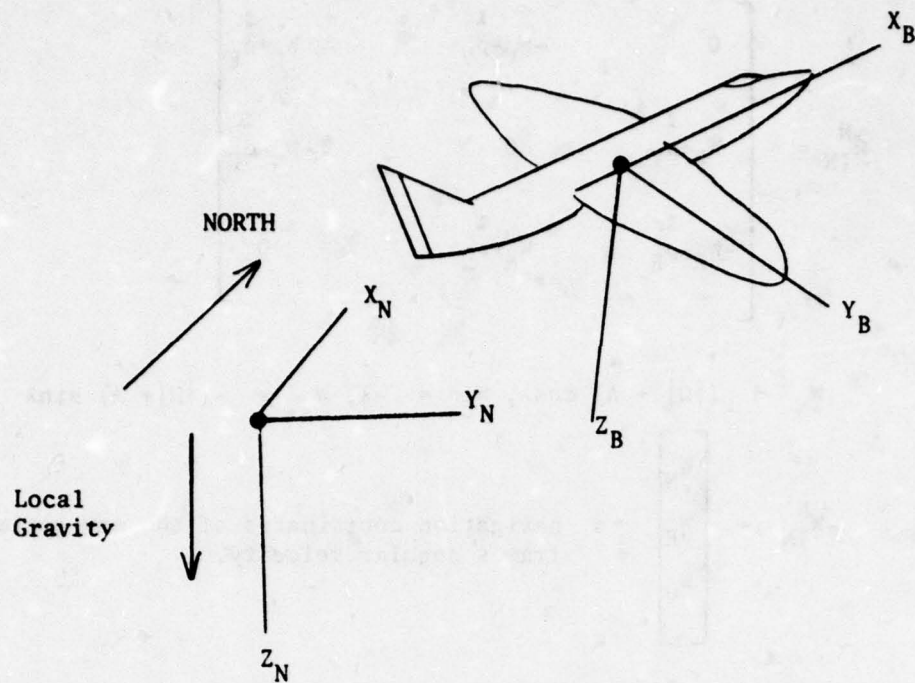


FIGURE A-1. Coordinate Systems

A-2. Direction Cosine Transformation Integration. The body to navigation coordinate transformation is obtained by solution of

$$\dot{C}_B^N = C_B^N \tilde{\Omega}_{IB} - \tilde{\Omega}_N C_B^N \quad (A-1)$$

where

$$\tilde{\Omega}_{IB} = \begin{bmatrix} 0 & -r & q \\ r & 0 & -p \\ -q & p & 0 \end{bmatrix}$$

$p, q, r$  = body axis components of aircraft angular velocity, which are measured by gyro triad.

$$\ddot{\alpha}_{IN}^N = \begin{bmatrix} 0 & -\dot{w}_V - \dot{\rho}_V & \dot{w}_E + \dot{\rho}_E \\ \vdots & \vdots & \vdots \\ w_V + \dot{\rho}_V & 0 & -\dot{w}_N - \dot{\rho}_N \\ \vdots & \vdots & \vdots \\ -\dot{w}_E - \dot{\rho}_E & w_N + \dot{\rho}_N & 0 \end{bmatrix}$$

$$w_N = (|\Omega| + \Lambda) \cos \lambda, w_E = -\lambda, w_V = -(|\Omega| + \Lambda) \sin \lambda$$

$$w_{IN}^N = \begin{bmatrix} w_N \\ w_E \\ w_V \end{bmatrix} = \text{navigation coordinates of the navigation frames angular velocity.}$$

$\lambda, \Lambda$  = latitude and longitude

$|\Omega|$  = earth rotation rate

$\dot{\rho}_N, \dot{\rho}_E, \dot{\rho}_V$  = integration filter attitude and heading corrections.

The relationship between the direction cosine transformation and roll ( $\phi$ ), pitch ( $\theta$ ), and heading ( $\psi$ ) is

$$C_B^N = \begin{bmatrix} c\theta c\psi & c\theta s\psi & -s\theta \\ -s\psi c\phi + s\theta c\psi s\phi & c\phi c\psi + s\phi s\theta s\psi & s\phi c\theta \\ s\psi s\phi + s\theta c\psi c\phi & -s\phi c\psi + c\phi s\theta s\psi & c\phi c\theta \end{bmatrix}^T$$

where  $s(\cdot) = \sin(\cdot)$  and  $c(\cdot) = \cos(\cdot)$

A-3. Position and Velocity Integration. The velocity differential equations are

$$\begin{bmatrix} \dot{v}_N \\ \dot{v}_E \\ \dot{v}_V \end{bmatrix} = C_B^N \begin{bmatrix} A_X \\ A_Y \\ A_Z \end{bmatrix} - C_{OR} \begin{bmatrix} v_N \\ v_E \\ v_V \end{bmatrix} + \begin{bmatrix} 0 \\ 0 \\ g \end{bmatrix} + \begin{bmatrix} \dot{\Delta v}_N \\ \dot{\Delta v}_E \\ \dot{\Delta v}_V \end{bmatrix} \quad (A-2)$$

where

$A_x, A_y, A_z$  = body axis components of the acceleration vector,  
measured by the strapped down accelerometer triad.

$V_N, V_E, V_V$  = north, east and vertical velocity components.

$$C_{OR} = \begin{bmatrix} 0 & 2|\Omega|\sin\lambda + \frac{V_E \tan\lambda}{R_E + h} & -\frac{V_N}{R_E + h} \\ -2|\Omega|\sin\lambda - \frac{V_E \tan\lambda}{R_E + h} & 0 & -2|\Omega|\cos\lambda - \frac{V_E}{R_E + h} \\ \frac{V_N}{R_E + h} & 2|\Omega|\cos\lambda + \frac{V_E}{R_E + h} & 0 \end{bmatrix}$$

$C_{OR}$  = matrix defining the Coriolis acceleration effect.

$R_E$  = earth radius

$g = g_0 \left[ 1 - \left( \frac{2h}{R_E} \right) \right]$  = gravity magnitude

$\dot{\Delta V}_N, \dot{\Delta V}_E, \dot{\Delta V}_V$  = integration filters' velocity error corrections.

The position differential equations are:

$$\begin{bmatrix} \dot{\lambda} \\ \dot{\lambda} \\ \dot{h} \end{bmatrix} = \begin{bmatrix} V_N R_E \\ V_E / R_E \cos\lambda \\ -V_V \end{bmatrix} + \begin{bmatrix} \dot{\Delta N} / R_E \\ \dot{\Delta E} / R_E \cos\lambda \\ \dot{\Delta h} \end{bmatrix} \quad (A-3)$$

where

$h$  = altitude

$\dot{\Delta N}, \dot{\Delta E}, \dot{\Delta h}$  = integration filter's position error corrections.

A.4

Predicted Time Differences. A precision earth model is used to compute geographical range between each transmitter and the receiver. These ranges are converted to propagation times using the Loran propagation velocity and a model of the secondary phase effects. Master and slave propagation times are differenced to obtain time difference prediction ( $TD_A$ ,  $TD_B$ ).

Propagation time estimates for each transmitter are computed by applying a Loran signal propagation model over the distance propagated. This model consists of primary and secondary phase effects. Total estimated propagation time ( $T_s$ ) between a transmitter (s) and the reference position is computed as:

$$T_s = \frac{\rho_s(\lambda, \Lambda)}{c_0} + T_{CS} \quad (A-4)$$

where

$\rho_s$  = arc length between the transmitter and aircraft position  $(\lambda, \Lambda)$

$c_0$  = the propagation velocity

$T_{CS}$  = secondary phase which accounts for the additional phase delay of the Loran groundwave signal over a signal traveling through a standard sea level atmosphere.

Equations for the arc length,  $\rho_s$ , are given in reference [15]. Time difference A and time difference B are computed as:

$$\hat{TD}_A = T_A - T_M + E_A \quad (A-5)$$

$$\hat{TD}_B = T_B - T_M + E_B$$

where

$E_A$ ,  $E_B$  = the known emission delays

A.5

Differential Baro/Inertial Mechanization. The vertical velocity and altitude corrections that are used in the baro/inertial vertical channel are:

$$\begin{aligned}\dot{\Delta V}_V &= K_{2D}(h_B - h) \\ \dot{\Delta h} &= K_{1D}(h_B - h)\end{aligned}\quad (A-6)$$

where

$K_{1D}$ ,  $K_{2D}$  = the baro/inertial feedback gains

$h_B$  = airborne baro altimeter measurement

A.6

Differential Loran/Inertial Integration Filter Mechanization. The integration filter transforms the difference between the measured time differences,  $TD_A$ ,  $TD_B$ , and the predicted time difference  $\hat{TD}_A$ ,  $\hat{TD}_B$  into corrections for the inertial position, velocity, heading, attitude and gyro biases. The transformation is written as

$$\begin{bmatrix} \dot{\Delta N} \\ \dot{\Delta E} \\ \dot{\Delta V}_N \\ \dot{\Delta V}_E \\ \vdots \\ \dot{\rho}_N \\ \vdots \\ \dot{\rho}_E \\ \vdots \\ \dot{\rho}_V \end{bmatrix} = K(t) \begin{bmatrix} A & B \\ C & D \end{bmatrix} \begin{bmatrix} TD_A - \hat{TD}_A \\ TD_B - \hat{TD}_B \end{bmatrix} \quad (A-7)$$

where

$K(t)$  = the integration filter's gain matrix.

The filter gain matrix can be computed in different ways depending on the performance requirements of the integration filter (see Sections 5.5 and 5.6).

DEPARTMENT OF DEFENSE

that also to 01-2 has 0-2 0-1 and members of 00000 and exercise set  
members also in battle are 0-2 and in 00-1 members has 0-0 and

other portion multiple operations used set

$$\begin{bmatrix} A_{11} & A_{12} \\ A_{21} & A_{22} \end{bmatrix} \quad \begin{bmatrix} 0 & A \\ 0 & 0 \end{bmatrix}$$

is given to a state, stage who awarded gains and win 0-0 0-1 0-0 0-1  
winning thereby not more because in 00000 has 0-0 0-1 0-0 0-1

in losses which may change in

**APPENDIX B**

level vision and it stores set

the figure notation but vision only one

**MATRIX DEFINITIONS**

$$\begin{bmatrix} 0 & 0 & 0 & 0 \\ 0 & 0 & 0 & 0 \\ 0 & 0 & 0 & 0 \\ 0 & 0 & 0 & 0 \end{bmatrix} = 0000$$

$$0000 = 00000000000000000000000000000000$$

## APPENDIX B. MATRIX DEFINITIONS

The matrices that appear in Equations 5-4, 5-5, 5-6, and 5-10 of main text Section 5.3 and Equation 5-23 of Section 5.6 are defined in this appendix.

The Loran geometric dilution factors are:

$$\begin{bmatrix} A & B \\ C & D \end{bmatrix} = C_0 \begin{bmatrix} \cos\psi_M - \cos\psi_A & \sin\psi_M - \sin\psi_A \\ \cos\psi_M - \cos\psi_B & \sin\psi_M - \sin\psi_B \end{bmatrix}^{-1}$$

where  $\psi_M$ ,  $\psi_A$ ,  $\psi_B$  are the angles between the master, slave A or slave B, respectively and north as measured from the aircraft position.

The errors in the locally level coordinate frame angular velocity caused by the system velocity and position errors are:

$$\Delta\omega_N = (-|\Omega|\sin\lambda \Delta N + \Delta V_E)/R_E$$

$$\Delta\omega_E = -\Delta V_N/R_E$$

$$\Delta\omega_V = [(-|\Omega|\cos\lambda - V_E/R_E \cos^2\lambda) \Delta N - \tan\lambda \Delta V_E]/R_E$$

The errors in computing the Coriolis acceleration are defined in terms of the following matrix:

$$\Delta\tilde{C}_{OR} = \begin{bmatrix} 0 & \tilde{\Delta C}_{12} & \tilde{\Delta C}_{13} \\ -\tilde{\Delta C}_{12} & 0 & \tilde{\Delta C}_{23} \\ -\tilde{\Delta C}_{13} & -\tilde{\Delta C}_{23} & 0 \end{bmatrix}$$

where

$$\tilde{\Delta C}_{12} = \{[2|\Omega|\cos\lambda + (V_E/R_E \cos^2\lambda)] \Delta N + \Delta V_E \tan\lambda\}/R_E$$

$$\tilde{\Delta C}_{13} = -\Delta V_N/R_E$$

$$\tilde{\Delta C}_{23} = \{2|\Omega|\sin\lambda \Delta N/R_N\} - V_E/R_E$$

The 18x18 matrix  $A_H$  is given in Table B-1. The terms in the matrix  $A_H$  not defined in Table B-1 are:

$$A_{1,14} = -A |V|/d_d$$

$$A_{1,15} = -B |V|/d_d$$

$$A_{2,14} = -C |V|/d_d$$

$$A_{2,15} = -D |V|/d_d$$

$$A_{3,1} = -[2|\Omega|\cos\lambda + (V_E/R_E \cos^2\lambda)]V_E/R_E$$

$$A_{3,3} = V_V/R_E$$

$$A_{3,4} = -2|\Omega|\sin\lambda - 2V_E \tan\lambda/R_E$$

$$A_{4,1} = \{[2|\Omega|\cos\lambda + (V_E/R_E \cos^2\lambda)]V_N - 2|\Omega|\sin\lambda V_V\}/R_E$$

$$A_{4,3} = 2|\Omega|\sin\lambda + V_E \tan\lambda/R_E$$

$$A_{4,4} = (\tan\lambda V_N + V_V)/R_E$$

$$A_{5,1} = |\Omega|\sin\lambda/R_E$$

$$A_{7,1} = [|\Omega|\cos\lambda + V_E/R_E \cos^2\lambda]/R_E$$

$$A_{7,4} = \tan\lambda/R_E$$

The nonzero terms of the 18x2 matrix  $A_B$  are:

$$A_{B3,2} = V_N/R_E$$

$$A_{B4,2} = 2|\Omega|\cos\lambda + V_E/R_E$$

The nonzero terms of the 2x18 matrix  $A_C$  are:

$$A_{C2,1} = 2|\Omega|\sin\lambda V_E/R_E$$

$$A_{C2,3} = -V_N/R_E$$

Table B-I. Matrix A<sub>H</sub> Definition

=

$$A_{C2,4} = -2|\Omega| \cos \lambda - V_E / R_E$$

$$A_{C2,5} = -A_E$$

$$A_{C2,6} = A_N$$

$$A_{C2,11} = C_{B3,1}^N$$

$$A_{C2,12} = C_{B3,2}^N$$

$$A_{C2,13} = C_{B3,3}^N$$

The  $2 \times 2$  matrix  $A_V$  that defines the dynamics of the differential baro/inertial system is defined as

$$A_V = \begin{bmatrix} K_{1D} & 1 \\ -K_{2D}^{-2} g_0 / R_E & 0 \end{bmatrix}$$

The  $18 \times 1$  vector of terms  $d_H$  that are input to the differential equation for the horizontal channel errors is defined as

$$-A\sigma_W \sqrt{\frac{2|V|}{d_d}} U_A - B\sigma_W \sqrt{\frac{2|V|}{d_d}} U_B$$

$$-C\sigma_W \sqrt{\frac{2|V|}{d_d}} U_A - D\sigma_W \sqrt{\frac{2|V|}{d_d}} U_B$$

$$g_{DN} + \Delta A_{DN}$$

$$g_{DE} + \Delta A_{DE}$$

$$G_{DN}$$

$$G_{DE}$$

$$G_{DV}$$

$$0$$

$$0$$

$$0$$

$$0$$

$$0$$

$$0$$

$$\sigma_W \sqrt{\frac{2|V|}{d_d}} U_A$$

$$\sigma_W \sqrt{\frac{2|V|}{d_d}} U_B$$

$$\sigma_{GBnx} \sqrt{\frac{2}{\tau_g}} U_x$$

$$\sigma_{GBny} \sqrt{\frac{2}{\tau_g}} U_y$$

$$\sigma_{GBnz} \sqrt{\frac{2}{\tau_g}} U_z$$

where

$$\begin{bmatrix} \Delta A_{DN} \\ \Delta A_{DE} \\ \Delta A_{DV} \end{bmatrix} = C_B^N \begin{bmatrix} \Delta A_{Dx} \\ \Delta A_{Dy} \\ \Delta A_{Dz} \end{bmatrix}$$

$$\begin{bmatrix} G_{DN} \\ G_{DE} \\ G_{DV} \end{bmatrix} = C_B^N \begin{bmatrix} G_{Dx} \\ G_{Dy} \\ G_{Dz} \end{bmatrix}$$

$\Delta A_{Dx}, \Delta A_{Dy}, \Delta A_{Dz}$  = Accelerometer measurement errors that are dependent on aircraft dynamics

$G_{Dx}, G_{Dy}, G_{Dz}$  = gyro measurement errors that are dependent on aircraft dynamics

$U_A, U_B$  = white noise with unit power spectral densities for exponentially correlated Loran warpage models

$U_x, U_y, U_z$  = white noise with unit power spectral densities for exponentially correlated gyro noise models

The accelerometer and gyro measurement errors ( $A_{Dx}, A_{Dy}, A_{Dz}, G_{Dx}, G_{Dy}, G_{Dz}$ ) account for the presence of the inertial sensor error sources shown below.

<u>ERROR SOURCE</u>	<u>SYMBOL</u>	<u>UNITS</u>
X, Y, Z Gyro Scale Factor Errors	GS	%
X, Y, Z Gyro Mass Unbalance Drift	GM	°/hr/G <sub>2</sub>
X, Y, Z Gyro Anisoelastic Drift	GA	°/hr/G
X, Y, Z Accelerometer Noise (1σ)	AN	μg
X, Y, Z Accelerometer Noise Time Constant	TA	sec
X, Y, Z Accelerometer Scale Factor Error	AS	%

The gyro measurement errors that are maneuver sensitivity are modeled as

$$\begin{bmatrix} G_{Dx} \\ G_{Dy} \\ G_{Dz} \end{bmatrix} = -[GS] \begin{bmatrix} p \\ q \\ r \end{bmatrix} + [GM] \begin{bmatrix} Ax \\ Ay \\ (Az-g) \end{bmatrix} - [GA] \begin{bmatrix} Ax^2 \\ Ay^2 \\ (Az^2-g)^2 \end{bmatrix}$$

where

$[GS]$  = 3 x 3 diagonal matrix of gyro scale factor errors

$[GM]$  = 3 x 3 diagonal matrix of gyro mass unbalances

$[GA]$  = 3 x 3 diagonal matrix of gyro anisoelastic errors

$[p \ q \ r]^T$  = body axis angular rates

$[Ax \ Ay \ Az]^T$  = body axis components of the acceleration vector

measured by the strapped down accelerometer triad.

For accelerometer measurement errors that include both accelerometer noise and maneuver sensitivity terms are modeled as

$$\begin{bmatrix} \Delta A_{Dx} \\ \Delta A_{Dy} \\ \Delta A_{Dz} \end{bmatrix} = \begin{bmatrix} A_{Nx} \\ A_{Ny} \\ A_{Nz} \end{bmatrix} - [AS] \begin{bmatrix} A_x \\ A_y \\ A_z \end{bmatrix}$$

where

$[AS]$  = 3 x 3 diagonal matrix of accelerometer scale factor errors

$[A_{Nx}, A_{Ny}, A_{Nz}]^T$  = 3 x 1 vector of accelerometer noises with standard deviation = AN and time constant = TA.

The 2x1 vector that is input to the differential equations for the vertical channel errors is

$$\underline{d}_V = \begin{bmatrix} -\dot{D} - K_{1D} U_{BA} \\ -K_{2D} U_{BA} + \Delta A_{DV} \end{bmatrix}$$

where  $U_{BA}$  is a white noise representation of the barometric altimeter noise. The 2x18 matrix  $H_1$  that takes into account Equation A-7 (of Appendix A) in relating the error vector  $\underline{x}_H$  to the integration filter 18x2 gain matrix  $K(t)$  is

$$H_1 = \begin{bmatrix} \overset{+2+}{1} & 0 & | & \overset{+16+}{0} \\ 0 & 1 & | & 0 \end{bmatrix}$$

The 2x3 matrix,  $H_2$ , that transforms the three receiver tracking errors into north and east position errors is

$$H_2 = \begin{bmatrix} A & B & -(A+B) \\ C & D & -(C+D) \end{bmatrix}$$

The 18x18 state transition matrix  $\Phi_H(t_{j+1}, t_j)$  is given in Table B-2. The terms in the matrix  $\Phi_H$  not defined in Table B-2 are:

$$\Phi_{1,14} = -\Delta t A |V|/d_d$$

$$\Phi_{1,15} = -\Delta t B |V|/d_d$$

$$\Phi_{2,14} = -\Delta t C |V|/d_d$$

$$\Phi_{2,15} = -\Delta t D |V|/d_d$$

$$\Phi_{3,1} = -\Delta t [2|\Omega|\cos\lambda + (V_E/R_E \cos^2\lambda)] V_E/R_E$$

$$\Phi_{3,3} = \Delta t V_V/R_E + 1$$

$$\Phi_{3,4} = -\Delta t [2|\Omega|\sin\lambda - 2V_E \tan\lambda/R_E]$$

$$\Phi_{4,1} = \Delta t \{ [2|\Omega|\cos\lambda + (V_E/R_E \cos^2\lambda)] V_N - 2|\Omega|\sin\lambda V_V \}/R_E$$

$$\Phi_{4,3} = \Delta t [2|\Omega|\sin\lambda + V_E \tan\lambda/R_E]$$

$$\Phi_{4,4} = \Delta t (\tan\lambda V_N + V_V)/R_E + 1$$

$$\Phi_{5,1} = \Delta t |\Omega|\sin\lambda/R_E$$

$$\Phi_{7,1} = \Delta t [|\Omega|\cos\lambda + V_E/R_E \cos^2\lambda]/R_E$$

$$\Phi_{7,4} = \Delta t \tan\lambda/R_E$$

The nonzero terms of the 2x18 matrix  $\Phi_C(t_{j+1}, t_j)$  are

$$\Phi_{C2,1} = 2\Delta t |\Omega|\sin\lambda V_E/R_E$$

$$\Phi_{C2,3} = -\Delta t V_N/R_E$$

$$\Phi_{C2,4} = -\Delta t [2|\Omega|\cos\lambda + V_E/R_E]$$

$$\Phi_{C2,5} = -fA_E$$

Table B-II. Matrix  $\Phi_H(t_{j+1}, t_j)$  Definition\*

1	0	$\Delta t$	0	0	0	0	0	0	0	0	0	0	0	0	0	0	0	0	0	0
0	1	0	$\Delta t$	0	0	0	0	0	0	0	0	0	0	0	0	0	$\Phi_{2,14}$	$\Phi_{2,15}$	0	0
$\Phi_{3,1}$	0	$\Phi_{3,3}$	$\Phi_{3,4}$	0	- $\Delta t \gamma_V$	$\Delta t E$	0	0	0	$\int C_{B_{1,1}}^N$	$\int C_{B_{1,2}}^N$	$\int C_{B_{1,3}}^N$	0	0	0	0	0	0	0	0
$\Phi_{4,1}$	0	$\Phi_{4,3}$	$\Phi_{4,4}$	$\Phi_{4,V}$	0	- $\Delta t \gamma_E$	0	0	0	$\int C_{B_{2,1}}^N$	$\int C_{B_{2,2}}^N$	$\int C_{B_{2,3}}^N$	0	0	0	0	0	0	0	0
$\Phi_{5,1}$	0	0	- $\Delta t/R_E$	1	$\Delta t \gamma_V$	- $\Delta t \gamma_E$	$\int C_{B_{1,1}}^N$	$\int C_{B_{1,2}}^N$	$\int C_{B_{1,3}}^N$	0	0	0	0	0	0	0	$\int C_{B_{1,1}}^N$	$\int C_{B_{1,2}}^N$	$\int C_{B_{1,3}}^N$	
0	0	$\Delta t/R_E$	0	- $\Delta t \gamma_V$	1	$\Delta t \gamma_N$	$\int C_{B_{2,1}}^N$	$\int C_{B_{2,2}}^N$	$\int C_{B_{2,3}}^N$	0	0	0	0	0	0	0	$\int C_{B_{2,1}}^N$	$\int C_{B_{2,2}}^N$	$\int C_{B_{2,3}}^N$	
$\Phi_{7,2}$	0	0	$\Phi_{7,4}$	$\Delta t \gamma_E$	- $\Delta t \gamma_N$	1	$\int C_{B_{3,1}}^N$	$\int C_{B_{3,2}}^N$	$\int C_{B_{3,3}}^N$	0	0	0	0	0	0	0	$\int C_{B_{3,1}}^N$	$\int C_{B_{3,2}}^N$	$\int C_{B_{3,3}}^N$	
0	0	0	0	0	0	0	1	0	0	0	0	0	0	0	0	0	0	0	0	0
0	0	0	0	0	0	0	0	0	1	0	0	0	0	0	0	0	0	0	0	0
0	0	0	0	0	0	0	0	0	0	1	0	0	0	0	0	0	0	0	0	0
0	0	0	0	0	0	0	0	0	0	0	1	0	0	0	0	0	0	0	0	0
0	0	0	0	0	0	0	0	0	0	0	0	1	0	0	0	0	0	0	0	0
0	0	0	0	0	0	0	0	0	0	0	0	0	1	0	0	0	0	0	0	0
0	0	0	0	0	0	0	0	0	0	0	0	0	0	1	0	0	0	0	0	0
0	0	0	0	0	0	0	0	0	0	0	0	0	0	0	1	0	0	0	0	0
0	0	0	0	0	0	0	0	0	0	0	0	0	0	0	0	1	0	0	0	0
0	0	0	0	0	0	0	0	0	0	0	0	0	0	0	0	0	1	0	0	0
0	0	0	0	0	0	0	0	0	0	0	0	0	0	0	0	0	0	1	0	0
0	0	0	0	0	0	0	0	0	0	0	0	0	0	0	0	0	0	0	1	0

$\Phi_H =$

\* All integrations are over the interval  $[t_{j+1}, t_j]$ .

$$\Phi_{C2,6} = fA_N$$

$$\Phi_{C2,11} = fC_{B3,1}^N$$

$$\Phi_{C2,12} = fC_{B3,2}^N$$

$$\Phi_{C2,13} = fC_{B3,3}^N$$

The  $2 \times 2$  matrix  $\Phi_V$ , the state transition matrix for the vertical channel, is defined as

$$\Phi_V = \begin{bmatrix} 1 + \Delta t K_{1D} & \Delta t \\ \Delta t (-K_{2D} - 2g_0/R_E) & 1 \end{bmatrix}$$

The  $18 \times 1$  vector of terms that are input to the difference equations for the simulation of the horizontal channel errors is defined as:

	$-A\sigma_W \sqrt{\frac{2 V }{d_d \Delta t}} U_{Aj}^* - B\sigma_W \sqrt{\frac{2 V }{d_d \Delta t}} U_{Bj}^*$
	$-C\sigma_W \sqrt{\frac{2 V }{d_d \Delta t}} U_{Aj}^* - D\sigma_W \sqrt{\frac{2 V }{d_d \Delta t}} U_{Bj}^*$
	-----
	$\Delta A_{DNj}$
	$\Delta A_{DEj}$
	-----
	$G_{DNj}$
	$G_{DEj}$
	$G_{DVj}$
	-----
	0
	0
	0
	-----
$d_{Hj}^*$	0
	0
	0
	-----
	$\sigma_W \sqrt{\frac{2 V }{d_d \Delta t}} U_{Aj}^*$
	$\sigma_W \sqrt{\frac{2 V }{d_d \Delta t}} U_{Bj}^*$
	-----
	$\sigma_{GBnx} \sqrt{\frac{2}{\tau_g \Delta t}} U_{xj}^*$
	$\sigma_{GBny} \sqrt{\frac{2}{\tau_g \Delta t}} U_{yj}^*$
	$\sigma_{GBnz} \sqrt{\frac{2}{\tau_g \Delta t}} U_{zj}^*$

where

$U_{Aj}^*, U_{Bj}^*$  = sequences of zero mean, unit variance, uncorrelated random variables for exponentially correlated Loran warpage models.

$U_x^*, U_y^*, U_z^*$  = sequences of zero mean, unit variance, uncorrelated random variables for exponentially correlated gyro noise models.

$\Delta A_{DNj}, \Delta A_{DEj}$  =  $j^{th}$  sample of the accelerometer errors  $\Delta A_{DN}$  and  $\Delta A_{DE}$

$G_{DNj}, G_{DEj}, G_{DVj}$  =  $j^{th}$  sample of the gyro errors  $G_{DN}$ ,  $G_{DE}$  and  $G_{DV}$ .

The  $2 \times 1$  vector that is input to the difference equations for the vertical channel simulation is

$$\underline{d}_{Vj}^* = \begin{bmatrix} - \left( \frac{dD}{dh} \right) V_V - K_{1D} U_{BAj}^* \\ -K_{2D} U_{BAj}^* + \Delta A_{DD} \end{bmatrix}$$

where  $U_{BAj}^*$  is a sequence of zero mean, uncorrelated random variables with standard deviation equal to  $\sigma_{BA} \sqrt{\tau_g / \Delta t}$ .

During flight tests, errors resulting from motion and its derivatives caused small inertial/inertial latencies and phase errors off the route planned thus, signs need even, strong velocity bias correction can occur at low or high altitude and not enough time interval off route signs off the course of having added at altitude and most beginning and some velocity and direction latencies

$$(e^2)_{\text{Gn}} \approx \pi - 1/(e_{\text{Gn}} \sin \theta) = (e_{\text{Gn}} \sin \theta)^{-1} \approx 1 - e^{-2} \approx 0.86$$

$$(e^2)_{\text{Gn}} \approx 1 - (e_{\text{Gn}} \sin \theta)^2 \approx 1 - (e_{\text{Gn}} \sin \theta)^2$$

## APPENDIX C

### DIFFERENTIAL LORAN/INERTIAL ERROR EXPRESSIONS

$$(e^2)_{\text{Gn}} \approx 1 - (e_{\text{Gn}} \sin \theta)^2 + (e_{\text{Gn}} \cos \theta)^2 + (e_{\text{Gn}} \sin \theta)(e_{\text{Gn}} \cos \theta)$$

$$(e^2)_{\text{Gn}} \approx 1 - (e_{\text{Gn}} \sin \theta)^2 + (e_{\text{Gn}} \cos \theta)^2 + (e_{\text{Gn}} \sin \theta)(e_{\text{Gn}} \cos \theta)$$

## APPENDIX C. DIFFERENTIAL LORAN/INERTIAL ERROR EXPRESSIONS

The Laplace transforms of the position error, velocity error, east misalignment angle, and heading error for the north channel in a differential Loran/inertial system, where Loran is used to damp out position and velocity errors, have been derived in Section 5.5 of the main text. The following expressions for the differential position and velocity error are derived from the equations in Table 5-II:

$$\begin{aligned}\Delta N_D(s) &= \{-(2s\zeta\omega_n + \omega_n^2)[A n_A(s) + B n_B(s) - (A+B)n_M(s)] + s \Delta N_D(t_0) \\ &\quad - s^2[-A W_A(s) - B W_B(s)] + g_{DN}(s) + \Delta A_{BN}(s) \\ &\quad + \Delta V_N(t_0) - [A_E \rho_V](s)\}/D_2(s) \\ &\quad - g\{G B_E(s) + G_{nE}(s) + (\Omega_N + \frac{V_E}{R_E}) \rho_V(s) + \rho_E(t_0)\}/D_3(s) \quad (C-1)\end{aligned}$$

$$\begin{aligned}\Delta V_N(s) &= \{-s\omega_n^2[A n_A(s) + B n_B(s) - (A+B)n_M(s)] - \omega_n^2 \Delta N_D(t_0) \\ &\quad - s\omega_n^2[-A W_A(s) - B W_B(s)] \\ &\quad + (s+2\zeta\omega_n)[-[A_E \rho_V](s) + \Delta A_{BN}(s) + g_{DN}(s) + \Delta V_N(t_0)]\}/D_2(s) \\ &\quad - g(s+2\zeta\omega_n)\{G B_E(s) + G_{nE}(s) + \left(\Omega_N + \frac{V_E}{R_E}\right) \rho_V(s) + \rho_E(t_0)\}/D_3(s) \quad (C-2)\end{aligned}$$

where

$$D_2(s) = s^2 + 2\zeta\omega_n s + \omega_n^2$$

This equation for heading misalignment is derived from Eqn. 5-15.

$$\rho_V(s) = G B_V(s)/s \quad (C-3)$$

For all error sources except east gyro bias  $GB_E$  and east gyro noise  $GB_{nE}$ , the error expressions were simplified by assuming that  $g/R$  is negligible. Also, in the above equations the gains  $K_1$  and  $K_2$  have been replaced by the natural frequency  $\omega_n$  and damping factor  $\zeta$  determined from the 2nd order characteristic equation, i.e.,  $K_2 = \omega_n^2$  and  $K_1 = 2\zeta\omega_n$ .

As indicated in Section 5.2, this study considers the error sources in Eqns. (C-1), (C-2), and (C-3) as either noise processes or biases. Consequently, these math models can be used with the above equations to derive the standard deviations of the position, velocity and heading errors.

To compute the effect of aircraft acceleration ( $A_E$ ) on the system performance a conservative assumption is made that the time duration ( $t_T^+ - t_T^-$ ) of the east acceleration is short relative to the system time constant; consequently, it is assumed the aircraft maneuver introduces a step change in the north velocity error equal to  $\rho_V(t_T)[V_E(t_T^+) - V_E(t_T^-)]$ . This velocity error and the peak position error that occurs after the aircraft maneuver represent the effect of the aircraft maneuver on system performance.

To save repeating the derivations for each error source, the derivation for the effects of accelerometer noise, accelerometer bias, and an aircraft maneuver are given, and the results for the other error sources listed.

#### Gravity Deflections (Equivalent to Accelerometer Noise)

The transfer functions between the gravity deflection and position and velocity errors are

$$\begin{aligned}\Delta N_D(s) &= \frac{g_{DN}(s)}{D_2(s)} \\ \Delta V_N(s) &= \frac{(s+2\zeta\omega_n)g_{DN}(s)}{D_2(s)}\end{aligned}$$

Gravity deflections are modeled as an exponentially correlated process whose power spectral density satisfies

$$S_{gDN}(\omega) = 2|v_N|\sigma_{gD}^2/d_g (\omega^2 + v_N^2/d_g^2)$$

where  $\sigma_{gD}^2$  is the gravity deflection variance and  $d_g$  its correlation distance. The variances of the position error and velocity error caused by the gravity deflections are

$$\sigma_{ND}^2 = \frac{1}{2\pi} \int_{-\infty}^{\infty} \frac{[2\alpha|v_N|\sigma_{gD}^2/d_g] d\omega}{D_2(j\omega)D_2(-j\omega)(-j\omega+|v_N|/d_g)(j\omega+|v_N|/d_g)}$$

$$\sigma_{ND}^2 = \frac{\sigma_{gD}^2 \tau_{gD} (1+2\tau_{gD}\zeta\omega_n)}{2\zeta\omega_n^3 (1+2\zeta\omega_n\tau_{gD} + \tau_{gD}^2\omega_n^2)}$$

$$\begin{aligned} \sigma_v^2 &= \frac{2\alpha|v_N|\sigma_{gD}^2}{2\pi} \int_{-\infty}^{\infty} \frac{(j\omega+2\zeta\omega_n)(-j\omega+2\zeta\omega_n) d\omega}{D_2(j\omega)D_2(-j\omega)(-j\omega+|v_N|/d_g)(j\omega+|v_N|/d_g)} \\ &= \frac{[2\zeta(1+2\zeta\omega_n\tau_{gD}) + \omega_n] \sigma_{gD}^2 \tau_{gD}}{2\zeta\omega_n^2 (1+2\zeta\omega_n\tau_{gD} + \tau_{gD}^2\omega_n^2)} \end{aligned}$$

where

$$\tau_{gD} = d_g / |v_N|$$

For accelerometer noise  $\sigma_{gD}^2$  is the variance and  $\tau_{gD}$  the correlation time.

Accelerometer Bias. The transfer function between accelerometer bias and the position error and velocity error is

$$\Delta N_D(s) = \frac{\Delta A_{BN}}{sD_2(s)}$$

$$\Delta V_N(s) = \frac{(s+2\zeta\omega_n)\Delta A_{BN}}{sD_2(s)}$$

The accelerometer bias  $\Delta A_{BN}$  has a standard deviation,  $\sigma_{AB}$ . The standard deviations of the steady state position and velocity errors caused by the accelerometer bias are

$$\sigma_{N_D} = \left[ \lim_{s \rightarrow 0} \left| \frac{s}{sD_2(s)} \right| \right] \sigma_{AB}$$

$$\sigma_{N_D} = \sigma_{AB}/\omega_n^2$$

$$\sigma_V = 2\zeta\sigma_{AB}/\omega_n$$

East Gyro Bias. For an east gyro bias with standard deviation  $\sigma_{GBE}$ , the position and velocity standard deviations are

$$\sigma_{ND} = R_E \sigma_{GBE} / 2\zeta\omega_n$$

$$\sigma_V = R_E \sigma_{GBE}$$

East Gyro Noise. For exponentially correlated east gyro noise, the position and velocity variances are

$$\sigma_{ND}^2 = \frac{g\tau g^2 R_E (2+\omega_n^2 \tau^2) \sigma_{GBnE}^2}{2\zeta\omega_n^3 \left[ 1 + 2\zeta\omega_n \tau g + \omega_n^2 \tau^2 + 2\zeta\omega_n g \tau g^3 R_E^{-1} \right]}$$

$$\sigma_V^2 = \frac{g\tau g^2 R_E \sigma_{GBnE}^2}{2\zeta\omega_n^3} \left[ \frac{4\zeta^2 \omega_n^2 (2\zeta\omega_n \tau + \omega_n^2 \tau^2 + 1) + (1 + 2\zeta\omega_n \tau g) g R_E^{-1}}{1 + 2\zeta\omega_n \tau g + \omega_n^2 \tau^2 + 2\zeta\omega_n g \tau g^3 R_E^{-1}} \right]$$

Loran Noise. The noises on the three Loran signals are uncorrelated and since the bandwidth of the integration filter is lower than the receiver's tracking loop bandwidth, the Loran noises are modeled as white noises with constant power spectral density  $S_L$ . The equation for the power spectral density is

$$S_L = 10^{-1.1S/N} \text{GRP}/2 N_p \omega_0^2$$

where

$S/N$  = Loran signal to noise ratio with the signal strength defined in terms of the pulse amplitude at the cycle being tracked by the receiver.

GRP = Group Repetition Period (nominally 0.1 seconds for Loran C and 0.05 second for Loran D)

$N_p$  = Number of pulses in each Loran pulse group ( $N_p = 8$  for Loran C and  $N_p = 16$  for Loran D)

$\omega_0$  = Loran carrier frequency  
=  $2\pi 10^5$  rad/sec

For this analysis the assumption is made that the three Loran S/Ns are equal. With this noise model, the position and velocity error variances are

$$\sigma_{ND}^2 = (A^2 + B^2 + AB) \omega_n (4\zeta^2 + 1) S_L / 2\zeta$$

$$\sigma_V^2 = (A^2 + B^2 + AB) \omega_n^3 S_L / 2\zeta$$

Loran Warpage. The Loran warpages,  $\Delta W_A$  and  $\Delta W_A'$ , are modeled as uncorrelated, exponential random processes with variance  $\sigma_W^2$  and correlation distance  $d_d$  (see Eqn. 5-11). The differential position error and velocity error variances resulting from the Loran warpages are

$$\sigma_{ND}^2 = \frac{(A^2 + B^2) \sigma_W^2}{2\tau_W \zeta \omega_n} \left[ \frac{(2\zeta \omega_n \tau_W + \omega_n^2 \tau_W^2)}{(1 + 2\zeta \omega_n \tau_W + \omega_n^2 \tau_W^2)} \right]$$

$$\sigma_V^2 = \frac{(A^2 + B^2) \tau_W \omega_n^3 \sigma_W^2}{2\zeta} \left[ \frac{1}{1 + 2\zeta \omega_n \tau_W + \omega_n^2 \tau_W^2} \right]$$

where

$$\tau_W = d_d / |V|$$

#### Aircraft Acceleration Effects

The heading misalignment is a major source of position and velocity error during aircraft maneuvers, since it couples part of the east aircraft acceleration into the north velocity channel (see Eqn. C-2). As discussed earlier in this section, a worst case assumption will be made that the duration of a nonzero east acceleration is short relative to the integration filter's time constant. Consequently, the effect of an aircraft east acceleration, or change in east velocity, is to cause a step increase in the north velocity error equal to  $\rho_V(t_T) [V_E(t_T^+) - V_E(t_T^-)]$ . The effect of this maneuver on position error is cause for the position error to increase for a short period of time, then to decrease back to zero. The effect on position error is represented by the position error peak. By using Eqn. C-1 the peak in the position error uncertainty is

$$\sigma_{ND} \Big|_{peak} = .35 \sigma_{\rho V} |V_E(t_T^+) - V_E(t_T^-)| / \omega_n$$

The heading misalignment increased during the flight according to Eqn. C-1. The increase in heading uncertainty caused by the z gyro bias is

$$\sigma_{\rho V} = t \sigma_{GBV}$$

## APPENDIX D

## DIFFERENTIAL BARO/INERTIAL ERROR EXPRESSIONS

## APPENDIX D. DIFFERENTIAL BARO/INERTIAL ERROR EXPRESSIONS

The sensitivities of the differential baro/inertial altitude and vertical velocity errors to the major error sources in the vertical channel are derived in this appendix.

The differential equations for the vertical channel errors are given in Equations 5-18 and 5-19 in Section 5 of the main text. Taking Laplace transforms of these equations and using Cramer's Rule to solve for the differential altitude and vertical velocity errors gives the following results:

$$\begin{aligned}\Delta h_D(s) = & \{s[-K_{1D} U_{BA}(s) - \dot{D}(s)] - K_{2D} U_{BA}(s) + \Delta A_{BZ}(s) \\ & + \Delta V_v(t_o) - [A_E \rho_N](s) + [A_N \rho_E](s)\} / G_2(s)\end{aligned}\quad (D-1)$$

$$\begin{aligned}\Delta V_v(s) = & \{(2K_{1D}g_o R_E^{-1} - sK_{2D}) U_{BA}(s) + K_{2D} \dot{D}(s) \\ & + (s+K_{1D}) [\Delta V_v(t_o) - [A_E \rho_N](s) + [A_N \rho_E](s) + \Delta A_{BZ}(s)]\} / G_2(s)\end{aligned}\quad (D-2)$$

where

$$G_2(s) = s^2 + s K_{1D} + (K_{2D} + 2g_o R_E^{-1})$$

From these equations, the uncertainties in the differential altitude and vertical velocity caused by the baro altimeter noise, accelerometer bias, D value gradient, ( $dD/dh$ ), and north and east misalignments have been derived. The results for the baro altimeter noise and accelerometer bias are listed below, followed by derivations for the effects of the D value gradient and the misalignments.

### BARO ALTIMETER NOISE

The baro altimeter noise is modeled as white noise, with power spectral density  $S_B = \tau_B \sigma_{BA}^2$ , where  $\tau_B$  is the noise correlation time and  $\sigma_{BA}$  its standard deviation. The variances of the altitude and vertical velocity errors caused by the noise are

$$\sigma_{hD}^2 = \omega_{nD} (4\zeta_D^2 + 1) \tau_B \sigma_{BA}^2 / 2\zeta_D$$

$$\sigma_{vv}^2 = \omega_{nD}^3 \tau_B \sigma_{BA}^2 / 4\zeta_D$$

where

$$K_{1D} = 2\zeta_D \omega_{nD}$$

$$K_{2D} = 2g_0 R_E^{-1} = \omega_{nD}^2$$

#### ACCELEROMETER BIAS

The Z accelerometer bias standard deviation is denoted  $\sigma_{BAZ}$  and the steady state altitude and vertical velocity uncertainties caused by the bias are

$$\sigma_{hD} = \sigma_{BAZ} / \omega_{nD}$$

$$\sigma_{vv} = 2\zeta_D \sigma_{BAZ} / \omega_{nD}$$

#### D VALUE GRADIENT

The D value, which is the difference between pressure altitude and altitude above sea level, changes as a function of altitude. D value versus altitude curves are given in Figure 5-3. As an error source in the differential baro/inertial vertical channel, D value causes differential altitude and velocity errors during an aircraft vertical maneuver. For constant altitude,  $\dot{D} = 0$ . To develop expressions for the altitude and velocity errors during a maneuver, consider an aircraft descent with a constant vertical velocity  $V_v$ . For a D value gradient  $dD/dh$ , the D value time rate of change is

$$\dot{D} = \left( \frac{dD}{dh} \right) V_v$$

Laplace transforms for the altitude and velocity errors caused by  $\dot{D}$  are

$$\Delta h_D(s) = - \left( \frac{dD}{dh} \right) v_v / G_2(s)$$

$$\Delta v_v(s) = - K_{2D} \left( \frac{dD}{dh} \right) v_v / s G_2(s)$$

Taking the inverse Laplace transforms of the above equations gives

$$\Delta h_D(t) = - \left( \frac{dD}{dh} \right) v_v e^{at} \sin bt/b \quad (D-3)$$

$$\Delta v_v(t) = \left( \frac{dD}{dh} \right) v_v \{ [1 - e^{at}] [\cos bt - a \sin bt/b] \} \quad (D-4)$$

where  $a = -\zeta_D \omega_{nD}$

$$b = \omega_{nD} \sqrt{1 - \zeta_D^2}$$

Eqn. D-3 shows that the steady state differential altitude error is zero and the peak differential altitude error is

$$|\Delta h_D|_{\text{peak}} = 0.35 \left( \frac{dD}{dh} \right) v_v / \omega_{nD} \quad \text{for } \zeta_D = 1$$

The steady state vertical velocity error is  $|\Delta v_v|_{ss} = \left( \frac{dD}{dh} \right) v_v$

NORTH AND EAST MISALIGNMENTS. The north and east misalignments,  $\rho_N$  and  $\rho_E$ , contribute to the vertical channel errors only during horizontal aircraft maneuvers. To develop analytical expressions for these effects, a worst case assumption is made that the duration of the nonzero north and east accelerations are short relative to the baro/inertial filter's time constant. With this assumption the effect of the misalignments during an aircraft maneuver on performance can be approximated as an increase in the vertical velocity error during the maneuver, followed by a decay of the velocity error to zero, and a temporary buildup of the altitude error before it decays to zero. The peak uncertainty in the vertical velocity caused by the maneuver is

$$\sigma_{vv}^2 \Big|_{\text{peak}} = |v_E(t_T^+) - v_E(t_T^-)|^2 \sigma_{\rho N}^2$$

$$+ |v_N(t_T^+) - v_N(t_T^-)|^2 \sigma_{\rho E}^2$$

where  $\sigma_{\rho N}^2$  and  $\sigma_{\rho E}^2$  are the variancies of the north and east misalignments, respectively, and  $t_T^+$ ,  $t_T^-$  define the beginning and ending times of the maneuver. The peak uncertainty in altitude following the maneuver is

$$\sigma_{hD} \Big|_{\text{peak}} = .35 \sigma_{vv} / \omega_{nD} \quad \text{for } \zeta_D = 1$$

**DIFFERENTIAL LORAN/DOPPLER/AHRS POSITIONING** - A. KINGSTON

At the present time, differential positioning is being developed by the Defense and Aerospace industries using DOR (Differential Orbiting Reference) techniques and acoustic propagation velocity measurements. The former technique is based upon a single reference satellite which transmits time signals to two or more receiving stations. The latter technique uses a reference station which transmits time signals to two or more receiving stations.

The primary advantage of the acoustic propagation velocity technique is that it does not require a reference satellite.

It is the purpose of this paper to describe the basic principles of the acoustic propagation velocity technique and to show how it can be used to develop a system for determining position and velocity of a vehicle.

**APPENDIX E**

**DIFFERENTIAL LORAN/DOPPLER/AHRS**

**ERROR EXPRESSIONS**

## APPENDIX E. DIFFERENTIAL LORAN/DOPPLER/AHRS ERROR EXPRESSIONS

The position and velocity errors of an integrated differential Loran/Doppler/AHRS system are parameterized in terms of Doppler, AHRS and Loran measurements. A second order integration technique, which has position and velocity damping, is assumed in the system, and steady state errors during aircraft cruise and peak errors during aircraft turns are derived.

The differential equations describing the position and velocity errors of the system are given by Equations 5-20, 5-21 and 5-22. Taking Laplace transforms of these equations and solving for the differential Loran position error and north velocity error gives:

$$\begin{aligned}\Delta N_D(s) = & \{-(2s\zeta\omega_n^2 + \omega_n^2)[A n_A(s) + B n_B(s) - (A+B)n_M(s)] + s \Delta N_D(t_0) \\ & - s^2[+A W_A(s) + B W_B(s)] \\ & + \Delta V_N(t_0) + s\varepsilon V_N(s)\}/D_2(s)\end{aligned}\quad (E-1)$$

$$\begin{aligned}\Delta V_N(s) = & \{-s\omega_n^2[A n_A(s) + B n_B(s) - (A+B)n_M(s)] - \omega_n^2 \Delta N_D(t_0) \\ & + s\omega_n^2[+A W_A(s) + B W_B(s)] \\ & + (s+2\zeta\omega_n)[s\varepsilon V_N(s) + \Delta V_N(t_0)]\}/D_2(s)\end{aligned}\quad (E-2)$$

where

$$D_2(s) = s^2 + 2\zeta\omega_n s + \omega_n^2$$

The Doppler and AHRS errors are present in the velocity error  $\varepsilon E_N(s)$ . Assuming a small pitch angle  $\theta$  and a small vertical velocity  $V_V$ , the error  $\varepsilon V_N(s)$  becomes

$$\begin{aligned}\varepsilon V_N = & \cos\psi \delta V_H + \sin\psi[-\cos\phi \delta V_D + \sin\phi \delta V_Z] \\ & - V_E \delta\psi + V_V[\cos\psi \delta\theta + \sin\psi \delta\phi]\end{aligned}\quad (E-3)$$

Comparison of Equations E-1 and E-2 and Equations C-1 and C-2 shows that the Loran noise and the Loran Warpage affect both the differential Loran/Doppler/ ARHS system and differential Loran/inertial system position and velocity errors the same. Consequently the analytical results in Appendix C for the effects of the Loran error sources apply to this analysis. In the remainder of this appendix, the effects of the Doppler and AHRS errors are listed.

#### Doppler Bias

For cruise conditions, the position and velocity errors caused by Doppler biases, along the three body axes, are

$$\Delta N_D(s) = s [\cos\psi \epsilon V_{HB}(s) - \sin\psi \epsilon V_{DB}(s)]/D_2(s)$$

$$\Delta V_N(s) = (s+2\zeta\omega_n)s [\cos\psi \epsilon V_{HB}(s) - \sin\psi \epsilon V_{DB}(s)]/D_2(s)$$

The standard deviations for the steady state position and velocity errors are:

$$\sigma_{N_D} = 0$$

$$\sigma_V = 0$$

During turns, the heading  $\psi$  will change value and the position and velocity errors will have non-zero transients. However the transients caused by the Doppler biases are negligible when compared to the position and velocity transients caused by AHRS heading errors. The effect of the AHRS heading error is listed below.

#### Doppler Scale Factor

The position and velocity errors caused by Doppler scale factors error, during cruise are:

$$\Delta N_D(s) = s \cos\psi V_H \epsilon SF_H(s)/D_2(s)$$

$$\Delta V_N(s) = (s+2\zeta\omega_n) s \cos\psi V_H \epsilon SF_H(s)/D_2(s)$$

### Doppler Scale Factor (cont.)

The steady state position and velocity standard deviations are:

$$\sigma_{N_D} = 0$$

$$\sigma_V = 0$$

The transient errors caused by the changing heading  $\psi$  and constant scale factor error during turns are negligible, compared to effects of AHRS heading errors.

### Doppler Noise

The transfer functions between the Doppler velocity noise and the position and velocity errors are:

$$\Delta N_D(\omega) = \frac{j\omega \{ \cos\psi n_{DH}(\omega) + \sin\psi [-\cos\phi n_{DD}(\omega) + \sin\phi n_{DV}(\omega)] \}}{(-\omega^2 + 2j\zeta\omega_n + \omega_n^2)}$$

$$\Delta V_D(\omega) = \frac{(j\omega)(j\omega + 2\zeta\omega_n) \{ \cos\psi n_{DH}(\omega) + \sin\psi [-\cos\phi n_{DD}(\omega) + \sin\phi n_{DV}(\omega)] \}}{(-\omega^2 + 2j\zeta\omega_n + \omega_n^2)}$$

Assuming the three Doppler noise components have equal power spectral densities,  $S_D$ , and the noise bandwidth is wide relative to  $\omega_n$ , the position variance is

$$\sigma_{N_D}^2 = \frac{S_D}{4\zeta\omega_n}$$

The Doppler noise components contribute directly to the system velocity error, as can be seen from the velocity error equation by letting  $\omega$  be significantly larger than  $\omega_n$ . Therefore the velocity error variance is approximately

$$\sigma_V^2 = S_D / \tau_D$$

where  $\tau_D$  is the correlation time of the Doppler radar frequency tracker.

### AHRS Heading Error

For cruise conditions, the position and velocity errors contributed by an AHRS heading error are

$$\Delta N_D(s) = \frac{-sV_E \delta\psi(s)}{D_2(s)}$$

$$\Delta V_N(s) = \frac{-(s+2\zeta\omega_n) sV_E \delta\psi(s)}{D_2(s)}$$

The steady state position and velocity variances caused by a AHRS heading error are

$$\sigma_{N_D}^2 = 0$$

$$\sigma_V^2 = 0$$

The AHRS heading error is the dominant cause of position and velocity errors during aircraft turns. To compute the magnitude of the position and velocity error transients, a worst case assumption is made that the aircraft turn is short relative to the system's time constant ( $1/\zeta\omega_n$ ). With this assumption, the Doppler/AHRS velocity error  $\epsilon V_N$  can be modeled with a step increase equal to  $-[V_E(t_\tau^+) - V_E(t_\tau^-)]\delta\psi(t_\tau)$  at the time of the turn. The east velocity change that occurs during the turn is  $[V_E(t_\tau^+) - V_E(t_\tau^-)]$ . From Equations E-1 and E-2, the position and velocity errors caused by the step change in  $\epsilon V_N$  satisfy

$$\Delta N_D(s) = \frac{-V_E(t_\tau^+) - V_E(t_\tau^-) \delta\psi(t_\tau)}{s^2 + 2\zeta\omega_n s + \omega_n^2}$$

$$\Delta V_N(s) = \frac{-(s+2\zeta\omega_n) [V_E(t_\tau^+) - V_E(t_\tau^-)] \delta\psi(t_\tau)}{s^2 + 2\zeta\omega_n s + \omega_n^2}$$

By taking the inverse Fourier transforms of the above equations, the peaks of the position and velocity error transients are determined to be

$$\sigma_{N_D}|_{\text{peak}} = .37 |V_E(t_\tau^+) - V_E(t_\tau^-)| \sigma_{\psi/\omega_n}$$

$$\sigma_v \Big|_{\text{peak}} = |v_E(t_\tau^+) - v_E(t_\tau^-)| \sigma_\psi$$

for a unity damping factor,  $\zeta$ .

#### AHRS Roll and Pitch Errors

As is the case with AHRS heading errors, the steady state position and velocity errors caused by roll and pitch errors are zero. The transient position and velocity errors caused during turn are negligible compared to the transients caused by the AHRS heading error.

REPORT OF OPERATIONAL & TEST EVALUATION OF THE GPS SYSTEM  
FOR THE C-130 AIRCRAFT AND HELICOPTER IN SUPPORT OF THE  
JOINT CASUALTY COLLECTION AND MEDICAL EVACUATION MISSIONS  
IN AFGHANISTAN

AN ASSESSMENT OF THE PERFORMANCE OF THE GPS SYSTEM  
FOR THE C-130 AIRCRAFT AND HELICOPTER IN SUPPORT OF THE  
JOINT CASUALTY COLLECTION AND MEDICAL EVACUATION MISSIONS  
IN AFGHANISTAN

AN ASSESSMENT OF THE PERFORMANCE OF THE GPS SYSTEM  
FOR THE C-130 AIRCRAFT AND HELICOPTER IN SUPPORT OF THE  
JOINT CASUALTY COLLECTION AND MEDICAL EVACUATION MISSIONS  
IN AFGHANISTAN

## **APPENDIX F**

### **GPS OPERATIONAL PERFORMANCE**

#### **LIMITATIONS**

## APPENDIX F. GPS OPERATIONAL PERFORMANCE LIMITATIONS

The position and velocity accuracy provided by the GPS user receiver is directly related to the receivers ability to measure pseudo-range and pseudo-range-rate. These two quantities are measured using two types of tracking loops; one which tracks the PRN code modulation on the received navigation signal, and the other which tracks the carrier phase. For each of these loops to operate properly, the uncertainty in the function not being directly tracked (phase or code) must be controlled. The code tracking loop requires that the carrier frequency be known within 10's of Hz while the carrier tracking loop requires that the code phase be known within a small fraction of a chip. The dependence of the carrier loop on proper code tracking is fairly high while the opposite condition is not as critical.

### F.1 CODE TRACKER

One common configuration of the code tracking loop is the delay lock loop implementation for which Equations F-1 and F-2 describe the performance.

$$\sigma_R = W \left[ \frac{B_L \left\{ .5 \left( \frac{I}{S} \right)_{PD} + \left( \frac{I}{S} \right)_{PD}^2 \right\}}{B_{PD}} \right]^{1/2} \quad (F-1)$$

$$\left( \frac{I}{S} \right)_{RF} = \left( \frac{I}{S} \right)_{PD} \frac{10^7}{B_{PD}} \quad (F-2)$$

where

$\sigma_R$  = range error ( $1\sigma$ ) in feet

W = Chip width in feet (96.2 ft.)

$B_L$  = Delay lock loop noise bandwidth

$(I/S)_{PD}$  = Interference to signal power in pre-detection bandwidth

$(I/S)_{RF}$  = Interference power to signal power ratio in receiver RF bandwidth (interference noise is assumed uniformly distributed over 10 MHz).

$B_{PD}$  = Pre-detection bandwidth (bandwidth before square law detection).

Reference [27] provides a derivation of Equation F-1. Because an unknown 50 bps data stream is present on the navigation signal, the pre-detection bandwidth cannot be smaller than 50 Hz.

Figure F-1 is a graph showing the performance provided by Equations F-1 and F-2. Curves providing range accuracies ( $1\sigma$ ) of 1, 4, 10, 12, and 15 feet are shown as a function of  $(I/S)_{RF}$  and  $B_L$ . The 1 foot curve is predicted as the best performance obtainable due to equipment implementation (nonlinearity, drifts) limitations, the 4 feet curve is the specified GPS tracking accuracy, the 12 feet curve corresponds to GPS degraded tracking mode specified as Hold-On-By-Your-Teeth (HOBYT) and the 15 feet curve corresponds to the lock limit ( $3\sigma_R \approx 1/2$  chip). Also shown is the  $(I/S)_{RF}$  that will be present in the system.

## F.2 CARRIER TRACKER

A very common carrier tracking loop configuration is the Costas loop where performance is described by the following equations:

$$\sigma_{RR} = \frac{C}{f_t \cdot 2\pi\sqrt{\left(\frac{S}{I}\right)_L} T} \quad (F-3)$$

$$\left(\frac{S}{I}\right)_L = \left(\frac{S}{I}\right)_{PD} \left[ \frac{4\left(\frac{S}{I}\right)_{PD}}{1 + 4\left(\frac{S}{I}\right)_{PD}} \right] \frac{B_{PD}}{B_n} \quad (F-4)$$

$$\left(\frac{S}{I}\right)_{RF} = \left(\frac{S}{I}\right)_{PD} \cdot \frac{B_{PD}}{10^7} \quad (F-5)$$

where

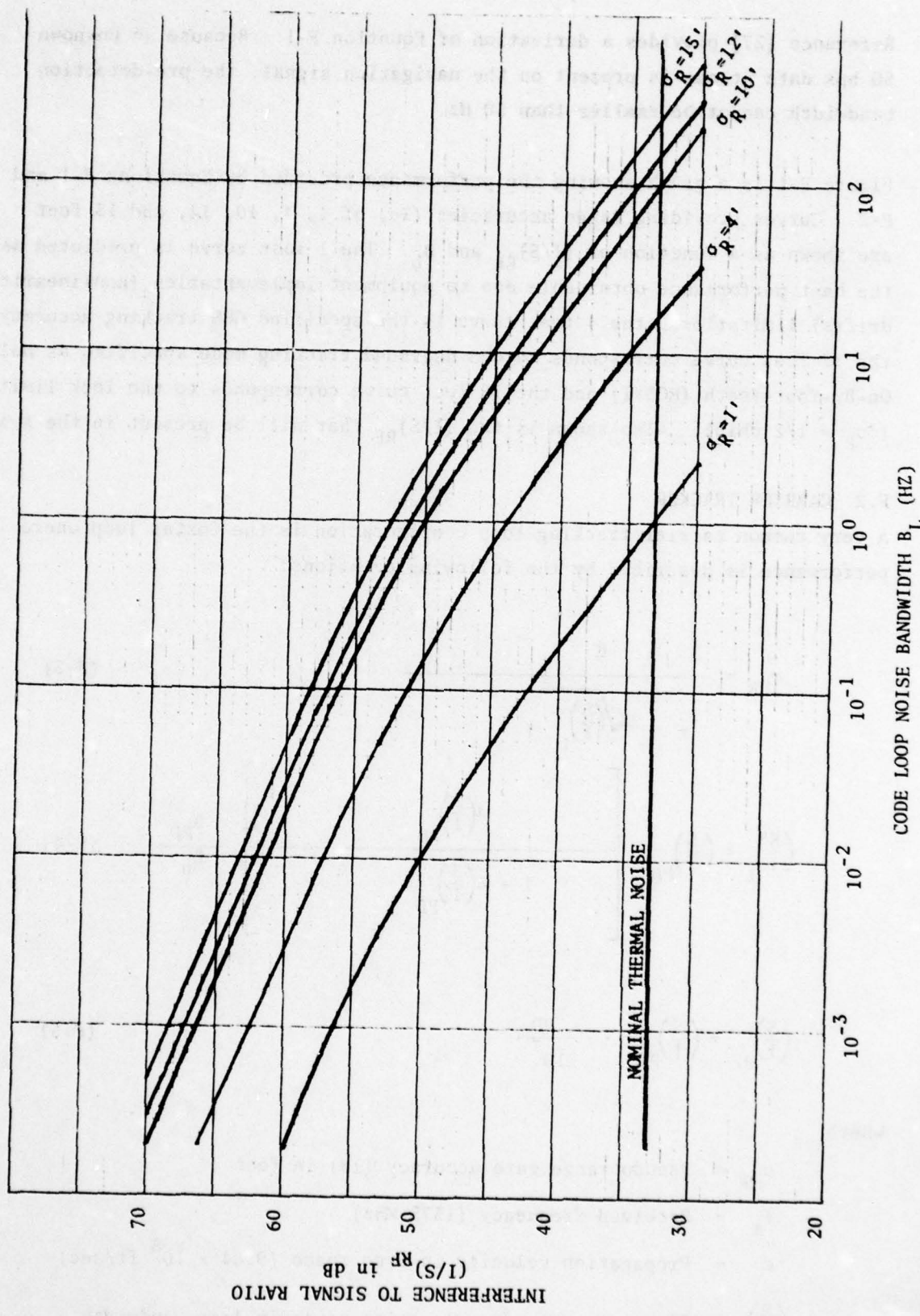
$\sigma_{RR}$  = Pseudo range rate accuracy ( $1\sigma$ ) in feet

$f_t$  = Received frequency (1575 MHz)

$c$  = Propagation velocity in free space ( $9.84 \times 10^8$  ft/sec)

$\left(\frac{S}{I}\right)_L$  = Signal to interference noise power in loop bandwidth

FIGURE F-1  
CODE TRACKING LOOP PERFORMANCE LIMITS



F-4

$T$  = Measurement sampling time (specified at 0.1 sec)

$B_n$  = Noise bandwidth of Costas loop

Reference [28] provides a derivation of Equations F-3 and F-4.

For the Costas Loop to remain locked with good probability a  $(S/I)_L$  of greater than 16 (12dB) is required. This represents a 6 dB degradation in threshold with respect to a conventional phase locked loop which is caused by the effective squaring in the loop. In the graph shown in Figure F-2 this constraint was imposed to generate the curves of  $\sigma_{RR}$  versus  $(I/S)_{RF}$  and  $B_n$ .

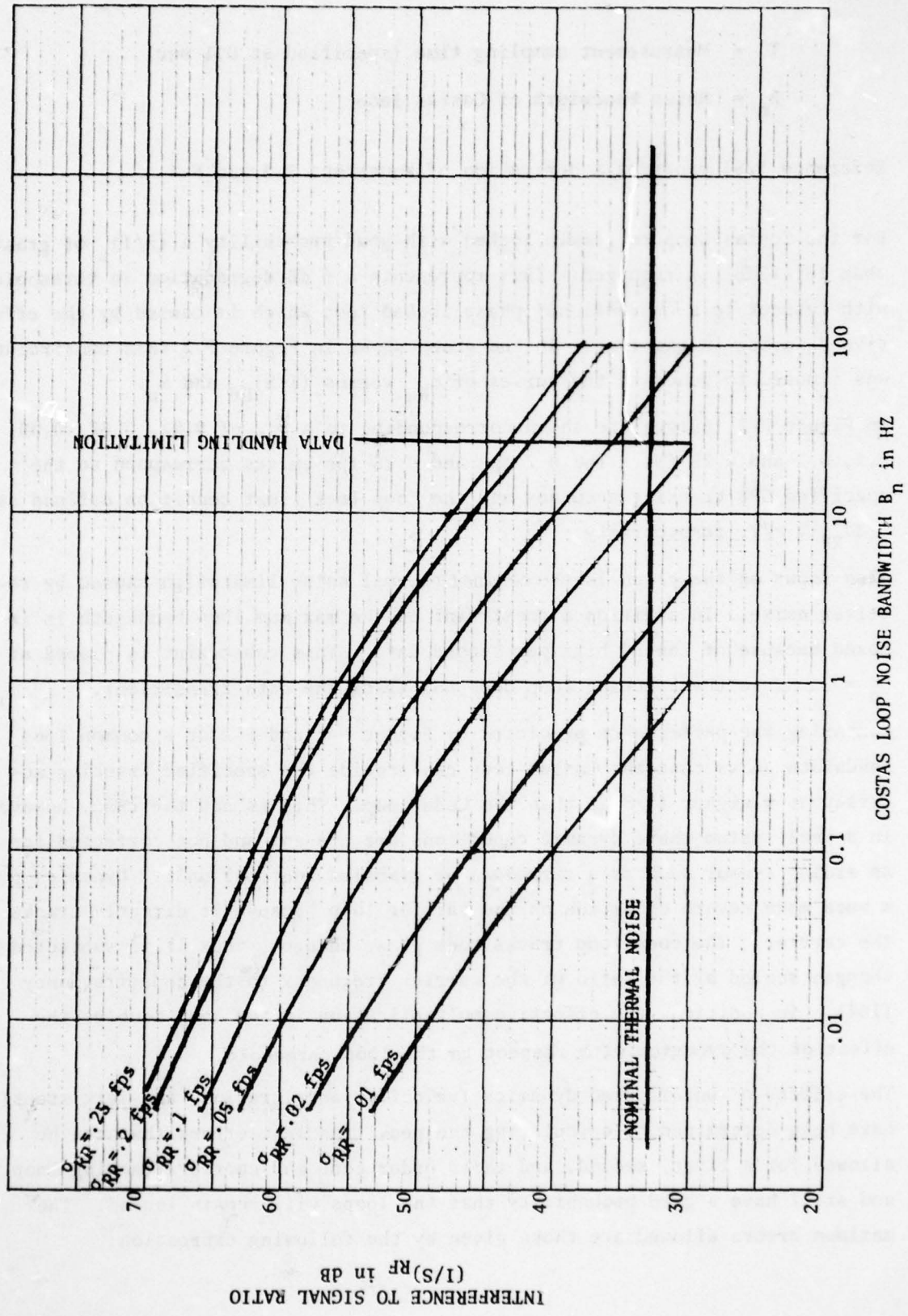
In Figure F-2, curves are shown corresponding to a  $\sigma_{RR}$  of 0.01, 0.02, 0.05, 0.1, 0.2 and 0.25 fps. The 0.2 fps and 0.25 fps curves correspond to the specified GPS tracking accuracy and the loop lock limit condition defined as  $3(2\sigma_{RR}) \approx \pi/2$ , respectively.

Also shown on the graph is the nominal thermal noise limitation caused by receiver noise. In addition a constraint on the maximum loop bandwidth is imposed because of the 50 bits per second data. This constraint is placed at  $B_n = 25$  Hz so the tracking loop does not track the data transitions.

Comparing the performance predicted by Figure F-1 and F-2 at a common loop bandwidth shows that the Costas loop can provide the specified tracking accuracy at a higher  $(I/S)_{RF}$  than the Code loop. This is not the case, however, in a real system where dynamic conditions are present and not corrected for by an aiding sensor such as a strapdown or gimbaled inertial unit. Dynamics pose a much more severe condition on the carrier loop because it directly tracks the carrier. The code loop tracks code phase changes, thus it is subjected to changes scaled by the ratio of the carrier frequency to the code frequency (154). In addition, the effective multiplication in the loop doubles the effect of the dynamics with respect to the loop threshold.

The effects of uncorrected dynamics (velocity, acceleration, and jerk steps) have been determined by calculating the peak transient errors that can be allowed for a first, second, and third order code and carrier tracking loop and still have a good probability that the loops will remain locked. The maximum errors allowed are those given by the following expression:

FIGURE F-2  
CARRIER TRACKING LOOP PERFORMANCE LIMITS



AD-A072 148 LEAR SIEGLER INC GRAND RAPIDS MICH INSTRUMENT DIV F/G 17/7  
FEASIBILITY STUDY FOR INTEGRATED FLIGHT TRAJECTORY CONTROL (AIR--ETC(U))  
JAN 77 M BIRD F33615-74-C-3083

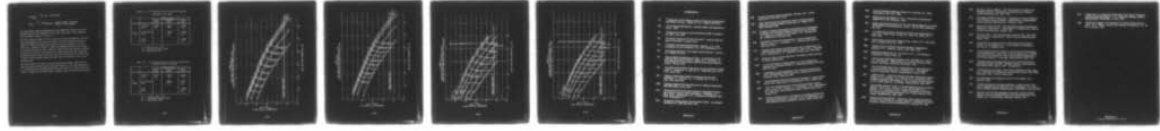
UNCLASSIFIED

AFFDL-TR-77-120

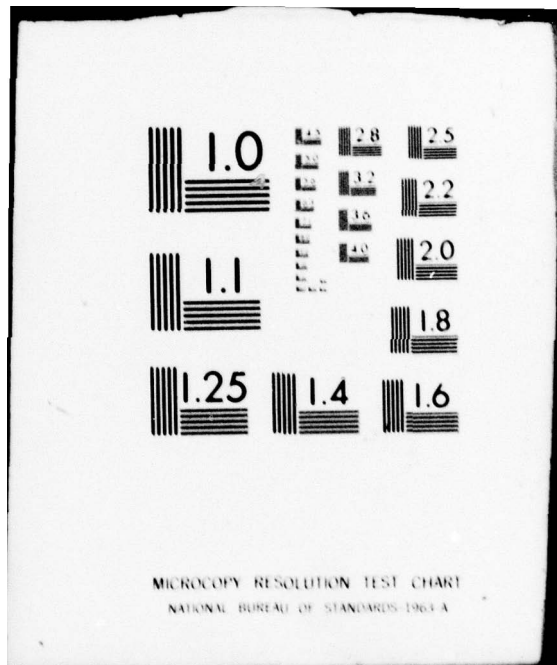
NL

4 OF 4

AD  
A072148



END  
DATE FILMED  
9-79  
DDC



$$\epsilon_{\text{range}} \Big|_{\max} = \frac{W}{2} - 3\sigma_R; \text{ code tracker}$$

$$\epsilon_{\phi} \Big|_{\max} = \frac{\pi}{4} - 3(\sigma_{RR})_{\text{radians}}; \text{ carrier tracker (including effect of loop squaring)}$$

The calculations conducted determined the loop bandwidth required so that the maximum error was not exceeded for the various step inputs. The expressions used are shown in Tables F-I and F-II.

The curves shown in Figure F-3 and F-4 show the limitation imposed on the code loop (superimposed on the curves of Figure F-1) for two specific conditions. Figure F-3 shows the maximum uncorrected acceleration allowed for a second order loop. Similarly, Figure F-4 shows the maximum uncorrected jerk allowed if a third order loop is used. Figures F-5 and F-6 show the limitation imposed on the carrier loop for the condition of a second order loop with uncorrected acceleration changes and a third order loop with uncorrected jerk, respectively. As shown, similar changes present much more severe constraints on the carrier tracking loops.

The curves shown can be used to provide predicted performance constraints on the GPS receiver code and carrier loops when operated in an aided configuration. In the aided mode the tracking errors which can be present are those caused by errors in outputs of the aiding sensor, sampling times, and computational delays.

TABLE F-I. Peak Transient Error for Code Tracking Loop  
Code Rate = 10.23 MHz

		Order of Loop		
		First Order	Second Order	Third Order
$\epsilon_r _{\max}$	Velocity Step	$\frac{.25\delta v}{B_n}$	$\frac{.242\delta v}{B_n}$	$\frac{.261\delta v}{B_n}$
	Acceleration Step	-	$\frac{.293\delta a}{B_n^2}$	$\frac{.279\delta a}{B_n^2}$
	Jerk Step	-	-	$\frac{.579\delta J}{B_n^3}$

$\delta v$  = velocity step in fps

$\delta a$  = acceleration step in  $\text{fps}^2$

$\delta J$  = jerk step in  $\text{fps}^3$

TABLE F-II. Peak Transient Error for Carrier Tracking Loop  
Received Carrier = 1575 MHz

		Order of Loop		
		First Order	Second Order	Third Order
$\epsilon_\phi _{\max}$	Velocity Step	$\frac{2.5\delta v}{B_n}$	$\frac{2.43\delta v}{B_n}$	$\frac{2.62\delta v}{B_n}$
	Acceleration Step	-	$\frac{2.95\delta a}{B_n^2}$	$\frac{2.8\delta a}{B_n^2}$
	Jerk Step	-	-	$\frac{5.82\delta J}{B_n^3}$

$\delta v$  = velocity step in fps

$\delta a$  = acceleration step in  $\text{fps}^2$

$\delta J$  = jerk step in  $\text{fps}^3$

FIGURE F-3  
CODE TRACKING LOOP PERFORMANCE LIMITS  
SECOND ORDER LOOP SUBJECTED TO STEPS OF ACCELERATION

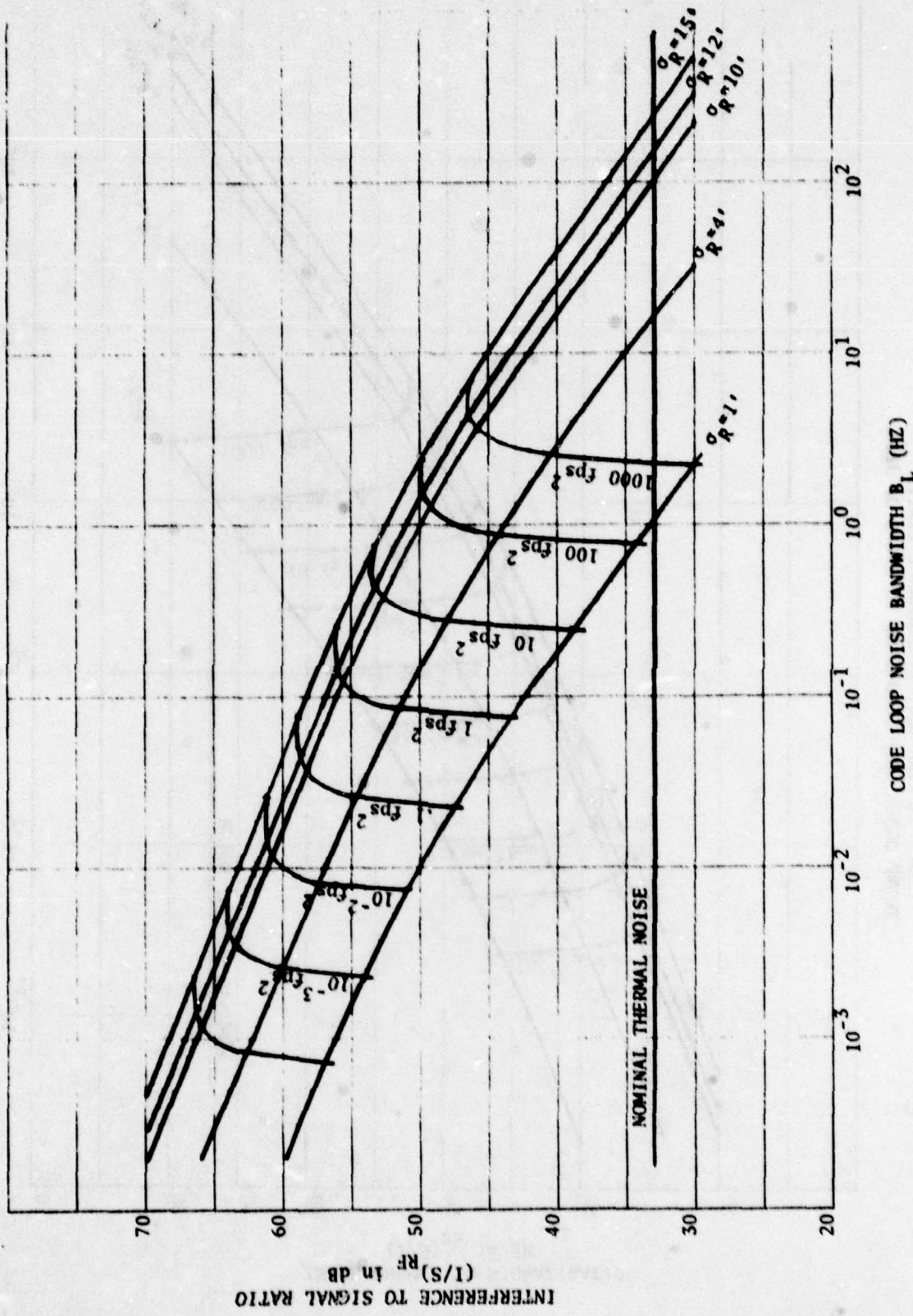


FIGURE F-4  
CODE TRACKING LOOP PERFORMANCE LIMITS  
THIRD ORDER LOOP SUBJECTED TO STEPS OF JERK

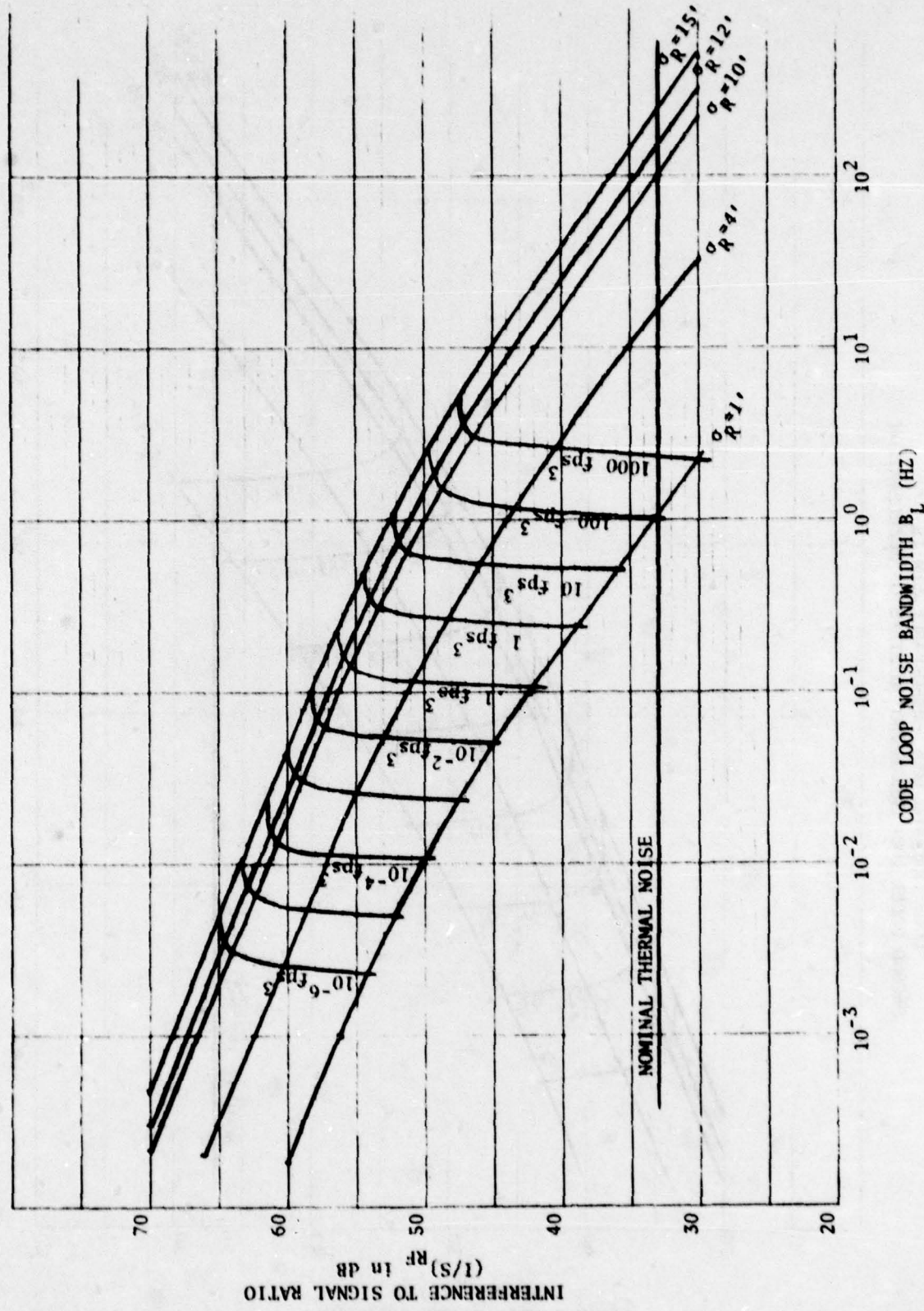


FIGURE F-5  
CARRIER TRACKING LOOP PERFORMANCE LIMITS  
SECOND ORDER LOOP SUBJECTED TO STEPS OF ACCELERATION

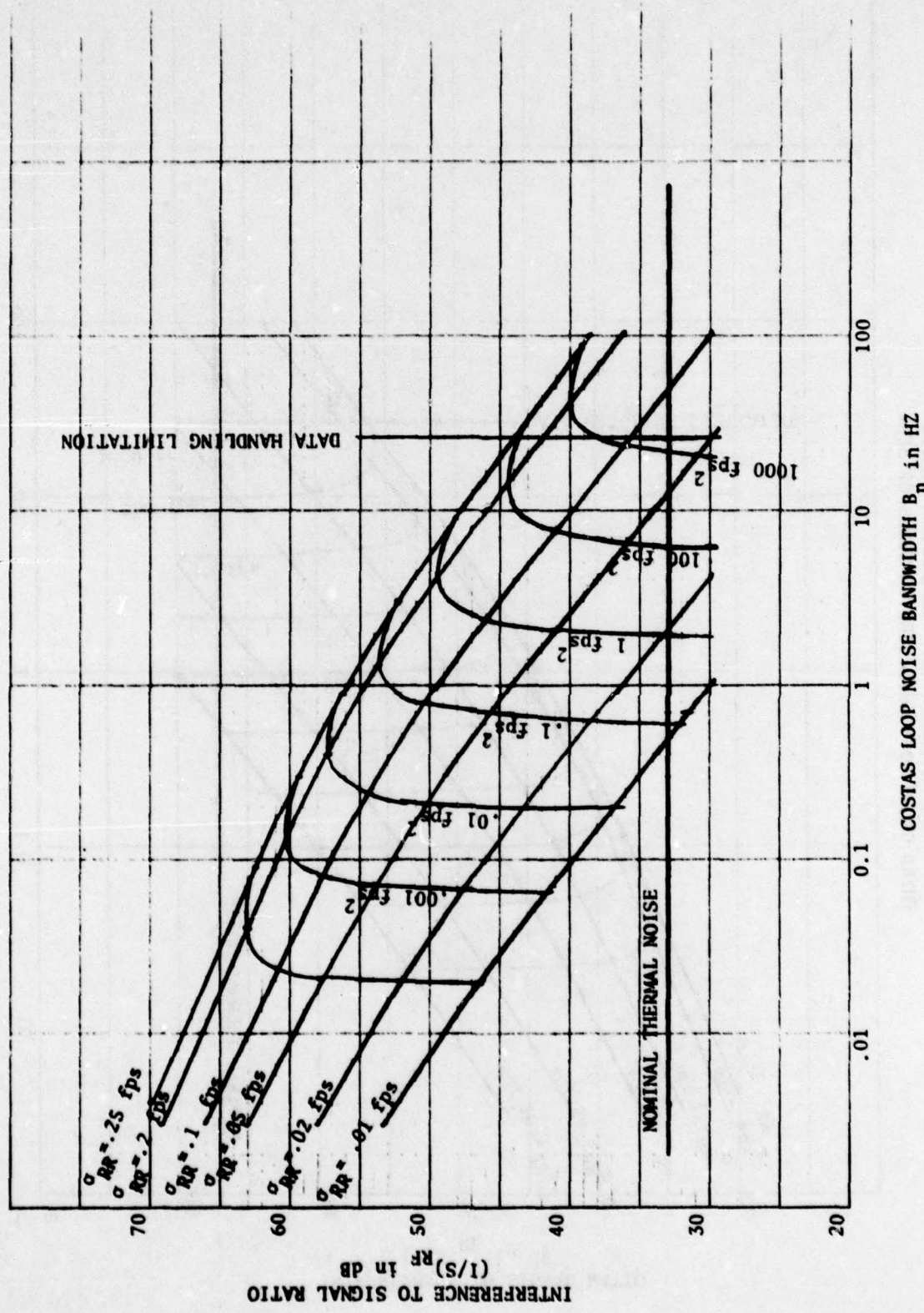
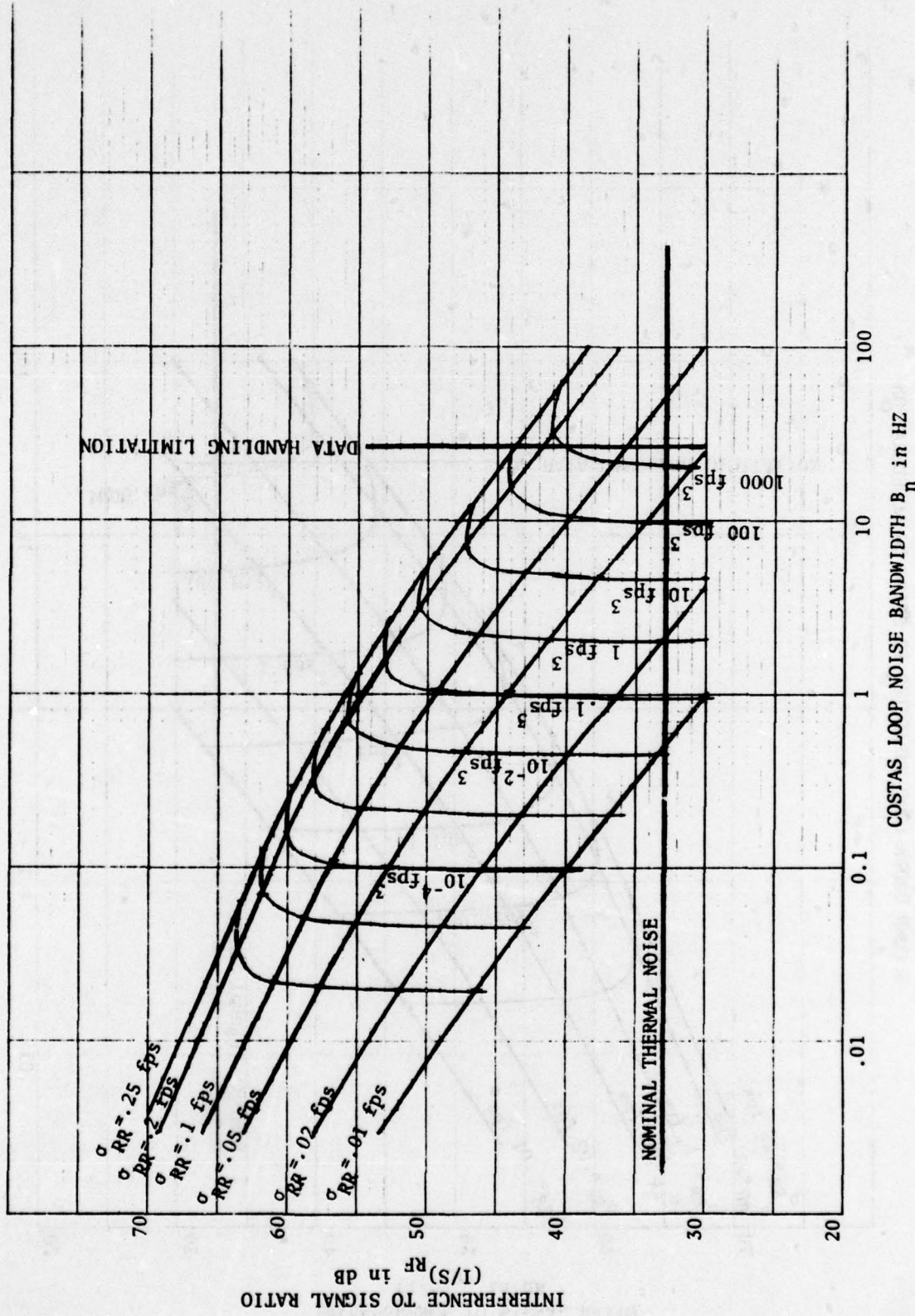


FIGURE F-6  
CARRIER TRACKING LOOP PERFORMANCE LIMITS  
THIRD ORDER LOOP SUBJECTED TO STEPS OF JERK



## REFERENCES

- [1] "Cockpit and Control Display Design Criteria for Tactical STOL and VSTOL Aircraft", Musgrove, J. S., AFFDL-TR-72-72.
- [2] "C-141 Aircraft Simulation", LSI Inter-Office Correspondence, 4 Dec., 1975.
- [3] "Employment Concept for Advanced Medium STOL Transport", Hq. MAC, June 1975.
- [4] "Terminal Configured 737 Hits Problems", Aviation Week and Space Technology, 6 January 1975.
- [5] "Computer-Generated Map Displays", Warner, J. S., FAA Symposium on Area Navigation, Jan. 1972, Washington, D. C.
- [6] "Simulator Evaluation of the Flight Profile Indicator", Gaynor, M., AFFDL TR 70-67.
- [7] "Manual Digital Positioning in 2 Axes: A Comparison of Joy-stick and Track Ball Controls", Mehr, M. H., and Mehr, E., Proceedings of the 16th Annual Meeting of the Human Factors Society, October 1972.
- [8] "Terminal Area Guidance Algorithms for Automated Air-Traffic Control", Erzberger, H. and Lee, H., NASA tech note, TN D-6773, April 1972.
- [9] "Optimum Horizontal Guidance Techniques for Aircraft", Erzberger, H., and Lee, H., J. Aircraft, Vol. 8, No. 2, Feb. 1971, pp 95-101.
- [10] "Military Standard Climatic Extremes for Military Equipment", MIL-STD-210A, 2 Aug. 1957.
- [11] "Recent Advances in Accurate Airborne Computation of Secondary Plan for Loran C Radio Navigation", Fredricks, R. J., Bird, M. W., and Wheeler, K. A., Institute of Navigation, June 1975, Washington D. C.
- [12] "Strapdown Attitude System Kalman Filter Study", Lear Siegler Publication No. GRR-004-0973, 1973.

- [13] Inertial Navigation Systems Analysis, Britting, K.R., Wiley-Interscience, New York, 1971.
- [14] USAF ASD Request for Proposal for Multi-Function Inertial Reference Assembly (MIRA), Solicitation No. E33615-76-R-3132, 18 March 1976.
- [15] Computer Program Development Specification for Navigational Computer of F-4E Digital Modular Avionics System AN/ARN-101 - Type B5, prepared by Lear Siegler, Inc., Specification No. CB1001-010, 5 October 1975.
- [16] Estimation Theory with Applications to Communications and Control, Sage, A.P. and Melsa, J.L., McGraw-Hill Book Co., New York, 1971.
- [17] "Kalman Filter Design and Performance for an Operational F-4 Loran Inertial Weapon Delivery System", Bird, M.W., Wierenga, R.D., and TenCate, J.V., NAECON, Dayton, Ohio, May 1976.
- [18] Reference Data for Radio Engineers, 5th Edition, IT&T, (Howard W. Sams Publications).
- [19] "C-141 All-Weather Landing System for Lower Minimums", Appendix B, Lockheed Georgia Co., Engineering Report ER-8081, Oct. 12, 1965.
- [20] "Application of Area Navigation in the National Aerospace System", FAA/Industry RNAV Task Force, Department of Transportation, FAA, February 1973.
- [21] "Area Navigation Waypoint Designation Standards", Report #FAA-RD-73-122, Department of Transportation, FAA, August 1975.
- [22] "4-D Area Navigation System Description and Flight Test Results", Lee, H.Q., Neuman, F., and Hardy, G.H., NASA Report No. TND-7874, Ames Research Center, Moffett Field, Calif., August 1975.
- [23] "Software Engineering of a Navigation and Guidance System for Commercial Aircraft", Lachmann, S.G. and McKinstry, R.G., AIAA Digital Avionics Symposium, Boston, Mass, April 1975.

- [24] **Avionics Navigation Systems**, Kayton, M. and Fried, W., Wiley Interscience, New York, 1969.
- [25] **GPS Control/User Segments**, Vol. I, Introduction and Summary, SAMSO TR 74-182, February, 1974.
- [26] **System Segment Specification for the User System Segment of the NAV STAR Global Positioning System**, Phase 1, SS-US-101B, September 30, 1974.
- [27] "A Comparison of Binary Delay-Lock Track Loop Implementation", Gill, W.J., IEEE Trans. on AES, Vol. AES, Vol. AES 2, No. 4, July, 1966.
- [28] **Telecommunication Systems Engineering**, Lindsey, W.C. and Simon, M.K., Prentice Hall, Inc., 1973.
- [29] "Failure Detection Without Excessive Hardware Redundancy", Maybeck, P.S., NAECON, Dayton, Ohio, May, 1976.
- [30] **Reliability Engineering**, Ed. Von Alven, W.H., Arinc Research Corporation, Prentice Hall, Inc.
- [31] "Tactical and Long Range Navigation in the AN/ARN 101", Perfitt, T.E. and Pickel E., IEEE Position Location and Navigation Symposium, San Diego, California, November, 1976.
- [32] "The US Candidate Microwave Landing System, A New Generation of Avionics/Ground Equipment", Sebring, J.R., AIAA Digital Avionics Conference, Boston, Massachusetts, April, 1975.
- [33] "ADSEL/DABS - A Selective Address Secondary Surveillance Radar", Bowes, R.C., Drouilhet, P.R., Weiss, H.G., and Stevens, M.C., AGARD Conference Proceedings No. 188 on Plans and Developments for Air Traffic Systems, Cambridge, Massachusetts, May, 1975.
- [34] "Intermittent Positive Control, A Ground-Based Collision Avoidance System", Perle, M.E., Horwitz, B.M., Mc Farland, A.L., Beusch, J.V., and Senve, K.D., AGARD Conference Proceedings No. 188 on Plans and Developments for Air Traffic Systems, Cambridge, Massachusetts, May, 1975.
- [35] **Advisory Circular #90-45A: "Approval of Area Navigation Systems for Use in the US National Aerospace System"**, Department of Transportation, Federal Aviation Administration, February 21, 1975.

- [36] **Advisory Circular #90-63: "ATC Procedures for Random Area Navigation Routes", Department of Transportation, Federal Aviation Administration, May, 1973.**
- [37] **FAA/Industry RNAV Task Force: "Application of Area Navigation in the National Airspace System", Department of Transportation, Federal Aviation Administration, February, 1973.**
- [38] **Report #FAA-RD-73-122: "Area Navigation Waypoint Designation Standards. Final Report", Department of Transportation, Federal Aviation Administration, August, 1975.**
- [39] **Ten Year Plan: "The National Aviation System Plan, 1973-1982", Department of Transportation, Federal Aviation Administration, March, 1973.**
- [40] **"Some System Considerations for MLS Airborne Processors", Beneke, J. and Wightman, C. J. of the Institute of Navigation, Vol. 22, No. 1, Spring, 1975.**
- [41] **"United States Program to ICAO for a New Non-Visual Approach and Landing System", Del Balzo, J. M. and Jones, S. R., AGARD Conference Proceedings No. 188 on Plans and Developments for Air Traffic Systems", Cambridge, Massachusetts, May, 1975.**
- [42] **"Message Specification (Interim) for Joint Tactical Information Distribution System (JTIDS)", MITRE, Bedford, Massachusetts, DCB Exhibit 7501, March, 1976. (Confidential)**
- [43] **"Communication Terminal: Time Division Multiple Access, Seek Bus - AWACS 411L" Boeing Procurement Specification, 204-15956, November, 1973. (Secret, Restricted)**
- [44] **Correspondence from Hughes Aircraft to Lear Siegler, Inc., Summer, 1975.**
- [45] **"Relative Navigation by Passive Ranging in a Synchronous Time Division Multiple Access Data Net", E. A. Westbrook, R. C. Snodgrass, MITRE, Bedford, Massachusetts, MTR-2966, U, March, 1975.**
- [46] **Seek Bus Time Division Multiple Access Data Link Into Digital Modular Avionics AN/ARN-101(V), Final Technical Study, Lear Siegler, Inc., Grand Rapids, Michigan, Spring, 1975.**

- [47] "Flight Test of an Integrated TDMA Data Link/Loran-C Navigation and Synchronization System", E. A. Westbrook, MITRE, Bedford, Massachusetts, MTR-2850, U, June, 1974.
- [48] "Differential Omega in the Domestic Air Traffic Control Environment", H. G. Miller, Journal of the Institute of Navigation, Vol. 22, No. 2, Summer 1975.

#### Reference-5

\*U.S. Government Printing Office: 1979 - 657-002/413